Analysis of the influencing factors of dynamic loads acting on the operating systems of beam balanced bascule bridges

D. Antohe

Delft University of Technology

TU Delft

anteagroup

Challenge the future

Analysis of the influencing factors of dynamic loads acting on the operating systems of beam balanced bascule bridges

By

D. Antohe

in partial fulfilment of the requirements for the degree of

Master of Science
in Civil Engineering

at Delft University of Technology,

Thesis committee:	Prof. dr. ir. A.V. Metrikine,	TU Delft
	Em. Prof. ir. F.S.K. Bijlaard,	TU Delft
	Ir. K. Sektani,	TU Delft and Antea Group
	Dr. ir. A. Tsouvalas	TU Delft

PREFACE

This thesis was written as a completion of the Civil Engineering master education at Delft University of Technology. The research was carried out in cooperation with the Faculty of Civil Engineering and Geosciences and the Dutch engineering company Antea Group.

The Structural Engineering master curriculum at Delft University of Technology helped me develop an immense interest on the design of bridges, especially steel bridges. After completing an internship within Antea Group company that was mainly focused on developing calculation models for the design of movable bridges, I decided that this is the part that I want to focus my thesis research on. Together with my direct supervisor from Antea Group, Kodo Sektani, we decided that a dynamic analysis of the operating systems of movable bridges would be an interesting choice and a good fit for me.

Firstly, I want to express my immense gratitude to my company supervisor, Kodo Sektani, who was more than a mentor. His experience in the design of movable bridges and his guidance during the graduation period were essential in finalising my thesis. Thank you also for all the advice given throughout this period, and for preparing me for postgraduate life.

Further, my gratitude goes to Andrei Metrikine, Frans Bijlaard and Apostolos Tsouvalas for being part of my committee and taking the time to revise my research and guide me towards a successful completion of this thesis. Furthermore, I want to thank Antea Group for offering me the opportunity to perform this research under their surveillance, and for letting me be part of a working environment. Special thanks to George Bitter for sharing his expertise in the mechanical engineering field.

Last, but not least, I want to express my eternal gratitude to my friends and family. They have provided the biggest moral and financial support since I came to Delft and especially during these last 10 months. I want to also express my gratitude to my brother Raoul for being the one that introduced me to this world and for always being there helping, questioning me, teaching me and sharing his experience.

D. Antohe
Delft, 2016

ABSTRACT

There are functional movable bridges in The Netherlands dating since the 1950s. If these bridges were to be reassed based on the current design code for movable bridges, then more than 90% will not meet the exigencies stated there. However, if these bridges were to be reassed based on field measurements, then this percentage will be lowered considerably. Then why should existing bridges be reassed with the rules for new bridges? This research intends to lower the conservativeness of the current design codes based on an analytical approach, by including both the theoretical considerations behind the standards and the real data given by field measurements of an existing movable bridge. The aim is to create a dynamic model which reduces the gap between theory and reality. Since the available measurements were performed on a beam balanced type of movable bascule bridge, only this type is analysed. The model is created for a straight rack type of mechanism, and the parameters are afterwards adjusted so that the behaviour of a curved rack type of operating mechanism is simulated properly. The bridge is modelled by means of equations of motion which are intended to simulate its behaviour in two situations: a complete opening cycle of the bridge and an emergency brake. The entire structure is considered as a three degrees of freedom model, interconnected by spring-dashpot elements that consider the stiffness and damping of the mechanical components of the bridge. The results are obtained at the level of the electro-motor, the movable deck and the balance part which includes the counterweight. The model predictions are obtained in terms of angular displacements, angular velocities and angular accelerations of the deck and/ or the balance part and the electro-motor torque. When the results obtained for the deck and balance part are compared with the same variables obtained from either the design standard or the measurements, there is an almost perfect match. The model predictions are always below the theoretical values, showing that the code is indeed conservative regarding these parameters. Moreover, the model predictions are also close to the measured variables, proving that the model is closer to the reality. The outcome in terms of the electro-motor torque cannot be properly verified. The data from measurements is insuffiecient and characterized by some uncertainty, thus pertinent conclusions in terms of the electro-motor torque cannot be drawn. The only viable conclusion observable for the electro-motor torque is that the predictions are always below the design electro-motor torque, proving again the conservative nature of the standard with regard to this variable. The research proved to be accurate in modelling the behaviour of the bridge structure, including the rack, the movable deck, the hanger, the balance beam and the counterweight, but the model can be improved further on the side of the electro-motor. Recommendations are given at the end in terms of additional modelling procedures, other measurements that should be performed and more components that could be accounted for.

CONTENTS

1. INTRODUCTION

In countries with low coastal zones and/or a high number of inland active waterways, movable bridges represent an economical alternative for the problem of carrying a railroad or a highway over an active waterway. A movable bridge usually has to open to marine traffic upon demand, thus the position of the movable span(s) is referred to as either closed or open. A closed movable bridge obstructs the waterway for marine traffic, while an open one permits marine traffic on the waterway. The difference between the two positions is important as different loading cases are used to design a bridge that can open versus a bridge that is permanently closed.

There are different types of movable bridge, but the use of a bascule type of bridge holds some advantages over the other types (i.e. vertical lifting bridge and swing bridge):

- It is easier to integrate within the environment;
- There is no obstruction in the waterway;
- It has unlimited clearance.

A rather important component of movable bridges is constituted by the operating equipment, its design playing a crucial role in the design of movable bridges. The operating equipment can be either mechanically or hydraulically operated and the choice depends on several factors. The most important factor for the design is the loading. Aside from the regular loads, which are present almost in every stage during operation, there are additional loads that need to be considered. The additional loads are caused by the behaviour of the bridge and of the operating equipment during motion. For instance, when applying a brake to the bridge while in motion, some back and forth movements can be observed, which give rise to these additional loads. Thus, it is trivial to analyse and understand the dynamic behaviour of the structure and the influence of various components on it.

1.1. Purpose

There are many factors that play a role in the behaviour of movable bridges. Some of them include the stiffness of various components of the bridge, the loading distribution on the operating system, the offsets due to tolerances etc. The provisions given in the Dutch Design Code for the design of movable bridges (VOBB) regarding these factors have proven to be too conservative for some projects.

The lack of information regarding the behaviour of operating mechanisms under dynamic loading constitutes one of the reasons that motivated the research behind this paper. It is questioned whether the rules given in VOBB are too favourable, giving rise to a rather conservative approach. The use of mathematical models and simulations should provide a clarification on whether the design code follows a conservative path and should lead to an optimization of the existing design of movable bridges.

1.1.1. Reference Project

South Holland Province carries out regular maintenance work on the bridges that are under its management. During the past few years regular reassessment of some existing bridges have shown that there were carried out more operations for these bridges than were specified in VOBB. Since the mentioned standard is applicable in practice, the question that arose was how the actual loads on the operational system relate to this standard.

Figure 1.1 Juliana Bridge - Caption

The province wanted, on the basis of measurements on some of its bridges, to build a framework which could justify in some cases the possibility to deviate from the provisions of this standard. Antea Group obtained an order to measure the Juliana Bridge in Vianen and compare the obtained results with calculation results in accordance with the standard. Techno Physics has been appointed to carry out the measurements and assists Hollandia in ensuring that the traffic measures, guidance and coordination are implemented.

The comparisons drawn by Antea Group will be further used in this report in order to make an additional comparison with the dynamic model of the bridge which will be later on developed. By correlation, the reliability of the above mentioned standard will be tested.

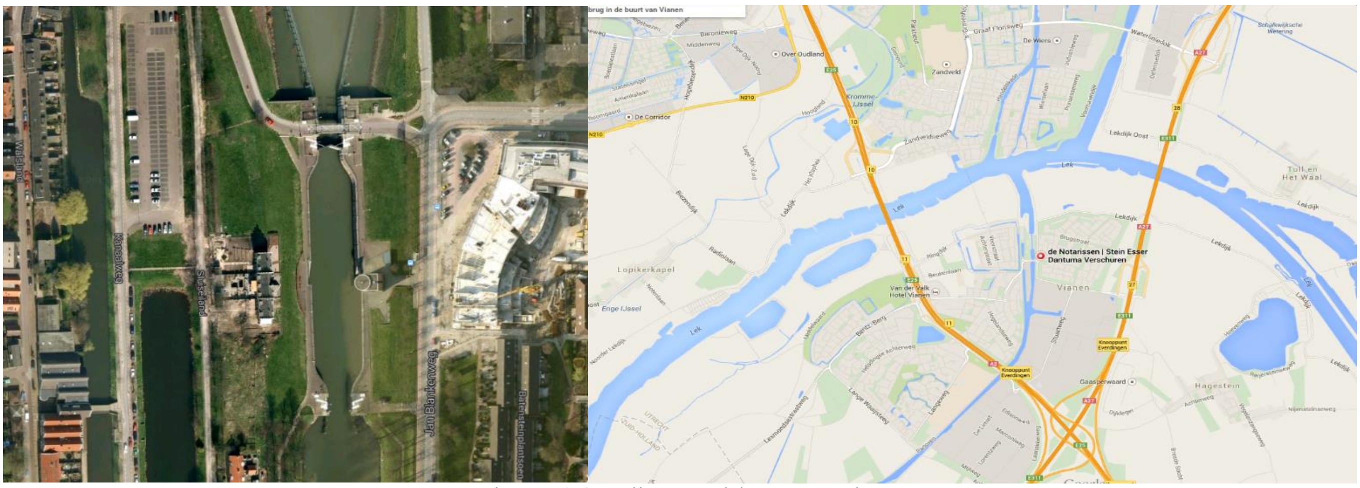

Figure 1.2 Juliana Bridge - Location

1.1.2. Research Objective

As previously stated, optimization of the current design of movable bridges implies investigating the dynamic behaviour of movable bridges, with an emphasis on its influence on the operating equipment. The main objective of this thesis is to analyse the loads acting on the operating equipment due to the influence of dynamic considerations. Therefore, another objective can be defined in terms of the factors that influence the magnitude and effects of these loads, and the manner in which they can be adapted so that the structural safety is not compromised.

1.2. Research Question

Main Question

"Is the calculation of dynamic loads for movable bridges according to VOBB leading to accurate and reliable results or is it too conservative? How could the design be improved towards a more realistic outcome?"

Sub-questions

In order to answer the main question, a set of sub-question have been established. Once answered, these sub-questions should provide an answer to the main question:

1. What is the background of the rules given in the Dutch Design Code for movable bridges?
2. What is the influence of the motion of the bridge structural frame?
3. What is the influence of the motion of the operating equipment?
4. What are the factors influencing the dynamic behaviour of movable bridges?
5. What is the effect of considering the stiffness of bridge components?
6. What is the effect of also considering the damping?
7. What is the result of adapting various factors on the behaviour of the operating mechanism and of the structure?

1.3. Limitations

Movable bridges can be dynamically analysed from different perspectives and it is quite a broad domain to be tackled. This project intends to analyse in depth the beam balanced type of bascule bridge. With respect to this subcategory, the focus (Figure 1.4) is put on the motion of these bridges caused by loads acting on the superstructure and the operating system. In this context, by superstructure it is understood the system formed by the steel structure, the movable deck and the counterweight. Analogously, the operating system is analysed at three distinct levels: the operating mechanism, the operating machinery and the motor shafts.

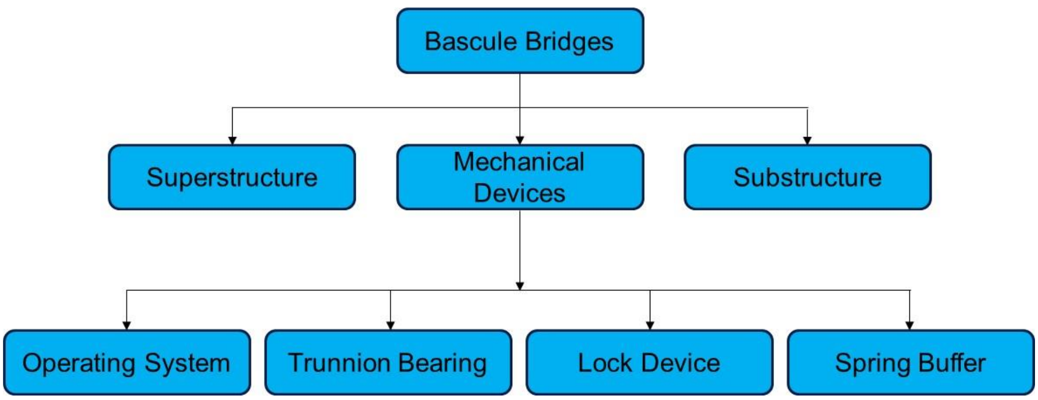

Figure 1.3 Main Focus Overview

The main idea is to create a mathematical model simulating the motion of the entire bridge. By means of mass moments of inertia, elements' stiffness, damping etc. the superstructure's geometrical characteristics will be reduced to the motor shaft. Moreover, the component elements of the operating mechanism with its characteristics will be also reduced and results will be obtained by equilibrium of the torsional moments occurring in every component part of the bridge reduced to the motor shaft. In order to start the model development, a generalized prototype will be implemented in Matlab software, including the operating mechanism, the motor shaft and the rest of the bridge, each with its corresponding geometrical properties. From there on, the model will be further on developed by splitting the rest of the bridge components into the above mention entities, so that the outcome on each structural component is obtained.

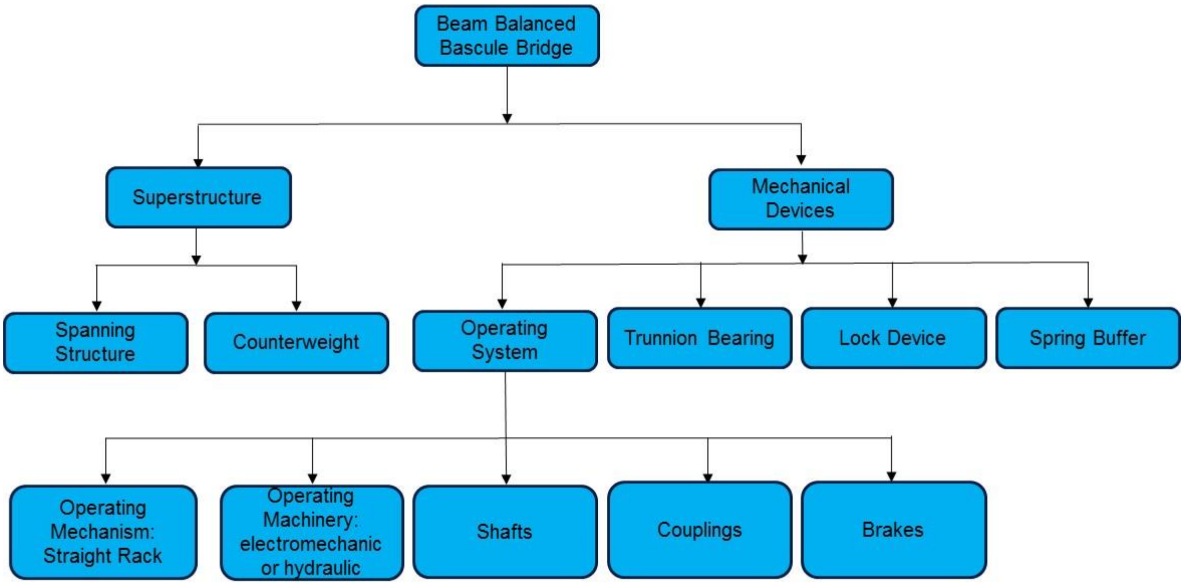

Figure 1.4 Main focus for Balanced Beam Bascule Bridges

1.4. Project Structure

This project is divided into four sections. Firstly, the motivation and purpose are defined in the first chapter. Following, the literature review with respect to movable bridges, the loads acting on them and more specifically on the operating systems is described in chapter 2. Chapter 3 is concerned with the dynamic model development, starting from a two degrees of freedom model and evolving to a three degrees of freedom model. The equations of motion of various components of the bridge are developed and the stiffness and damping coefficients are determined. The implementation of the equations of motion is done using Matlab software and the scripts can be found in the relevant appendices. The verification of the model developed in Chapter 3 is done briefly at the end of this chapter by analysing the eigenvalue problem. The complex verification will be elaborated in Chapter 4, where by means of comparison with theoretical models according to the VOBB standard and measurements from the reference project, the basic conclusions can be drawn. Finally, Chapter 5 describes in detail the conclusions drawn from the previous chapters and recommendations for further work are provided. A scheme of the project structure and the flow is outlined in Figure 1.5.

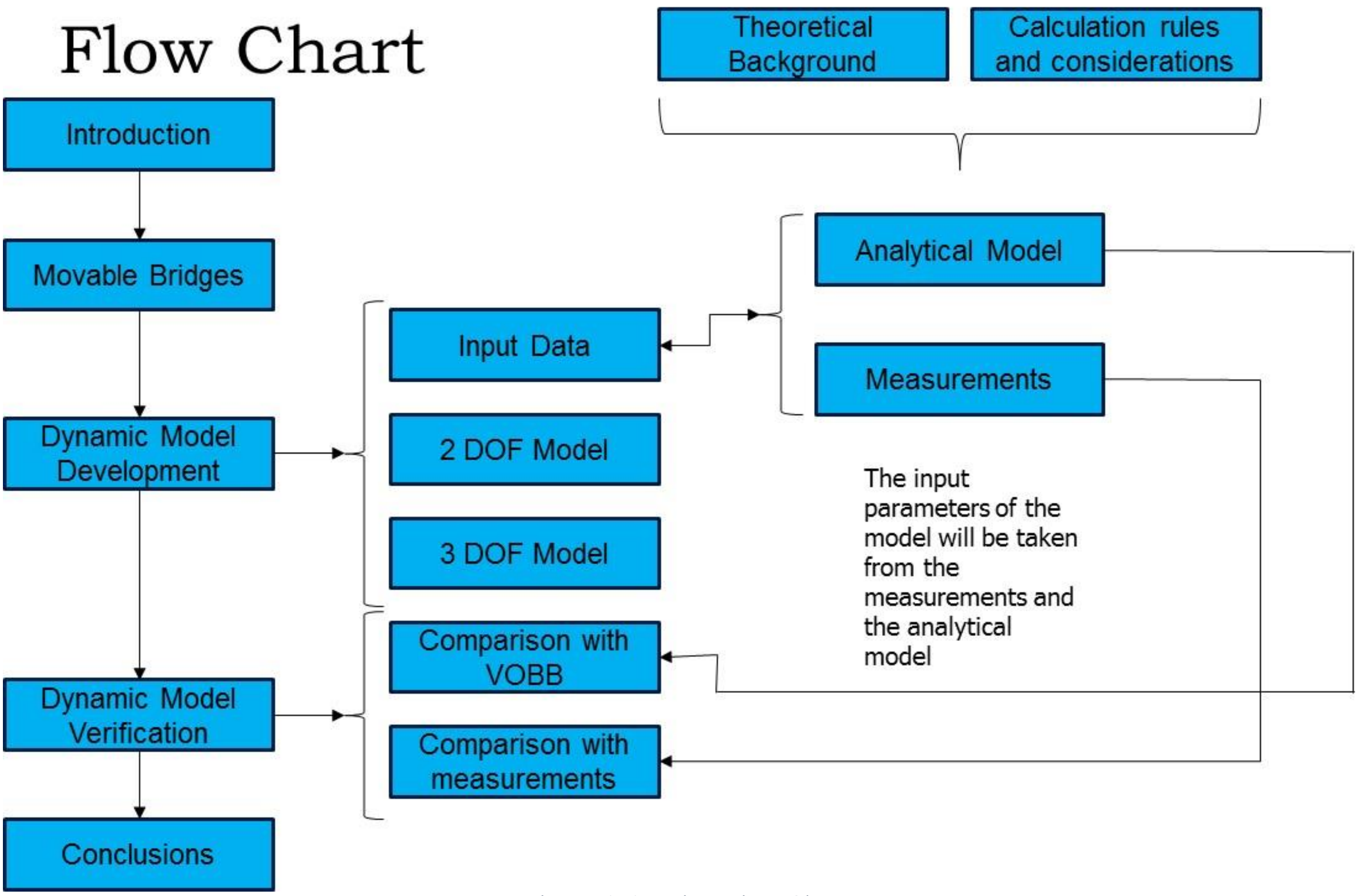

Figure 1.5 Project Flow Chart

2. MOVABLE BRIDGES

Bridges have already been available for thousands of years. Some of the earliest versions included the short spanned fixed bridges over small waterways. In time, these structures have undergone a major development, becoming an important feature in the infrastructure domain. However, fixed bridges were not always feasible because they impede the waterway and larger ships are not be able to pass. In order to overcome this problem, a solution was thought in the form of bridges with a movable span. A major impact on the development of movable bridges was the beginning of the industrial revolution. Also, the increasing number of ships used for shipping goods and the demands regarding larger clearances for ships and not denying them access to certain regions (e.g. cities, ports) contributed to the development of movable bridges.

The motion of all movable bridge spans results from a combination of rotational and translational movement; the differences between types coming from the axes selected for these displacements. Based on primary displacement and axes of displacement, according to ICE (Institution for Civil Engineers) movable bridge spans are usually categorized as follows:

- rotation about a fixed transverse horizontal axis (trunnion bascule)
- rotation about a transverse horizontal axis that simultaneously translates longitudinally (rolling bascule)
- rotation about a fixed vertical axis (swing)
- translation along a fixed vertical axis (vertical lift)
- translation along a fixed horizontal axis (retractile and transporter)
- rotation about a fixed longitudinal axis (gyratory)
- rotation about multiple transverse horizontal axes (folding)

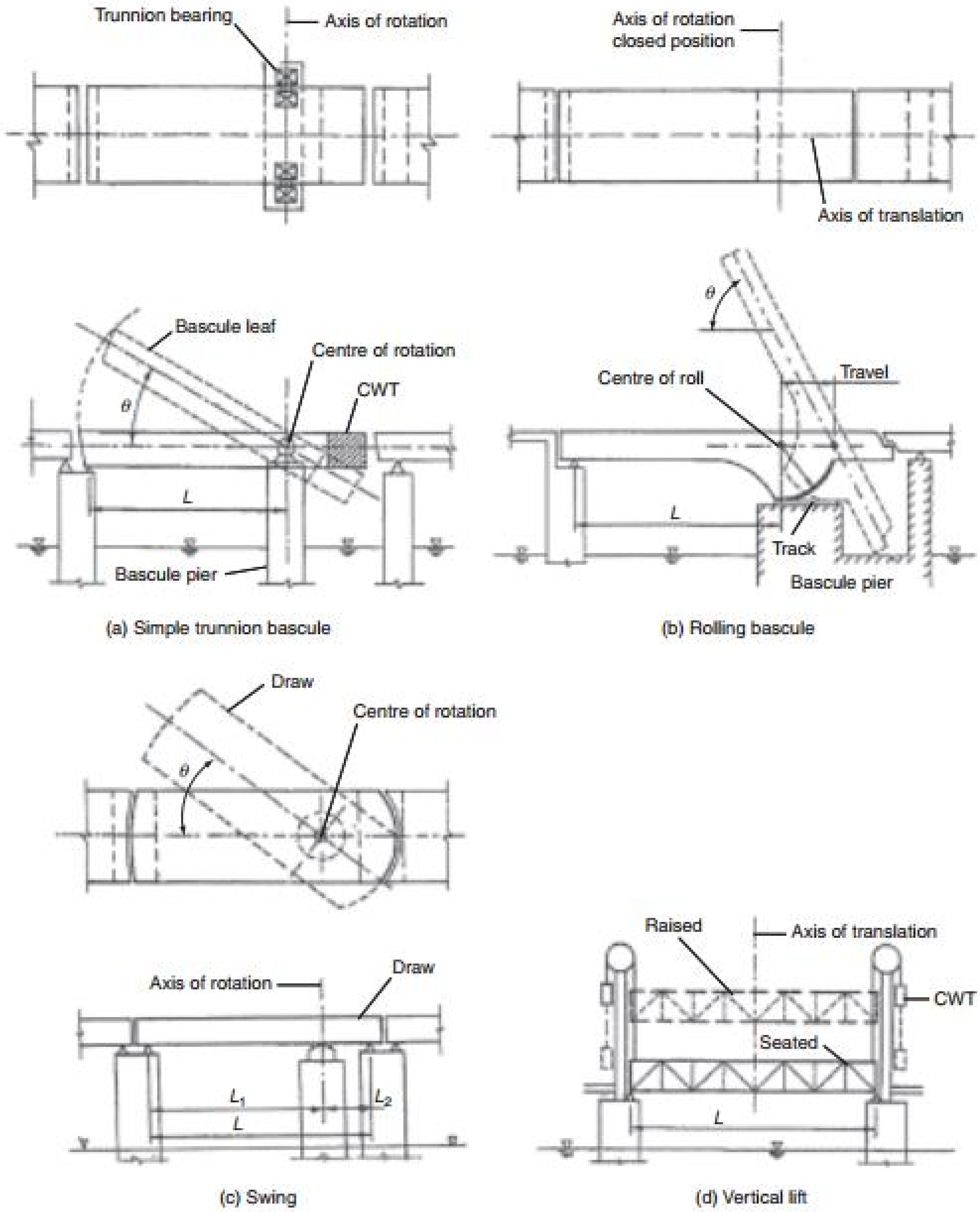

Figure 2.1 Types of movable bridges

In Figure 2.1 (a) a simple trunnion bascule bridge can be depicted for which the counterweight is fixed to the bascule girders. In this case the bascule leaf rotates about a fixed horizontal axis. The trunnion bascule bridge can be further on distinguished by the location of the counterweight. To this extend, Figure 2.1 (b) shows a single-leaf rolling bascule bridge having the counterweight located below the deck. The rolling bascule types of bridges have as a defining feature the fact that together with a rotation about a horizontal axis a translation is also occuring. Swing type of bascule bridges (Figure 2.1 (c)) are most commonly designed with symmetrical swing spans (L_1=L_2), but there were also bridges that were constructed with L_2=0. A vertical lift span as depicted in Figure 2.1 (d) moves in vertical direction along a fixed vertical axis so that clearance for navigation is obtained.

2.1. Bascule Bridges

The term bascule bridge has different meanings in the international market than in the Netherlands. Although the types of bridges depicted in Figure 2.2 are commonly categorized as bascule bridges internationally, in the Netherlands each type of bridge is regarded as a different type.

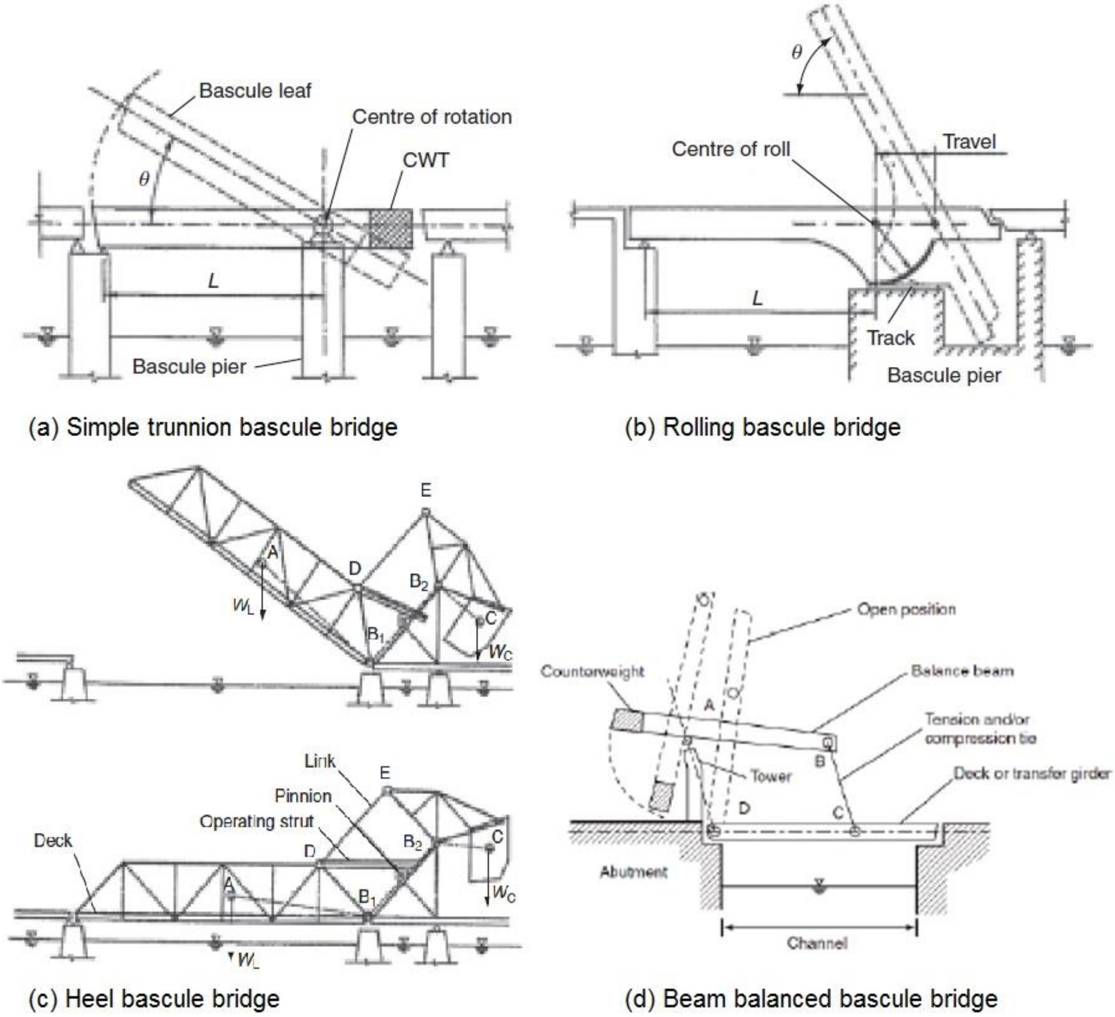

Figure 2.2 Main types of bascule bridges

Figure 2.2 (a) depicts a simple trunnion bascule bridge with a counterweight connected to the bascule girders. The trunnions are usually fixed to the bascule leaf and rotation is possible through the bearings mounted on the bascule pier. However, there are also trunnions that do not rotate, but the leaf rotates against them through bearings belonging to the bascule girder. The counterweight is intended to fully or partially balance the leaf structure. There are many types of trunnion bascule, which can be distinguished through the location of the counterweight. For instance, a rolling bascule is characterized by a rotation about a horizontal axis and simultaneous translation. The majority of rolling bascules are balanced by counterweights fixed to the bascule girder. Moreover, the counterweights can be located above the deck, below it, or outside of the moving span. In Figure 2.2 (b) a single-leaf rolling bascule bridge with the counterweight located below the deck can be observed. Another interesting type of bascule bridge is the Strauss bascule. Such a bridge can be depicted in Figure 2.2 (c) in the form of a heel trunnion with rotating counterweight. All Strauss bascules have as a defining feature the parallelogram connecting the counterweight to the leaf. The motion of the leaf occurs about a fixed horizontal axis.

2.1.1. Beam Balanced Bascule Bridge

One of the earliest form of movable bridges can be traced back to the medieval times at castles, in the form of the drawbridge. Even though the drawbridge was implemented as a military defence mechanism, in time it served as a concept for the "Dutch style" bascule bridge, more specifically the balanced beam bascule bridge (Figure 2.2 (d)). Compared to bascule bridges, they have the advantage of simpler piers and a high architectural potential, but the disadvantage that they can only be used for rather reduced spans.

Beam balanced bascule bridges have counterweights positioned in the overhead balance frames (as shown in Figure 2.2 (d)) to assist in the lifting operation of the deck. The bridge shown consists of a movable deck (C-D), tie rods (A-D), a balance frame including counterweights (A-B-E), and a portal support frame. In order to guarantee equilibrium at every position during lifting, it is necessary to locate the pin connections in the balance frame at the vertices of a parallelogram (A-B-C-D). Secondly, the virtual line between pivot B and the center of gravity of the whole balance frame E, should be parallel to the virtual line between pivot C and the center of gravity of the deck.

In order to ensure a feasible design of beam balanced bascule bridges, the following provisions should be considered:

-Offset columns can be used to allow larger rotational movement of the deck.

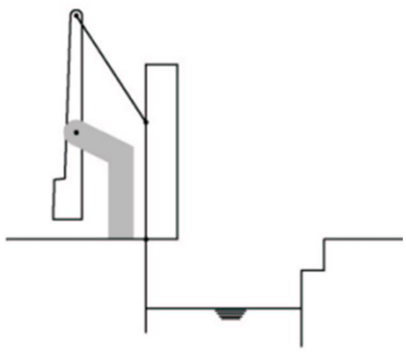

Figure 2.3 Beam Balance Bascule Bridge - Offset Columns

-Any vibrations in the deck are transmitted to the frame.

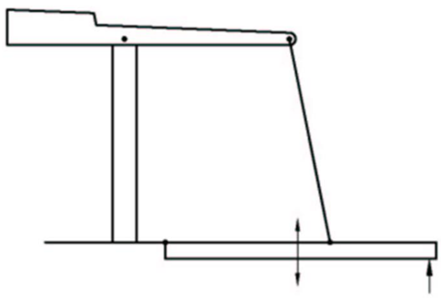

Figure 2.4 Beam Balance Bascule Bridge - Pivot Point of the Hanger inside the Deck

-If the pivot is positioned at the end of the deck at its neutral axis then no vibrations are transmitted to the frame.

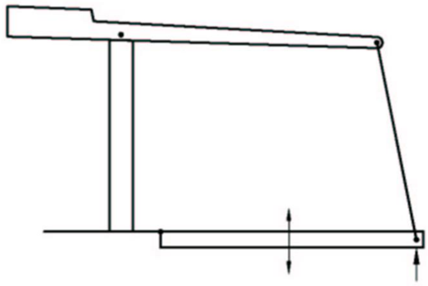

Figure 2.5 Beam Balanced Bascule Bridge - Pivot Point of the Hanger at the end of the Deck

-Secondary beams attached at the ends of the deck can also be provided to avoid transmitting vibrations to the frame.

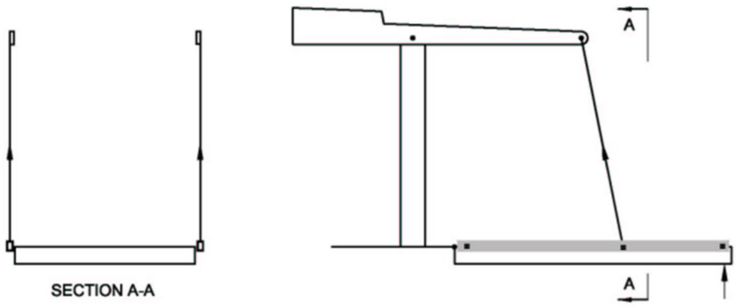

Figure 2.6 Beam Balanced Bascule Bridge - Secondary Beams at the end of the Deck

Additionally, these types of bridges are considered when the waterway does not exceed 20m. For spans larger than 20m this arrangement proves itself disadvantageous because it requires:

- use of excessive counterweights;
- excessive power to operate;
- use of an elevated bridge or use of a counter-balance pit to lengthen the counterbalance arms.

2.1.2. Steel Structure

The design of the steel structure for movable bridges has had a remarkable development since World War II. The enormous development of the welding technology during the war made possible the replacement of riveted constructions by much lighter welded structures, especially in case of main girders and cross girders. A very important phase of the design of bascule bridges is to limit the moving dead load which determines the size of the counterweight, the size of the main structural elements and the machinery.

The deck construction with riveted main girders and cross girders, rolled stringers and decking has gradually been replaced with an orthotropic deck design .As a consequence, the mass per m^2 of the deck structure has been reduced to almost half (from about 360 kg / m^2 to 200 kg / m^2). Due to this reduction in the weight, the counterweight box has been reduced considerably. For balance beam bascule bridges this has led to the disappearance of the wide counterweight box. Now the counterweight requires only some space within the balance frame. Additionally, a lighter structure results in decreased loads on the substructure.

2.1.3. Operating System

The aim of the motion work is not only to open and close the bridge, but also to gradually reduce the speed of the spanning structure in the achievement of the end positions, by delaying. To avoid vibration or whip of the bridge due to traffic, the bridge must be pressed on its bearings. Currently, the operating systems are designed with either a mechanical or hydraulic drive for the main drive, while the auxiliary operating machinery are mechanical. The choice between mechanical or hydraulic drive is usually influenced by the client’s preference and the final costs.

Mechanical drives are rather simple configurations that are based on machinery design principles developed before the creation of movable bridges. Nowadays, these principles are combined with modern systems like speed reducers and bearings to improve the performance of the drive and reduce the level of maintenance. A more effective solution for movable bridge design has proven to be the introduction of hydraulic machinery. This is because the hydraulics can meet more closely the power demands, requiring a good speed control over various power requirements. Although it is a more effective system, the hydraulic drive requires more specialized knowledge and maintenance than for mechanical drives.

Movable bridges which were built long before the last war, tend to have a job where the main and auxiliary drives functions are separated during the movement. These movement works are rather complicated and therefore costly. In the subsequent driving mechanisms these functions are combined. Some examples are:

- A shell structure (Figure 2.7).
Two pinions mounted on the counterweight box and running at constant speed move along a tooth path, which is anchored to the concrete structure in the foundation. When these pinions come into contact with the shell, then the movement of the bridge is converted into a rotational movement of the shell. The speed the bridge will decrease. The role of the shell forces is to initiate the movement, causing the counterweight box to press against the front bearings attached to the foundation deck.

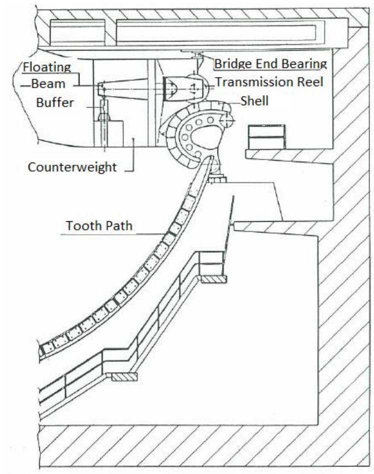

Figure 2.7 Shell Structure Drive [1]

-The Panama wheel (Figure 2.8).
This type of motion work was first applied to the locks of the Panama Canal. The Panama wheel, driven by a constant speed rotating pinion, is provided with a lever (push pull rod) which is hinged to the counterweight box. The position of the Panama wheel is now such that at the closing of the bridge the velocity at the location of the front bearings is zero. Setting up is effected by means of a push pull rod arranged in the buffer.

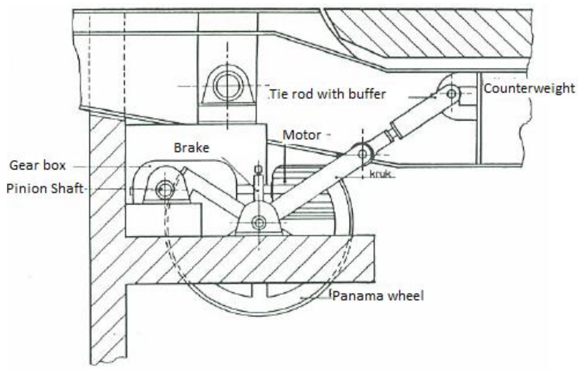

Figure 2.8 Panama Wheel Drive [1]

- Curved racks (Figure 2.9).
Previously, these were used virtually in every drawbridge; for bascule bridges, they were hardly used. A pinion, driven at constant speed, engages in a rack mounted on the tooth path. The curvature at the end of the rack allows for the delay in the closed position of the spanning structure. Here a buffer is also created in the rack bar for sufficient contact pressure at the location of the pre-imposition.

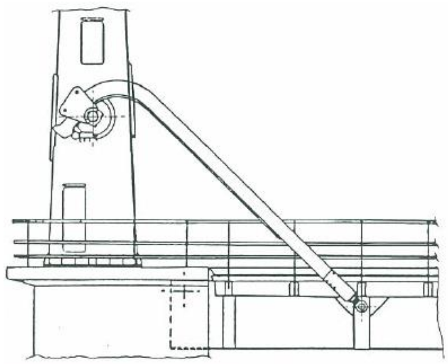

Figure 2.9 Curved Rack Drive [1]

Over the past twenty years the above movement operation had to be replaced with simpler mechanical drive systems. Electrical controls provide acceleration and deceleration of the bridge. This shift has been influenced by:

- High labour costs and difficult manufacturing of shell, Panama wheel, curved rack;
- Delay operation only took place during the closed position of the bridge;
- The movement operations were sensitive to temperature effects;
- The availability of low-cost electrical / electronic systems for controlling velocities and accelerations.

Recent examples of drive mechanisms worth mentioning are:

- Movement work with straight racks, where the speed of movement is controlled by means of the rotational speed of the engine (Figure 2.10);
- Drive with hydraulic cylinders: acceleration and deceleration are hydraulically controlled. The bridge balance can only partly achieve sufficient bearing pressure (Figure 2.11).

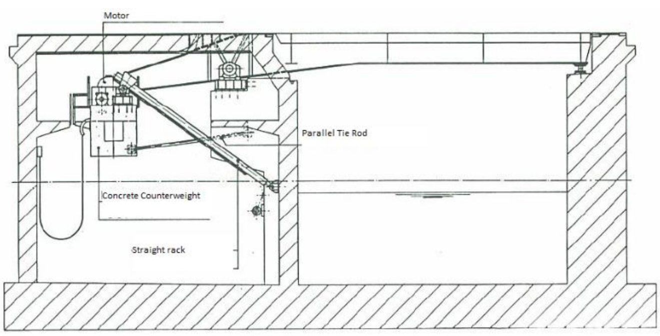

Figure 2.10 Straight Rack Drive [1]

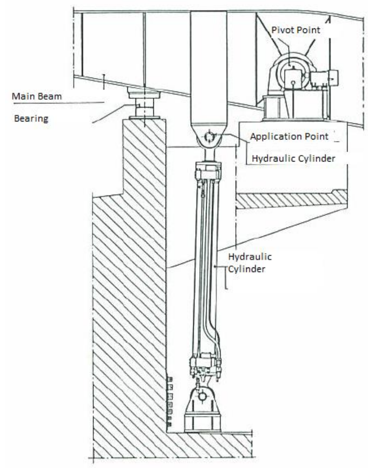

Figure 2.11 Hydraulic Cylinders Drive [1]

Generally, the movable bridge machinery can be divided into two types: a span drive machinery and a stabilising machinery. While the span drive machinery ensures the motion of the bridge and stabilises the span when the fully closed position is not achieved, the stabilising machinery restrains the bridge when it is in rest position and in motion, but it does not accelerate it. The stabilising machinery can be thought as passive, while the span drive machinery is active. The main objective of span drives is to convert the rotational output of the prime mover to the required rotational input in order to move the bridge. In Figure 2.12 three types of span drives can be depicted, which are commonly used for swing bridges, bascules and vertical lift bridges. A basic mechanical drive (Figure 2.12 (a)) consists of an electric motor connected to an input shaft of a primary speed reducer. Between the motor and the speed reducer, a brake is coupled, and it is considered the primary brake. The output torques from the primary reducer are transmitted to a secondary reducer via shafts, then through pinion shafts the output is transmitted to the pinion which engages the rack and consequently moves the span. The hydraulic piston motor drive (Figure 2.12 (b)) is similar to the mechanical drive, but in this configuration the electric motor and the primary reducer are replaced by piston hydraulic motors. Another type of span drive is the hydraulic cylinder drive (Figure 2.12 (c)), for which the output is transmitted to the span by a linear type of action.

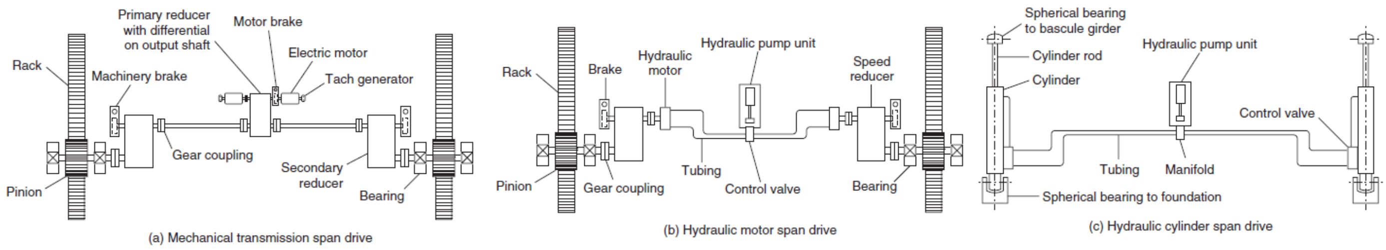

Figure 2.12 Types of span drives [1]

The stabilising machinery includes all the elements that keep the span in closed position and can include trunnions, live load buffers and locking devices. The way in which a bridge is locked is of utter most importance. For bridges that are locked by the main drive, as in the case of bridges with panama wheel, rack, shell and other drives, firstly the stroke of the buffer and / or deformation of the steel structure must be worn out, before the bridge moves along.

This paper will further on discuss the mechanically-driven operating mechanism, with an emphasis on the curved rack for balance beam bascule bridges.

2.2. Behavior of the Drive Mechanism under Dynamic Loading

In the past the dynamic behavior of a movable bridge has been hardly included in the assessment of the ultimate and serviceability limit states of the drive mechanism. However, if a functional bridge is considered, then often when applying a brake during the open position, back and forth movements of the bridge structure occur. Although when accelerating this is less visible, this phenomena can also be observed when starting to open from the closed position. In some instances these movements are so strong that the bridge can be referred to as a “humping bridge”. Therefore, it is useful to investigate the influence of these movements on the interplay of forces in the drive mechanism.

The main idea is to find the torsional moments and forces due to these phenomena and reduce them at the level of the drive mechanism. Since these parts are four times more loaded during the opening cycle [2], when dimensioning the drive mechanism they should be considered. Moreover, since most components of the bridge rotate and the load itself is of a fluctuating nature, it is obvious that the number of variations to which a component is subject during the lifetime of a bridge is so large that the loads serve also as basis for fatigue design.

The torsional moments and forces that occur while starting and stopping the bridge are not only decisive for the capacity of the component parts of the bridge under dynamic loading. For example, they are decisive when the braking loads are exceeding the allowable value for the respective load case. Thus, also the dynamic behavior of the bridge will need to be considered when assessing the static strength. Usually there are two major factors that determine the value of the load. Firstly, the ratio of the mass moments of inertia of the bridge and the counterweight reduced to the motor shaft and the sum of the mass moments of inertia of the components of the motor shaft. Secondly, the ratio between the reduced stiffness of the drive mechanism on the motor shaft and the nominal torsional moment on the motor is of utter importance. These factors, together with other ones, will be discussed later on, and their influence on the analysis of the bridge will be enhanced.

For beam balanced bascules with respect to the size of the masses, three parts stand out. These are: the motor shaft with the relatively heavy rotating parts, the counterweight and the spanning structure. These components are mutually coupled by means of elastic members including: the drive mechanism, the main beams, the balancing parts, cables, etc.. On the basis of these main parts, one can generally have a movable bridge transformed into a system with three masses or mass moments of inertia connected in series by means of springs.

In order to determine the natural frequencies of the component elements: bridge structure, counterweight, and drive mechanism in an effective manner, it is necessary to convert the geometrical and material characteristics so that they fit within the considered calculation model. There are two possibilities: either transformation to a translational system or conversion to a rotating system. For the translational system the geometry, the stiffness and the mass of the bridge remain unchanged, while the drive mechanism at the location of the connection to the bridge is considered as a spring-mass system. In a rotational system, all the masses and stiffness’s are reduced with respect to an axis, preferably the one of the motor shaft. In Figure 2.13 the schematization of the beam balanced bascule bridge considered in the current standards [3] can be observed. In this figure J represents the mass moment of inertia of the considered component and C is the torsional spring constant.

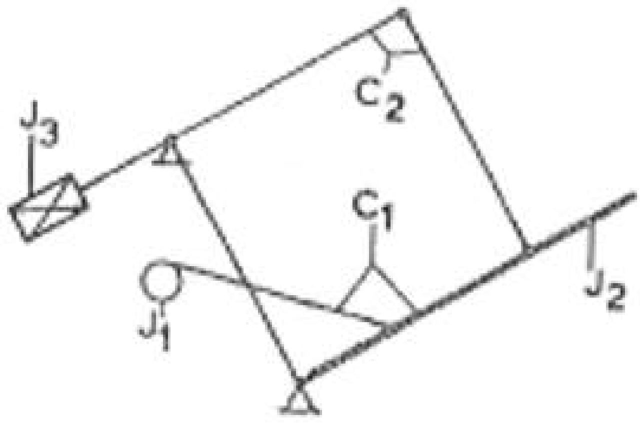

where :
J_3 is the mass moment of inertia of the balance part
J_2 is the mass moment of inertia of the deck
J_1 is the mass moment of inertia of the operating system
C_2 is the rotational stiffness of the drive mechanism reduced to the hanger rod
C_1 is the rotational stiffness of the drive mechanism reduced to the motor shaft

Figure 2.13 Beam Balanced Bascule Bridge Schematization [2]

In this project a similar approach will be followed. Initially, the system will be modelled as a two degrees of freedom rotational system, in which the mass moment of inertia of the motor will be considered connected by means of a spring-dashpot element to the mass moment of inertia of the bridge structure, which will include the counterweight. Afterwards, the bridge structure will be divided into two degrees of freedom, connected by another spring-dashpot element. More specifically, the deck of the bridge and the balance part including the counterweight connected by the hanger rod will replace the bridge structure previously considered.

2.3. Operational Phases and Situations

A movable bridge should be analysed in three states: in open position, in closed position and in motion while opening or closing. The main focus of this project is related to the dynamic loads occurring during the operational phases of a movable bridge, thus the closed position state will not be considered here. According to VOBB [3], all the situations that occur during a complete moving cycle must be considered:

a. Setting-up or unlocking the bridge;
b. Crawling;
c. Acceleration of the bridge;
d. Uniform movement of the bridge;
e. Delay of the bridge movement;
f. Crawling after delay;
g. Inhibiting, delaying the bridge;
h. Braking, holding the bridge in a position;
i. Closing from open or any intermediate position;
j. Landing effect on the bearings;
k. Keeping in position effect on the bearings;
l. Setting-up, locking or centering of the bridge;
m. Emergency stop at full speed.

Generally, the setting-up process of the bridge is preceded by a load occurring in the system, which is the load necessary to move the bridge without the influence of acceleration forces. This load is generated by the self-weight of the bridge, wind and variable deck weight. When beginning to open the bridge, at the moment when the stroke of the buffer has just been removed and the bridge starts moving upwards, large tensile forces may be exerted on the tie rod, rack etc.

The interference of the torques and forces due to braking and setting-up of the bridge are caused by the dynamic components generated when a brake is applied. Usually it is assumed that these dynamic loads at the termination of the setting-up and braking are damped sufficiently, but this will not be the case for bridges with very low natural frequencies. In this case, when the acceleration and deceleration forces play an important role, the drive should have the acceleration and deceleration characterized by a sinusoidal function. After a delay, the bridge usually has a certain speed, the so-called creep speed. The bridge is then decelerated by means of the applied brake until it is brought to a stop. Depending on the creep speed and the stiffness of the drive mechanism, there can occur considerable loads.

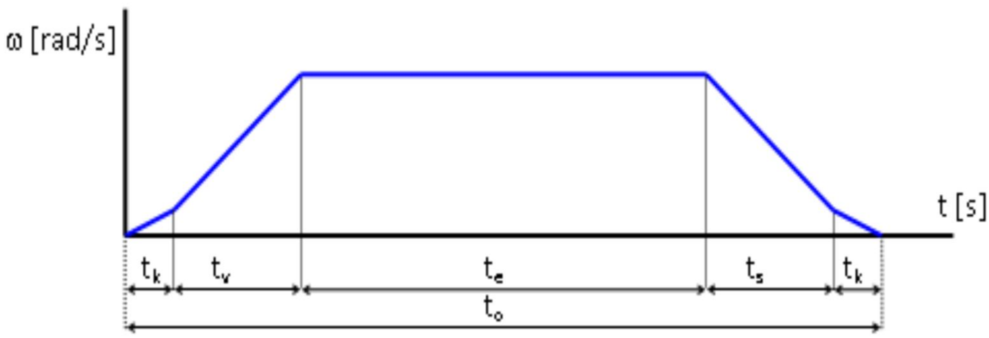

Figure 2.14 Angular velocity of the motor function of time

An angular velocity of a motor expressed as function of time can be observed in Figure 2.14. In the first instance a starting motor torque is necessary to move the bridge. This gives rise to a sudden acceleration, which is accompanied by creep. The time t_k during which creep phenomenon occurs in the beginning is defined here. As the creep phenomenon starts to wear off, the motor runs normally, accelerating towards full speed. The time corresponding to this acceleration is denoted with t_v. When full speed is attained, the angular velocity of the motor is maintained constant for the amount of time t_e, until the deceleration is employed in order to bring the bridge in open position. The deceleration time is then denoted with t_s. After the deceleration period creep phenomenon is present again until the bridge reaches a stop.

The torques occurring in the motor of the operating system of bascule bridges are decisive for understanding the overall behavior of the bridge. Figure 2.15 depicts the evolution of the torque in time for the situation in which the motor accelerates from zero speed to maximum operating speed. When the motor starts at zero speed it develops a torque called starting motor torque. A high starting torque is usually required in applications that are difficult to start like bridges, cranes etc.. As the motor tries to acquire full speed a minimum torque is necessary, called pull-up torque. The highest torque available, before it decreases, is the break-down torque. The accelerating torque needed to accelerate the inertia load is defined as the difference between the available motor torque and the load torque. Another torque that is important is the full load torque or braking torque which is necessary to produce the rated power of the motor at full load speed. It can be expressed as:

$$M_t = 9550 P_{kw} / n_r$$

where:

M_t *is the full-load torque* (Nm)

P_{kw} *is the rated power* (kW)

n_r *is the rated rotational speed* (rpm)

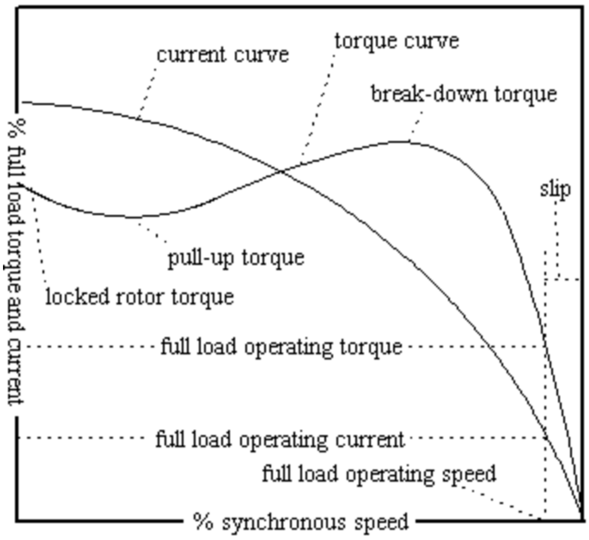

Figure 2.15 Torques in electrical induction motors

In this project the motion of the electro-motor will be simulated by means of calculated or measured angular displacements, angular velocities and angular accelerations. In this manner, the main results will be obtained in terms of torsional moments acting on the electro-motor. Additionally, only three loading situations will be considered:

- Start opening the bridge from closed position;
- Accelerating/ decelerating from closed or intermediate position;
- Emergency brake at full speed.

2.4. Load Cases and Load Combinations

2.4.1. Characteristic values for Loads

Movable bridges are designed differently than fixed bridges. Even though a movable bridge in closed position can be designed as a fixed bridge, in open position or in motion it is subjected to additional loads that are important for the performance of the operating system. These additional loads will be further discussed in this chapter as well as the corresponding load combinations. The main focus is directed towards load cases which are relevant for the investigation of the influence of dynamic loads on the operating system, more specifically when the bridge is in the operational phase.

Wind Load

Movable bridges are subjected to wind loading both in open and closed position. Due to its dynamic character, the wind load is probably one of the most complex loads acting on movable bridges. It can be seen as a beneficial load, for instance when is acting in the same direction with the bridge movement, or as a detrimental load when it acts opposite to the movement, requiring more power for the operation of the bridge. Due to its complexity, the wind load is dependent upon several factors further mentioned:

- Movable bridge availability;
- Waterway type;
- Maximum clearance in closed position;
- Location;
- Distance between water level and highest point of the deck;
- Surface roughness.

The characteristic value of the dynamic wind pressure perpendicular to the affected surface for the bascule type of bridge shall be determined as follows:

$$p_{w;rep} = C_{\dim} \cdot C_t \cdot \phi_w \cdot p_w$$

where :

- $C_{\dim}$ is a factor that accounts for the geometrical dimensions of the bridge - $C_{\dim} = 0.95$;
- C_t is the wind shape factor taken from Figure 2.16;
- ϕ_w is the dynamic amplification factor for wind - $\phi_w = 1.15$;
- p_w is the wind pressure, which based on the height of highest point of the spanning structure, is determined with:

$$p_w = \frac{1}{2} \cdot \rho \cdot \left\{ U_R \cdot \frac{\ln(\frac{h}{z_0})}{\ln(\frac{z_{ur}}{z_0})} \right\}^2 \cdot \left\{ 1 + \frac{7}{\ln(\frac{h}{z_0})} \right\}$$

where :

- ρ is the air density - $\rho = 1.25 kg/m^3$;
- U_R is the hourly averaged wind speed measured at 10m above ground level, taken from table 3 in VOBB [3];

- h is the highest vertical clearance with respect to the average water level. If the average water level is above the adjacent terrain, then the last level shall be used. The highest point of the spanning structure has to be determined based on the considered position of the bridge. The minimum value for h is 4 m;
- z_0 is the roughness height, taken from table 3 in VOBB [3];
- z_{ur} is the height above the ground level at which the hourly averaged wind speed U_R is determined - $z_{ur} = 10\ m$.

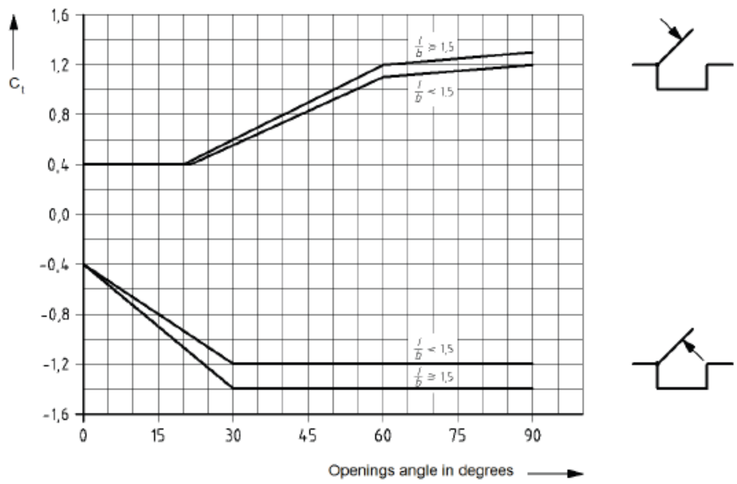

Figure 2.16 Wind Shape Factor

The wind load for bascule type of bridges is reduced to a torsional moment acting upon the pivot point of the bridge, and the characteristic value of this torque is established with:

$$M_{w;brug;rep} = S \cdot p_{w;rep}$$

where :

- S is the moment of inertia (in m³) with respect to the rotational axis of the bridge; for bascule bridges only the surface affected by wind needs to be considered.

During the measurement performed in the reference project no wind was present, thus the model will be initially analysed without wind. After a comparison is drawn between the developed model and the measurements and calculation models, the wind load will be added as an external load acting on the structure so that its influence is observed. For this latter situation, only a comparison with the calculation models according to VOBB can be made.

Snow Load

When bascule bridges are in the operational phase, the snow load can be neglected.

Traffic Load

A bridge in closed position should be designed according to Eurocodes. The traffic load is one of the most decisive loads for the design of the bridge structure. However, during operation, there is no traffic on the deck, thus the traffic load can be neglected.

Temperature

The VOBB states that in general is recommended to prevent deformations of the bridge caused by temperature changes because they may affect different components of the mechanical equipment. Even though the standard gives provisions for the analysis of temperature changes during the operational phase of a bridge, in this study this influence will not be considered.

Self-weight

The self-weight is one of the loads that determines the required torsional moment of the drive. It is considered for all the bridge components, and in order to determine it reference is made to NEN 6702 for the characteristic values of the components' densities.

Excess Load

The excess load is defines as the load that is not balanced by the self-weight of the movable bridge. This type of load should be considered when its magnitude is dependent on the position of the bridge. The magnitude of this load will be obtained from the measurements performed in the reference project.

Variable Deck Weight

Rain, wearing and/ or replacement of the asphalt layer during the lifetime of a bridge can lead to variations of the deck weight in time. This variation should be considered through a difference of $\pm 50N/m^2$ in case of electro-mechanical and hydraulic driven bridges with a steel deck. In this study a variable load of $50N/m^2$ is considered.

Friction

The operational phase of a movable bridge implies rotation of various components around pivot points, pinions etc.. During these rotations friction occurs, which has to be reduced as much as possible. The reduction is done by means of bearings mounted in the pivot points, which are characterized by a certain friction factor giving rise to a certain friction load which must be equilibrated during operation. In this case the influence of friction is not considered.

Dynamic Load

The dynamic load can be caused by:

- Acceleration and deceleration;
- Phenomena caused by the onset of brake(s) and engine(s);
- Speed differences between the drive and bridge;
- Recoil after braking and deceleration;
- The completion of clearances and spring buffers;
- Interference.

VOBB standard provides times for acceleration/ deceleration during normal operation and during an emergency stop, for delaying a bridge etc. Thus, in case of an emergency stop, the maximum allowable time within which the bridge from nominal speed has to come to a stop for a surface of the spanning structure of less than $125m^2$ is 3s. This consideration will be taken into account when modelling the brake situation.

2.4.2. Load Combinations

The loads acting on the superstructure will be considered for two different situations:

a. Bridge in motion while opening;
b. Bridge in open position.

The loads acting on the operating system of a movable bridge must be analysed in four different states:

a. During normal operation;
b. During emergency operation;
c. When the locking mechanism is active;
d. When the setting-up, locking and centring mechanism is active.

In relation to the above mentioned situations and the load combinations recommended in VOBB, in order to investigate the pure dynamic behaviour of bascule bridges, five loading situations are considered:

1. BS1 – Normal operation;

   This loading situation is intended to analyse the behaviour of the bridge in normal operation, during a full opening and closing moving cycle. The bridge is opened normally, kept in open position for 30s and then is normally closed. Initially the situation is analysed without the influence of wind loading, but in the end the torsional moment due to wind will be accounted for.

2. BS2 – Measured excess load;

   The current loading situation and the next one are employed for the reference project as a manner to obtain valuable input data. In this case the excess load is measured in the following way: the bridge is normally opened until the straight rack is in a straight line with the pinion shaft, then pressure gauges are placed in the middle of the spanning structure, the bridge is slowly closed and a light brake is applied, followed by the measurement of the overall excess load. The bridge is normally open at 30cm above the abutment and then it closed. The obtained excess load from the measurements performed on Julianabrug will be used later on as an input value.

3. BS3 – Measured stiffness of the operating system;

   The stiffness of the operating system is obtained as follows: the bridge is normally open until the straight rack is in a straight line with the pinion shaft and is kept in that position. The zero position due to the excess load is set in the spring buffers and the pinion shaft. Then a weight is put in position 1, in the middle of the spanning structure. New positions are defined in both buffers and the pinion shaft and the weight is removed from the bridge. The new zero position due to the excess load is set in the spring buffers and the pinion shaft. The weight is now put on the bridge in position 2, at the end of the spanning structure. New positions are redefined in both buffers and the pinion shaft, the weight is removed from the bridge and the bridge is normally closed. The obtained stiffness will be further used as an input value.

4. BS4 – Emergency stop while opening;

   The bridge is normally opened until 30°. When a 30° angle with the horizontal is reached, an emergency stop is employed. Then the bridge is normally closed.

5. BS5 – Emergency stop while closing.

   The bridge is completely opened, kept 30s in open position and then is closed until a 30° angle with the horizontal is reached. When the 30° angle is reached an emergency stop is employed and then the bridge is normally closed.

2.5. Influencing Factors

The torques and forces exerted on movable bridges due to running phenomena of the drive mechanism, are so large that they must be considered in the design of the operating system. The influence of the following parameters is very important:

- The starting motor torque

In order to use three-phase alternating current motors with a slip-ring the torque rotor resistance must be adjusted to a certain value. This torque corresponds to the open position of the bridge, however, it is bound to a minimum. In order to prevent the bridge from moving in the wrong direction at moderate wind loads ($400N/m^2$), between the moment that the brake is released and the motor is switched on and the moment when the first resistor is switched off, the initial torque for moving an average bridge cannot be less than 1.6 times the nominal motor torque.
In short circuit and induction motors with a slip-ring, motors with fixed rotor resistance, the initial torque will also have to be able to bring the bridge into motion. This is generally 1.8 - 2.25 times the required nominal motor torque.

- The braking torque

The brake generally has two functions. In the first place, the brake must be able to bring the bridge subjected to moderate wind load to a stop. In addition, the braking torque must be sufficient to maintain the bridge open during high wind loads (750 N / m2). This holding torque is for the average bridge about 2.7 times the nominal motor torque.
In connection with the associated costs, it is recommended for M_{max} not to be greater than 1 – 1.5 times the nominal motor torque.

- The factor α

This factor is closely linked to the moment of inertia on the brake disc. Together with the mass moments of inertia of the components of the motor shaft and the mass moments of inertia of the bridge and the counterweight reduced to the motor shaft, determines the magnitude of the torques and forces which are exerted on the operating mechanism. It might be recommended to use a value based on the type of drive mechanism and the type of bridge.
In practical calculations the impact of the efficiency of the drive mechanism has to be considered also. It is recommended that a distinction is made between the influence during acceleration and the influence during deceleration or braking. Assuming a constant value of 0.8 for the efficiency rate, it can be deduced that for accelerating, respectively decelerating or braking the following applies:

$$\alpha = \frac{1.25\sum J_2}{\sum J_1 + 1.25\sum J_2} \quad and: \alpha = \frac{\sum J_2}{\sum J_1 + 0.8\sum J_2}$$

$where:$

ΣJ_1 : Is the sum of the mass moments of inertia of parts on the motor shaft and the reduced mass moments of inertia of other rotating parts e.g. a revolving anchor of an emergency motor.
ΣJ_2 : Is the sum of the mass moments of inertia of the bridge and counterweight reduced to the motor shaft.

- Clearances

For bridges where the torques and forces change direction, the clearances must be reduced to a minimum.

- The stiffness of the drive mechanism

Clearances in the drive should be avoided by not making the stiffness of the drive mechanism infinitely large. It is therefore recommended that between the gearbox and the pinion shaft an intermediate shaft with limited stiffness, or another elastic element is applied.

- Acceleration/ deceleration expressed as a function

In a controlled speed rate drive one can give in the end a function to the acceleration or deceleration. An example of this is an acceleration (deceleration) in accordance with a sine function. Such a variation of the acceleration (deceleration) would be, when taken in reference with the interplay of forces, considered very beneficial: in reality, however, it may be slightly different.

- Damping effect

The required load on the drive is only 3.6% smaller than in the case without damping. For the following peak values the load is decreased significantly.

- Scale effect

Since the stiffness of the pinion shaft determines the stiffness of the drive mechanism to a large extent, it can be therefore stated that a change of scale, provided that the product between the factor α and the ratio between the setting-up motor torque M_1 and the nominal motor torque M_{nom} does not change, has almost no influence on the values of c_1 and c_2.

3. DYNAMIC MODEL DEVELOPMENT

The dynamic model will be created by means of equations of motion. The equations of motion are used to describe the behaviour of a physical system in terms of motion as a function of time. The mathematical relations are described in terms of generalized coordinates and time. The dynamic motion is of interest in this case, and the method to derive the differential equations that the system satisfies is Newton's second law for rotational degrees of freedom.

Initially, the entire bridge will be modelled as a two degrees of freedom system, one simulating the electromotor and the other the bridge structure. The connection between the two is done through a spring-dashpot element meant to simulate the stiffness and damping of the mechanical devices located between the deck and the motor. After having this model and performing an eigenvalue analysis, a three degrees of freedom model will be created. The bridge structure will be considered as a two degrees of freedom system, the rotation of the balance part and the rotation of the deck, which will be connected by a spring-dashpot element simulating the hanger rod.

Two loading situations will be considered: normal operation and brake situation. For the normal operation the VOBB loading situations of starting to open from closed position and accelerating/ decelerating the bridge from open or intermediate position are covered. In case of the brake situation, the loading situation of brake at full speed is modelled. For each of the two considered loading situations two sub-models will be created. The idea is to be able to compare the developed models with the results obtained from the calculation models according to VOBB, and with the measurements performed in the reference project. Thus, a model for comparison with the theory and a model comparison with the measurements will be developed, each of them for the two above mentioned loading situations. The model developed for the comparison with the theory will be called further on the theoretical model and the one for the comparison with the measurements, the measurements' model.

After developing the models, an eigenvalue analysis is performed in order to investigate the modes of vibration and verify them. In order to solve the eigenvalue problem a linearization of the system of equations of motion without damping will be performed.

3.1. Two Degrees of Freedom Model

The structure will be modelled as a two degrees of freedom system, the electro-motor characterized by a mass moment of inertia J_1 and the bridge structure characterized by a mass moment of inertia J_2. The two extreme parts are interconnected by a spring-dashpot element replacing the behavior of the operating equipment including the curved rack, the shafts and the beveled gear. The equivalent stiffness of the operating equipment K_{eq} is obtained by considering all these elements connected in series. The damping C is obtained by considering a critical damping ratio $\xi = 5\%$. This value is the maximum recommended value for the critical damping ratio characterizing steel elements.

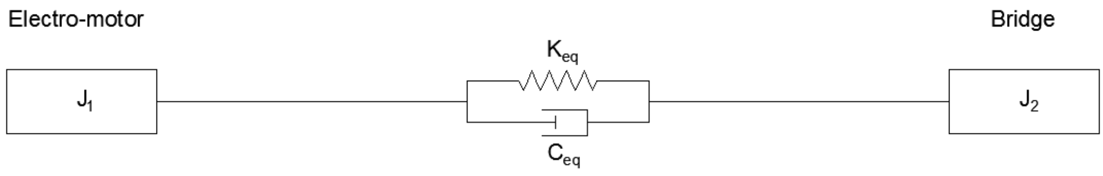

Figure 3.1 Two Degrees of Freedom Model Schematization

3.1.1. Input Data

Firstly, the initial geometry of the bridge has to be defined. This is done by considering the data from the reference project, also available in **Error! Reference source not found.**. Then the geometrical characteristics of the considered elements are input. Based on the steel material parameters and the geometrical characteristics of the elements, the stiffness and damping of the mechanical devices are calculated. The stiffness of the mechanical devices is calculated as an axial stiffness:

$$K = \frac{E_{steel} \cdot A_{hgl}}{L_{hgl}}$$

The final stiffness of the mechanical devices has to be a rotational stiffness, thus it will be multiplied with the squared radius of the pinion shaft:

$$K_{eq} = \frac{E_{steel} \cdot A_{hgl}}{L_{hgl}} \cdot R_{rond}^{\ 2}$$

In order to find the rotational damping, the mass moment of inertia of the mechanical devices has to be computed. Having the mass of the mechanical devices and knowing the radius of the pinion shaft, the mass of moment of inertia of the mechanical devices is:

$$I_{eq} = \frac{1}{2} \cdot m_{eq} \cdot R_{rond}^{\ 2}$$

Then, the rotational damping is expressed as:

$$C_{eq} = 2 \cdot \xi \cdot \sqrt{K_{eq} \cdot I_{eq}}$$

For the sub-model that will be compared to the measurements the stiffness is taken directly from the reference project, since one of the loading cases was meant to provide this parameter. Another two important variables that will be considered are the transmission factor and efficiency of the mechanical devices. The transmission factor accounts for the gearboxes present and the motor shafts. In case of the model developed for theory comparison, the transmission factor will be considered unitary because the input motion parameters are already reduced at the level of the pinion shaft. For the measurements' comparison the transmission factor with its real value accounting for the gearboxes and the motor shafts will be considered in order to reduce the measured input motion parameters from the electro-motor to the pinion shaft.

Input Data - 2 DOF Model

Variable Description	Notation	Value	Units
Mass Moment of Inertia of the Electro-motor	J_1	2.373	kg m^2
Mass Moment of Inertia of the Bridge	J_2	6427000	kg m^2
Cross-Sectional Area of the Rack	A_{hgl}	0.027	m^2
Length of the Rack	L_{hgl}	6.447	m
Pinion Shaft Radius	R_{rond}	0.05	m
Steel Density	ρ_{steel}	7850	kg/m^3
Mass of the Mechanical Devices	m_{eq}	1366.442	kg
Mass Moment of Inertia of the Mechanical Devices	I_{eq}	1.708052	kg m^2
Viscous Damping Ratio	ξ	5	%
Axial Stiffness of the Mechanical Devices - Theory	K_{theory}	1.4E+08	N/m
Rotational Stiffness of the Mechanical Devices - Theory	$K_{eqtheory}$	350000	N m
Axial Stiffness of the Mechanical Devices - Measurements	K_{meas}	1.33E+08	N/m
Rotational Stiffness of the Mechanical Devices - Measurements	K_{eqmeas}	333155	N m
Damping of the Mechanical Devices - Theory	$C_{eqtheory}$	77.31871	N s m
Damping of the Mechanical Devices - Measurements	C_{eqmeas}	75.43514	N s m
Mechanical Devices Efficiency	η	1	
Mechanical Devices Transmission Factor - Theory	i_{twk}	1	
Mechanical Devices Transmission Factor - Measurements	i_{twk}	0.005251	

Table 3.1 Input Data for the Two Degrees of Freedom Model

Secondly, the motion parameters of the electro-motor, which will represent the external loading on the system, are described in terms of angular displacement, angular velocity and angular acceleration of the electro-motor. An additional external load is considered for the bridge structure, which is a torque due to the self-weight of the bridge, reduced on the motor shaft. A differentiation is done in terms of the external loads applicable for the loading situations considered, namely normal operation and brake situation, and a further one has to be done with respect to the sub-models developed for each loading situation (i.e. for comparison with the theory and for comparison with the measurements).

3.1.2. Equations of Motion

The equations of motion are derived by applying Newton's second law. The resulting system of equations will describe the motion of the entire bridge:

$$J_1 \cdot \ddot{\varphi}_1 + C_{eq} \cdot (\dot{\varphi}_1 - \dot{\varphi}_2) + K_{eq} \cdot (\varphi_1 - \varphi_2) = M_{motor}$$
$$J_2 \cdot \ddot{\varphi}_2 + C_{eq} \cdot (\dot{\varphi}_2 - \dot{\varphi}_1) + K_{eq} \cdot (\varphi_2 - \varphi_1) = M_{selfweight}$$

In matrix form, the system can be written as follows:

$$M \cdot \underline{\ddot{\varphi}} + C \cdot \underline{\dot{\varphi}} + K \cdot \underline{\varphi} = \underline{F}$$

where

$M = \begin{bmatrix} J_1 & 0 \\ 0 & J_2 \end{bmatrix}$ is the mass matrix of the system;

$C = \begin{bmatrix} C_{eq} & -C_{eq} \\ -C_{eq} & C_{eq} \end{bmatrix}$ is the damping matrix of the system;

$K = \begin{bmatrix} K_{eq} & -K_{eq} \\ -K_{eq} & K_{eq} \end{bmatrix}$ is the stiffness matrix of the system;

$\underline{F} = \begin{Bmatrix} M_{motor} \\ M_{selfweight} \end{Bmatrix}$ is the torque vector;

$\underline{\ddot{\varphi}} = \begin{Bmatrix} \ddot{\varphi}_1 \\ \ddot{\varphi}_2 \end{Bmatrix}$ is the angular accelerations vector;

$\underline{\dot{\varphi}} = \begin{Bmatrix} \dot{\varphi}_1 \\ \dot{\varphi}_2 \end{Bmatrix}$ is the angular velocitites vector;

$\underline{\varphi} = \begin{Bmatrix} \varphi_1 \\ \varphi_2 \end{Bmatrix}$ is the angular displacements vector.

The complete Matlab scripts for the two degrees of freedom model can be found in Appendix 2.

3.1.3. Normal Operation

The normal operation (Figure 3.2) consists of an external loading applied to the electro-motor in terms of angular velocity and an external loading applied to the bridge in the form of a torque accounting for the self-weight of the bridge structure. In order to obtain the input motion parameters of the electro-motor, the angular velocity is numerically integrated and numerically differentiated to obtain the angular acceleration and angular displacement, respectively. The numerical integration is based on the computation of the cumulative integral with trapezoidal integration, while the numerical differentiation is based on the computation of the slope of a secant line through two nearby points. By imposing these electro-motor motion parameters and the external torque due to the self-weight of the bridge structure, the torque acting on the electro-motor and the motion of the bridge structure are found.

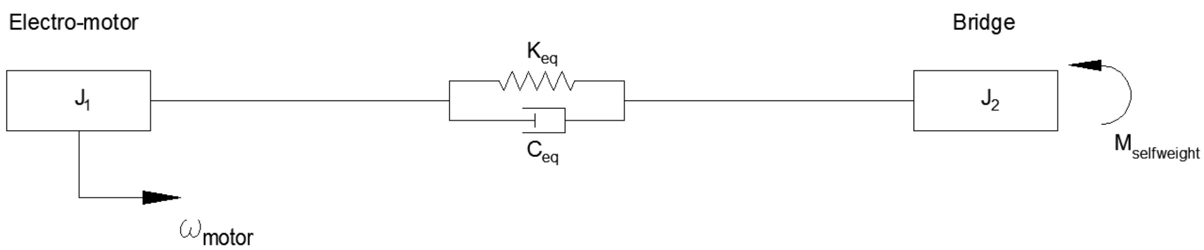

Figure 3.2 Two Degrees of Freedom Model for Normal Operation - Mechanical Scheme

The two models considered for this loading situation, theoretical model and measurements' model, are characterized by similar principles, but the input motion parameters and the stiffness of the mechanical devices will differ. In Figure 3.3 and Figure 3.4 the input motion parameters can be observed for this loading situation.

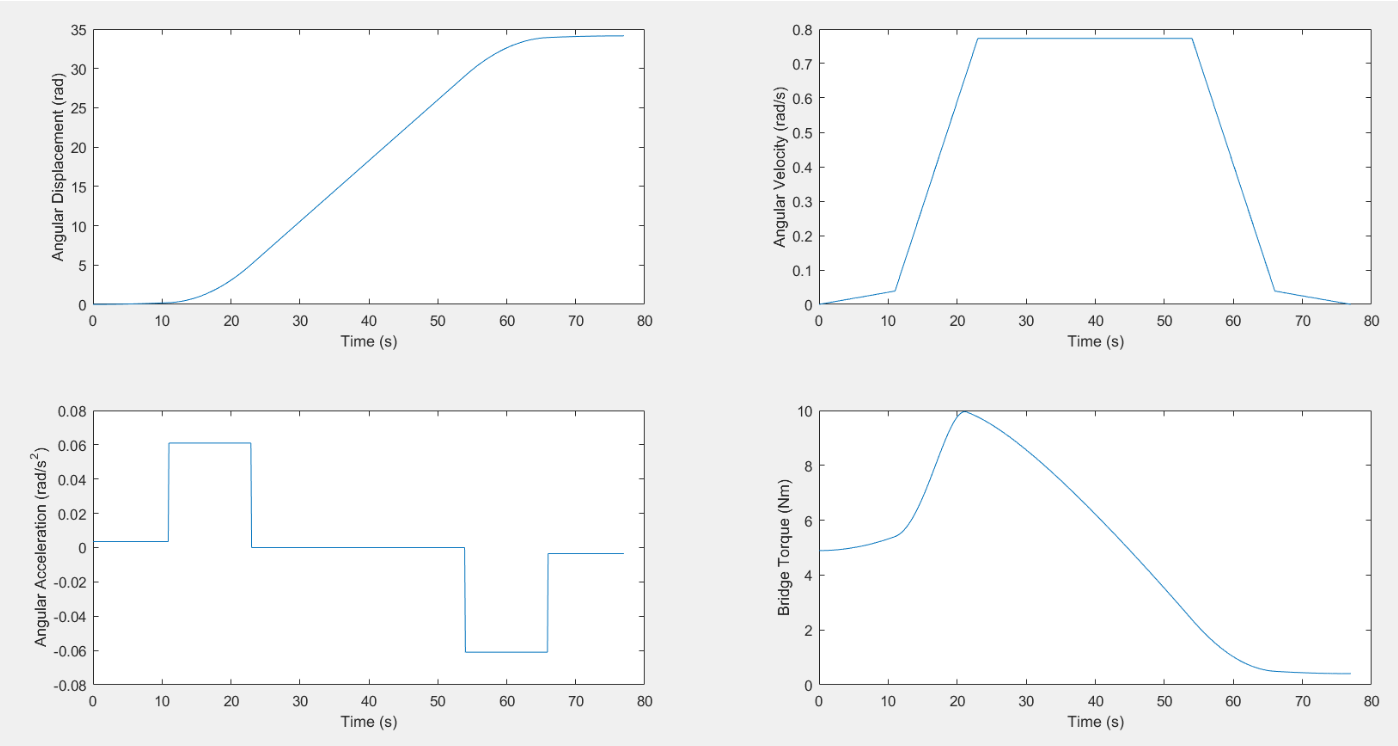

Figure 3.3 Motion Parameters – 2DOF - Normal Operation – Theoretical Model

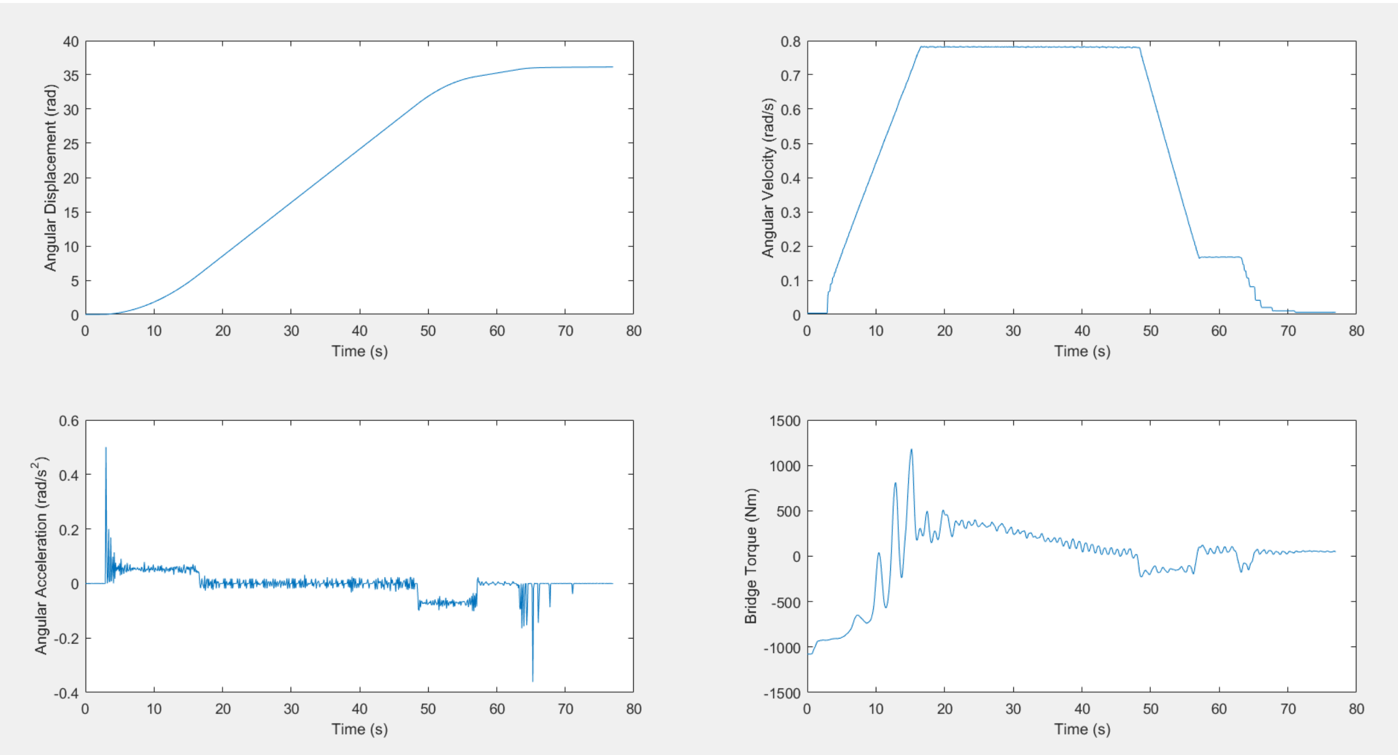

Figure 3.4 Motion Parameters – 2DOF - Normal Operation – Measurements' Model

3.1.4. Brake Situation

In case of the brake situation (Figure 3.5) an external loading simulating a brake at a certain time will be applied to the system. The difference between the normal operation model and the brake situation model can be observed at the level of the input motion parameters.

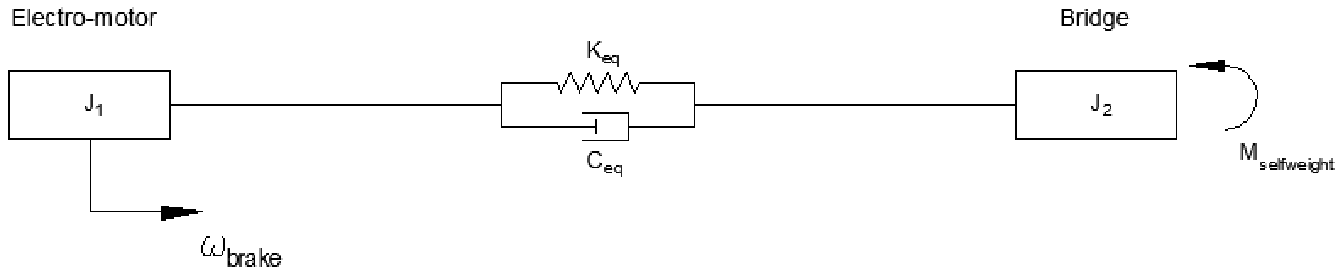

Figure 3.5 Two Degrees of Freedom Model for Brake Situation - Mechanical Scheme

In case of the theoretical model, this loading situation is similar to the normal operation, but the algorithm is created so that from a certain time t_{brake}, when the brake is applied, the bridge has to come to a stop in 3s. Therefore, the input angular velocity is modified so that after the brake is applied the angular velocity decreases to zero in a linear manner. The rest of the electro-motor motion input parameters will be obtained from the newly defined angular velocity. In case of the torque due to the self-weight of the bridge structure, the variable is modified so that after the time t_{brake}+3s it will maintain the value attained at that point. Input motion parameters can be observed in Figure 3.6 and Figure 3.7 for the brake situation. In case of the measurements' model the input angular velocity is taken directly from the provided data from the reference project.

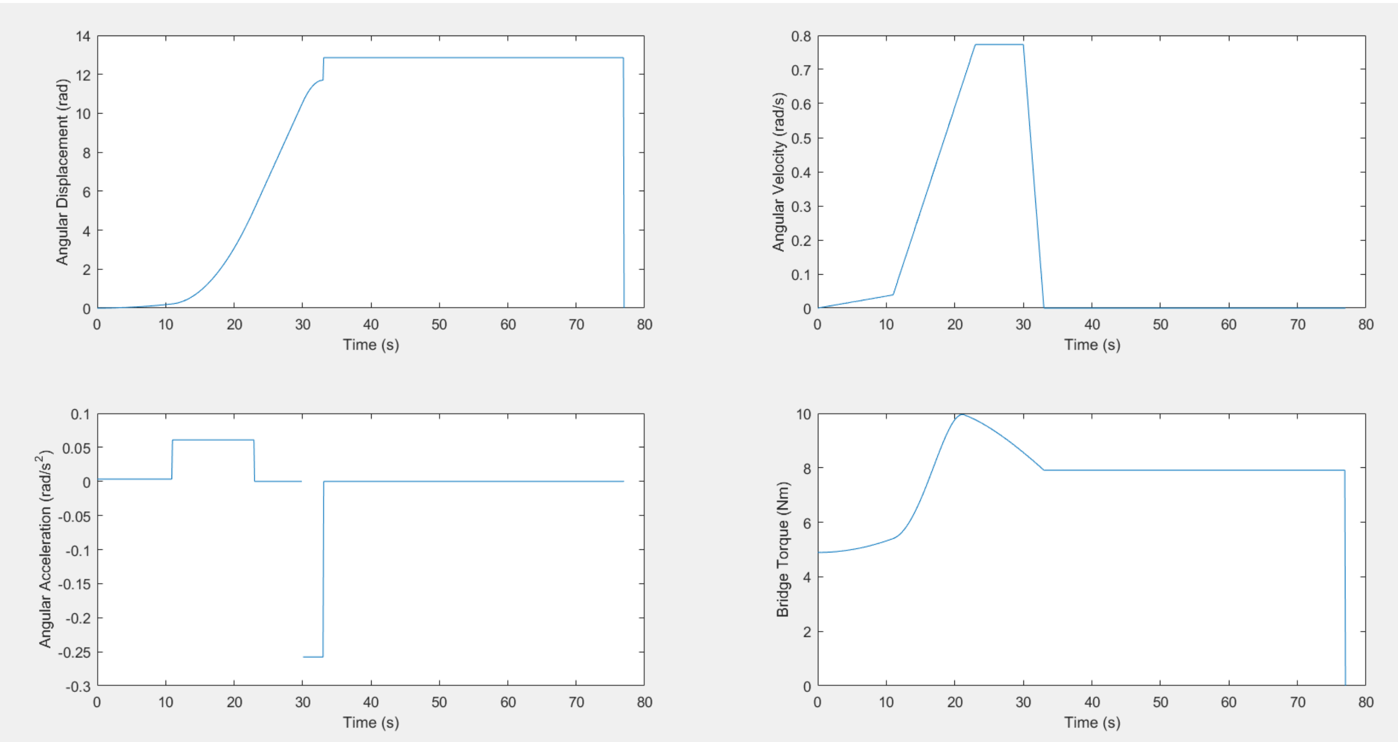

Figure 3.6 Motion Parameters – 2DOF - Brake Situation – Theoretical Model

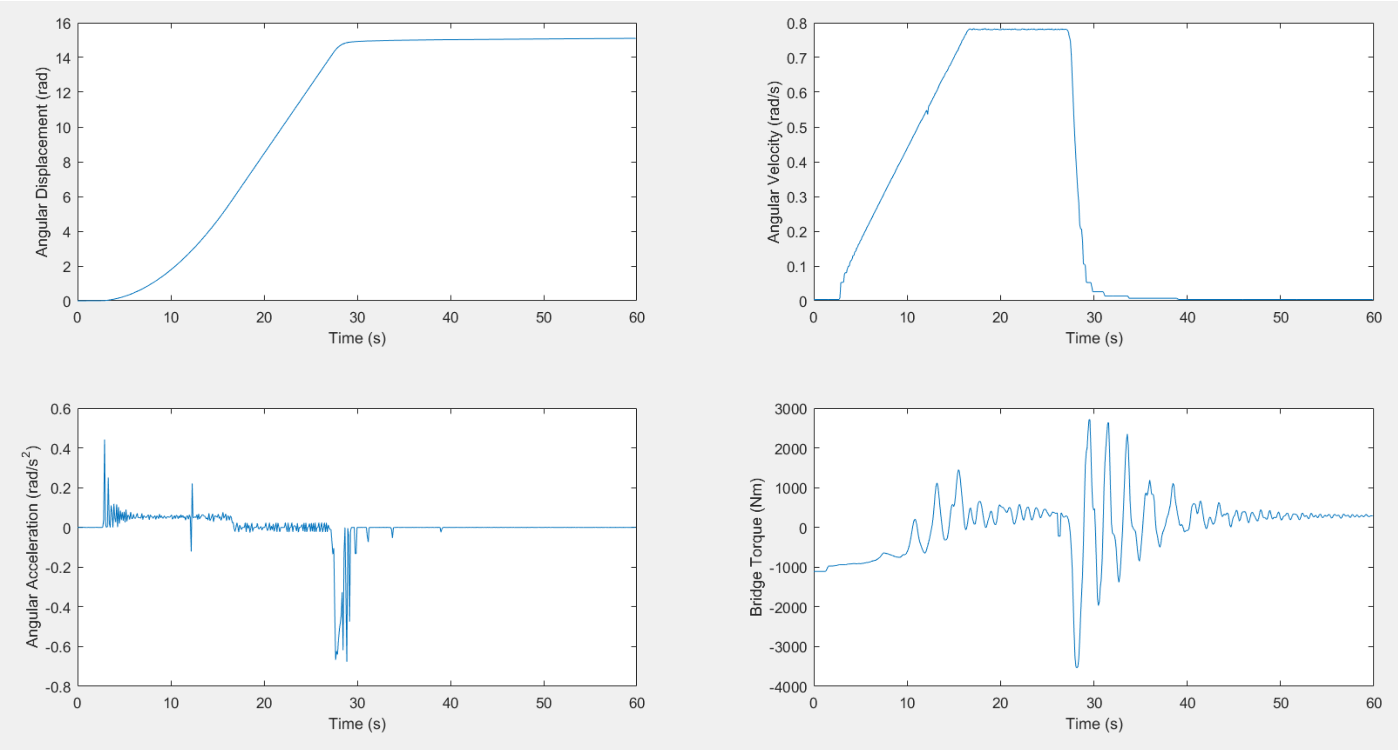

Figure 3.7 Motion Parameters – 2DOF - Brake Situation – Measurements' Model

3.1.5. Motivation for a more complex model

The analysis of the beam balanced bascule bridge as a two degrees of freedom system was basically a method to analyse the considerations in the research behind the design codes for movable bridges. Instead of only considering two masses connected by a spring element, a system comprising two masses connected by a spring-dashpot element was considered. In this manner, the damping of the mechanical devices was taken under consideration.

One of the drawbacks of considering only a two degrees of freedom system to model the bridge is that the behaviour of bridge's component parts cannot be analysed. Even though all the bridge structure's components are accounted for by means of mass moments of inertia and the torque exerted on the electro-motor due to the self-weight of the bridge structure, the results are in terms of the whole bridge structure and they cannot be decomposed at the component parts level. This is one of the reasons that motivated the development of a more complex model.

Another reason to pass to a more complex model consists in the fact that by replacing the bridge degree of freedom with two additional degrees of freedom, one of the movable deck and one of the balance part, the interaction between these two can be also analysed.

3.2. Three Degrees of Freedom Model

The simplicity of the previously developed two-degrees of freedom model motivated the analysis of a more complex system. The bridge structure in this case was divided into three elements: the movable deck, the hanger rod and the balance part including the counterweight. Two additional degrees of freedom were introduced, which will replace the single degree of freedom of the bridge in the previous model. The deck and the balance part are considered as rigid elements, interconnected by a spring-dashpot element modelling the hanger rod. The connection of the deck with the electro-motor is still realized through the previously considered mechanical devices. The mechanical scheme corresponding to this new system can be observed in Figure 3.8.

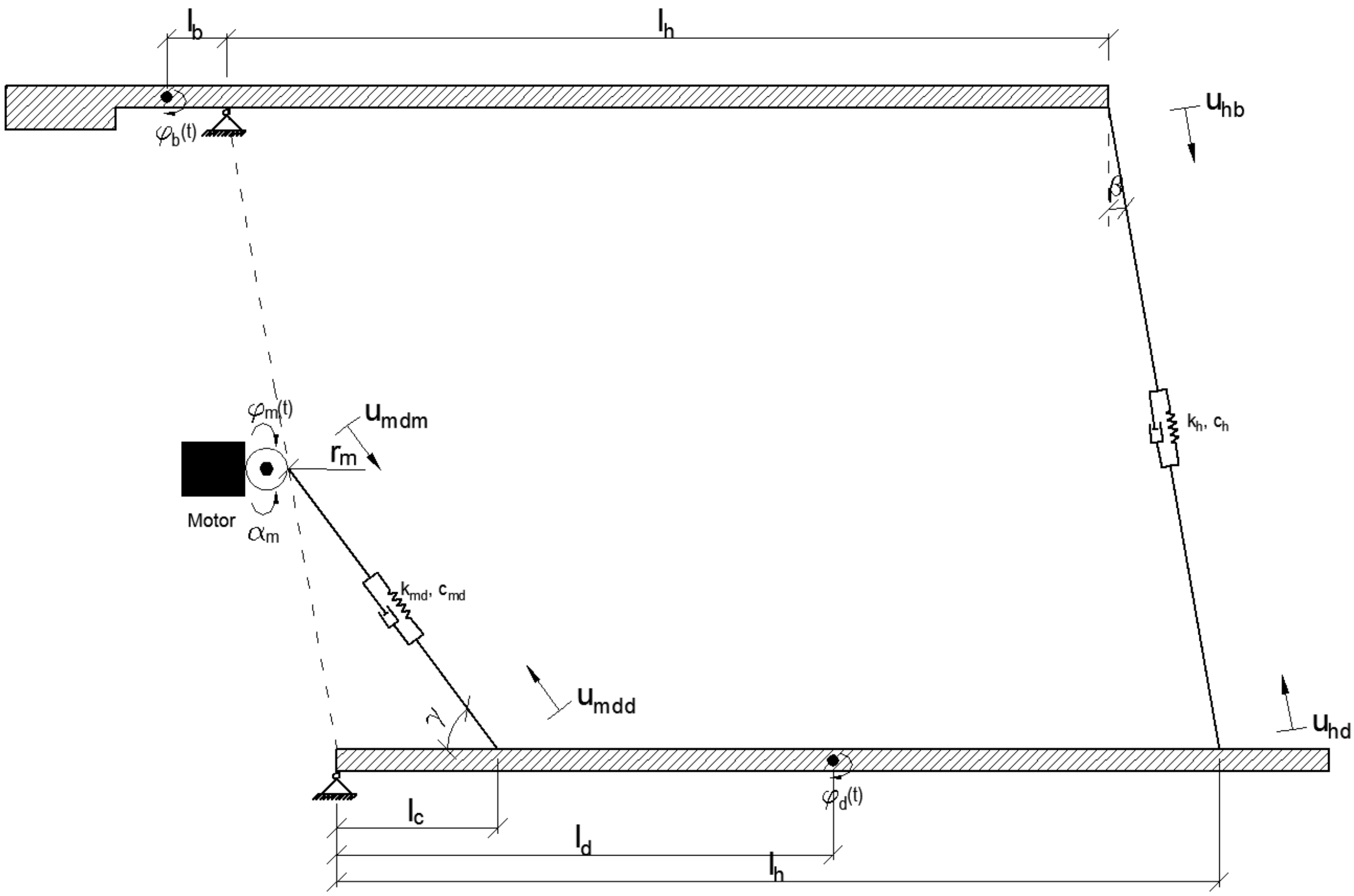

Figure 3.8 Beam Balanced Bascule Bridge – Mechanical Scheme

The spring-dashpot elements in this system are distributed under certain angles. The elongation/ compression of these springs give rise to forces that contribute to the moment equilibrium. Their contribution has to be accounted for and it will be later on shown.

3.2.1. Input Data

As in case of the two-degrees of freedom model, the initial geometry, the geometrical characteristics, material properties of the bridge are considered from Appendix 1. In this case more variables have to be considered because component parts of the bridge structure will be analysed. Following the same pattern as before, two models are developed for each loading: a theoretical model and a measurements' model. Based on this, some input variables will be different for each model. The stiffness and damping coefficients for this model will be derived for a translational type of spring-dashpot element.

Input Data - 3 DOF Model

Variable Description	Notation	Value	Units
Mass Moment of Inertia of the Electro-motor	J_m	2.373	kg m^2
Mass Moment of Inertia of the Balance Part	J_b	2138000	kg m^2
Mass of the Balance Part	m_b	74969	kg
Mass Moment of Inertia of the Deck	J_d	3980000	kg m^2
Mass of the Deck	m_d	46017	kg
Cross-Sectional Area of the Rack	A_{hgl}	0.027	m^2
Length of the Rack	L_{hgl}	6.447	m
Steel Modulus of Elasticity	E_{steel}	2.10E+11	N/m^2
Steel Density	ρ_{steel}	7850	kg/m^3
Mass of the Mechanical Devices	m_{md}	1366.442	kg
Viscous Damping Ratio	ξ	5	%
Stiffness of the Mechanical Devices	$k_{mdtheory}$	140000000	N/m
	k_{mdmeas}	133262000	N/m
Damping of the Mechanical Devices	c_{md}	3169.986	N s/m
Angle between the hanger and the vertical	β	0.231876	rad
Height of the hanger	H_{bal}	12.07	m
Length of the Hanger	L_{hanger}	12.40191	m
Mass of the Hanger	m_h	2000	kg
Cross-Sectional Area of the Hanger	A_{hanger}	0.020543	m^2
Stiffness of the Hanger	k_h	3.48E+08	N/m
Damping of the Hanger	c_h	83409.63	N s/m
Angle between the rack and the horizontal	γ	0.605643	rad
Distance from the hanger to the pivot point	l_h	12.25	m
Distance from the center of gravity of the balance part to the pivot point	l_b	2	m
Distance from the center of gravity of the deck to the pivot point	l_d	6.125	m
Distance from the rack to the pivot point	l_c	3.7	m
Pinion radius	r_m	0.05	m
Mechanical Devices Efficiency	η	1	
Mechanical Devices Transmission Factor	i_{twk}	0.005251	

Table 3.2 Input Data for the Three Degrees of Freedom Model

The external loading on the system will also be considered as in the two-degrees of freedom model. The input motion parameters will be approximately the same, with the exception that the bridge torque is not considered anymore. The self-weight of each component part of the bridge structure will be considered in each equation of motion. The electro-motor motion parameters are similar to the ones used for the two degrees of freedom system: angular displacement, angular velocity and angular acceleration.

3.2.2. Equations of Motion

The beam balanced bascule bridge will be modelled with rigid elements simulating the behaviour of the balance part and the deck, while the hanger and the mechanical devices are considered as spring-dashpot elements (Figure 3.8). The system is characterized by three angular degrees of freedom, the rotation of the balance part φ_b, the rotation of the movable deck φ_d and the rotation of the motor shaft φ_m. The main intent is to analyse the displacements that occur in these elements.

Let us first consider the bridge structure system composed of the balance part including the counterweight, the hanger rod and the deck. The free body diagram of this system can be depicted in Figure 3.9.

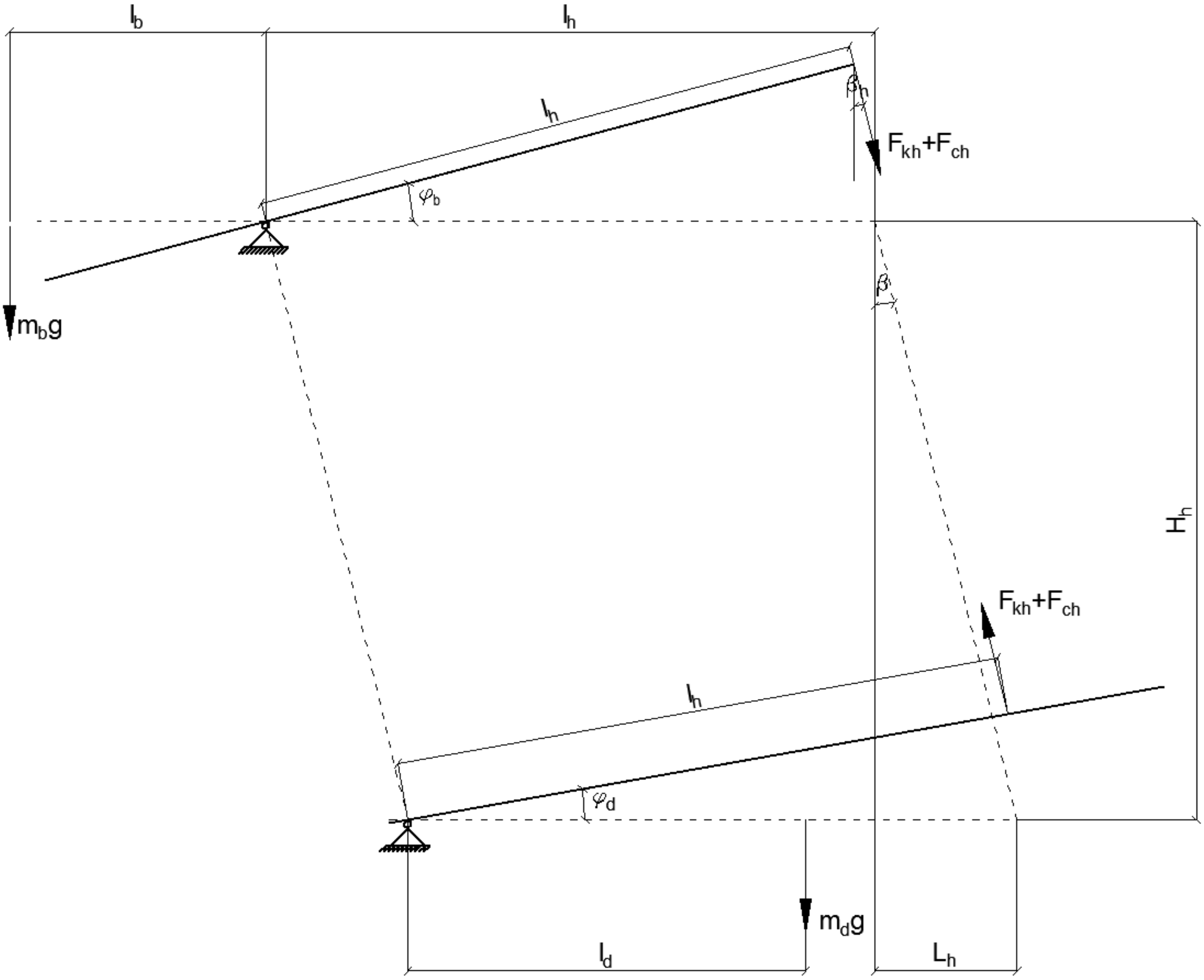

Figure 3.9 Mechanical Scheme for Bridge Structure Model

The equations of motion for this system are obtained as sum of the moments that act on the balance part or deck with respect to the rotational points:

$$J_b \cdot \ddot{\varphi}_b = m_b \cdot g \cdot l_b \cdot \cos(\varphi_b) - (F_{kh} + F_{ch}) \cdot (\cos \beta_h \cdot l_h \cdot \cos(\varphi_b) + \sin \beta_h \cdot l_h \cdot \sin(\varphi_b))$$
$$J_d \cdot \ddot{\varphi}_d = -m_d \cdot g \cdot l_d \cdot \cos(\varphi_d) + (F_{kh} + F_{ch}) \cdot (\cos \beta_h \cdot l_h \cdot \cos(\varphi_d) + \sin \beta_h \cdot l_h \cdot \sin(\varphi_d))$$

where:
J_b *is the mass moment of inertia of the balance part including the counterweight;*
J_d *is the mass moment of inertia of the deck;*
m_b *is the mass of the balance part including the counterweight;*
m_d *is the mass of the deck;*
l_b *is the distance from the center of gravity of the balance part to the upper pivot point;*
l_d *is the distance from the center of gravity of the deck to the lower pivot point;*
g *is the gravitational acceleration;*
β_h *is the angle between the hanger rod and the vertical axis during operation;*
l_h *is the distance from the connection point of the hanger with the deck/ balance part to the lower/ upper pivot point;*
F_{kh} *is the force in the hanger accounting for its stiffness;*
F_{ch} *is the force in the hanger accounting for its damping;*
φ_b, φ_d *are the rotational degrees of freedom of the balance part and the deck, respectively.*

φ_b, φ_d are the rotational degrees of freedom of the balance part/deck.

The forces that occur in the hanger are calculated based on the elongation of the hanger due to the considered degrees of freedom as follows:

$$F_{kh} = k_h \cdot u_h = k_h \cdot (D_h - H_h / \cos \beta)$$
$$F_{ch} = c_h \cdot \dot{D}_h$$

where:
k_h *is the axial stiffness of the hanger rod;*
c_h *is the damping of the hanger rod calculated with a 5% damping ratio coefficient;*
$H_h / \cos \beta$ *is the initial length of the hanger rod;*
H_h *is the projection on the vertical axis of the initial position of the hanger;*
β *is the initial angle between the hanger rod and the vertical axis;*
D_h *is the length of the hanger at each time moment;*

The length of the hanger at any position during operation can be expressed as follows:

$$D_h = \sqrt{H^2 + L^2} = \sqrt{(H_h + l_h \cdot \sin(\varphi_b) - l_h \cdot \sin(\varphi_d))^2 + (H_h \cdot \tan \beta + l_h \cdot (1 - \cos(\varphi_b)) - l_h \cdot (1 - \cos(\varphi_d)))^2}$$

And the first derivative of the elongation of the hanger is:

$$\dot{D}_h = D_h^{-1} \cdot \begin{bmatrix} l_h \cdot (H_h + \sin(\varphi_b) \cdot l_h - \sin(\varphi_d) \cdot l_h) \cdot (\cos(\varphi_b) \cdot \dot{\varphi}_b - \cos(\varphi_d) \cdot \dot{\varphi}_d) + l_h \cdot (H_h \cdot \tan\beta - l_h \cdot \cos(\varphi_b) + \\ + l_h \cdot \cos(\varphi_d)) \cdot (\sin(\varphi_b) \cdot \dot{\varphi}_b - \sin(\varphi_d) \cdot \dot{\varphi}_d) \end{bmatrix}$$

In Figure 3.10 the angular displacements of the previously developed model for a theoretical input can be observed. The bridge structure is moving upwards and it stabilizes around 1.57rad. This displacement is too large since the theoretical maximum opening angle of the bridge is 1.465rad. The upward movement of the bridge structure is possible because the force necessary to keep the structure in closed position is incorporated in the rack, via a pre-stressing force that is occurring in the disc springs of the buffer.

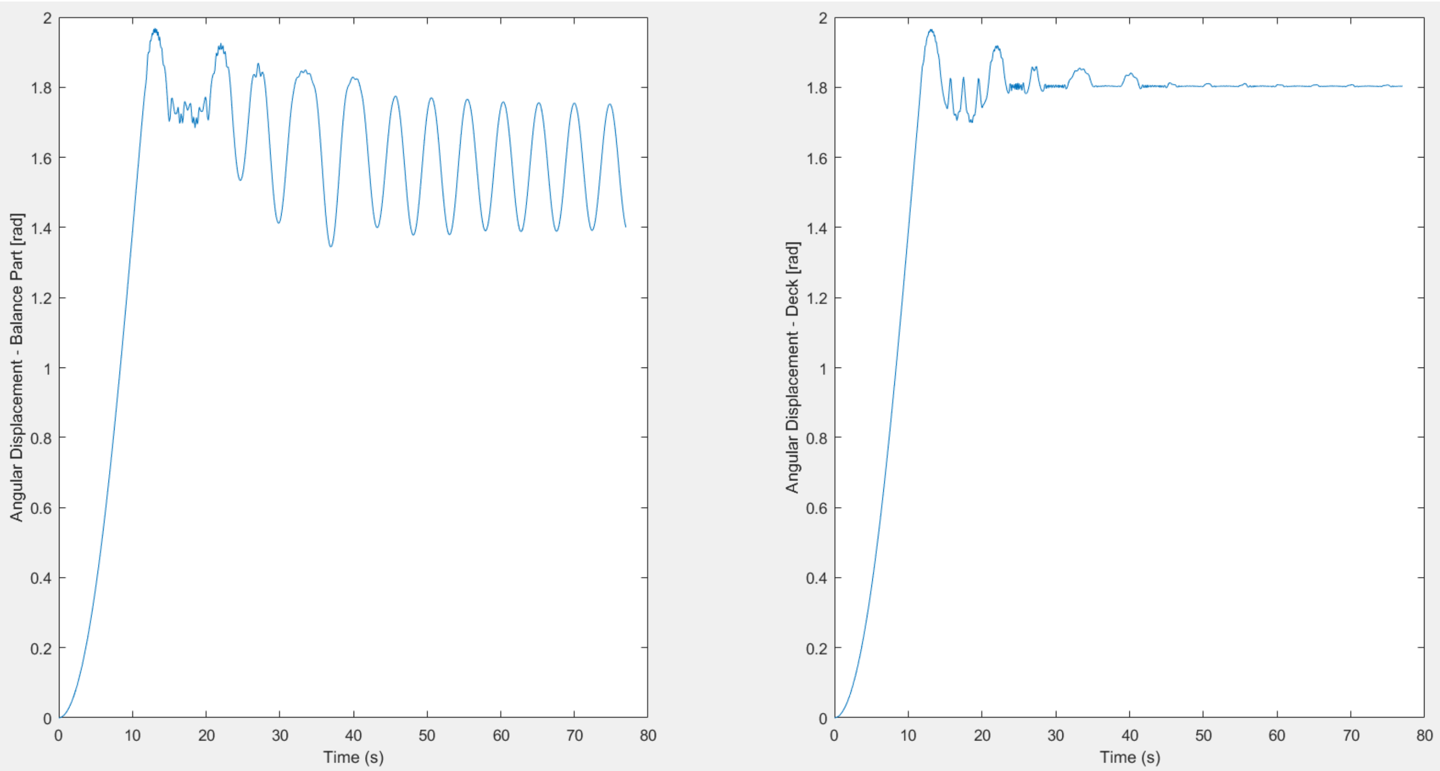

Figure 3.10 Bridge Structure Nonlinear Model - Angular Displacements in [rad]

Now the connection of the bridge structure with the operating system has to be developed. The deck is connected to the pinion shaft by means of an inclined curved rack. This will be modelled through a spring-dashpot element. The previously derived equations of motion will become:

$$J_b \cdot \ddot{\varphi}_b = m_b \cdot g \cdot l_b \cdot \cos(\varphi_b) - (F_{kh} + F_{ch}) \cdot (\cos\beta_h \cdot l_h \cdot \cos(\varphi_b) + \sin\beta_h \cdot l_h \cdot \sin(\varphi_b))$$

$$J_d \cdot \ddot{\varphi}_d = -m_d \cdot g \cdot l_d \cdot \cos(\varphi_d) + (F_{kh} + F_{ch}) \cdot (\cos\beta_h \cdot l_h \cdot \cos(\varphi_d) + \sin\beta_h \cdot l_h \cdot \sin(\varphi_d)) + (F_{kmd} + F_{cmd}) \cdot$$
$$(\cos(\gamma_1) \cdot l_c \cdot \sin(\varphi_d) + \sin(\gamma_1) \cdot l_c \cdot \cos(\varphi_d))$$

where:

γ_1 *is the angle between the rack and the horizontal axis;*

l_c *is the distance from the connection between the rack and the deck and the lower pivot point;*

F_{kmd} *is the force in the rack accounting for its stiffness;*

F_{cmd} *is the force in the rack accounting for its damping;*

The forces that occur in the rack are calculated based on the elongation of the rack due to the considered degrees of freedom (Figure 3.11). They are calculated as follows:

$$F_{kmd} = k_{md} \cdot u_r = k_{md} \cdot (D_1 - L_r)$$
$$F_{cmd} = c_{cmd} \cdot \dot{D}_1$$

where:
k_{cmd} *is the axial stiffness of the rack;*
c_{cmd} *is the damping of the rack calculated with a 5% damping coefficient;*
L_r *is the initial length of the rack;*
D_1 *is the length of the rack at any moment in time.*

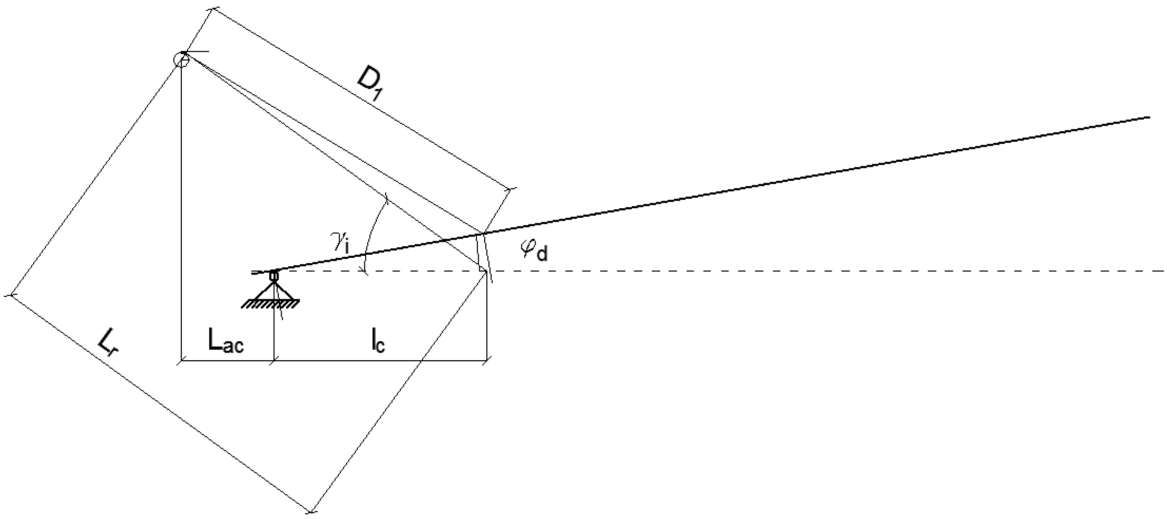

Figure 3.11 Derivation of the forces occurring in the rack

The length of the rack at any position during operation can be expressed as follows:

$$D_1 = \sqrt{H_1^{\,2} + L_1^{\,2}} = \sqrt{\begin{array}{l}(L_r \cdot \sin(\gamma_i) - l_c \cdot \sin(\varphi_d) + 2 \cdot r_m \cdot \varphi_m / 3.14)^2 + (L_r \cdot \cos(\gamma_i) - l_c \cdot (1 - \cos(\varphi_d)) + \\ + 2 \cdot r_m \cdot \varphi_m / 3.14)^2\end{array}}$$

where:
r_{m} *is the radius of the pinion shaft;*
φ_{m} *is the angular displacement of the motor reduced to the pinion shaft;*
L_{ac} *is the horizontal distance between the center of the pinion shaft and the lower pivot point;*

And the first derivative of the elongation of the rack is:

$$\dot{D}_1 = \frac{1}{2} \cdot D_1^{-1} \cdot \left[2 \cdot H_1 \cdot (-l_c \cdot \cos(\varphi_d) \cdot \dot{\varphi}_d + 2 \cdot r_m \cdot \dot{\varphi}_m / 3.14) + 2 \cdot L_1 \cdot (-l_c \cdot \sin(\varphi_d) \cdot \dot{\varphi}_d + 2 \cdot r_m \cdot \dot{\varphi}_m / 3.14)\right]$$

where:
$\dot{\varphi}_{\mathrm{m}}$ *is the angular velocity of the motor reduced to the pinion shaft;*

Figure 3.12 depicts the angular displacement of the deck obtained from theoretical input motion parameters for normal operation imposed on the last developed model. It can be observed that the displacement is increasing up until 1.239rad. This is lower than the expected maximum opening angle, but the shape of the angular displacement is in accordance with the theoretical result.

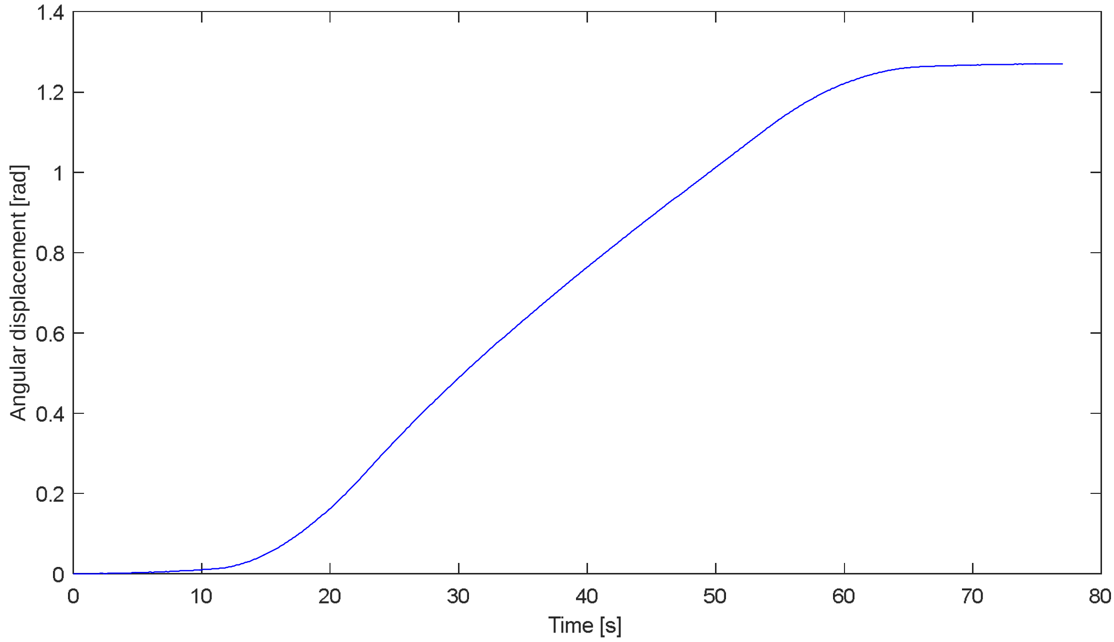

Figure 3.12 Bridge Structure Connected to the Pinion Shaft – Nonlinear Model – Angular Displacement of the Deck [rad]

In order to obtain the torque acting on the motor an additional equation of motion has to be considered around the pinion shaft:

$$J_m \cdot \ddot{\varphi}_m = (F_{kmd} + F_{cmd}) \cdot r_m + M_{motor} \quad ==> \quad M_{motor} = (F_{kmd} + F_{cmd}) \cdot r_m + J_m \cdot \ddot{\varphi}_m$$

where:

$\ddot{\varphi}_{\mathrm{m}}$ *is the angular acceleration of the motor reduced to the pinion shaft;*

J_{m} *is the mass moment of inertia of the electro-motor.*

In Figure 3.13, the torque on the electro-motor can be observed. This is a result from theoretical input motion parameters.

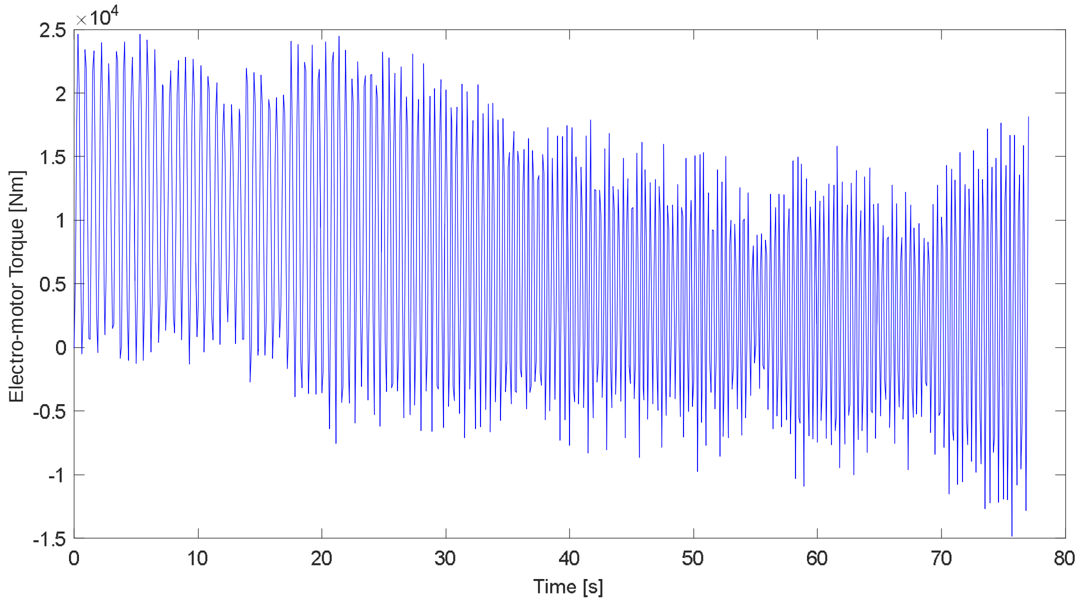

Figure 3.13 Motor Torque [Nm]

The complete equations of motion are as follows:

- Equation of motion of the balance part

$$J_b \cdot \ddot{\varphi}_b + (k_h \cdot (\sqrt{H^2 + L^2} - H_h / \cos\beta) + c_h \cdot D_h^{-1} \cdot (l_h \cdot H \cdot (\cos(\varphi_b) \cdot \dot{\varphi}_b - \cos(\varphi_d) \cdot \dot{\varphi}_d) + l_h \cdot L \cdot$$
$$(\sin(\varphi_b) \cdot \dot{\varphi}_b - \sin(\varphi_d) \cdot \dot{\varphi}_d))) \cdot (\frac{H}{\sqrt{H^2 + L^2}} \cdot l_h \cdot \cos(\varphi_b) + \frac{L}{\sqrt{H^2 + L^2}} \cdot l_h \cdot \sin(\varphi_b)) - m_b \cdot g \cdot l_b \cdot \cos(\varphi_b) = 0$$

- Equation of motion of the deck

$$J_d \cdot \ddot{\varphi}_d - (k_h \cdot (\sqrt{H^2 + L^2} - H_h / \cos\beta) + c_h \cdot D_h^{-1} \cdot (l_h \cdot H \cdot (\cos(\varphi_b) \cdot \dot{\varphi}_b - \cos(\varphi_d) \cdot \dot{\varphi}_d) + l_h \cdot L \cdot$$
$$(\sin(\varphi_b) \cdot \dot{\varphi}_b - \sin(\varphi_d) \cdot \dot{\varphi}_d))) \cdot (\frac{H}{\sqrt{H^2 + L^2}} \cdot l_h \cdot \cos(\varphi_d) + \frac{L}{\sqrt{H^2 + L^2}} \cdot l_h \cdot \sin(\varphi_d)) - (k_{md} \cdot (\sqrt{H_1^2 + L_1^2} - L_r) +$$
$$c_{cmd} \cdot D_1^{-1} \cdot \left[H_1 \cdot (-l_c \cdot \cos(\varphi_d) \cdot \dot{\varphi}_d + 2 \cdot r_m \cdot \dot{\varphi}_m / 3.14) + L_1 \cdot (-l_c \cdot \sin(\varphi_d) \cdot \dot{\varphi}_d + 2 \cdot r_m \cdot \dot{\varphi}_m / 3.14)\right]) \cdot$$
$$(\frac{L_1}{\sqrt{H_1^2 + L_1^2}} \cdot l_c \cdot \sin(\varphi_d) + \frac{H_1}{\sqrt{H_1^2 + L_1^2}} \cdot l_c \cdot \cos(\varphi_d)) + m_d \cdot g \cdot l_d \cdot \cos(\varphi_d) = 0$$

- Equation of motion of the motor

$$J_m \cdot \ddot{\varphi}_m + (k_{md} \cdot (\sqrt{H_1^2 + L_1^2} - L_r) + c_{cmd} \cdot D_1^{-1} \cdot (H_1 \cdot (-l_c \cdot \cos(\varphi_d) \cdot \dot{\varphi}_d + 2 \cdot r_m \cdot \dot{\varphi}_m / 3.14)$$
$$+ L_1 \cdot (-l_c \cdot \sin(\varphi_d) \cdot \dot{\varphi}_d + 2 \cdot r_m \cdot \dot{\varphi}_m / 3.14))) \cdot r_m = M_{motor}$$

The last obtained equations of motion are verified by means of the Lagrangian approach. In Newtonian mechanics, the approach previously used, the equations of motion are derived based on Newton's second law. Instead of using forces, Lagrangian mechanics used the energies of the system to derive the equations of motion. A function called the Lagrangian is used to express the dynamic behavior of the entire system. Since the system at hand contains both conservative and non-conservative forces, the general form of the Lagrange equation is going to be employed:

$$\frac{d}{dt}\left(\frac{\partial L}{\partial \dot{q}_r}\right) - \frac{\partial L}{\partial q_r} + \frac{\partial F}{\partial \dot{q}_r} = 0$$

where:

L *is the Lagrangian;*

q_r *represents the generalized coordinates of the system:* φ_b, φ_d *and* φ_m*;*

F *is the Rayleigh dissipation function.*

For this system the Lagrange equations are the following

$$\frac{d}{dt}\left(\frac{\partial L}{\partial \dot{\varphi}_b}\right)-\frac{\partial L}{\partial \varphi_b}+\frac{\partial F}{\partial \dot{\varphi}_b}=0$$
$$\frac{d}{dt}\left(\frac{\partial L}{\partial \dot{\varphi}_d}\right)-\frac{\partial L}{\partial \varphi_d}+\frac{\partial F}{\partial \dot{\varphi}_d}=0$$
$$\frac{d}{dt}\left(\frac{\partial L}{\partial \dot{\varphi}_m}\right)-\frac{\partial L}{\partial \varphi_m}+\frac{\partial F}{\partial \dot{\varphi}_m}=0$$

The Lagrangian function is expressed as the difference between the kinetic energy K and the potential energy P:

$$L = K - P$$

The kinetic energy K is expressed function of the coordinates of the system as follows:

$$K=\frac{1}{2}\cdot J_b\cdot \dot{\varphi}_b^{\,2}+\frac{1}{2}\cdot J_d\cdot \dot{\varphi}_d^{\,2}+\frac{1}{2}\cdot J_m\cdot \dot{\varphi}_m^{\,2}$$

The potential energy P accounts for the energy stored in the springs and the energy due to the self-weight of the elements and is expressed as follows:

$$P=\frac{1}{2}\cdot k_h\cdot u_h^{\,2}+\frac{1}{2}\cdot k_{md}\cdot u_r^{\,2}-m_b\cdot g\cdot l_b\cdot \sin(\varphi_b)+m_d\cdot g\cdot l_d\cdot \sin(\varphi_d)$$

The Rayleigh dissipation function is defined as:

$$F=\frac{1}{2}\cdot c_h\cdot \dot{u}_h^{\,2}+\frac{1}{2}\cdot c_{md}\cdot \dot{u}_r^{\,2}$$

The energies previously defined are defined in Maple software and the Lagrange equations are obtained. A detailed script of the process can be observed in Appendix 3. The resulting equations of motion are the following:

- Equation of motion of the balance part

$$J_b\cdot\ddot{\varphi}_b+(k_h\cdot(\sqrt{H^2+L^2}-H_h/\cos\beta)+c_h\cdot D_h^{-1}\cdot(l_h\cdot H\cdot(\cos(\varphi_b)\cdot\dot{\varphi}_b-\cos(\varphi_d)\cdot\dot{\varphi}_d)+l_h\cdot L\cdot$$
$$(\sin(\varphi_b)\cdot\dot{\varphi}_b-\sin(\varphi_d)\cdot\dot{\varphi}_d)))\cdot(\frac{H}{\sqrt{H^2+L^2}}\cdot l_h\cdot\cos(\varphi_b)+\frac{L}{\sqrt{H^2+L^2}}\cdot l_h\cdot\sin(\varphi_b))-m_b\cdot g\cdot l_b\cdot\cos(\varphi_b)=0$$

- Equation of motion of the deck

$$J_d\cdot\ddot{\varphi}_d-(k_h\cdot(\sqrt{H^2+L^2}-H_h/\cos\beta)+c_h\cdot D_h^{-1}\cdot(l_h\cdot H\cdot(\cos(\varphi_b)\cdot\dot{\varphi}_b-\cos(\varphi_d)\cdot\dot{\varphi}_d)+l_h\cdot L\cdot$$
$$(\sin(\varphi_b)\cdot\dot{\varphi}_b-\sin(\varphi_d)\cdot\dot{\varphi}_d)))\cdot(\frac{H}{\sqrt{H^2+L^2}}\cdot l_h\cdot\cos(\varphi_d)+\frac{L}{\sqrt{H^2+L^2}}\cdot l_h\cdot\sin(\varphi_d))-(k_{md}\cdot(\sqrt{H_1^{\,2}+L_1^{\,2}}-L_r)+$$
$$c_{cmd}\cdot D_1^{-1}\cdot\left[H_1\cdot(-l_c\cdot\cos(\varphi_d)\cdot\dot{\varphi}_d+2\cdot r_m\cdot\dot{\varphi}_m/3.14)+L_1\cdot(-l_c\cdot\sin(\varphi_d)\cdot\dot{\varphi}_d+2\cdot r_m\cdot\dot{\varphi}_m/3.14)\right])\cdot$$
$$(\frac{L_1}{\sqrt{H_1^{\,2}+L_1^{\,2}}}\cdot l_c\cdot\sin(\varphi_d)+\frac{H_1}{\sqrt{H_1^{\,2}+L_1^{\,2}}}\cdot l_c\cdot\cos(\varphi_d))+m_d\cdot g\cdot l_d\cdot\cos(\varphi_d)=0$$

- Equation of motion of the motor

$$J_m \cdot \ddot{\varphi}_m + (k_{md} \cdot (\sqrt{H_1^{\,2} + L_1^{\,2}} - L_r) + c_{cmd} \cdot D_1^{-1} \cdot (H_1 \cdot (-l_c \cdot \cos(\varphi_d) \cdot \dot{\varphi}_d + 2 \cdot r_m \cdot \dot{\varphi}_m / 3.14)$$
$$+ L_1 \cdot (-l_c \cdot \sin(\varphi_d) \cdot \dot{\varphi}_d + 2 \cdot r_m \cdot \dot{\varphi}_m / 3.14))) \cdot r_m = M_{motor}$$

Since the obtained equations of motion are identical both ways of derivation, namely Newtonian mechanics and Lagrangian mechanics, it can be concluded that the development of the system of equations has been performed correctly.

In order to further test the correctness of the obtained system of equations, linearization of the system will be employed. This is also beneficial for the eigenvalue analysis that will be later on performed. The linearization of the nonlinear differential equations is based on Taylor expansion series and nominal system trajectories. The obtained angular accelerations can be expressed as a function G depending on the angular displacements and angular accelerations:

$$\ddot{\varphi}_b = G_b(\varphi_b, \dot{\varphi}_b, \varphi_d, \dot{\varphi}_d)$$
$$\ddot{\varphi}_d = G_d(\varphi_b, \dot{\varphi}_b, \varphi_d, \dot{\varphi}_d, \varphi_m, \dot{\varphi}_m)$$
$$\ddot{\varphi}_m = G_m(\varphi_d, \dot{\varphi}_d, \varphi_m, \dot{\varphi}_m)$$

If it is assumed that under normal operating conditions the system works along the trajectories $\varphi_{bn}(t)$, $\varphi_{dn}(t)$ and $\varphi_{mn}(t)$, then these are called the nominal trajectories of the system. Further on, if it is assumed that the motion of the nonlinear system occurs in the vicinity of the nominal system trajectory, then the following can be written:

$$\varphi_b(t) = \varphi_{bn}(t) + \Delta\varphi_b(t)$$
$$\varphi_d(t) = \varphi_{dn}(t) + \Delta\varphi_d(t)$$
$$\varphi_m(t) = \varphi_{mn}(t) + \Delta\varphi_m(t)$$

where $\Delta\varphi_b(t),\ \Delta\varphi_d(t),\ \Delta\varphi_m(t)$ represent small quantities.

Then, for the motion of the system in close proximity to the nominal trajectory the following holds:

$$\ddot{\varphi}_{bn} + \Delta\ddot{\varphi}_b = G(\varphi_{bn} + \Delta\varphi_b, \dot{\varphi}_{bn} + \Delta\dot{\varphi}_b, \varphi_{dn} + \Delta\varphi_d, \dot{\varphi}_{dn} + \Delta\dot{\varphi}_d)$$
$$\ddot{\varphi}_{dn} + \Delta\ddot{\varphi}_d = G(\varphi_{bn} + \Delta\varphi_b, \dot{\varphi}_{bn} + \Delta\dot{\varphi}_b, \varphi_{dn} + \Delta\varphi_d, \dot{\varphi}_{dn} + \Delta\dot{\varphi}_d, \varphi_{mn} + \Delta\varphi_m, \dot{\varphi}_{mn} + \Delta\dot{\varphi}_d)$$
$$\ddot{\varphi}_{mn} + \Delta\ddot{\varphi}_m = G(\varphi_{dn} + \Delta\varphi_d, \dot{\varphi}_{dn} + \Delta\dot{\varphi}_d, \varphi_{mn} + \Delta\varphi_m, \dot{\varphi}_{mn} + \Delta\dot{\varphi}_m)$$

Applying Taylor expansion around the nominal points φ_{bn}, $\dot{\varphi}_{bn}$, φ_{dn}, $\dot{\varphi}_{dn}$, φ_{mn}, $\dot{\varphi}_{mn}$, results in a system of linear differential equations of the form:

$$\Delta\ddot{\varphi}_b + a_{11b} \cdot \Delta\dot{\varphi}_b + a_{01b} \cdot \Delta\varphi_b + a_{11d} \cdot \Delta\dot{\varphi}_d + a_{01d} \cdot \Delta\varphi_d = 0$$
$$\Delta\ddot{\varphi}_d + a_{12b} \cdot \Delta\dot{\varphi}_b + a_{02b} \cdot \Delta\varphi_b + a_{12d} \cdot \Delta\dot{\varphi}_d + a_{02d} \cdot \Delta\varphi_d + a_{12m} \cdot \Delta\dot{\varphi}_m + a_{02m} \cdot \Delta\varphi_m = 0$$
$$\Delta\ddot{\varphi}_m + a_{13d} \cdot \Delta\dot{\varphi}_d + a_{03d} \cdot \Delta\varphi_d + a_{13m} \cdot \Delta\dot{\varphi}_m + a_{03m} \cdot \Delta\varphi_m = 0$$

The corresponding coefficients in the above equations are evaluated at the nominal points as follows:

$$a_{11b} = -\frac{\partial G_b}{\partial \dot{\varphi}_b}(\varphi_{bn}, \dot{\varphi}_{bn}, \varphi_{dn}, \dot{\varphi}_{dn}) \qquad a_{01b} = -\frac{\partial G_b}{\partial \varphi_b}(\varphi_{bn}, \dot{\varphi}_{bn}, \varphi_{dn}, \dot{\varphi}_{dn})$$

$$a_{11d} = -\frac{\partial G_b}{\partial \dot{\varphi}_d}(\varphi_{bn}, \dot{\varphi}_{bn}, \varphi_{dn}, \dot{\varphi}_{dn}) \qquad a_{01d} = -\frac{\partial G_b}{\partial \varphi_d}(\varphi_{bn}, \dot{\varphi}_{bn}, \varphi_{dn}, \dot{\varphi}_{dn})$$

$$a_{12b} = -\frac{\partial G_d}{\partial \dot{\varphi}_b}(\varphi_{bn}, \dot{\varphi}_{bn}, \varphi_{dn}, \dot{\varphi}_{dn}, \varphi_{mn}, \dot{\varphi}_{mn}) \qquad a_{02b} = -\frac{\partial G_d}{\partial \varphi_b}(\varphi_{bn}, \dot{\varphi}_{bn}, \varphi_{dn}, \dot{\varphi}_{dn}, \varphi_{mn}, \dot{\varphi}_{mn})$$

$$a_{12d} = -\frac{\partial G_d}{\partial \dot{\varphi}_d}(\varphi_{bn}, \dot{\varphi}_{bn}, \varphi_{dn}, \dot{\varphi}_{dn}, \varphi_{mn}, \dot{\varphi}_{mn}) \qquad a_{02d} = -\frac{\partial G_d}{\partial \varphi_d}(\varphi_{bn}, \dot{\varphi}_{bn}, \varphi_{dn}, \dot{\varphi}_{dn}, \varphi_{mn}, \dot{\varphi}_{mn})$$

$$a_{12m} = -\frac{\partial G_d}{\partial \dot{\varphi}_m}(\varphi_{bn}, \dot{\varphi}_{bn}, \varphi_{dn}, \dot{\varphi}_{dn}, \varphi_{mn}, \dot{\varphi}_{mn}) \qquad a_{02m} = -\frac{\partial G_d}{\partial \varphi_m}(\varphi_{bn}, \dot{\varphi}_{bn}, \varphi_{dn}, \dot{\varphi}_{dn}, \varphi_{mn}, \dot{\varphi}_{mn})$$

$$a_{13d} = -\frac{\partial G_m}{\partial \dot{\varphi}_d}(\varphi_{dn}, \dot{\varphi}_{dn}, \varphi_{mn}, \dot{\varphi}_{mn}) \qquad a_{03d} = -\frac{\partial G_m}{\partial \varphi_d}(\varphi_{dn}, \dot{\varphi}_{dn}, \varphi_{mn}, \dot{\varphi}_{mn})$$

$$a_{13m} = -\frac{\partial G_m}{\partial \dot{\varphi}_m}(\varphi_{dn}, \dot{\varphi}_{dn}, \varphi_{mn}, \dot{\varphi}_{mn}) \qquad a_{03m} = -\frac{\partial G_m}{\partial \varphi_m}(\varphi_{dn}, \dot{\varphi}_{dn}, \varphi_{mn}, \dot{\varphi}_{mn})$$

The nominal points are considered at time $t = 0$, so all the quantities related to the nominal points will be null. The complete procedure and the results can be observed in Appendix 3. The final linear equations of motion are:

- Linear equation of motion of the balance part

$$J_b \cdot \ddot{\varphi}_b + \frac{c_h \cdot H_h^{\ 2} \cdot l_h^{\ 2}}{H_h^{\ 2} + H_h^{\ 2} \cdot (\tan\beta)^2} \cdot \dot{\varphi}_b + \left(\frac{k_h \cdot H_h^{\ 2} \cdot l_h^{\ 2}}{H_h^{\ 2} + H_h^{\ 2} \cdot (\tan\beta)^2} - \frac{k_h \left(\sqrt{H_h^{\ 2} + H_h^{\ 2} \cdot (\tan\beta)^2} - \frac{H_h}{\cos\beta} \right) \cdot H_h^{\ 2} \cdot l_h^{\ 2}}{(H_h^{\ 2} + H_h^{\ 2} \cdot (\tan\beta)^2)^{\frac{3}{2}}} \right.$$
$$\left. + \frac{k_h \left(\sqrt{H_h^{\ 2} + H_h^{\ 2} \cdot (\tan\beta)^2} - \frac{H_h}{\cos\beta} \right) \left(l_h^{\ 2} + H_h \cdot \tan\beta \cdot l_h \right)}{\sqrt{H_h^{\ 2} + H_h^{\ 2} \cdot (\tan\beta)^2}} \right) \cdot \varphi_b - \frac{c_h \cdot H_h^{\ 2} \cdot l_h^{\ 2}}{H_h^{\ 2} + H_h^{\ 2} \cdot (\tan\beta)^2} \cdot \dot{\varphi}_d - \left(\frac{k_h \cdot H_h^{\ 2} \cdot l_h^{\ 2}}{H_h^{\ 2} + H_h^{\ 2} \cdot (\tan\beta)^2} \right.$$
$$\left. - \frac{k_h \left(\sqrt{H_h^{\ 2} + H_h^{\ 2} \cdot (\tan\beta)^2} - \frac{H_h}{\cos\beta} \right) \cdot H_h^{\ 2} \cdot l_h^{\ 2}}{(H_h^{\ 2} + H_h^{\ 2} \cdot (\tan\beta)^2)^{\frac{3}{2}}} + \frac{k_h \left(\sqrt{H_h^{\ 2} + H_h^{\ 2} \cdot (\tan\beta)^2} - \frac{H_h}{\cos\beta} \right) \cdot l_h^{\ 2}}{\sqrt{H_h^{\ 2} + H_h^{\ 2} \cdot (\tan\beta)^2}} \right) \cdot \varphi_d = 0$$

- Linear equation of motion of the deck

$$
J_d \cdot \ddot{\varphi}_d - \frac{c_h \cdot H_h{}^2 \cdot l_h{}^2}{H_h{}^2 + H_h{}^2 \cdot (\tan\beta)^2} \cdot \dot{\varphi}_b - \Bigg(\frac{k_h \cdot H_h{}^2 \cdot l_h{}^2}{H_h{}^2 + H_h{}^2 \cdot (\tan\beta)^2} - \frac{k_h \left(\sqrt{H_h{}^2 + H_h{}^2 \cdot (\tan\beta)^2} - \dfrac{H_h}{\cos\beta} \right) \cdot H_h{}^2 \cdot l_h{}^2}{(H_h{}^2 + H_h{}^2 \cdot (\tan\beta)^2)^{\frac{3}{2}}}
$$

$$
+ \frac{k_h \left(\sqrt{H_h{}^2 + H_h{}^2 \cdot (\tan\beta)^2} - \dfrac{H_h}{\cos\beta} \right) \cdot l_h{}^2}{\sqrt{H_h{}^2 + H_h{}^2 \cdot (\tan\beta)^2}} \Bigg) \cdot \varphi_b + \left(\frac{c_h \cdot H_h{}^2 \cdot l_h{}^2}{H_h{}^2 + H_h{}^2 \cdot (\tan\beta)^2} + \frac{c_{md} \cdot L_r{}^2 \cdot (\sin\gamma_i)^2 \cdot l_c{}^2}{L_r{}^2 \cdot (\sin\gamma_i)^2 + L_r{}^2 \cdot (\cos\gamma_i)^2} \right) \cdot \dot{\varphi}_d
$$

$$
+ \Bigg(\frac{k_h \cdot H_h{}^2 \cdot l_h{}^2}{H_h{}^2 + H_h{}^2 \cdot (\tan\beta)^2} - \frac{k_h \left(\sqrt{H_h{}^2 + H_h{}^2 \cdot (\tan\beta)^2} - \dfrac{H_h}{\cos\beta} \right) \cdot H_h{}^2 \cdot l_h{}^2}{(H_h{}^2 + H_h{}^2 \cdot (\tan\beta)^2)^{\frac{3}{2}}}
$$

$$
+ \frac{k_h \left(\sqrt{H_h{}^2 + H_h{}^2 \cdot (\tan\beta)^2} - \dfrac{H_h}{\cos\beta} \right) \left(l_h{}^2 + H_h \cdot \tan\beta \cdot l_h \right)}{\sqrt{H_h{}^2 + H_h{}^2 \cdot (\tan\beta)^2}} + \frac{k_{md} \cdot L_r{}^2 \cdot (\sin\gamma_i)^2 \cdot l_c{}^2}{L_r{}^2 \cdot (\sin\gamma_i)^2 + L_r{}^2 \cdot (\cos\gamma_i)^2} -
$$

$$
\frac{k_{md} \cdot (\sqrt{L_r{}^2 \cdot (\sin\gamma_i)^2 + L_r{}^2 \cdot (\cos\gamma_i)^2} - L_r) \cdot L_r{}^2 \cdot (\sin\gamma_i)^2 \cdot l_c{}^2}{(L_r{}^2 \cdot (\sin\gamma_i)^2 + L_r{}^2 \cdot (\cos\gamma_i)^2)^{\frac{3}{2}}} +
$$

$$
\frac{k_{md} \cdot (\sqrt{L_r{}^2 \cdot (\sin\gamma_i)^2 + L_r{}^2 \cdot (\cos\gamma_i)^2} - L_r) \cdot (l_c{}^2 - L_r \cdot \cos\gamma_i \cdot l_c)}{\sqrt{L_r{}^2 \cdot (\sin\gamma_i)^2 + L_r{}^2 \cdot (\cos\gamma_i)^2}} \Bigg) \cdot \varphi_d -
$$

$$
\frac{c_{md} \cdot \dfrac{2}{3.14} \cdot (L_r \cdot \sin\gamma_i \cdot r_m + L_r \cdot \cos\gamma_i \cdot r_m) \cdot L_r \cdot \sin\gamma_i \cdot l_c}{L_r{}^2 \cdot (\sin\gamma_i)^2 + L_r{}^2 \cdot (\cos\gamma_i)^2} \cdot \dot{\varphi}_m - \Bigg(\frac{k_{md} \cdot \dfrac{2}{3.14} \cdot (L_r \cdot \sin\gamma_i \cdot r_m + L_r \cdot \cos\gamma_i \cdot r_m) \cdot L_r \cdot \sin\gamma_i \cdot l_c}{L_r{}^2 \cdot (\sin\gamma_i)^2 + L_r{}^2 \cdot (\cos\gamma_i)^2}
$$

$$
- \frac{k_{md} \cdot \dfrac{2}{3.14} \cdot (L_r \cdot \sin\gamma_i \cdot r_m + L_r \cdot \cos\gamma_i \cdot r_m) \cdot L_r \cdot \sin\gamma_i \cdot l_c \cdot (\sqrt{L_r{}^2 \cdot (\sin\gamma_i)^2 + L_r{}^2 \cdot (\cos\gamma_i)^2} - L_r)}{(L_r{}^2 \cdot (\sin\gamma_i)^2 + L_r{}^2 \cdot (\cos\gamma_i)^2)^{\frac{3}{2}}} +
$$

$$
\frac{k_{md} \cdot \dfrac{2}{3.14} \cdot (\sqrt{L_r{}^2 \cdot (\sin\gamma_i)^2 + L_r{}^2 \cdot (\cos\gamma_i)^2} - L_r) \cdot r_m \cdot l_c}{\sqrt{L_r{}^2 \cdot (\sin\gamma_i)^2 + L_r{}^2 \cdot (\cos\gamma_i)^2}} \Bigg) \cdot \varphi_m = 0
$$

- Linear equation of motion of the motor

$$
J_m \cdot \ddot{\varphi}_m - \frac{c_{md} \cdot \dfrac{2}{3.14} \cdot (L_r \cdot \sin\gamma_i \cdot r_m + L_r \cdot \cos\gamma_i \cdot r_m) \cdot L_r \cdot \sin\gamma_i \cdot l_c}{L_r^{\,2} \cdot (\sin\gamma_i)^2 + L_r^{\,2} \cdot (\cos\gamma_i)^2} \cdot \dot{\varphi}_d - \Bigg(\frac{k_{md} \cdot \dfrac{2}{3.14} \cdot (L_r \cdot \sin\gamma_i \cdot r_m + L_r \cdot \cos\gamma_i \cdot r_m) \cdot L_r \cdot \mathrm{si}}{L_r^{\,2} \cdot (\sin\gamma_i)^2 + L_r^{\,2} \cdot (\cos\gamma_i)^2}
$$

$$
- \frac{k_{md} \cdot \dfrac{2}{3.14} \cdot (L_r \cdot \sin\gamma_i \cdot r_m + L_r \cdot \cos\gamma_i \cdot r_m) \cdot L_r \cdot \sin\gamma_i \cdot l_c \cdot \left(\sqrt{L_r^{\,2} \cdot (\sin\gamma_i)^2 + L_r^{\,2} \cdot (\cos\gamma_i)^2} - L_r\right)}{\left(L_r^{\,2} \cdot (\sin\gamma_i)^2 + L_r^{\,2} \cdot (\cos\gamma_i)^2\right)^{\frac{3}{2}}} +
$$

$$
\frac{k_{md} \cdot \dfrac{2}{3.14} \cdot \left(\sqrt{L_r^{\,2} \cdot (\sin\gamma_i)^2 + L_r^{\,2} \cdot (\cos\gamma_i)^2} - L_r\right) \cdot r_m \cdot l_c}{\sqrt{L_r^{\,2} \cdot (\sin\gamma_i)^2 + L_r^{\,2} \cdot (\cos\gamma_i)^2}} \Bigg) \cdot \varphi_d + \frac{c_{md} \cdot \left(\dfrac{2}{3.14} \cdot L_r \cdot \sin\gamma_i \cdot r_m + \dfrac{2}{3.14} \cdot L_r \cdot \cos\gamma_i \cdot r_m\right)^{\wedge 2}}{L_r^{\,2} \cdot (\sin\gamma_i)^2 + L_r^{\,2} \cdot (\cos\gamma_i)^2} \cdot \dot{\varphi}_m
$$

$$
+ \Bigg(- \frac{k_{md} \cdot \dfrac{2}{3.14} \cdot (L_r \cdot \sin\gamma_i \cdot r_m + L_r \cdot \cos\gamma_i \cdot r_m) \cdot L_r \cdot \sin\gamma_i \cdot l_c}{L_r^{\,2} \cdot (\sin\gamma_i)^2 + L_r^{\,2} \cdot (\cos\gamma_i)^2}
$$

$$
+ \frac{k_{md} \cdot \dfrac{2}{3.14} \cdot (L_r \cdot \sin\gamma_i \cdot r_m + L_r \cdot \cos\gamma_i \cdot r_m) \cdot L_r \cdot \sin\gamma_i \cdot l_c \cdot \left(\sqrt{L_r^{\,2} \cdot (\sin\gamma_i)^2 + L_r^{\,2} \cdot (\cos\gamma_i)^2} - L_r\right)}{\left(L_r^{\,2} \cdot (\sin\gamma_i)^2 + L_r^{\,2} \cdot (\cos\gamma_i)^2\right)^{\frac{3}{2}}} -
$$

$$
\frac{k_{md} \cdot \dfrac{2}{3.14} \cdot \left(\sqrt{L_r^{\,2} \cdot (\sin\gamma_i)^2 + L_r^{\,2} \cdot (\cos\gamma_i)^2} - L_r\right) \cdot r_m \cdot l_c}{\sqrt{L_r^{\,2} \cdot (\sin\gamma_i)^2 + L_r^{\,2} \cdot (\cos\gamma_i)^2}} \Bigg) \cdot \varphi_m = 0
$$

The solution of the linear system of equations of motion can be observed in Appendix 3. The behavior of the linear system is similar to that of the nonlinear system, although as it can be observed in Figure 3.14, the angular displacement of the balance part is larger in case of the linear system. The maximum rotation in case of the linear system is larger than the maximum allowable value, thus it is clear that the nonlinear system is more reliable and close to the reality. The linear system will only be used for the eigenvalue problem.

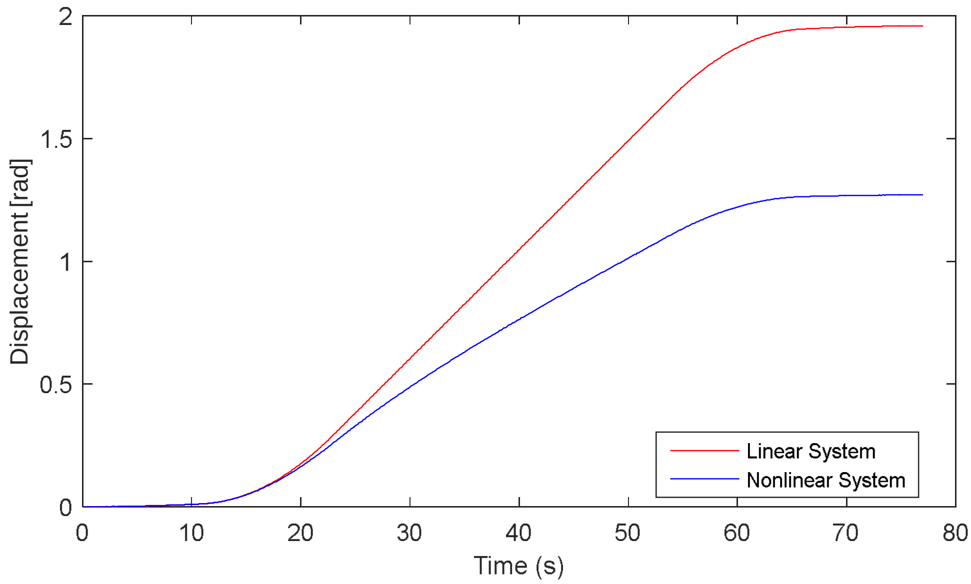

Figure 3.14 Angular Displacement of the Balance Part - Linear versus Nonlinear System

3.2.3. Normal Operation

The normal operation is intended to describe the motion of the electro-motor, the deck and the balance part produced by the imposed motion parameters in Figure 3.15 and Figure 3.16. The Matlab scripts for this situation can be found in Appendix 3.

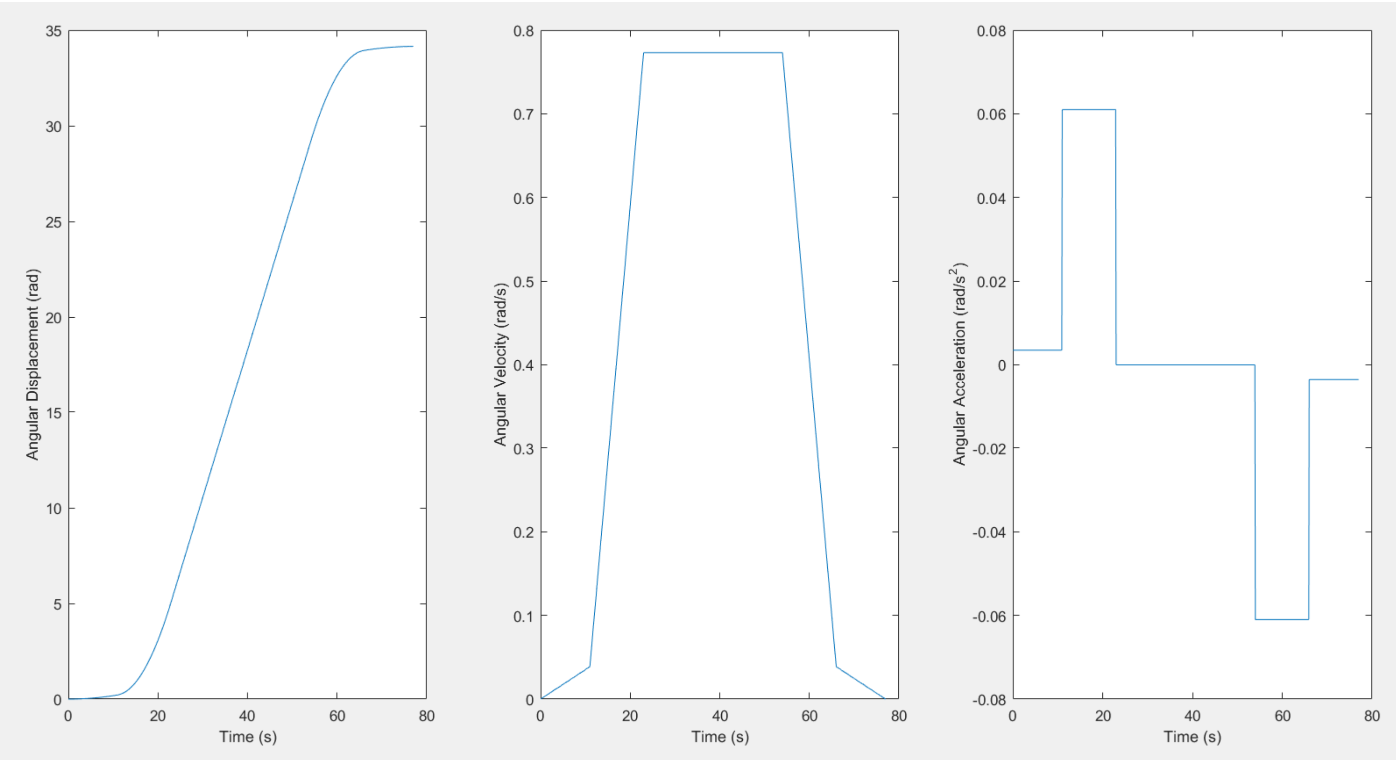

Figure 3.15 Motion Parameters - 3DOF - Normal Operation – Theoretical Model

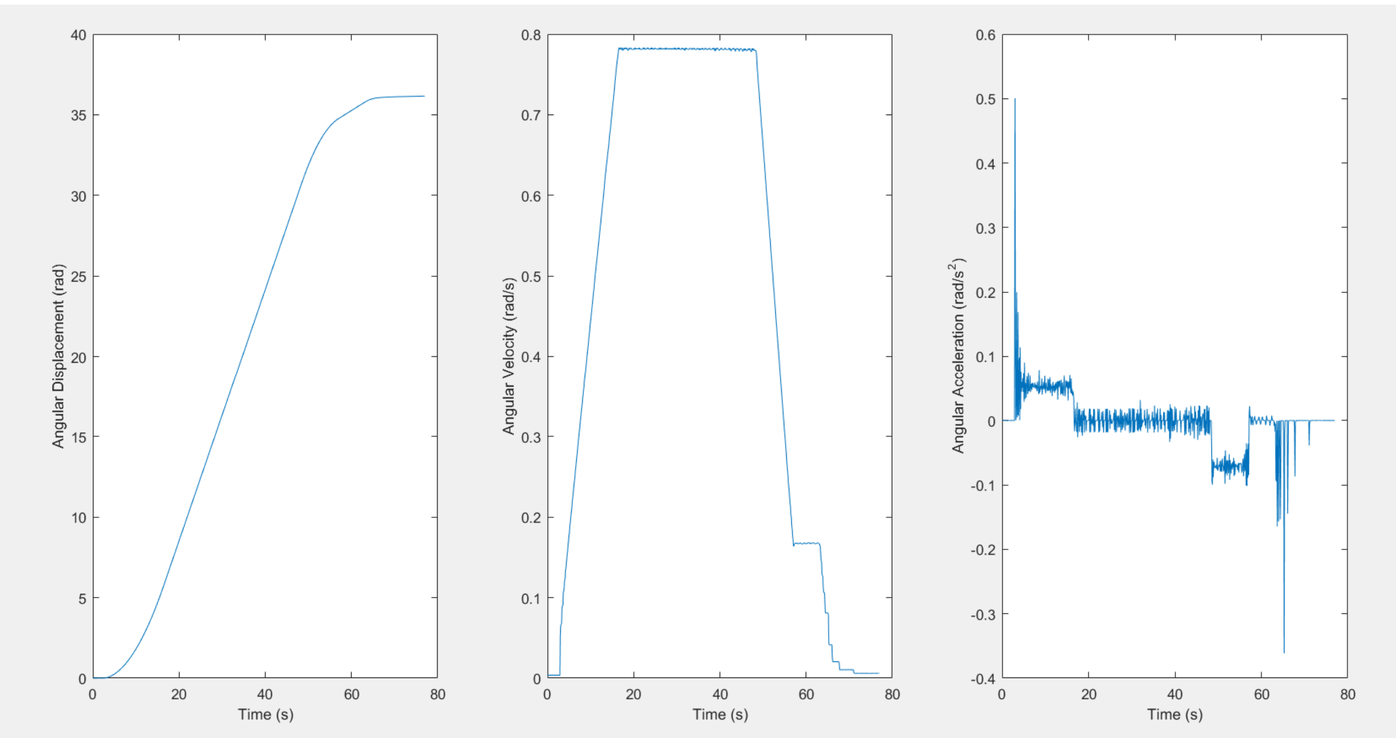

Figure 3.16 Motion Parameters - 3 DOF - Normal Operation – Measurements' Model

3.2.4. Brake Situation

The brake situation in this case considers the motion parameters in Figure 3.17 and Figure 3.18 and the complete Matlab scripts can be found in Appendix 3.

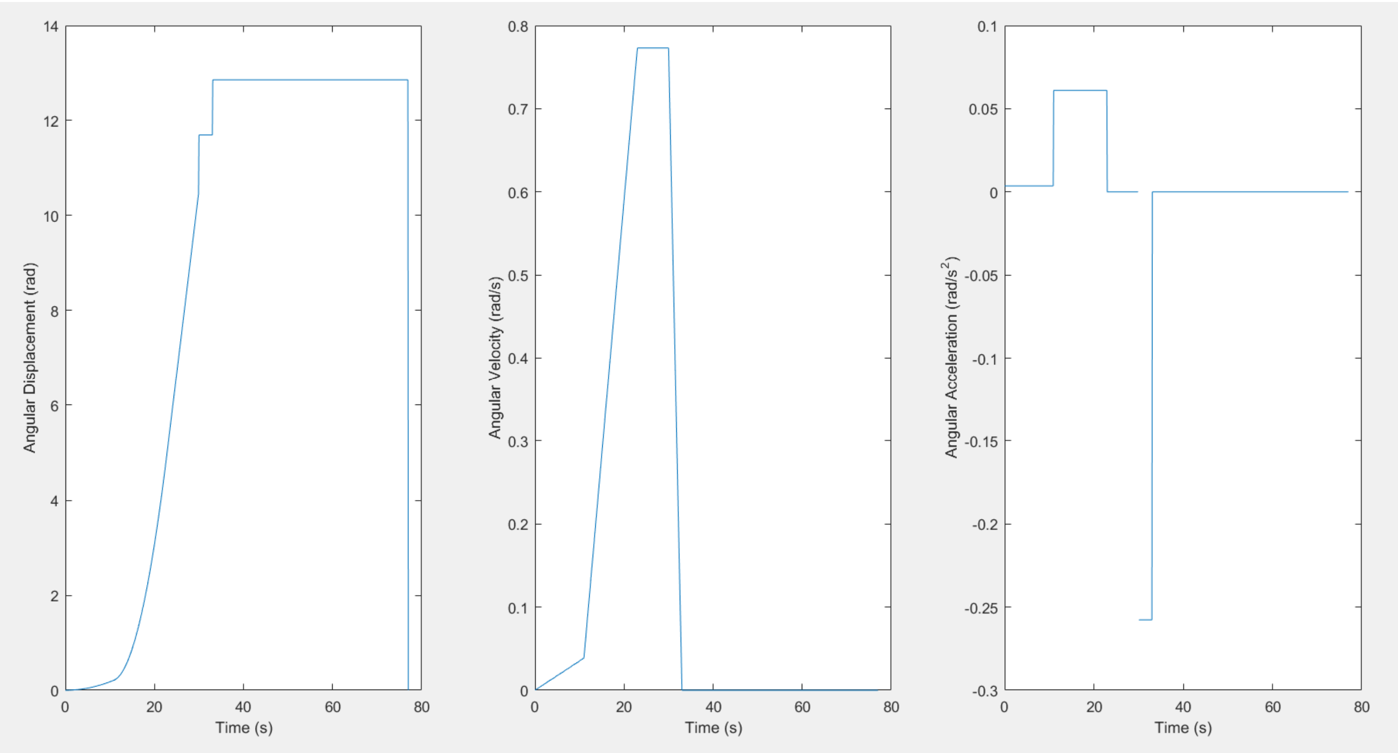

Figure 3.17 Motion Parameters - 3DOF - Brake Situation – Theoretical Model

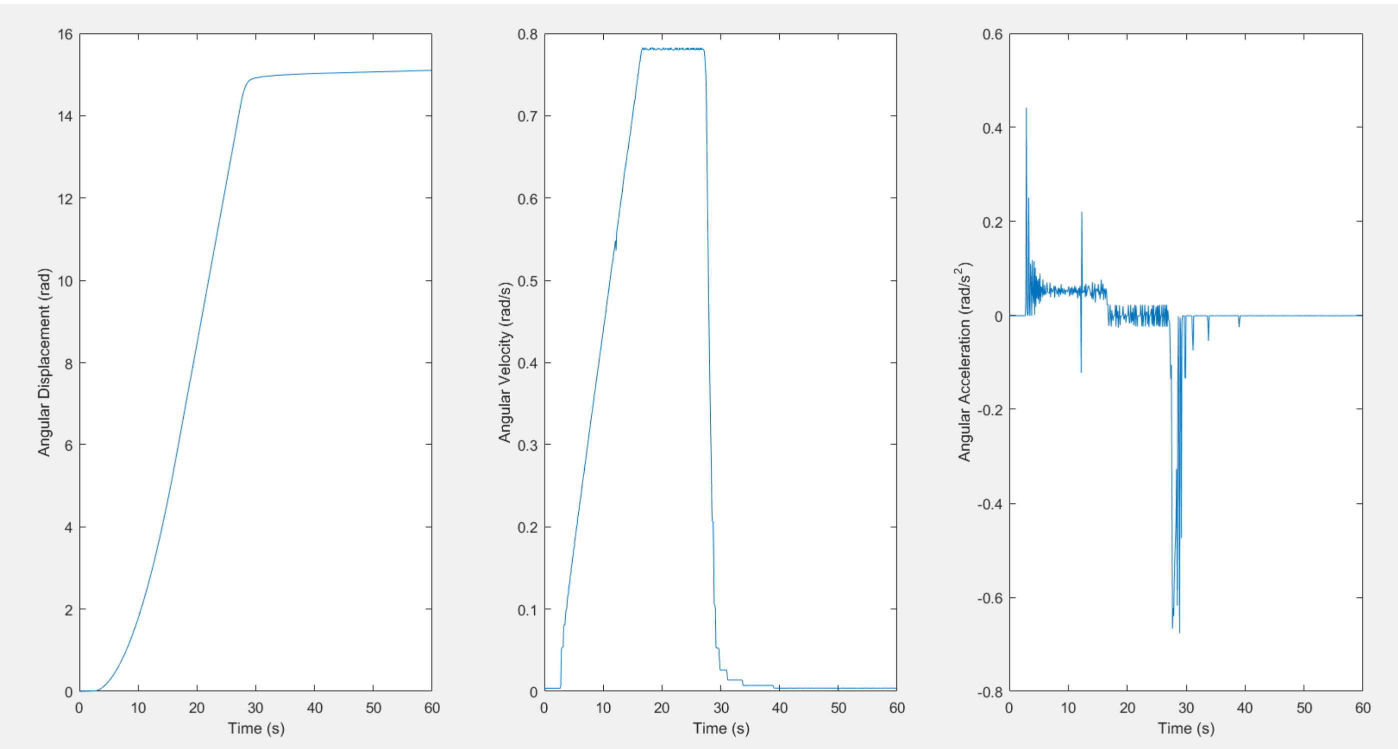

Figure 3.18 Motion Parameters - 3DOF - Brake Situation – Measurements' Model

3.2.5. Eigenvalue Problem

The natural frequencies and mode shapes are obtained by solving the eigenvalue problem. These are obtained in terms of eigenvalues and eigenvectors, which are essential in comprehending the motions of the system. It is also a method of verification of the accuracy of the developed equations of motion. The eigenvalue problem can be solved only for a linear system of differential equations. Thus, the linearized system from section 3.2.2 is used here. Moreover, the analysis will be conducted for the undamped system composed of the balance part, deck and the rack. The equation of motion of the motor will not be considered because the respective equation is used to either impose a motion to the bridge structure or to obtain the torque on the electro-motor.

By writing the mass matrix of this system and the stiffness matrix, Matlab software permits the use of the function “eig”, which computes the eigenvalues and eigenvectors of the system. The script for this analysis can be observed in Appendix 3. In Table 3.3 the obtained resonant frequencies of the system can be observed.

	[Hz]
1st Natural Angular Frequency	1.5995
2nd Natural Angular Frequency	30.9904

Table 3.3 Resonant Frequencies of the System

The eigenvalue analysis was performed on the undamped system, thus no decaying amplitude of the vibrations experienced by the two components of the bridge structure is observed. In Figure 3.19, the vibrations of the balance part and the deck, can be observed at the first natural frequency and at the second natural frequency. The balance part and the deck present an in-phase type of vibration at the first natural frequency in contrast to the out-of-phase vibration occurring at the second natural frequency.

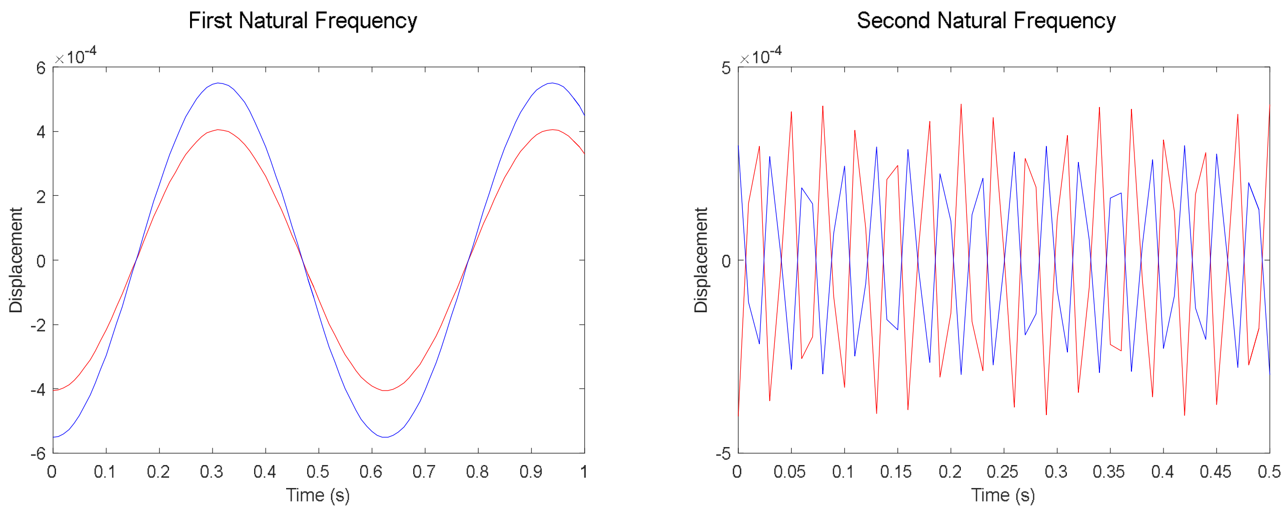

Figure 3.19 Vibrations of the Bridge Structure Components

4. DYNAMIC MODEL VERIFICATION

The results of the model developed in chapter 3.Dynamic Model Development will be analysed in this chapter. Firstly, a description of the performed measurements and the parameters available for the comparison is given. Then, the information necessary from the VOBB and the respective models will be described. Moreover, a short description of the filtering algorithm applied to the model predictions as well as to the measurements is going to be provided. Finally, comparisons will be drawn between the modelled results and the theoretical and measured respective data. The two loading situations will be analysed separately, starting with the parameters characterizing the bridge structure motion and ending with the analysis of the dynamic loads acting on the operating systems of beam balanced bascule bridges.

4.1. Description of the Measurement Campaign

South Holland Province carries out regular maintenance work at bridges that are under its management. Regular recalculations in accordance with VOBB performed during the past few years have shown that the operating systems of these bridges failed. Since the referenced standard is applicable in practice, the question that emerged is how the actual loads on the operating system can be related to this standard.

The province wants on the basis of measurements on a few bridges to develop a framework through which the possibility to deviate from the relevant standard can be justified. Antea Group is measuring the Juliana Bridge in Vianen and comparing those measurements with calculations carried out in the framework of the standard. Techno Physics has been appointed to carry out the measurements. It grants Hollandia assistance and ensures the traffic measures taken, guidance and coordination.

The Juliana Bridge (Figure 1.1) was recently renovated. This is also the reason why this bridge was chosen for this investigation. It is located on the courtyard of the Grand Vianen lock, situated between the Lek and the Merwede. It is a beam balanced type of bascule bridge. Juliana Bridge is operated by two so-called curved racks positioned on either side of the bridge. The bridge is driven by means of a gear unit coupled with an electric motor (Figure 4.1). The gearbox has two output shafts which are linked by two horizontal axes to two bevelled gearboxes. The bevelled gearboxes are then using vertical intermediate shafts connected to each open bevelled gear. The bevelled gear drives drive each a pinion, which then drive on either side of the bridge, the two gear curved racks. The drive further comprises of brake blocks, a flywheel electric motor and the necessary couplings.

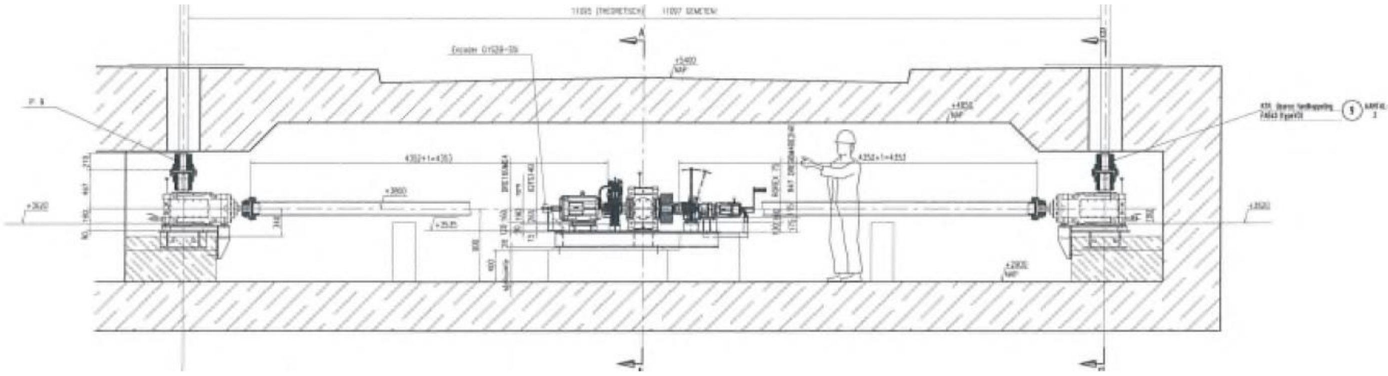

Figure 4.1 Operating System located in the Basement

The following variables and parameters were measured (Figure 4.2):

- The angular rotation of the spanning structure is recorded continuously by means of an angle measurement with an electronic spirit level;
- Motor torque before the brake (during movement cycle and the application of the brake) by means of strain gauges;
- Motor torque after the brake (during movement cycle and the application of the brake) by means of strain gauges;
- Motor speed by means of an infrared transmitter / receiver in combination with a reflector on the shaft ;
- Torque in both horizontal shafts, as close as possible to the motor by means of strain gauges;
- Torque in both vertical intermediate shafts, directly above the corner by means of strain gauges;
- Material stresses in both racks (deformation via strain gauges) in order to calculate the stiffness;
- Electric current, voltage, frequency and power through the drive motor offered by Emerson Industrial Automation;
- Deformation of the spring buffer during the movement cycle by means of an infrared laser;

- Total rotation of the upper side of the vertical shaft relative to the structural frame in an almost closed position, as a result of a well-defined load in order to be able to determine the elasticity of the components;
- The wind speeds are assumed zero, given that there was no wind during the measurements.

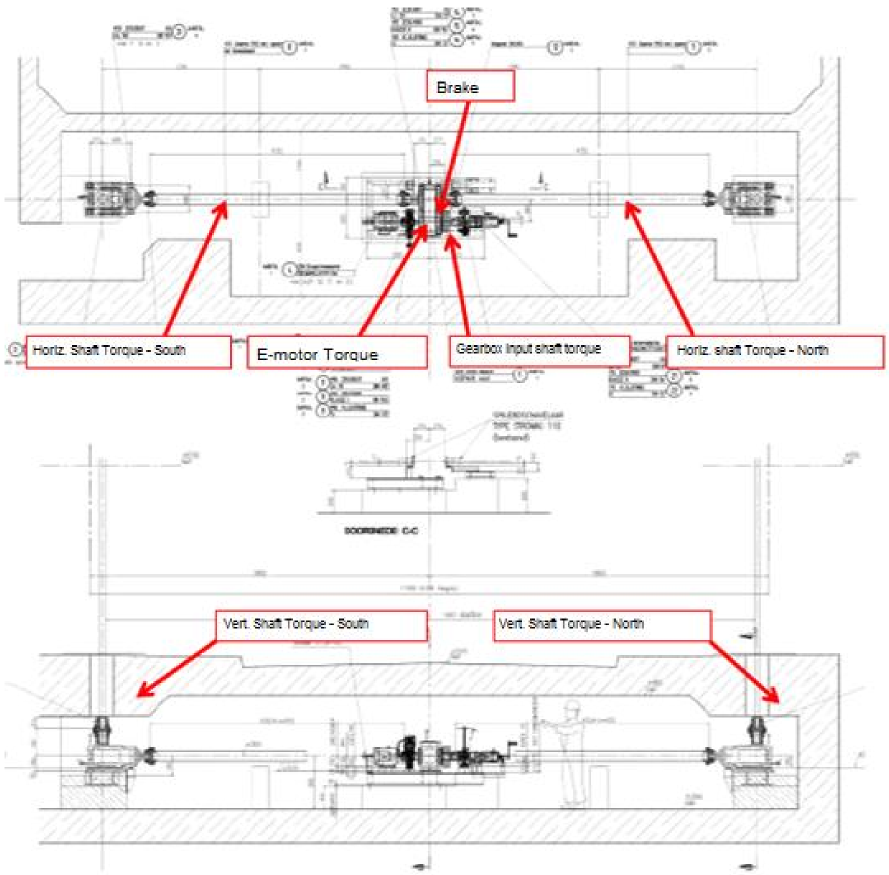

Figure 4.2 Measurement Locations for Various Parameters

In order to get a good impression of the progress of the loads in the operating system calculations according to VOBB are also performed. The theoretical calculations are performed in Mathcad. Here, the measurement results are compared with the calculations in accordance with VOBB.

The variability of the various parameters is accounted for by filtering every measurement sample at every 0.1 seconds. The calculations are carried out synchronously with the same step size, so that graphics can be superimposed. There are totally four computational models. The first calculation model is intended for the determination of the stiffness of the operating system. The second calculation is a calculation in accordance with VOBB for the measured situation. The third calculation takes into account the specific parameters of the bridge. The fourth calculation explains the basic VOBB calculation of the recorded data. The fourth calculation was performed because it became clear during measurements that the right-positioned gear and the gearboxes have extremely high resistance. Furthermore, it appears that the northern spring buffer in the curved rack was not properly functioning. The consequence of this situation is that the unavailability of information for this bridge is far beyond the norm. The standard does not provide requirements when one of the component parts of the bridge does not function properly.

4.2. VOBB Calculation Models

The theoretical calculation models are developed in accordance with the requirements prescribed in the VOBB. The parameters necessary for the comparisons which will be later on drawn have to be derived based on theoretical considerations. These parameters are the following:

- The angular displacement of the bridge structure;
- The angular velocity of the bridge structure;
- The angular acceleration of the bridge structure;
- The electro-motor torque due to the self-weight of the bridge structure;
- The angular displacement of the electro-motor;
- The angular velocity of the electro-motor;
- The angular acceleration of the electro-motor.

The last three mentioned parameters were actually used as input for the developed models (Appendix 1). The first four are going to be used as a theoretical reference, and will be compared with the results obtained from the model. The procedure for deriving the electro-motor torque due to the self-weight of the bridge and the derivation of the theoretical motion parameters of the bridge structure can be seen in Appendix 1.

4.3. Data Filtering

Data filtering has to be implemented in this project for the measurements data and the predictions of the dynamic model. In both cases the data is noisy and a filtering procedure is needed for the comparison between various parameters. The main principle behind data filtering implies that the considered variable is both slowly varying and also corrupted by random noise. Therefore, it is sometimes useful to replace each point with a local average of the surrounding points. The nearby points are quite close to the selected point, thus the averaging can reduce the level of noise without affecting greatly the value obtained.

Savitzky-Golay filter has proven to be a very efficient method for data smoothening. Instead of having the properties defined in a Fourier domain and then translated to a time domain, this filter derives the properties directly from a particular formulation of the smoothening problem in the time domain. Generally, a digital filter is applied to a series of equally spaced data values $f_i = f(t_i)$, where $t_i = t_0 + \Delta \cdot i$ for a constant data spacing Δ . In the simplest type of digital filter, the each data value is replaced by a linear combination of itself and a number of neighbouring points:

$$g_i = \sum_{n=-n_L}^{n_R} c_n \cdot f_{i+n}$$

where

n_L is the number of points situated in the left side of the chosen data point;

n_R is the number of point situated in the right side of the chosen data point.

The average of data points from f_{i-n_L} to f_{i+n_R} is called a moving window averaging and for an equal number of points located left and right of the data point, $n_L = n_R$, the coefficient $c_n = 1/n_L + n_R + 1$ is constant. The idea behind Savitzky-Golay filter is to approximate the data points within the moving window averaging by a higher order polynomial, usually quadratic or quartic. For each data point a polynomial is fit to all $n_L + n_R + 1$ points in the moving window by means of least-squares fitting. The least-squares fitting procedure is repeated for each window.

In Figure 4.3, the difference between the actual (unfiltered) data, the data smoothened by a moving window average filter and the data smoothened by the Savitzky-Golay filter can be observed. It is clear in the last graph that the Savitzky-Golay filter approximates more accurately the data. Moreover, the smoothened data shape is more similar to the shape resulted from the theoretical models of the same variable. In the above image a time span of 0.03125s was employed, and a quartic polynomial for the filter was used. The chosen time span of 0.03125s corresponds to a 32Hz frequency, which is higher than the second natural frequency found for the bridge structure. Although the frequency at which the data is filtered is higher than the second natural frequency of the bridge structure, the applied filter is a low frequency filter which removes all high frequency noise.

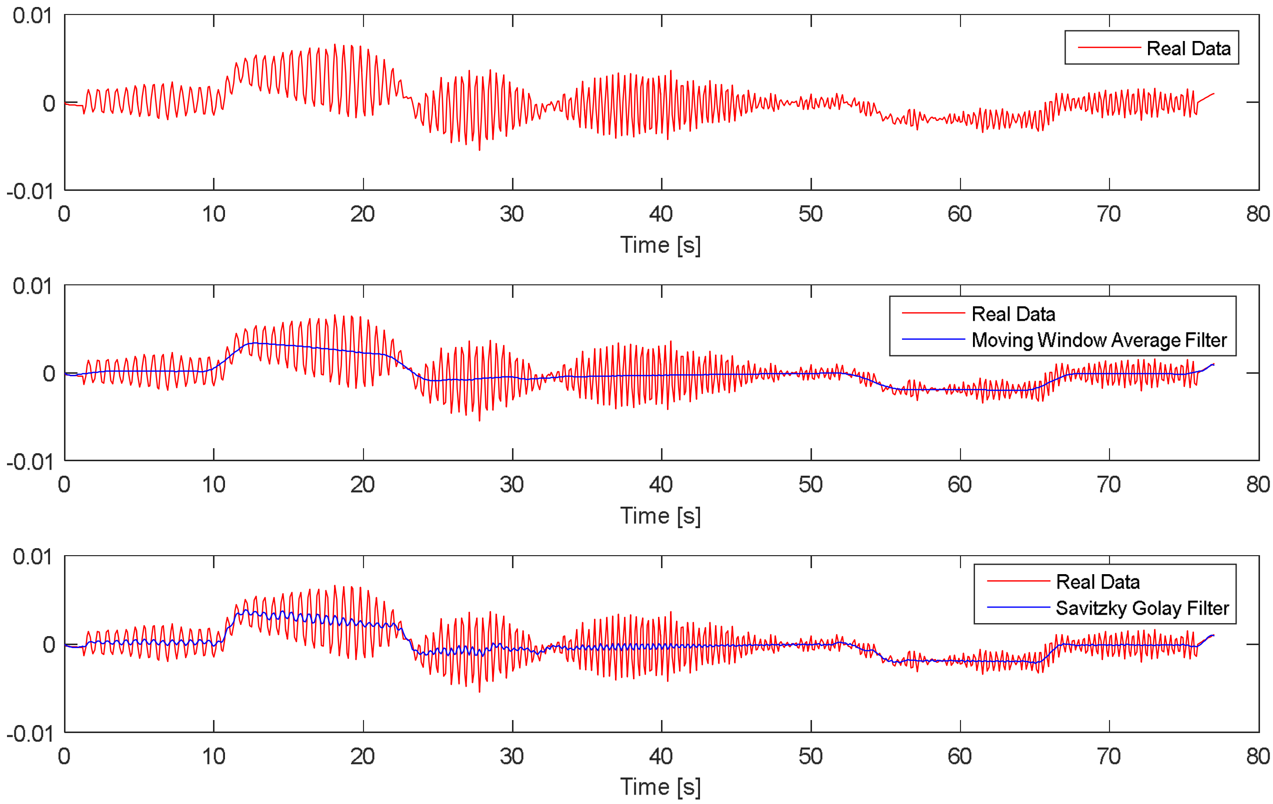

Figure 4.3 Filtering Techniques Comparison

In Figure 4.4 the data smoothening with Savitzky-Golay filter can be observed for different polynomial degrees under the same span of 0.03125s. The results are similar so the quartic polynomial will be chosen for data smoothening in order to reduce the computation time.

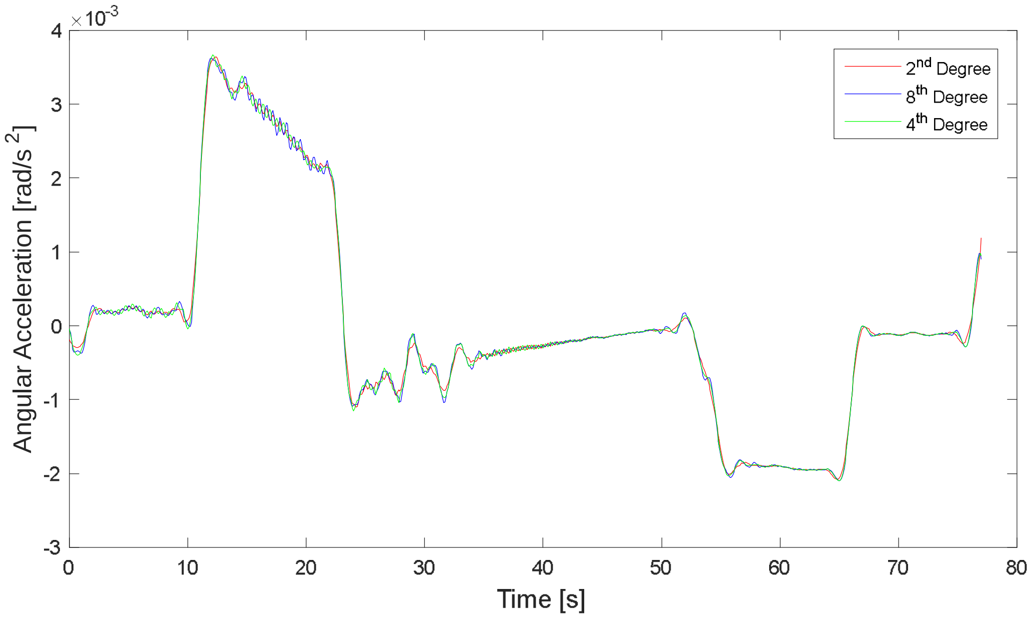

Figure 4.4 Savitzky-Golay Filter for different polynomial degrees

4.4. Model Comparisons with Theory and Measurements

The results from the dynamic model obtained in section 3.Dynamic Model Development will be hereafter compared to the theoretical results and the measurements. The variables to be considered in the comparison are the angular displacements, angular velocities and angular accelerations of the bridge structure and the electro-motor torque. The variables describing the motion of the bridge structure are going to be analysed first in order to adapt them for a curved rack type of operating mechanism. After adapting these variables, the torque acting on the electro-motor is going to be analysed. Firstly, the variables obtained for the normal situation are going to be considered, and afterwards the braking situation is going to be analysed.

4.4.1. Normal Operation

The models obtained for the normal operation will be in this sub-section compared with the theory and measurements. The analysis will start with the comparisons in terms of angular displacement of the bridge structure. Based on the remarks made for the angular displacements and modifications done at each stage, the rest of the variables will be later on analysed. Subsequently, a comparison will take place in terms of the angular velocities of the bridge structure and the angular accelerations. Finally, the focus will be placed on the torque occurring in the electro-motor.

Angular Displacements of the Bridge Structure

- **Theoretical Input Motion Parameters**

The angular displacements of the bridge structure can be analysed either in terms of the angular displacement of the balance part or in terms of the angular displacement of the deck. Firstly, the difference between the two previously mentioned angular displacements due to theoretical input motion parameters is plotted in Figure 4.5. It can be observed that the difference between the two constituent parts of the bridge structure is very small (0.75e-04), which is an expected result. The parallelogram shape of the balance beam bridge is always maintained, thus the angular displacements of the deck and the balance part have to be the same. For this reason, the analysed figures in the next sections will only investigate the balance part.

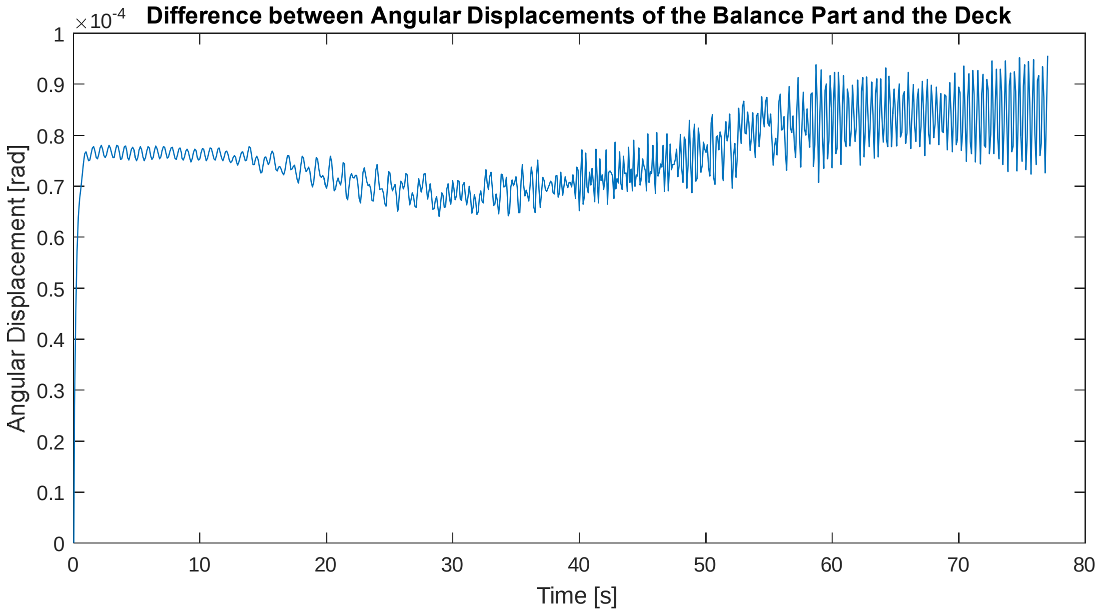

Figure 4.5 Difference between Angular Displacements of the Balance Part and the Deck - Normal Operation - Theoretical Input Motion Parameters

In Figure 4.6 the angular displacements of the bridge structure obtained from the model and the theory are compared. It is noticeable that the model follows a similar shape, but it does not reach the maximum angle that the theory imposes. According to theoretical considerations the bridge should have a maximum opening angle at the end of the opening process of 84° (1.465rad), but the model only achieves a maximum angle of 73° (1.27rad). This is mainly a geometrical problem, due to the fact that the model considers a straight rack, while the theory and the measurements are based on a curved rack type of mechanism. This difference will be accounted for by changing the magnitude of the input motion parameters. The adoption of a straight rack in the model is also observable by the fact that the theoretical angular displacement presents a delay in achieving the upward movement with respect to the model prediction. This delay is also the reason why the maximum theoretical angle is not achieved in the model.

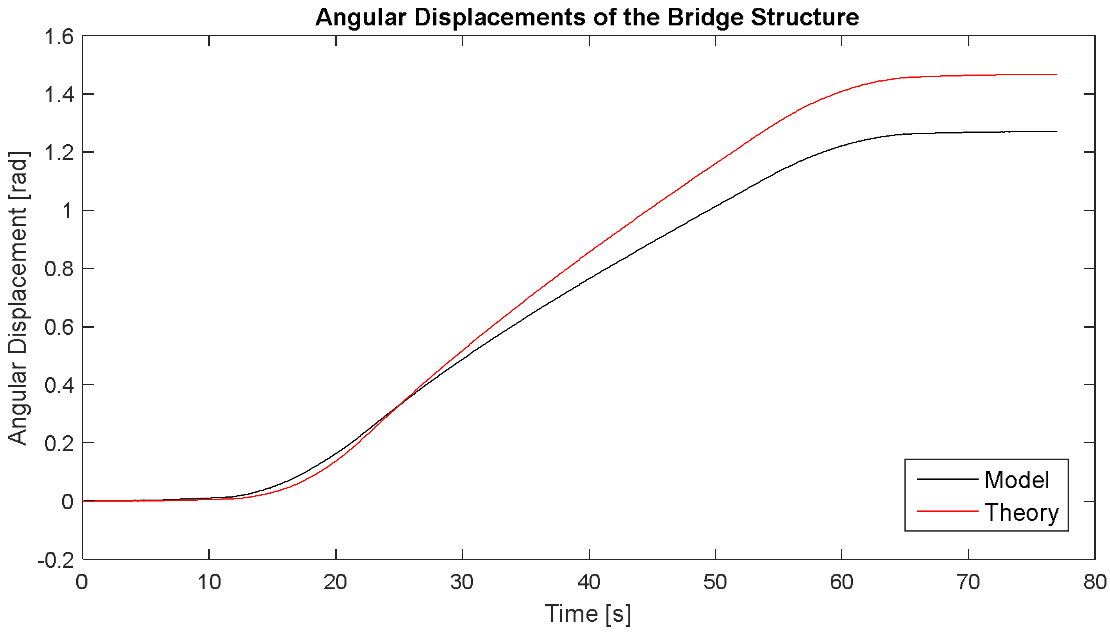

Figure 4.6 Angular Displacements of the Bridge Structure - Normal Operation - Model versus Theory

In Figure 4.7 the angular displacement obtained from the model for both increased input motion parameters and normal input motion parameters is shown. The theoretical angular displacement of the bridge structure is also plotted. The input motion parameters in the model are increased with 16.5% (red line) and 17% (blue line) in order to find the limits between which the maximum theoretical prescribed angle is achieved in the model. A close-up of the maximum opening angle for the increased input motion parameters angular displacement and the theoretical angular displacement is shown in Figure 4.8. It is clear that the bridge structure requires higher motion parameters in order to achieve this maximum angle. Thus, from now on an increase of 16.5% of the input motion parameters will be considered for this situation in order have appropriate comparisons between the theory and the model. In fact, by doing so, the presence of a curved rack in the simplified straight rack model is accounted for indirectly.

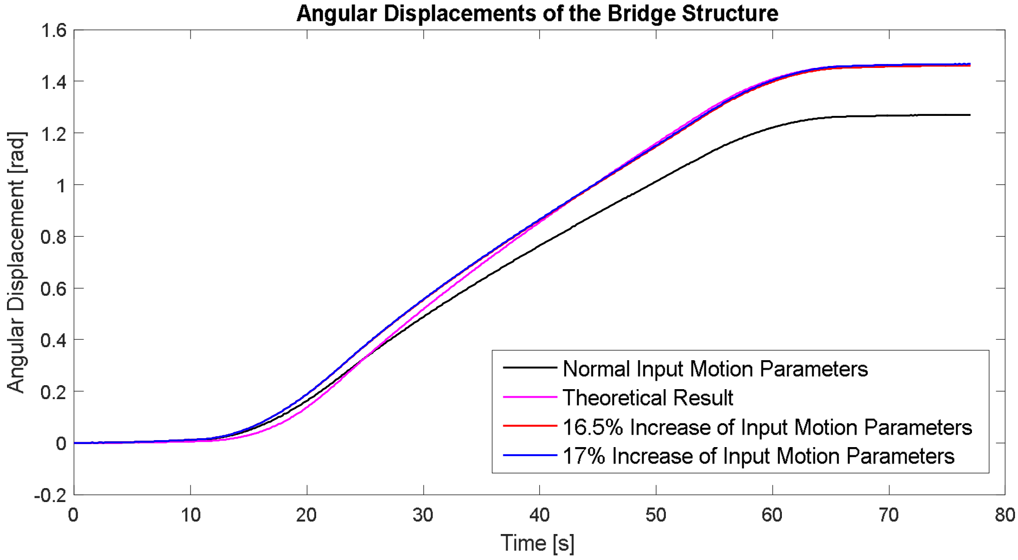

Figure 4.7 Angular Displacements of the Bridge Structure - Normal Operation - Different Theoretical Input Motion Parameters

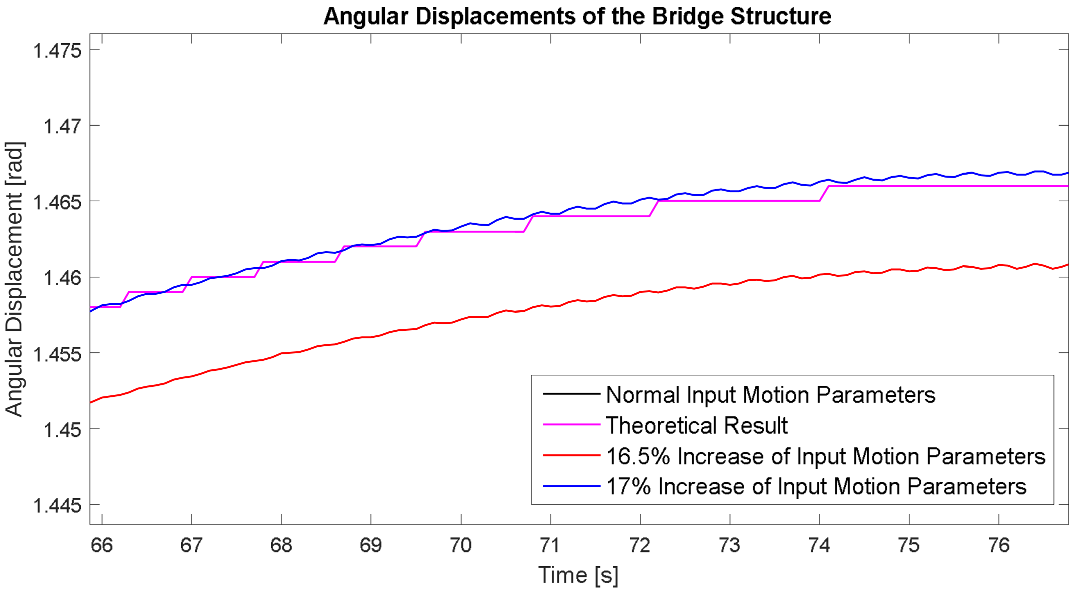

Figure 4.8 Angular Displacements of the Bridge Structure - Normal Operation - Close-up of the Maximum Opening Angle

- **Measured Input Motion Parameters**

Further on, the model obtained from measured input motion parameters is considered. If the difference between the angular displacements of the component parts of the bridge is again analysed, it can be observed (Figure 4.9) that the situation is similar to the previous one. The difference between the angular displacements of the balance part and the deck is again small (0.75e-04) and as before only one of the components suffices for the analysis. The component chosen here is the balance part, which will represent the behaviour of the entire bridge structure.

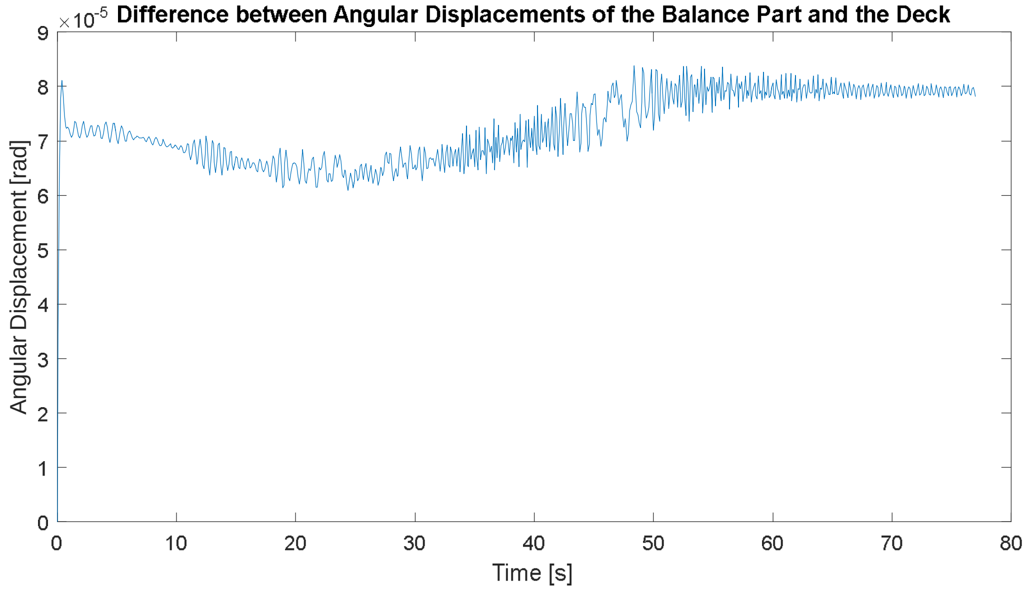

Figure 4.9 Difference between Angular Displacements of the Balance Part and the Deck - Normal Operation – Measured Input Motion Parameters

When the angular displacement of the bridge structure obtained from the model with measured input motion parameters is further analysed with the measured angular displacement of the bridge a difference between the maximum opening angles can be again observed (Figure 4.10). The measured variable attains a maximum value of 82° (1.438rad) at the end of the opening phase, while the modelled structure goes up until 76° (1.336rad). In order to find a maximum value of the angular displacement closer to the measured maximum value, the input motion parameters will be again increased. In case of the model obtained from measured input motion parameters, the upward movement of the bridge is obtained faster than for theoretical input motion parameters. The reason behind this faster upward movement is due to the measured input motion parameters for which the creep period before the acceleration period is much smaller, almost inexistent, when compared to the theoretical input motion parameters. In order to correct this matter, a delay of 10s is applied to the measured input angular velocity of the electro-motor. This delay also helps achieving a behaviour more similar to that of a curved straight rack type of mechanism. The straight rack model considered in this research is indirectly transformed by this delay into a model with a curved rack type of mechanism.

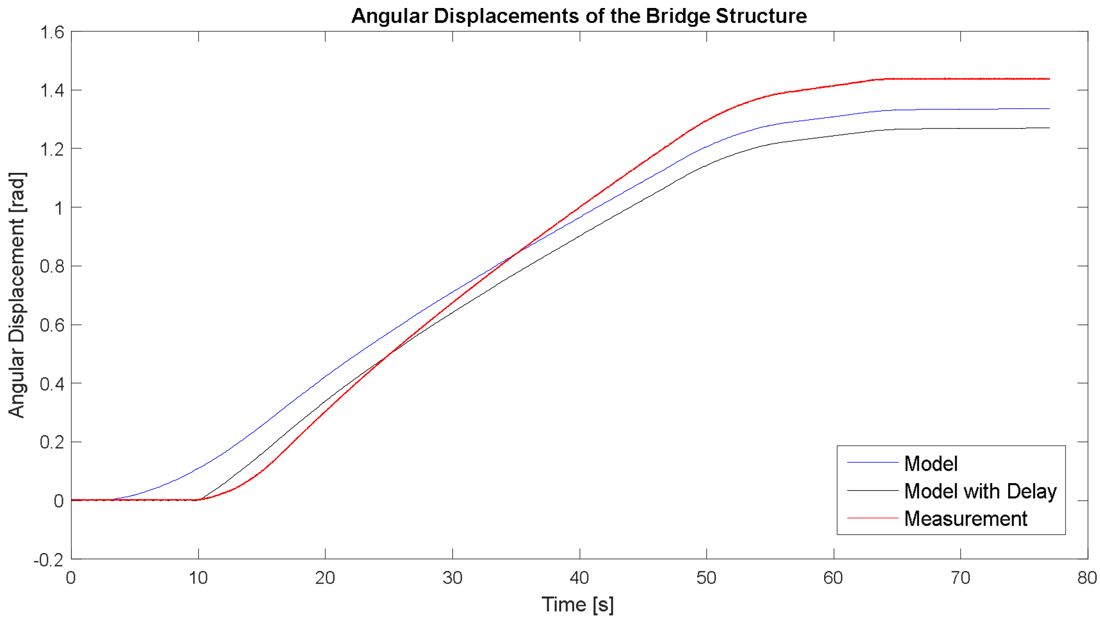

Figure 4.10 Angular Displacements of the Bridge Structure - Normal Operation - Model versus Measurements

Furthermore, an increase of the input motion parameters for the model based on measured input is applied to the model with a delay in order to be closer to the behaviour given by a curved rack type of mechanism. As depicted in Figure 4.11, an increase of the input motion parameters by 15% (red line) and 16% (blue line) positions the maximum measured angular displacement between the two predicted curves.

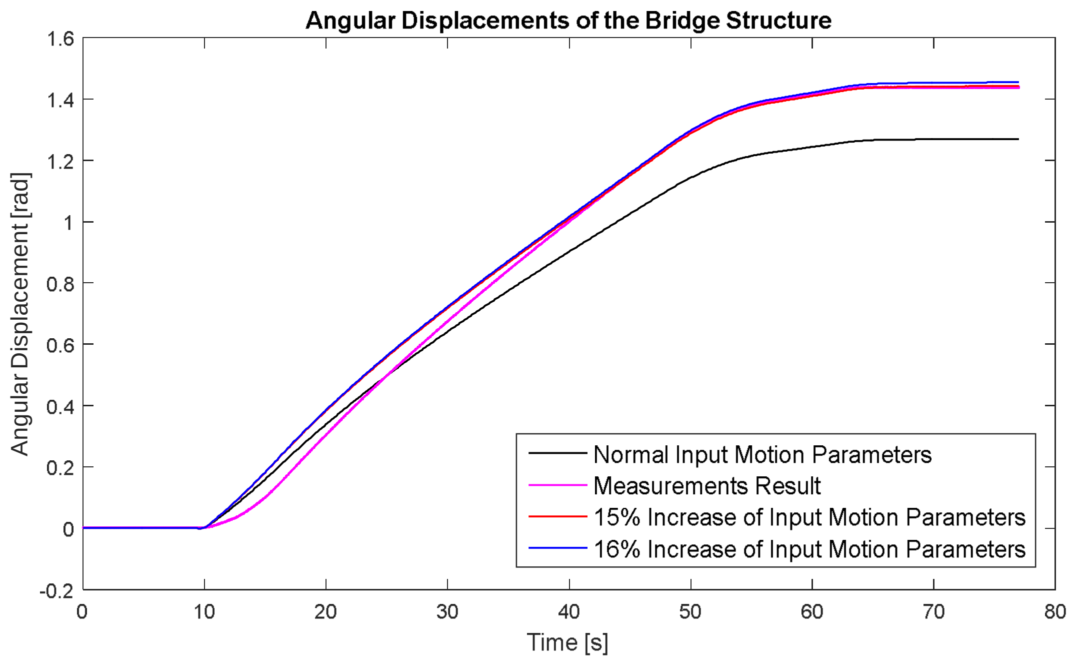

Figure 4.11 Angular Displacements of the Bridge Structure - Normal Operation - Different Measured Input Motion Parameters

A close-up of the maximum opening angle can be observed in Figure 4.12. A 16% increase of the measured input motion parameters would lead to a maximum opening angle of 83° (1.453rad), while a 15% increase leads to a maximum opening angle of 82° (1.435rad). For the following variables both the model with 15%

increase of measured input parameters and a delay as well as the initial model with a delay will be considered.

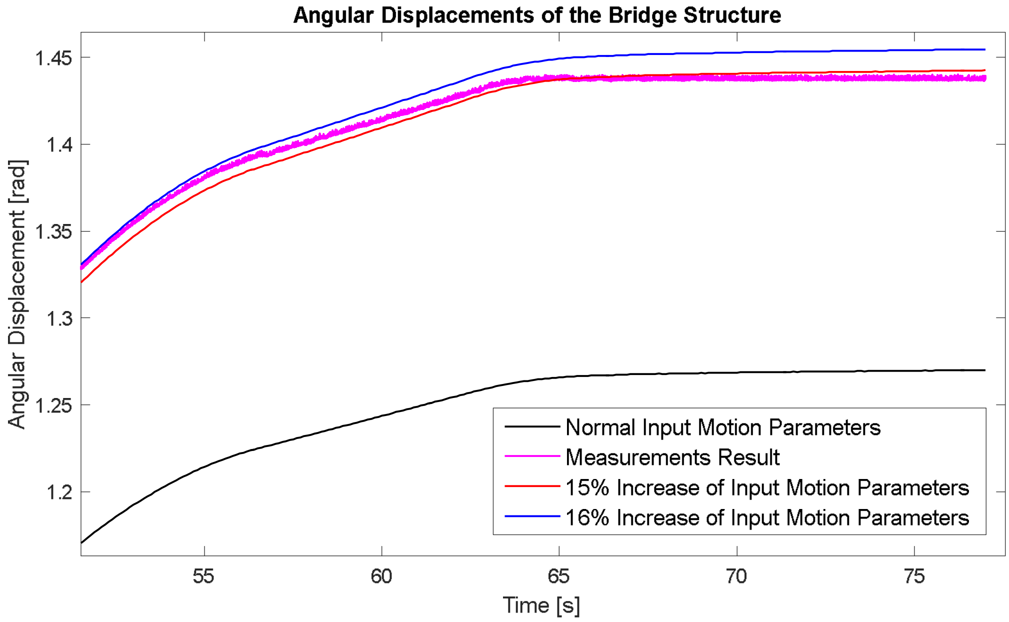

Figure 4.12 Angular Displacements of the Bridge Structure - Normal Operation - Close-up of the Maximum Opening Angle

Angular Velocities of the Bridge Structure

- **Theoretical Input Motion Parameters**

The angular velocity of the bridge structure can be compared both at the level of the deck and at the level of the balance part. For this reason, the difference between the two angular velocities is first analysed. In Figure 4.13 it is observed in the upper graph that this difference is very small, close to zero for the major part of the time span, and with a maximum difference of almost 4e-04 rad/s at two different positions. In order to understand this relative difference, below the graph containing the differences between angular velocities, the angular velocity of the electro-motor is plotted. It can be observed that the angular velocity of the balance part at 30s becomes larger than the angular velocity of the deck, while at 54s it becomes smaller. If at 54s the angular velocity of the electro-motor is also observed, then it can be motivated that just before the start of the deceleration period, the deck has a larger angular velocity as a result of the deceleration input, and then it stabilizes itself around the magnitude of the angular velocity of the balance part. Since the magnitude of this difference is very small, the effect is barely noticeable, and thus unimportant. Further on, only the predictions obtained for the balance part are going to be considered for the comparisons.

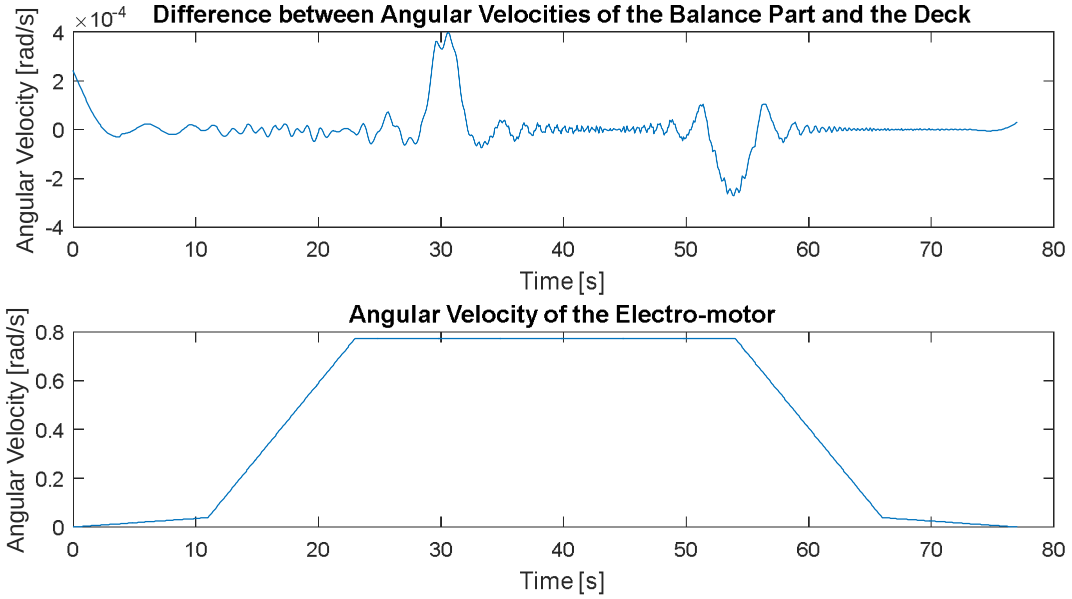

Figure 4.13 Difference between the Angular Velocities of the Balance Part and the Deck - Normal Operation – Theoretical Input Motion Parameters

The angular velocity of the bridge structure as obtained from the model and the one of the bridge structure obtained from the theory can be observed in Figure 4.14. The variable obtained from the model is the one under the real input motion parameters and as in case of the angular displacement it can be seen that the maximum angular velocity given by the theory is not achieved. However, a similar path is followed: it starts with an angular velocity due to creep, followed by an increase due to acceleration, then during the constant angular velocity of the electro-motor a slow decrease of the angular velocity of the bridge is observed, a faster decrease is then noticeable because of the deceleration and it ends with a slow decrease to zero during creep phenomenon.

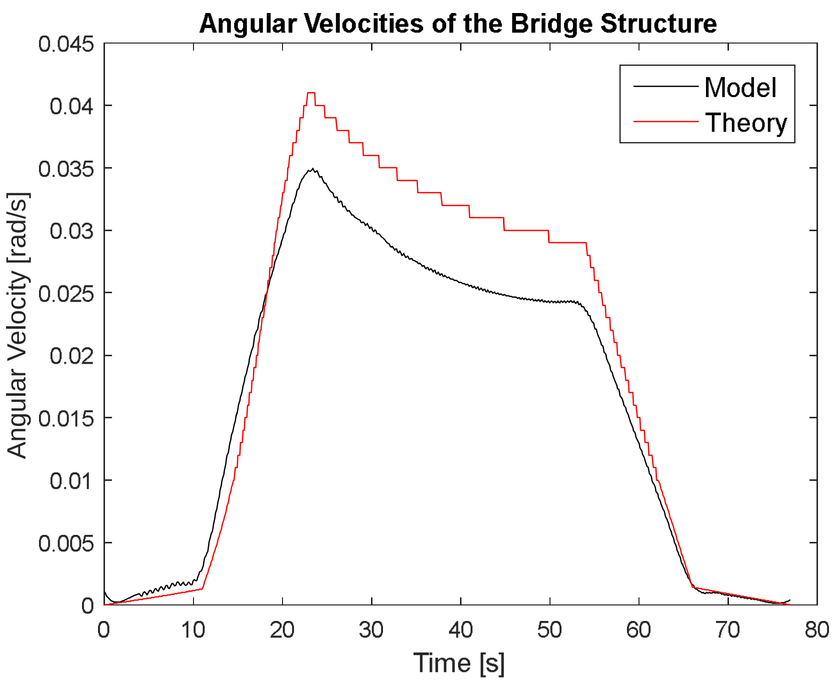

Figure 4.14 Angular Velocities of the Bridge Structure - Normal Operation - Model versus Theory

In Figure 4.15 the angular velocity of the bridge structure from the model is compared to the one from theory for unchanged input motion parameters and for a 16.5% increase of the theoretical input motion parameters. Moreover, the input angular velocity on the electro-motor is also shown as a reference. The normal input motion parameters lead, as previously mentioned, to an angular velocity of the bridge structure lower than the one obtained from theory. However, the increase of 16.5% of the input motion parameters shifts the predictions closer to the theoretical values. For both the bridge structure and the electro-motor a similar shape is observable, but the magnitude of the variables is lower for the former. This is because the rack acts as a transmission element between the operating system and the bridge structure, and it also transforms the motion of a rotating element into a linear motion that lifts the bridge.

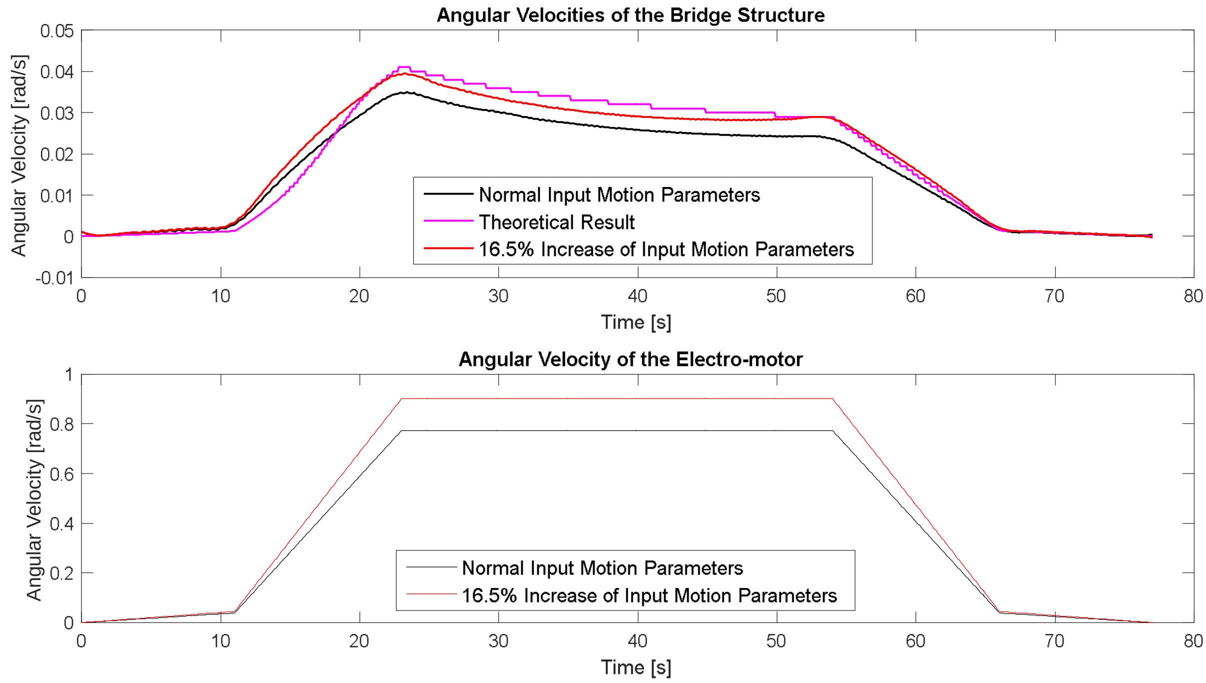

Figure 4.15 Angular Velocities of the Bridge Structure and Electro-motor - Normal Operation - Different Theoretical Input Motion Parameters

- **Measured Input Motion Parameters**

When the results given by the measured input motion parameters are analysed, a very small difference between the angular velocities of the balance part and the deck is present. In Figure 4.16, the difference is plotted and also the measured angular velocity of the electro-motor with the applied 10s delay before accelerating. There is again present a larger relative difference between the deck and the balance part just before the deceleration period, and afterwards the difference is null until the end of the motion. The angular velocity of the balance part will be further on used to draw comparisons with the results obtained from the measurements.

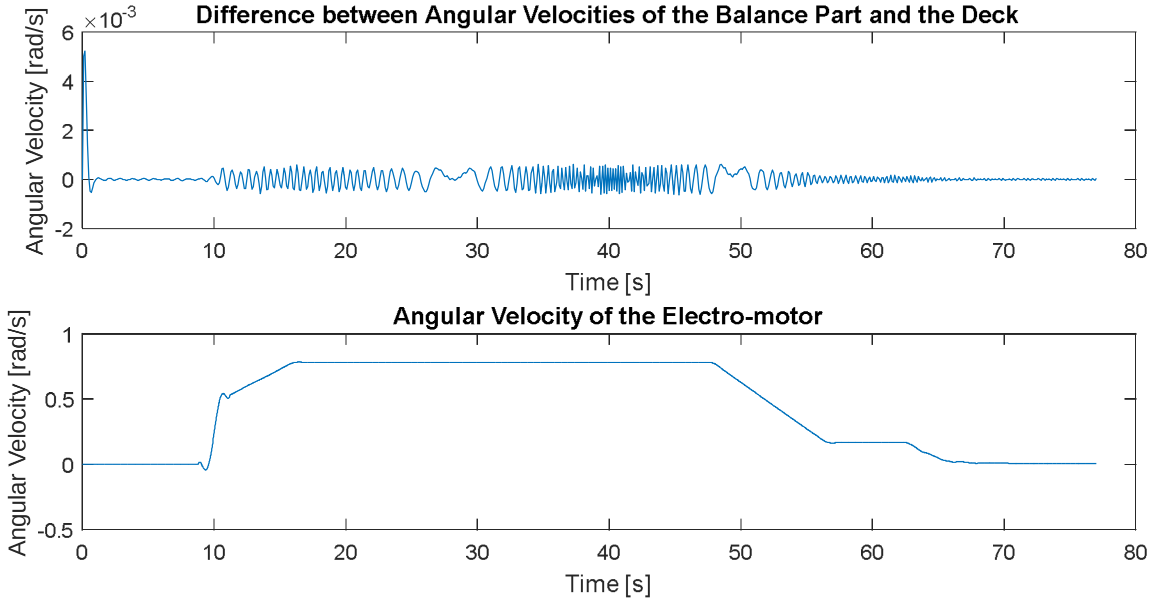

Figure 4.16 Difference between the Angular Velocities of the Balance Part and the Deck - Normal Operation - Measured Input Motion Parameters

In Figure 4.17 the model predictions for the delayed motion are compared with the measurements. The maximum attained angular velocity from the model is around 0.035 rad/s, while for the measurements is at 0.043 rad/s. The angular velocity obtained from the model with a delayed initial motion follows a similar path as the measured angular velocity of the bridge structure. Before 50s, the model predictions have a lower magnitude than the measurements, but after the start of deceleration the angular velocity from the model is again in agreement with the measured one. Between 32s and 45s, an irregularity in the shape of the measured angular velocity can be observed. This is a malfunctioning that occurred during the measurements, due to a temporary wind gust and this irregularity can be ignored.

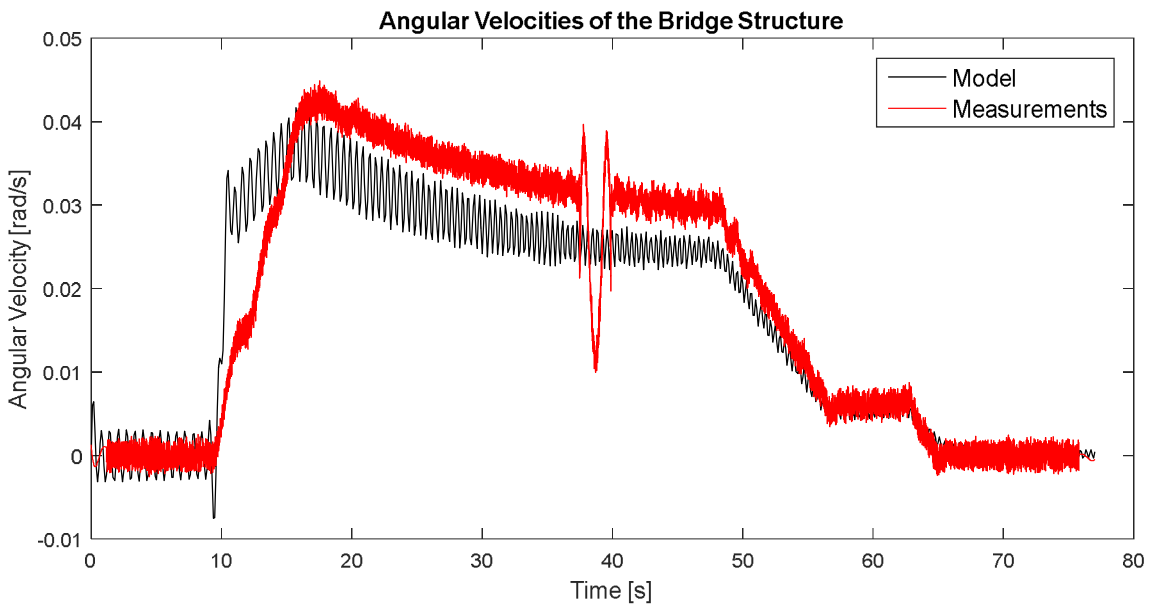

Figure 4.17 Angular Velocity of the Bridge Structure - Normal Operation - Model versus Measurements

Again, with an increase of the measured input motion parameters and the applied delay, the model predictions shift closer to the measurements with respect to the maximum values. In Figure 4.18 the results for different measured input motion parameters can be depicted as well as the input angular velocity. The results of the model are following a similar path as the input angular velocity. An exception is present during the period of uniform electro-motor angular velocity, when the bridge structure does not have a constant angular velocity, but it decreases slowly.

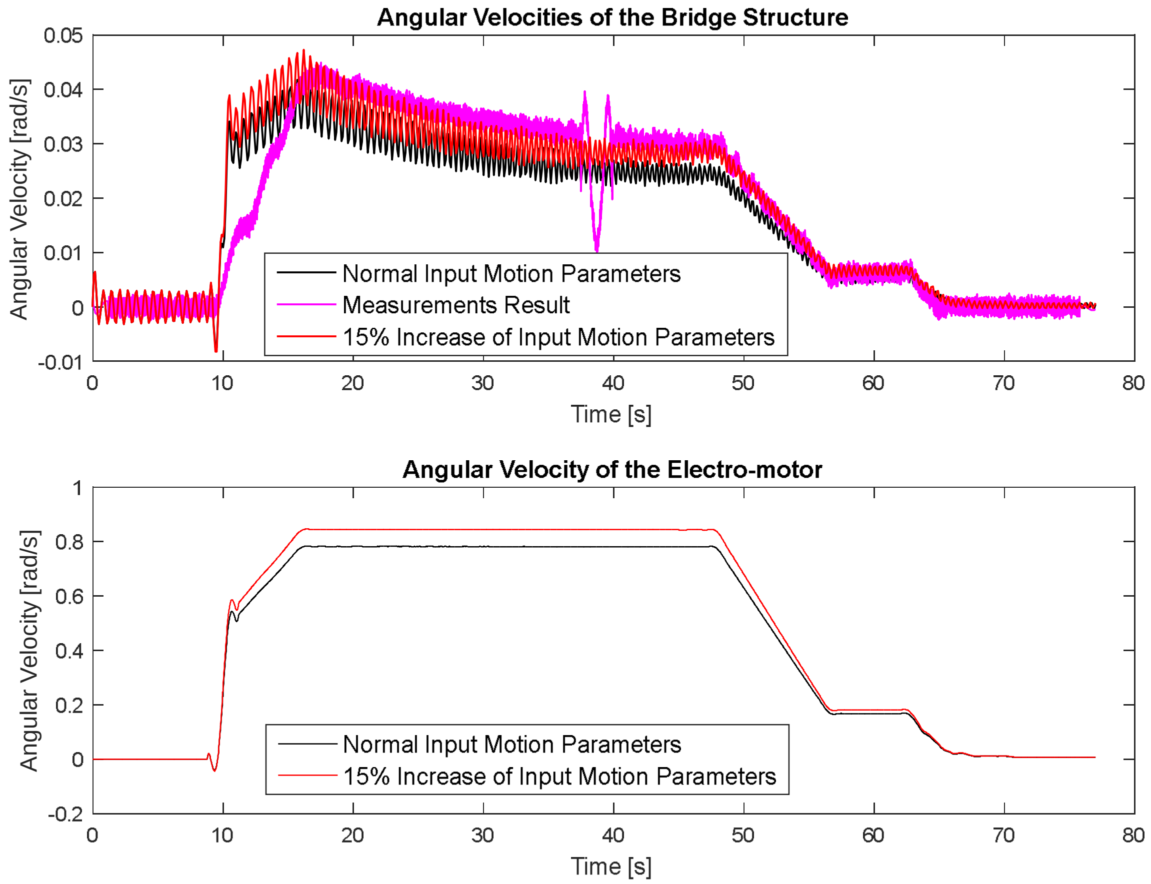

Figure 4.18 Angular Velocities of the Bridge Structure and Electro-motor - Normal Operation - Different Measured Input Motion Parameters

Angular Accelerations of the Bridge Structure

- **Theoretical Input Motion Parameters**

The angular acceleration of the bridge structure is noticeable for both the balance part and the deck. If the difference between the two component parts is analysed for the theoretical input parameters, then a very small variation, close to zero, is observable (Figure 4.19). Thus, only one component, the balance part, is further used to draw comparisons with the theoretical angular acceleration of the bridge structure.

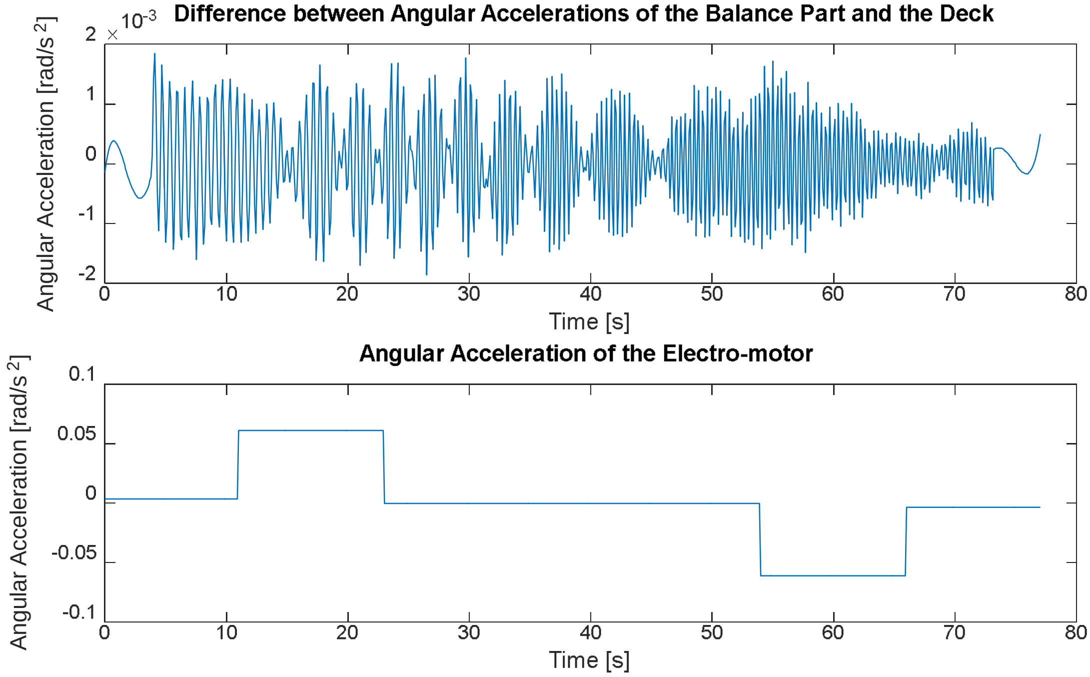

Figure 4.19 Difference between the Angular Accelerations of the Balance Part and the Deck - Normal Operation - Theoretical Input Motion Parameters

In Figure 4.20, the angular acceleration obtained from the model is compared with the theoretical angular acceleration. Overall similarities are present for both graphs: in the beginning there is no acceleration of the bridge, followed by an acceleration in order to lift the bridge up, then almost no acceleration is present during uniform movement of the bridge, followed by a deceleration meant to bring the bridge to a stop and zero acceleration until the end of the operational phase.

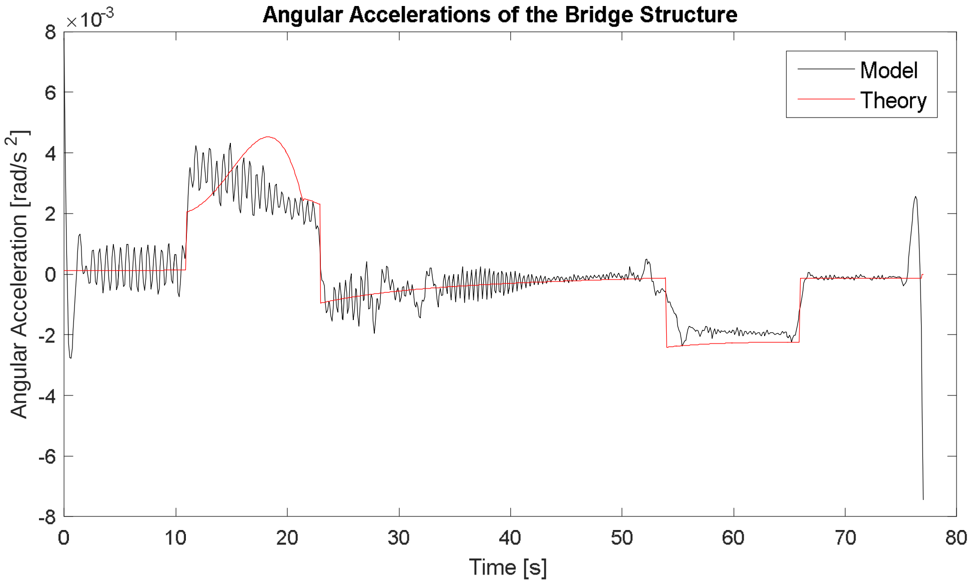

Figure 4.20 Angular Accelerations of the Bridge Structure - Model versus Theory

If the 16.5% increase of the theoretical input motion parameters is applied, then the comparison with the model and the theoretical result can be seen in Figure 4.21. This figure also contains the input theoretical angular acceleration and it can be observed that the magnitude of the input is decreased when looking at the bridge structure. This happens because the rack can also be considered to have a transmission factor, which diminishes the input so that the bridge opens until the prescribed maximum angle.

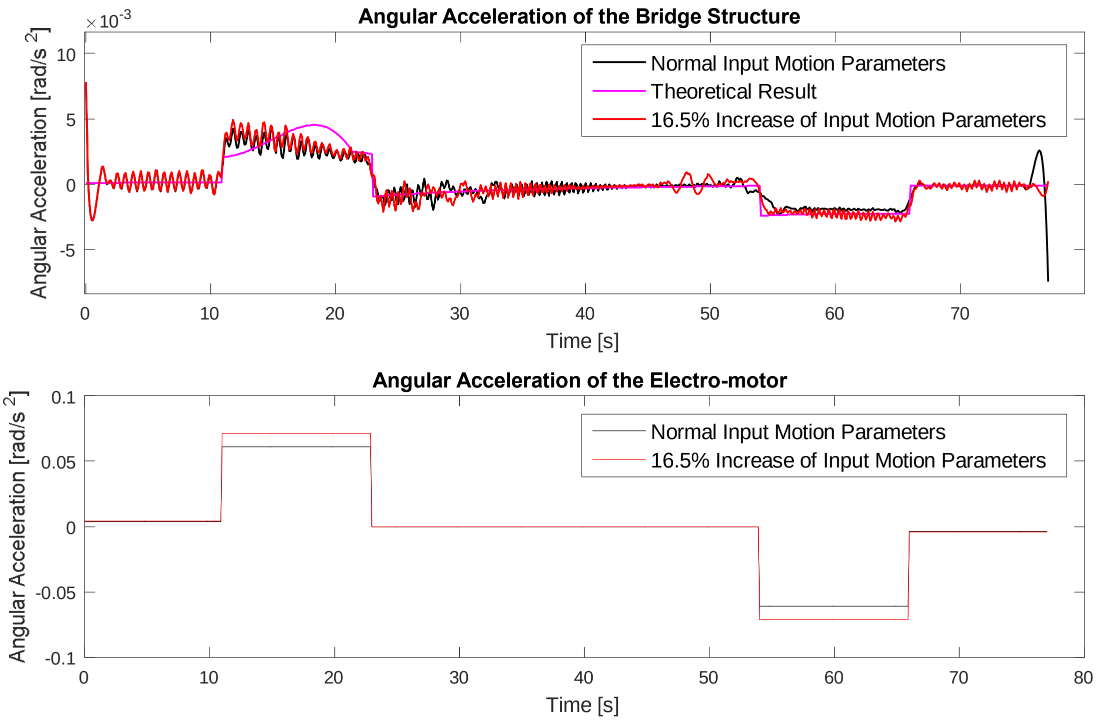

Figure 4.21 Angular Accelerations of the Bridge Structure and Electro-motor - Normal Operation - Different Theoretical Input Motion Parameters

- **Measured Input Motion Parameters**

If the angular acceleration of the bridge structure given by measured input motion parameters with an initial 10s delay is analysed, then the difference between the considered component parts of the bridge structure can be depicted in Figure 4.22. Again, a small variation is observable between the angular accelerations of the balance part and the deck, which is a consequence of the modelling considerations of balanced beam bascule bridges. The parallelogram shape that is maintained during the entire operational phase results in negligible differences between the angular displacements of the balance part and the deck, and in turn results in negligible differences between the angular accelerations. In the beginning, a larger difference relative to the differences along the entire considered period is observable which is mainly caused by the filtering procedure. But the magnitude of the starting acceleration is very small, thus it can be considered null.

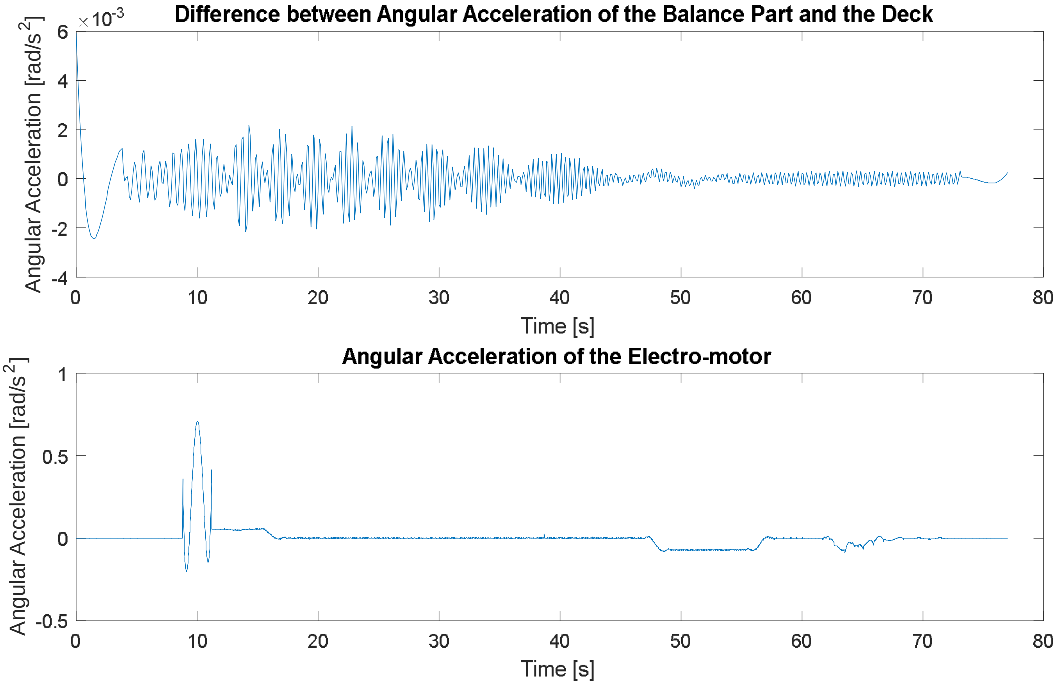

Figure 4.22 Difference between the Angular Accelerations of the Balance Part and the Deck - Normal Operation - Measured Input Motion Parameters

The filtering procedure malfunction can be observed also when looking at the measured data (Figure 4.23). The angular acceleration obtained from the measurements is computed by numerical differentiation. The only measured parameter for the bridge structure is the opening angle, thus through numerical differentiation the angular acceleration of the bridge structure is obtained. The measured angular acceleration of the bridge structure is compared with the angular acceleration obtained from the model with a 10s initial delay, and for the beginning and end of the operational phase an increase or decrease can be observed due to the approximation done by the filter method. These differences are relatively small, and can be considered null. The overall behaviour in terms of angular acceleration is similar for both model and measured data, except some higher vibration peaks present during the acceleration period. The straight rack type of mechanism considered in the model has an influence also here. The model predictions in terms of angular acceleration do not reach the maximum measured angular acceleration of the bridge structure after the deceleration period, thus an increase will be applied to the input. Between 35s and 45s an anomaly in the measured parameter can be observed. This anomaly was also present for the measured angular velocity, and is due to a malfunctioning that occurred during the measurements' campaign. Thus, it can be further on ignored.

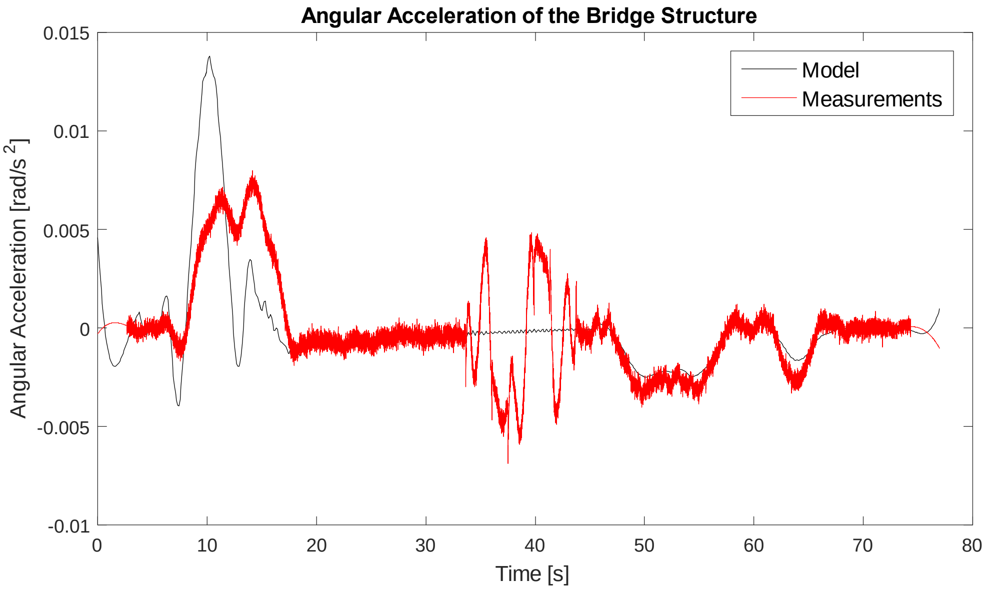

Figure 4.23 Angular Acceleration of the Bridge Structure - Normal Operation - Model versus Measurements

When comparing the results from the measurements with the results obtained from an increase of 15% of the input motion parameters, the difference is barely noticeable (Figure 4.24). The measurements' results depict a higher acceleration in the beginning, then a period of no acceleration, followed by a deceleration of the bridge structure. The model follows the same path, but it has a smaller acceleration in the beginning and continues by matching the measurements' results. Some of the anomalies present in the measurements' data during the period of null acceleration, between 30s and 45s, are due to the subsequent derivation of the measured data, and this anomalies were also observable at the level of the measured angular velocity. Thus, these increases and decreases of the angular acceleration can be neglected.

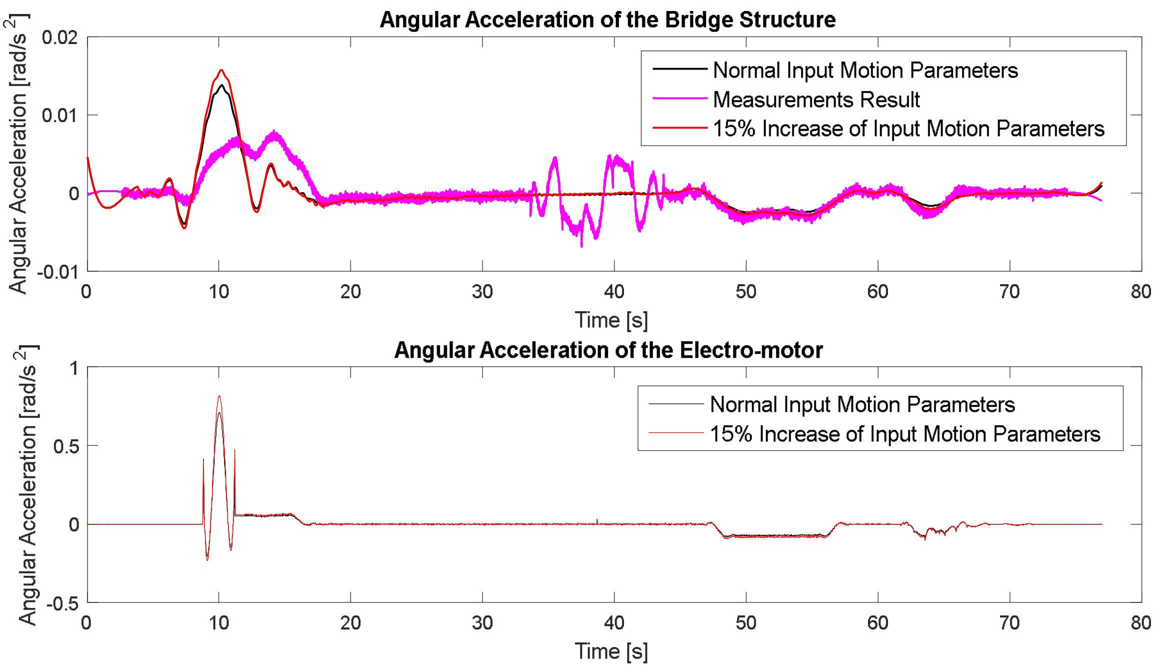

Figure 4.24 Angular Accelerations of the Bridge Structure and Electro-motor - Normal Operation - Different Measured Input Motion Parameters

Electro-motor Torque

After analysing and adjusting the parameters characterizing the motion of the bridge structure, the electro-motor torque has to be found. By imposing the last considered equation of motion and accounting for all the changes of the bridge structure motion parameters, the electro-motor torque obtained from the model can be compared with both the theoretical and measurements' results.

- **Theoretical Input Motion Parameters**

When analysing the theoretical motor torque due to the self-weight of the bridge, even though the torque has a specific shape, the only consideration in the design is given to the maximum value. As depicted in Figure 4.25, a blue line marks the maximum value of the theoretical motor torque due to the self-weight of the bridge structure. Also, the results obtained from the model are plotted, and as it can be observed the magnitude of the torque is always below the maximum design theoretical value. This shows the conservative nature of the theory, which was one of the primary causes behind this research. On the other hand, if the shape of the torque obtained from the model is analysed, then the characteristic torques for electro-mechanical motors can be depicted: an initial torque of approximately 8 Nm, called starting motor torque is observed, then a decrease in the magnitude occurs, when a minimum torque, the pull-up torque, is necessary while the motor tries to acquire full speed, then an increase is observable up to a maximum available torque just before it starts decreasing. If the modelled torque is compared with the theoretical one at the end of this loading situation, then it can be observed that the results from the model with increased motion parameters are close to the theoretical torque due to the self-weight of the bridge. In case of the theoretical comparisons drawn before, the motion parameters of the bridge structure did not present a high delay (approximately 1s) with respect to the theoretically obtained motion parameters. So, if a delay in applying the input motion parameters were to be considered, then the effect would not be observable.

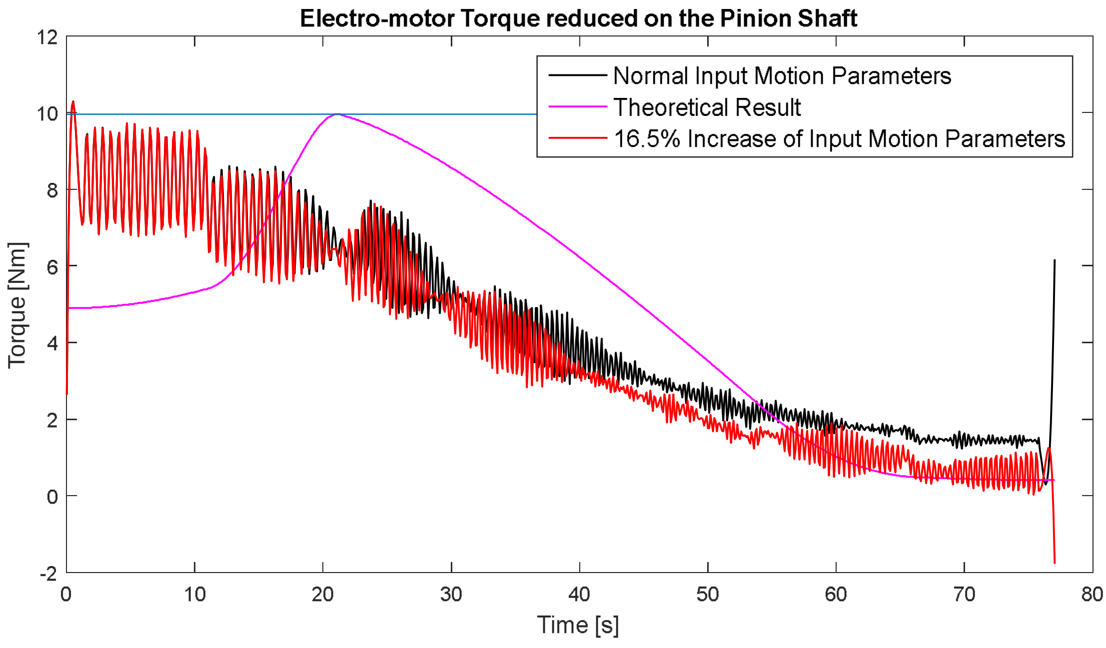

Figure 4.25 Electro-motor torque - Normal Operation - Model versus Theory for different input motion parameters

The typical torques occurring in electrical motors that were previously mentioned can be better depicted in Figure 4.26 when the modelled torque is plotted against the angular velocity of the motor. The plot includes all the data before the deceleration period.

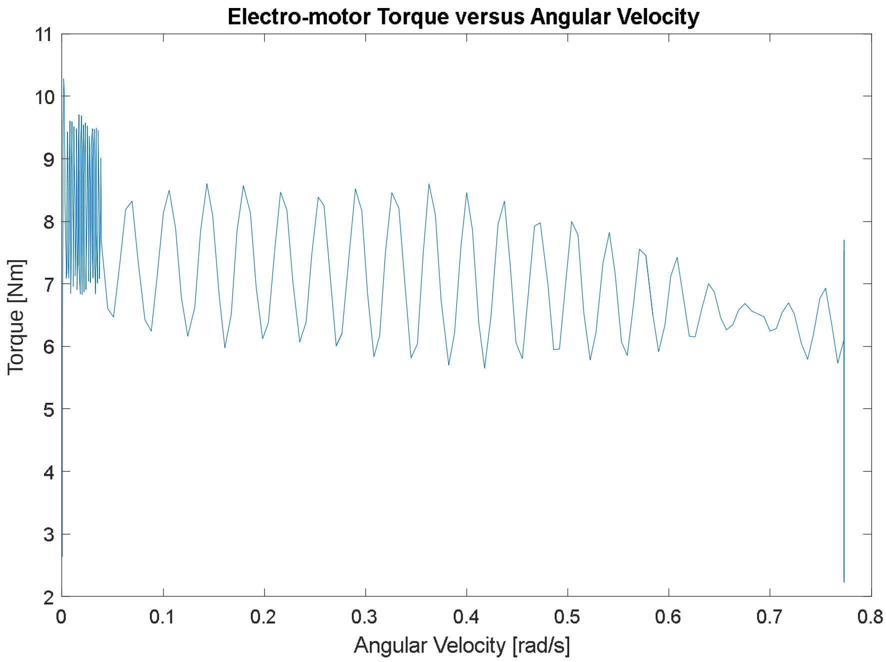

Figure 4.26 Electro-motor torque versus Angular Velocity - Normal Operation - Theoretical Input Motion Parameters

- **Measured Input Motion Parameters**

On the other hand, the measurements' results present more alternatives for choosing the electro-motor torque to be compared. In Figure 4.27 the measured torque on the electro-motor as well as the torque measured on the vertical shafts and reduced to the motor are shown. The torques on the vertical shafts can be taken for the southern part of the bridge, the northern one or for both. In this case, the measured torque from the vertical shaft was considered for only the southern part (red line), for only the northern part (blue line) and for the both parts. Normally, all these measured torques on the vertical shaft would have to coincide, but the malfunction of the southern spring buffer gives rise to differences. So, all of them will be considered. Additionally, there is a discrepancy between the torques on the vertical shaft reduced to the electro-motor and the one on the electro-motor. This is mainly caused by the varying efficiency of the main gearbox, so the consideration of the theoretical efficiency would not be valid in this case. For this reason, the torque measured on the electro-motor will not be considered. The comparisons will be drawn with respect to the measurements performed on the vertical shaft and the reduction of these results to the electro-motor will be done with the theoretical transmission factors and drive efficiency.

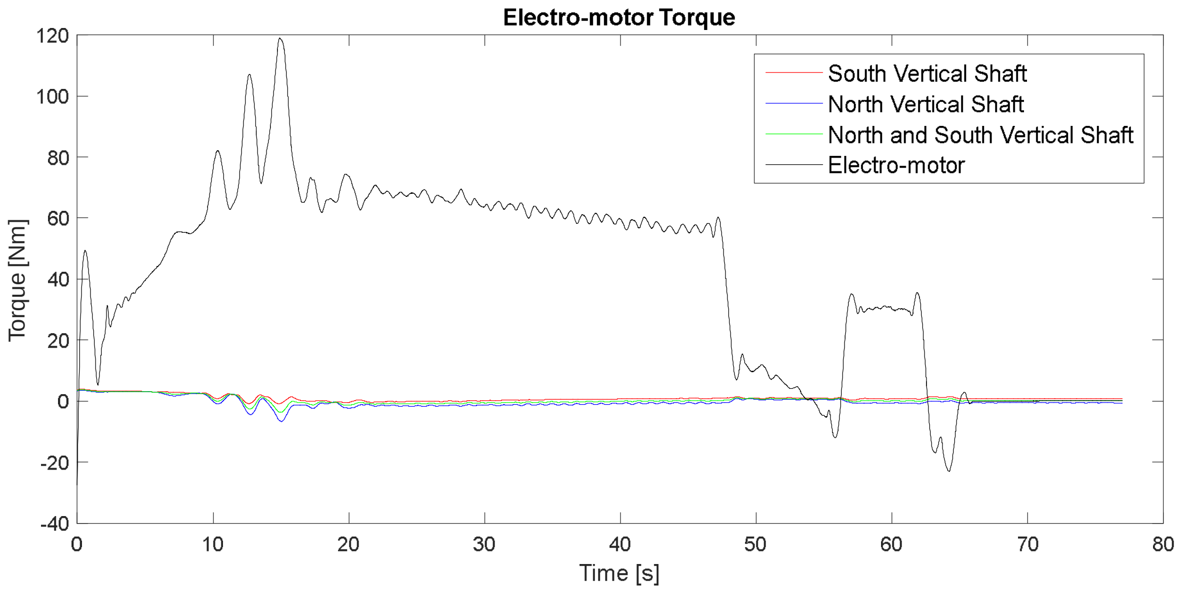

Figure 4.27 Electro-motor Torque - Different Measured Components reduced to the Electro-motor

Now, if the model is to be compared with the measured vertical shaft torques, then Figure 4.28 is enforced. The result from the model is located in terms of values above the measured results, but as it was previously stated the model was below the theoretical results. The initial starting torque obtained from the model with measured input is almost double the one from the measurements. After the initial starting torque, both the measurements and the model show a decrease of the electro-motor torque, however within the period of constant angular velocity (between 15s and 45s) an increase of the measured electro-motor torque is noticed in contrast with a decrease of the electro-motor torque obtained from the model. During the deceleration period, between 45s and 65s, both the model predictions and the measurements behave similarly, ending with magnitudes of the electro-motor torque that are close.

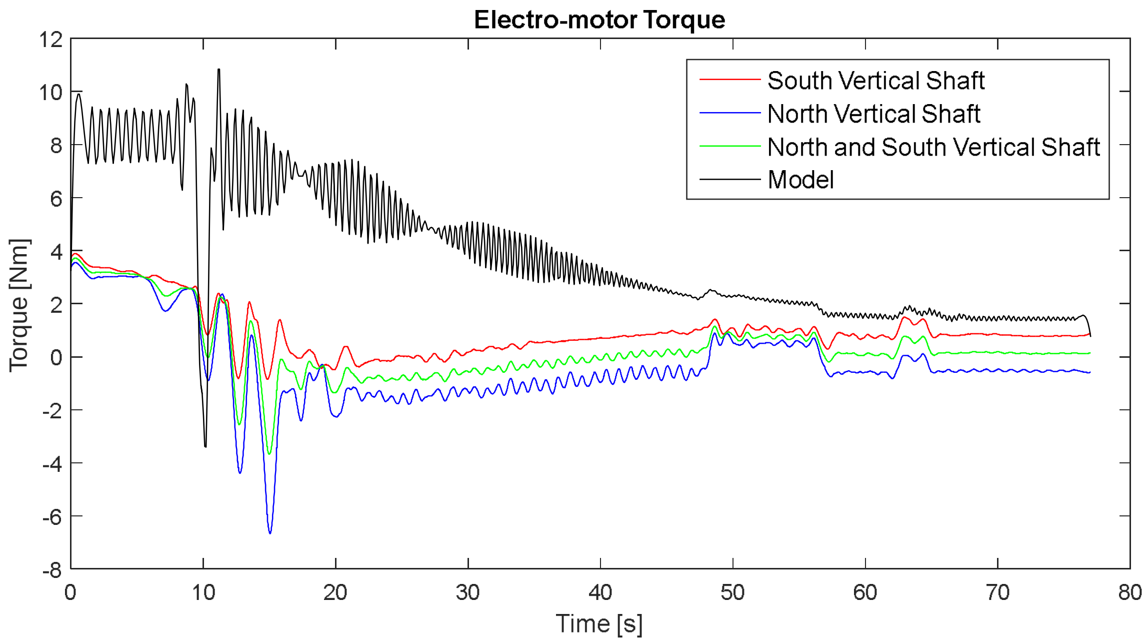

Figure 4.28 Electro-motor torque - Normal Operation - Model versus Measurements

The torques occurring in an electric motor can be better observed when the electro-motor torque is plotted against the angular velocity of the electro-motor (Figure 4.29). A high initial torque required to start the operation is visible in the beginning. Then it decreases to a minimum torque developed by the electric motor when it runs from zero to full speed. At the end of the acceleration period, between an angular velocity of 0.7 to 0.8 rad/s, the torque has a slight increase, which is the moment in which the break-down torque is attained. This is the highest torque at a higher speed that the motor can reach.

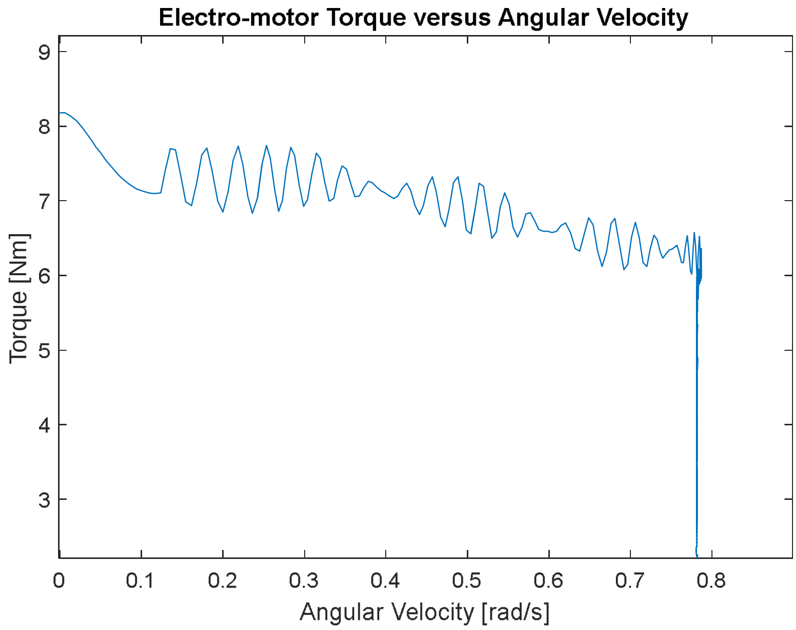

Figure 4.29 Electro-motor torque versus Angular Velocity - Normal Operation - Measured Input Motion Parameters

4.4.2. Braking Situation

In this sub-section the models obtained for the emergency brake situation will be analysed. Comparisons will be drawn between model predictions, theory and measurements. Firstly, the parameters characterizing the motion of the bridge structure will be described and adjusted, and afterwards the electro-motor torque will be analysed. As in case of the normal operation loading situation, the angular displacement, angular velocity and angular acceleration of the bridge structure will be adjusted in order to have a behaviour similar to a curved rack type of operating mechanism instead of the straight rack considered in the model.

Angular Displacements

- **Theoretical Input Motion Parameters**

In case of the model obtained from theoretical input motion parameters, the difference between the balance part and the deck can be observed in Figure 4.30. The magnitude of this difference is of the order of 10e-05, an insignificant value. This allows the consideration of the balance part to describe the motion of the bridge structure. Even though the differences depicted in the figure below are very small, variations can be observed, and of most importance are the ones occurring before and after the braking time of 25s. The application of the emergency brake gives rise to variations in the difference between the angular displacements of the two components, but this difference settles shortly after the brake around a constant value.

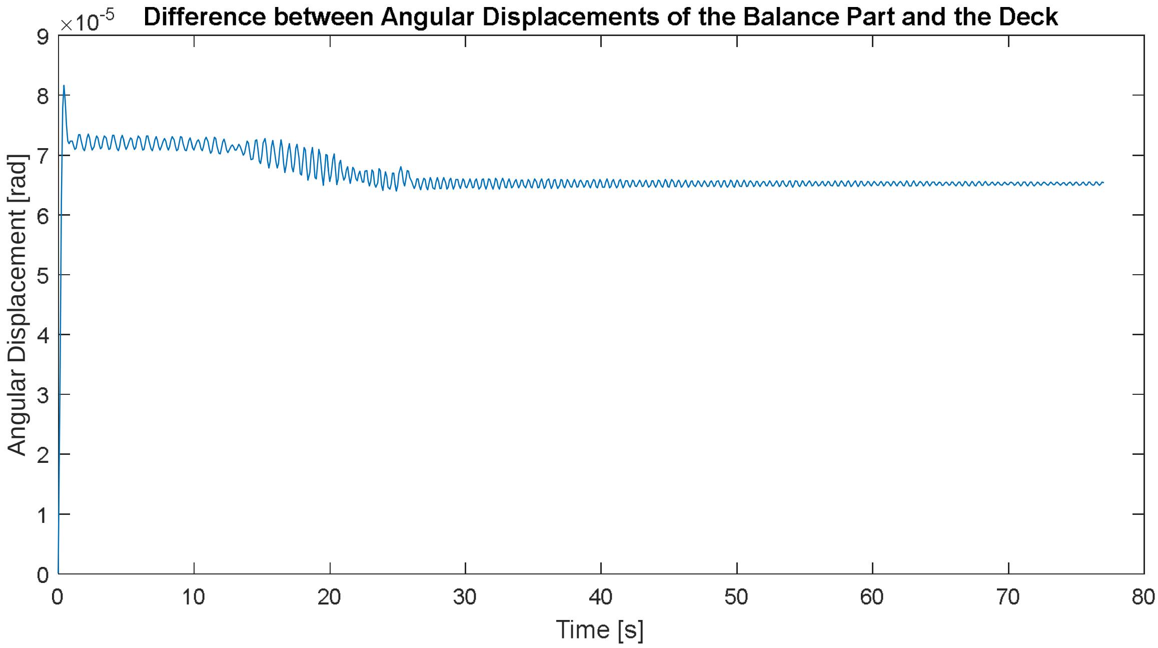

Figure 4.30 Difference between the Angular Displacements of the Balance Part and the Deck - Brake Situation - Theoretical Input Motion Parameters

In Figure 4.31 the angular displacement of the bridge structure obtained from the model and the one from theory for an emergency brake applied at 25s are shown. It can be noticed that the model prediction stops at a lower angle than the theory. This is again due to the modelling of a straight rack instead of the curved rack considered in the theory. In order to correct this, an increase of the theoretical input motion parameters will be applied.

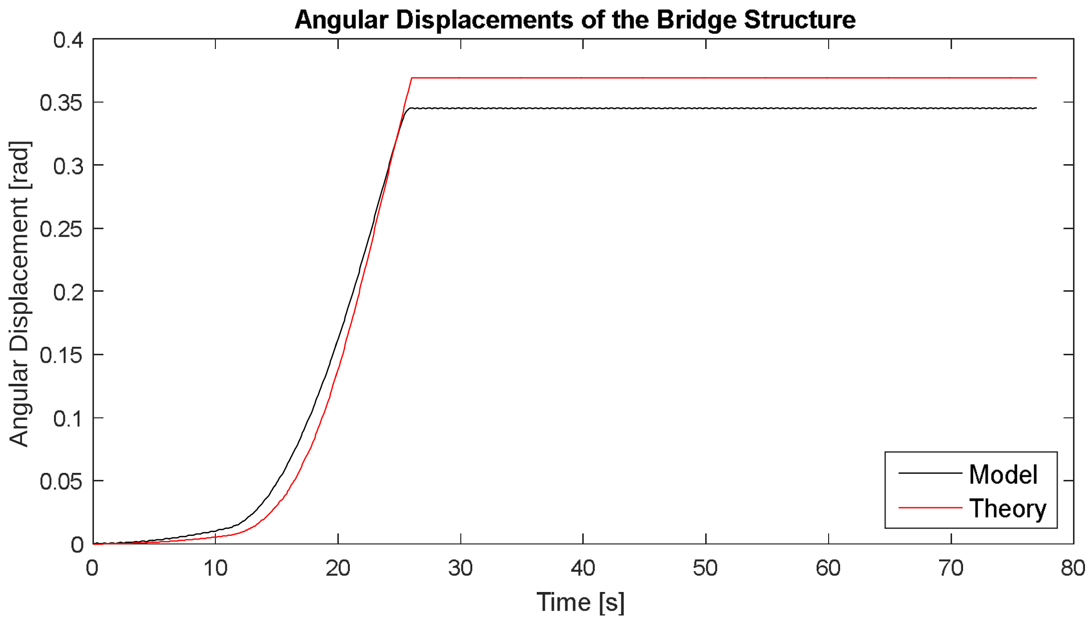

Figure 4.31 Angular Displacements of the Bridge Structure - Brake Situation - Model versus Theory

An increase of the input motion parameters results in an angular displacement obtained from the model closer to the theoretical one. This can be observed in Figure 4.32. The increase of the theoretical input motion parameters of 8% and 9% position the model prediction closer to the theory. For the angular velocity and angular acceleration obtained from the model with theoretical input, the 8% increase will be considered in order to have a more accurate model. This increase accounts indirectly for a curved rack type of mechanism instead of the straight rack considered in the model. On the other hand, if the focus is put on the period close to the braking time of 25s, then it can be observed both in Figure 4.32 and in Figure 4.33 that the bridge structure stops within the limit of 3s prescribed in the VOBB.

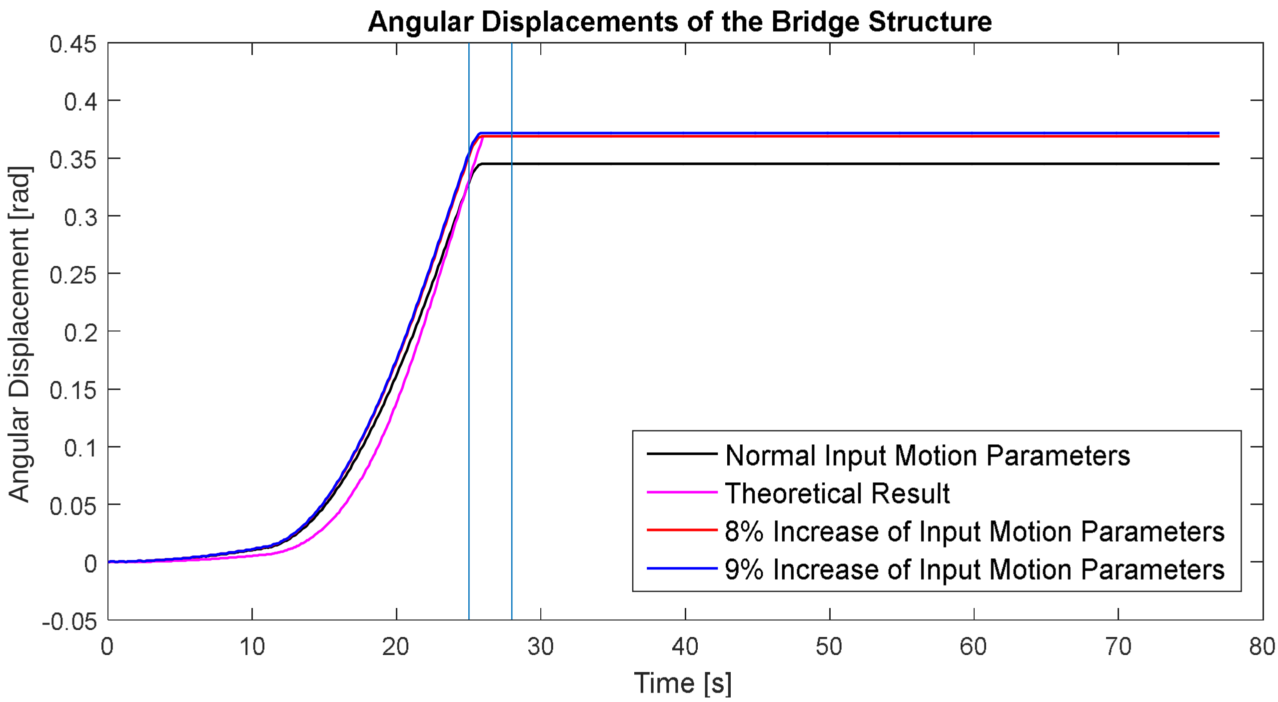

Figure 4.32 Angular Displacements of the Bridge Structure - Brake Situation - Different Theoretical Input Motion Parameters

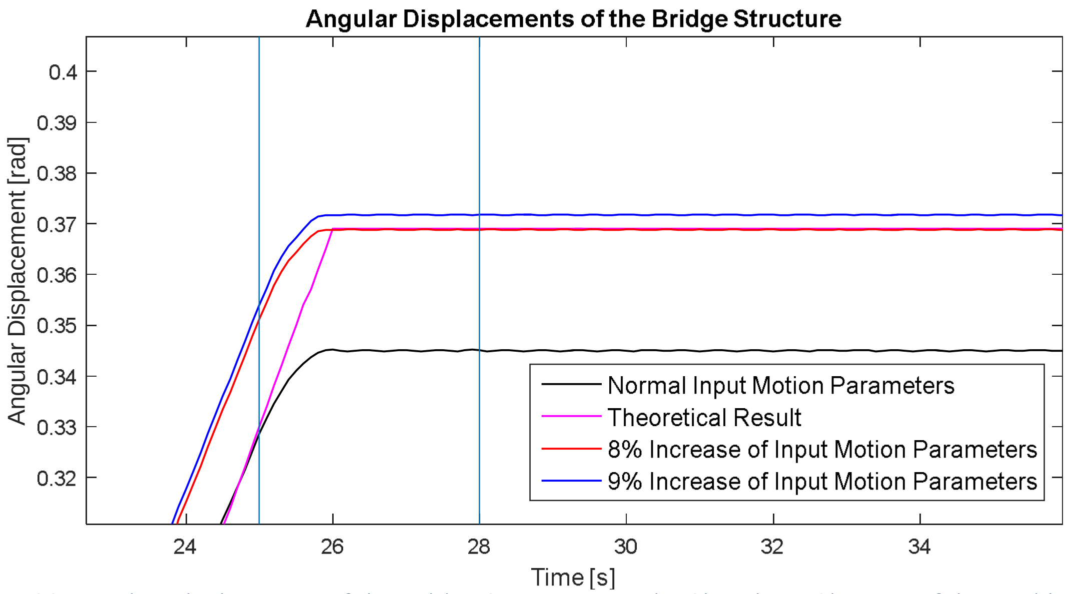

Figure 4.33 Angular Displacement of the Bridge Structure - Brake Situation - Close-up of the Braking Moment

- **Measured Input Motion Parameters**

When the measured input parameters are attributed to the model, the results will differ. In Figure 4.34 the difference between the angular displacement of the balance part and the deck can be depicted. As in case of the theoretical input motion parameters, this difference is very small, 10e-05, which is a negligible value. After the brake is applied, this difference gets stable around a value, showing the bridge has come to a stop. Taking into account these very small differences, it can be assumed that the deck and the balance part behave similarly, and only one of them could be considered for analysing the motion of the bridge structure, more specifically the balance part.

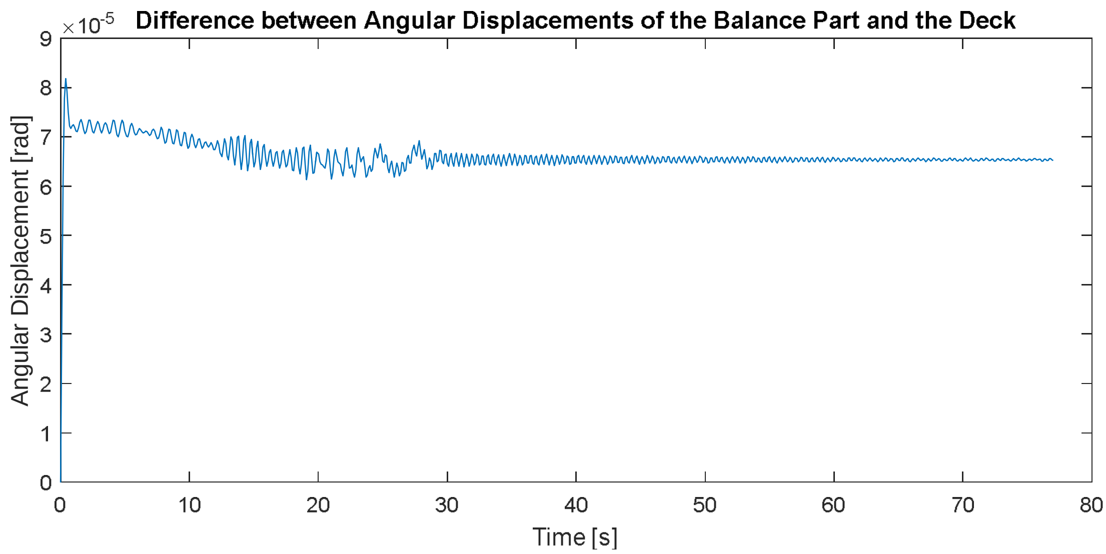

Figure 4.34 Difference between Angular Displacements of the Balance Part and the Deck - Brake Situation - Measured Input Motion Parameters

The comparison between the angular displacement obtained from the model and the one from the measurements can be seen in Figure 4.35. Under the measured input motion parameters, the model stops at a larger angle than the measurements. The influence of the broken spring buffer can be attributed as a cause for this difference. Also, the straight rack operating mechanism adopted in the model has an influence on the maximum angle attained through the model. Moreover, the straight rack affects the beginning of the operation phase by causing the model to lift faster than the measurements. In order to adjust the model in order to behave more like a model having a curved rack type of mechanism a delay of 10s is applied in the beginning.

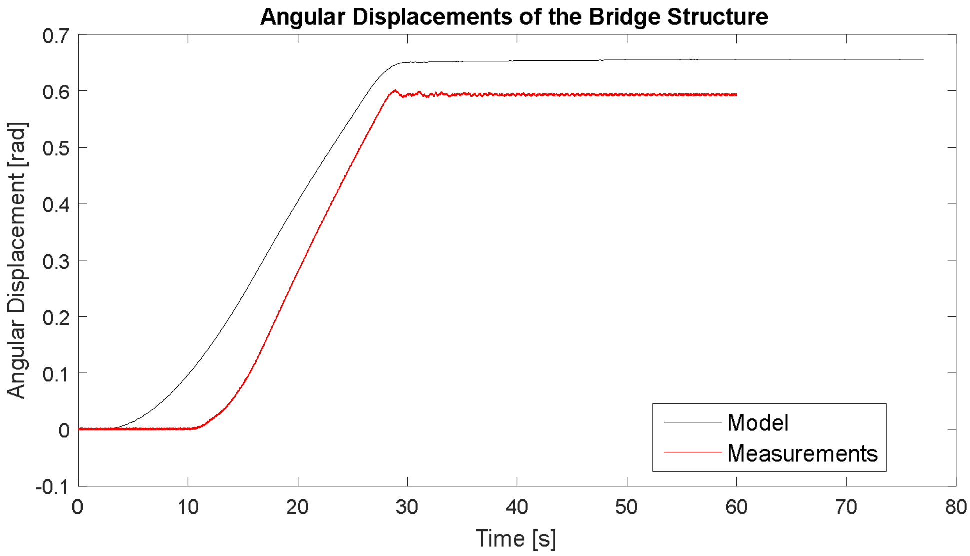

Figure 4.35 Angular Displacements of the Bridge Structure - Brake Situation - Model versus Measurements

The angular displacement of the bridge structure obtained for a delay of the measured input motion parameters as well as the measured angular displacement of the bridge structure can be seen in Figure 4.36. The model with a delayed initial motion (red line) is closer in shape and values to the measured angular displacement of the bridge structure. Unlike the normal operation loading case, there is no need for an increase of the input motion parameters besides this applied delay, because the maximum opening angle is obtained at the same level for both the measurements and the adjusted model. A close-up of the moment when the emergency brake is applied can be observed in Figure 4.37. The vibrations of the bridge structure measured angular displacement are more evident in this figure. The model is respecting more accurately the requirement of stopping within the 3s time limit after the application of the brake, and the vibrations are much smaller. This is a more desirable outcome, and if a measurement of a fully functional bridge would be considered, then this magnitude of the vibrations would be expected.

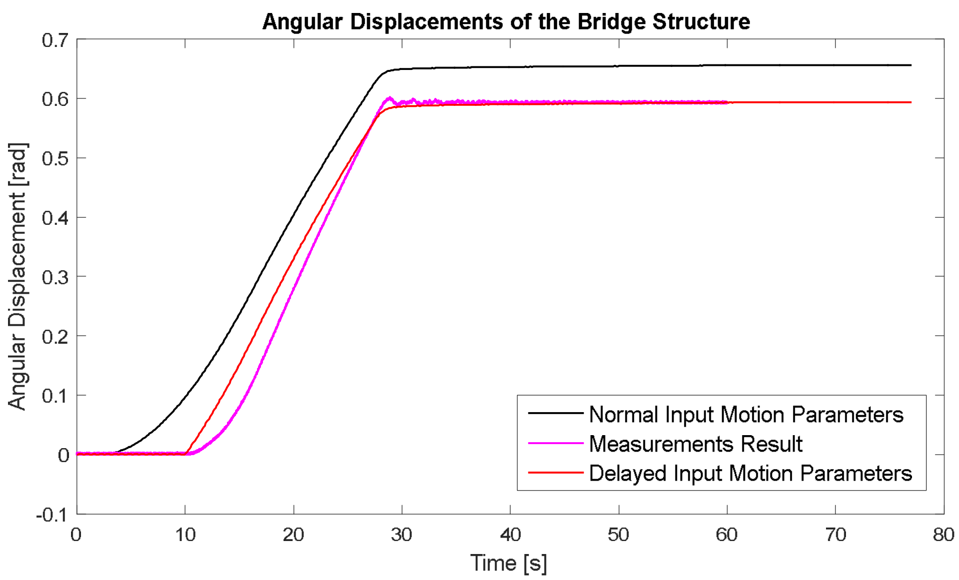

Figure 4.36 Angular Displacements of the Bridge Structure - Brake Situation - Different Measured Input Motion Parameters

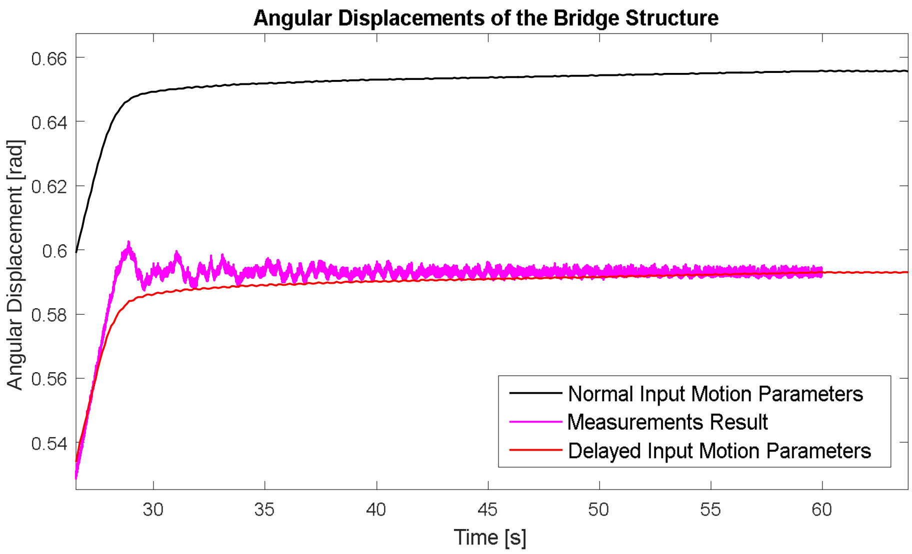

Figure 4.37 Angular Displacements of the Bridge Structure - Brake Situation - Close-up of Maximum Opening Angle

Angular Velocities

- **Theoretical Input Motion Parameters**

The difference between the angular velocities of the balance part and the deck obtained from theoretical input motion parameters can be observed in Figure 4.38. Moreover, the input theoretical velocity is plotted in order to observe the moment of the brake application. The magnitude of the differences is not very large, even negligible, 10e-03, but some variations can be observed especially before a uniform input angular velocity and in the period close to the application of the emergency brake. The moment in which the full speed is acquired by the electro-motor gives rise to a small variation between the parameters characterizing the balance part and the deck. Firstly, the deck will feel the effect of a uniform speed, and the balance part will tend to move faster. But this effect is immediately counteracted and a decrease of the difference is observable, with the deck having a short increase of the angular velocity. Then, the brake is applied, and again the deck is the one that will be affected first. The balance part is afterwards experiencing a decrease of the angular velocity with respect to the deck in order for the two to behave as a whole. Afterwards, the two components of the bridge structure start acting together, with the difference between the two angular velocities getting constant around a null value, implying also that the bridge has come to a stop. The small difference between the angular velocities of the two components permits the consideration of a single parameter to characterize the motion of the bridge structure. The component chosen here to characterize the motion of the bridge structure is the balance part.

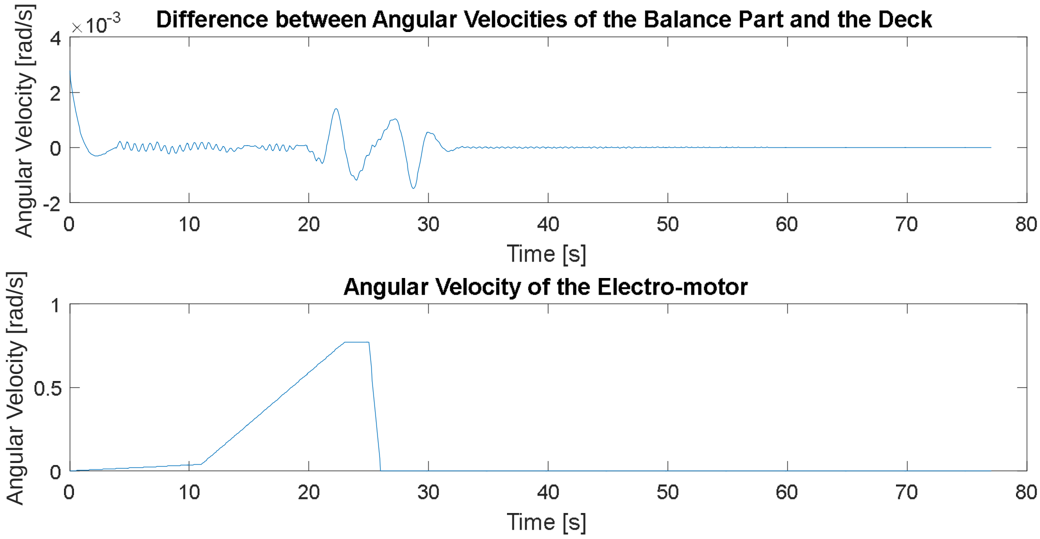

Figure 4.38 Difference between the Angular Velocities of the Balance Part and the Deck - Brake Situation - Theoretical Input Motion Parameters

In Figure 4.39 the angular velocity of the bridge structure obtained by modelling and the one from theory are plotted. It can be observed that the theoretical angular velocity experiences no vibrations after the brake, while the model has some small vibrations before it stabilizes around the null value. It is clear that some variations are expected after the brake, so the conservative nature of the theory can be again observed in this case. The maximum theoretical angular velocity is larger than the one obtained by modelling. This is caused by the straight rack type of operating mechanism adopted in the model, in contrast with the curved rack type of mechanism used in the theory. In order to adjust the model so that it behaves similar to a curved rack type of mechanism, an increase of the input motion parameters will be applied.

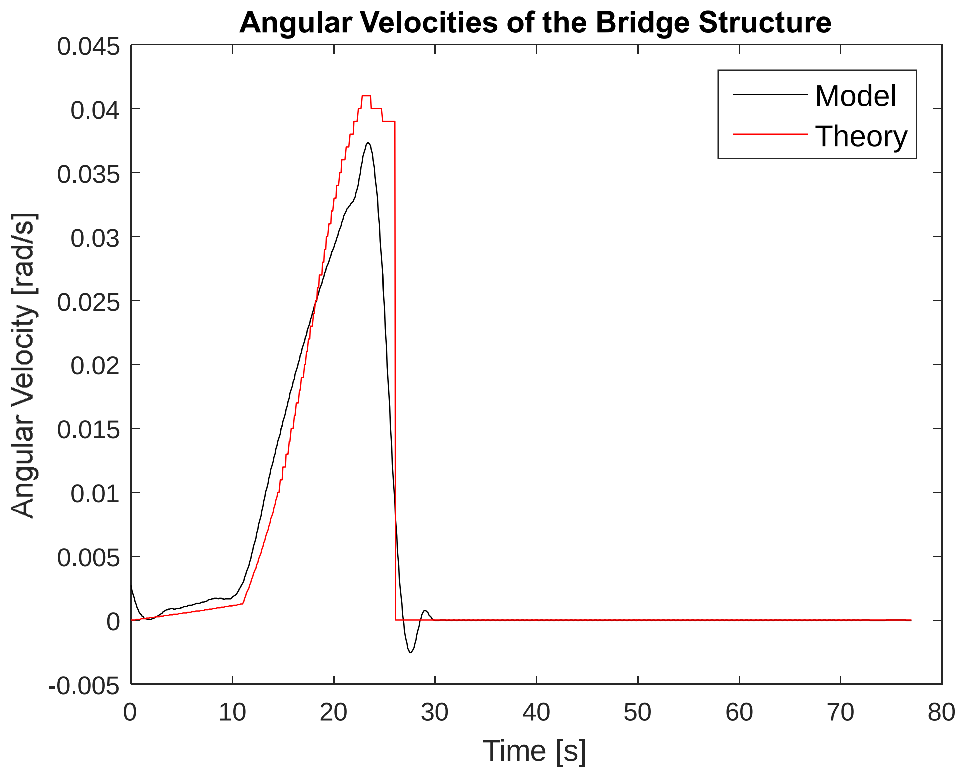

Figure 4.39 Angular Velocities of the Bridge Structure - Brake Situation - Model versus Theory

Figure 4.40 shows the angular velocity obtained for different theoretical input motion parameters and the one obtained from the theory. The angular velocity obtained from the model with an 8% increase of the input theoretical motion parameters comes closer to the maximum theoretical angular velocity. Moreover, the period between the time of application of the brake and the required time during which the bridge has to come to a stop is delimited by the blue lines in the plot. The input motion parameters are set to achieve a zero angular velocity in 1s, while the model predictions and theoretical angular velocity have to become null within 3s. Thus, it can be observed that the angular velocity obtained from the model achieves zero value within this time frame, however it has some small vibrations around the zero value for an additional 5s.

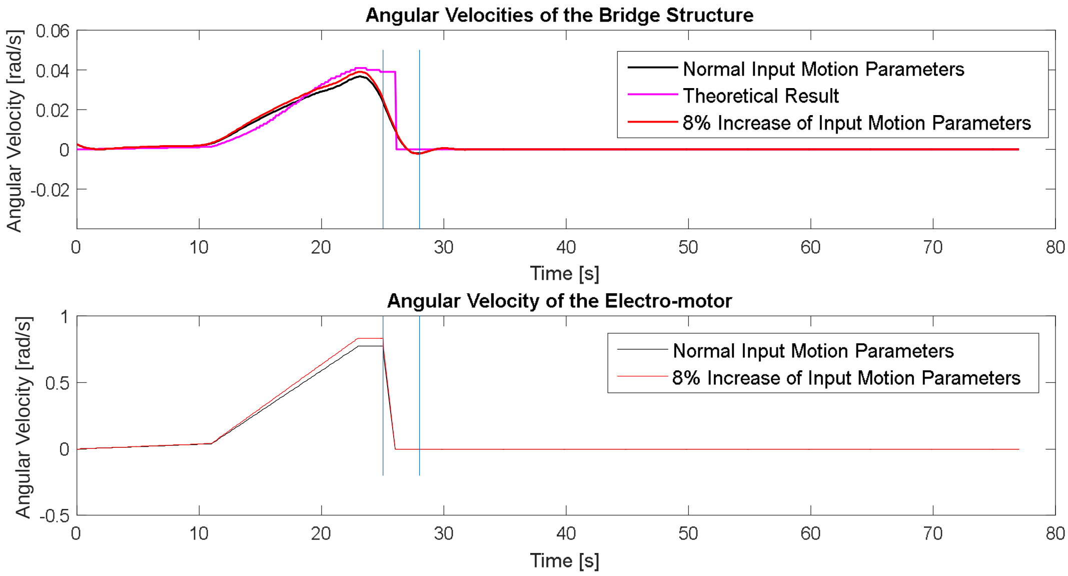

Figure 4.40 Angular Velocities of the Bridge Structure and Electro-motor - Brake Situation - Different Theoretical Input Motion Parameters

- **Measured Input Motion Parameters**

If the difference between the angular velocities of the balance part and the deck given by measured input motion parameters with an initial 10s delay is analysed, then the results can be observed in Figure 4.41. The differences are very small, 10e-03, and variations are more noticeable after the transit from the acceleration period to the uniform movement period. The balance part has an initial increase of the angular velocity, counteracted afterwards by a decrease with respect to the deck and a stabilization around the null value afterwards. During the braking period no variations are present in the difference between the angular velocities of the two components. These negligible differences permit the consideration of only one component of the bridge structure to be used to describe the motion of the bridge structure. The component chosen for further analysis is the balance part.

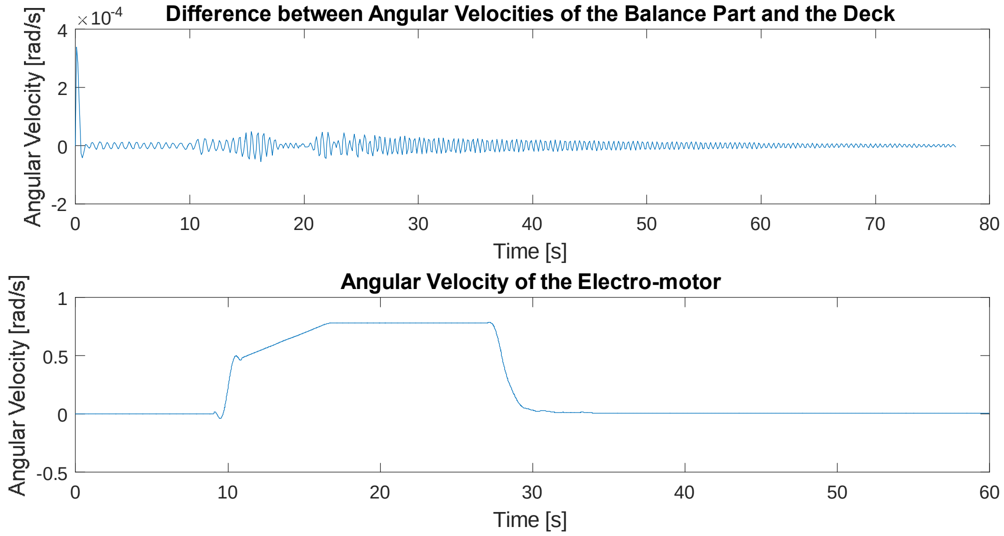

Figure 4.41 Difference between the Angular Velocities of the Balance Part and the Deck - Brake Situation - Measured Input Motion Parameters

In Figure 4.42 the angular velocities obtained from the model with an initial 10s delay and the measurements are plotted against each other. Moreover, the input measured angular velocity is also plotted. Both the model predictions and theory behave similarly, especially after the deceleration period. The angular velocity obtained from the model during the period of constant angular velocity (between 15s and 25s) is lower than the theoretical one, but during the deceleration period they are behaving similarly. The emergency brake gives rise to larger vibration for both the model and the theory, but after approximately 10s both angular velocities become zero, and only noisy data is observable.

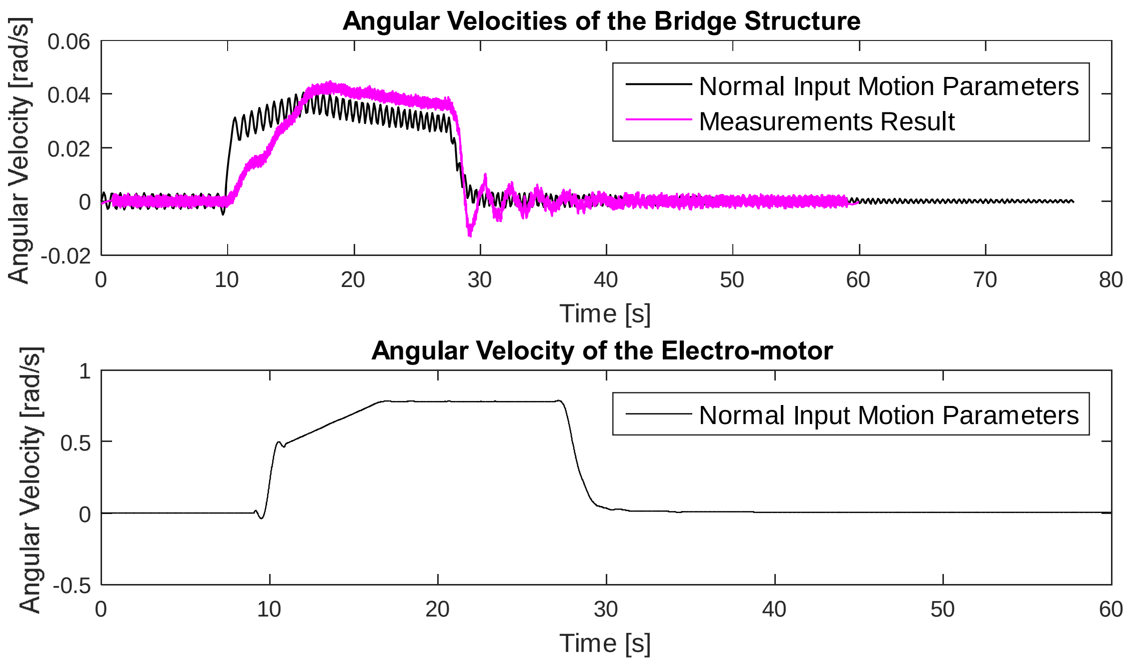

Figure 4.42 Angular Velocities of the Bridge Structure and Electro-motor - Brake Situation - Different Measured Input Motion Parameters

Angular Accelerations

- **Theoretical Input Motion Parameters**

The angular accelerations for the brake situation are now analysed. In Figure 4.43 the difference between the angular accelerations of the balance part and the deck obtained for theoretical input motion parameters with the initial 10s delay can be depicted. Moreover, the theoretical input angular acceleration is also shown in order to better understand some of the variations present for the two components of the bridge structure. Even though the differences are very small, 10e-03, the moment in which the brake is applied gives rise some variations. Just before the braking moment, at the end of the acceleration period, the balance part experiences a larger acceleration than the deck, and then it stabilises and becomes similar to the one in the deck. This is explainable by the fact that the deck achieves firstly a uniform acceleration, which is then transmitted to the balance part, giving rise to a larger difference of the angular accelerations for the two components. Afterwards, the period of uniform movement begins when the difference is almost zero. The application of the brake results in an initial higher angular acceleration of the deck, then a higher acceleration of the balance part with respect to the deck, and it ends in a constant difference between the two. Since the behaviour of the two components is similar in terms of angular acceleration, with a low order difference, the bridge structure behaviour can be considered to be characterized only by one of them. The component chosen hereafter to characterize the motion of the bridge structure is the balance part.

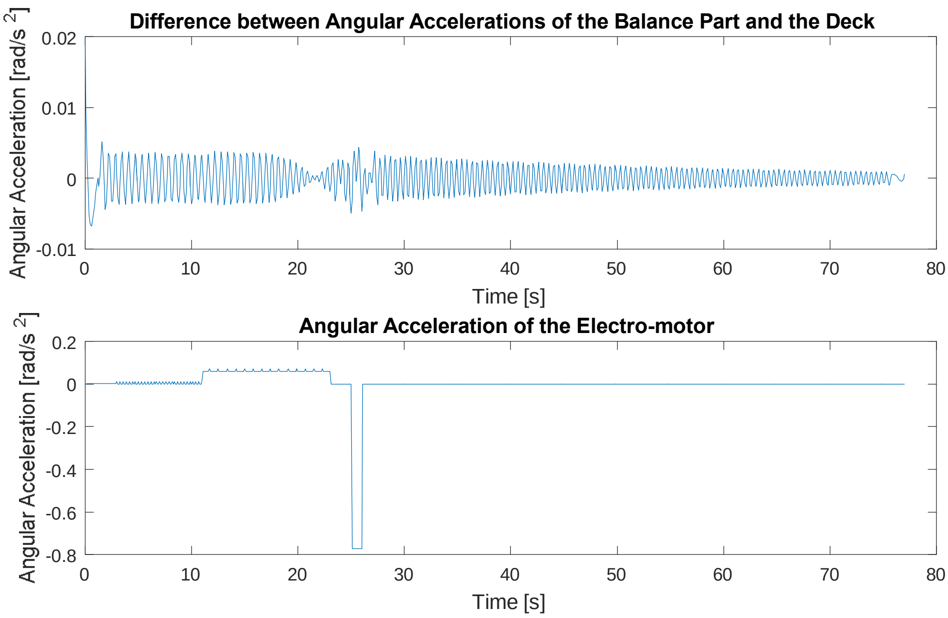

Figure 4.43 Difference between the Angular Accelerations of the Balance Part and the Deck - Brake Situation - Theoretical Input Motion Parameters

The angular acceleration of the bridge structure obtained from the model will be compared with the measured angular acceleration of the bridge structure in Figure 4.44. The input angular acceleration with the considered initial delay of 10s is also plotted in this figure. The magnitudes of the compared angular accelerations are very small, but differences can still be observed. The initial start of the angular acceleration obtained from the model can be considered zero because the starting and ending higher value are due to the filtering procedure. When the acceleration period starts, an increase of the angular acceleration is observed, which is similar to the theoretical result. Immediately after the acceleration period, the bridge start to decelerate due to the brake application. The model predictions show a higher deceleration than the theory. Moreover, after the brake is applied, the angular acceleration of the bridge goes towards zero within the 3s time frame, accompanied by some small variations until it becomes zero and the bridge stops.

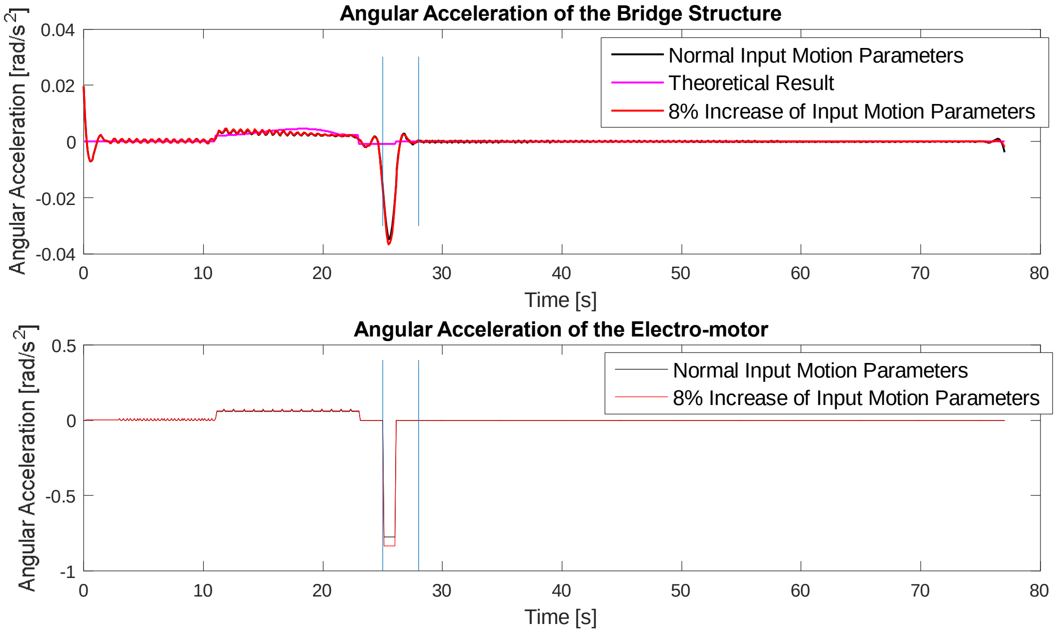

Figure 4.44 Angular Accelerations of the Bridge Structure and Electro-motor - Brake Situation - Different Theoretical Input Motion Parameters

- **Measured Input Motion Parameters**

The influence of the measured input motion parameters on the angular acceleration of the bridge structure is analysed firstly through the difference between the angular accelerations of the balance part and the deck. As it can be observed in Figure 4.45, the difference is almost null. An increase of the angular acceleration of the deck with respect to the one of the balance part just before the acceleration period occurs, but then the difference becomes constant around zero. Because the differences are very small, the bridge structure behaviour can be considered to be modelled only by one of the components. The balance part is chosen further as the component modelling the bridge structure motion.

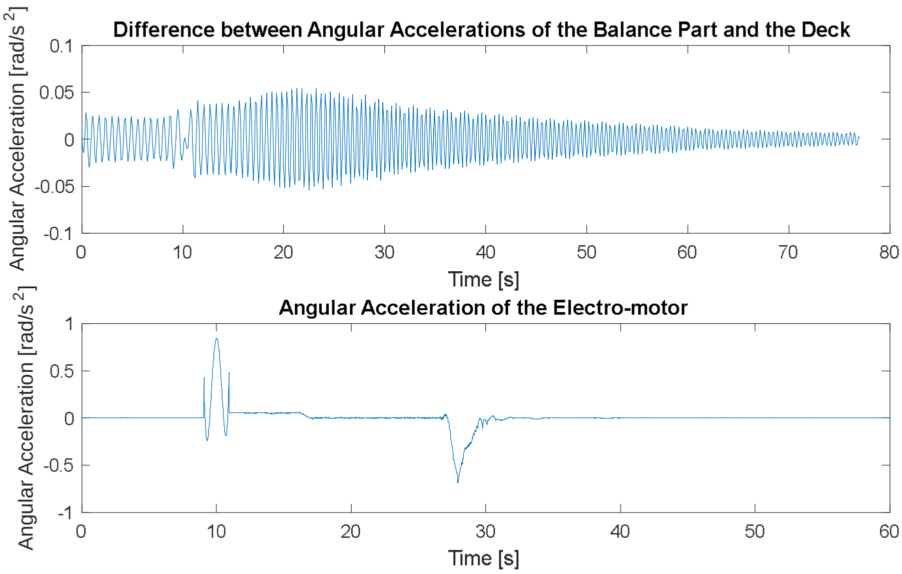

Figure 4.45 Difference between the Angular Accelerations of the Balance Part and the Deck - Brake Situation - Measured Input Motion Parameters

In Figure 4.46 the angular acceleration of the bridge structure obtained from the model is plotted against the measured angular acceleration of the bridge structure and the input angular acceleration with an initial 10s delay is also plotted. The model predictions show an initial acceleration peak higher than the measurements, but the angular acceleration becomes lower than the measurements shortly after this peak. Both the model and the measurements experience an almost zero angular acceleration after the acceleration period, followed by a deceleration impulse when the brake is applied. After the application of the brake, the angular acceleration experiences some vibrations as a reaction to the emergency brake, but this vibrations wear off after 5s.

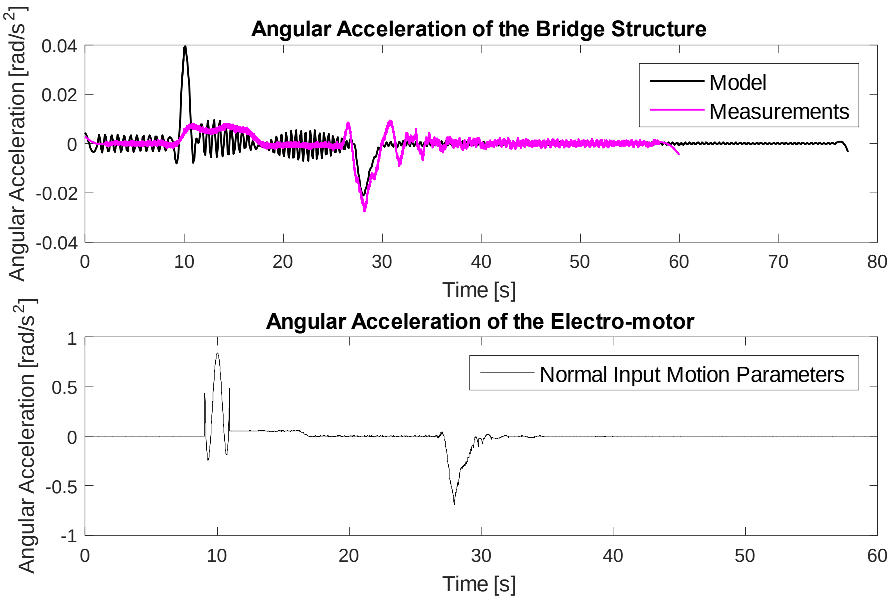

Figure 4.46 Angular Accelerations of the Bridge Structure and Electro-motor - Brake Situation – Model versus Measurements

Electro-motor Torque

After all the parameters characterizing the motion of the bridge structure were analysed and adjusted in order to have a behaviour more similar to the curved rack type of operating mechanism, the load acting on the electro-motor will be analysed. The load is defined in terms of the torque acting on the electro-motor which is obtained from the bridge structure motion parameters: angular displacements, angular velocities and angular accelerations.

- **Theoretical Input Motion Parameters**

Figure 4.47 depicts the electro-motor torque obtained from theoretical input motion parameters and the theoretical electro-motor torque due to the self-weight of the bridge. For both normal input motion parameters and an increase of these the torque can be observed. The torque obtained from the model remains below the design motor torque, which is the maximum theoretical electro-motor torque. When the brake is applied, the bridge has a reaction that results in an increase of the electro-motor torque, followed by a decrease and a stabilization around the value of the torque due to the self-weight of the bridge structure at the moment it stops.

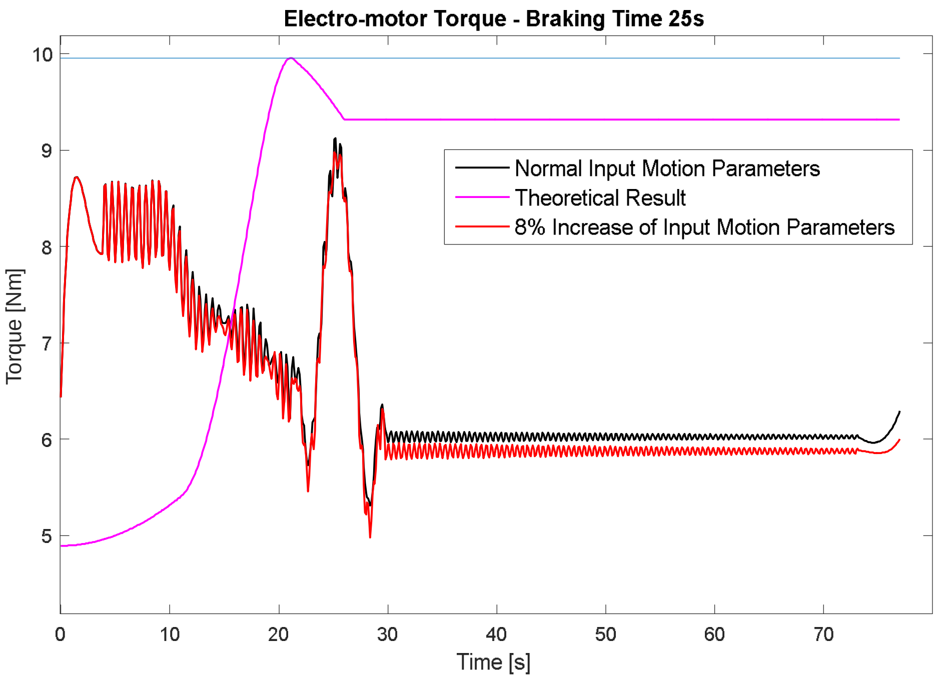

Figure 4.47 Electro-motor Torque - Brake Situation – Braking Time 25s - Model versus Theory

In Figure 4.48 different braking times were imposed on the model in order to investigate if the increase of the torque given by the reaction of the bridge to the brake remains below the maximum theoretical torque. The main idea was to see if a braking time below the initial braking time of 25s would be detrimental with respect to the maximum obtained torque. A brake was applied to the model gradually and the results of the electro-motor torque for a brake at 5s, 10s, 15s and 20s can be observed. Below 15s, the reaction is very small because the bridge just begins to accelerate and its angular velocity is very small. After 15s, the emergency brake gives a considerable reaction. The maximum reaction torque obtained from the model for a brake at 15s is almost the same at the ones between 15s and 20s and these are the largest that can be obtained (almost 9.8 Nm). After 20s, the value of the maximum reaction torque decreases and for a brake at 25s it is a little over 9 Nm. Since the maximum value of the torque obtained from the model is located always under the design theoretical torque (blue line), it can be concluded that the theory is rather conservative with respect to the maximum value of this parameter.

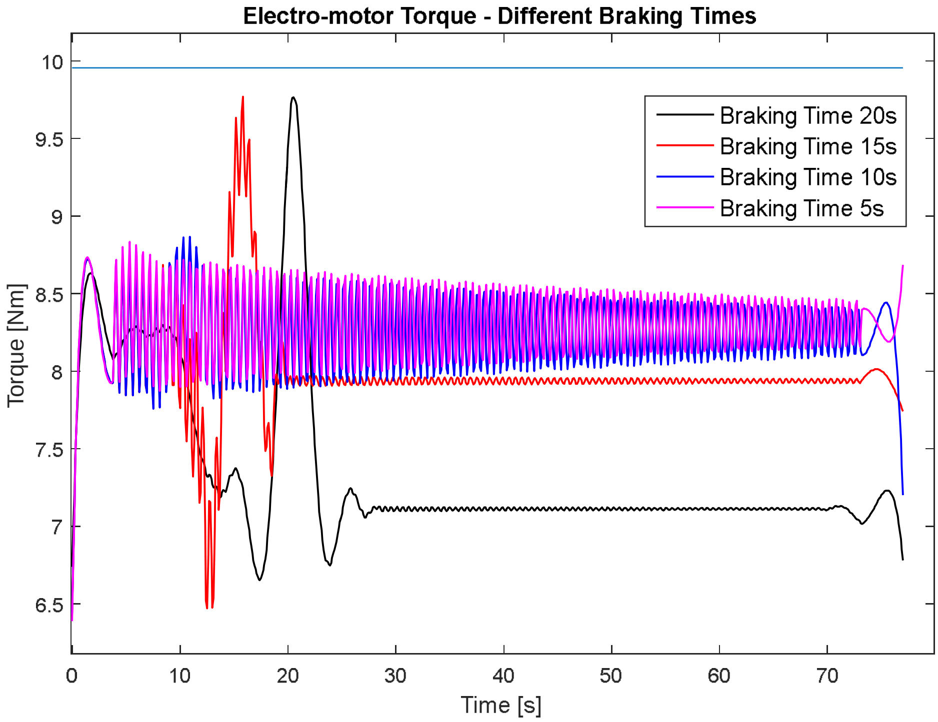

Figure 4.48 Electro-motor Torque - Brake Situation – Model for Different Braking Times versus Theory

The typical characteristics of torques occurring in electric motors can be better observed when the torque is plotted against the angular velocity of the electro-motor (Figure 4.49). The initial high torque necessary to lift the bridge is observable around 8 Nm, then it decreases during the acceleration period to a minimum torque, and at the end of this period an increase is observed at 0.7 rad/s, when the break-down torque is achieved.

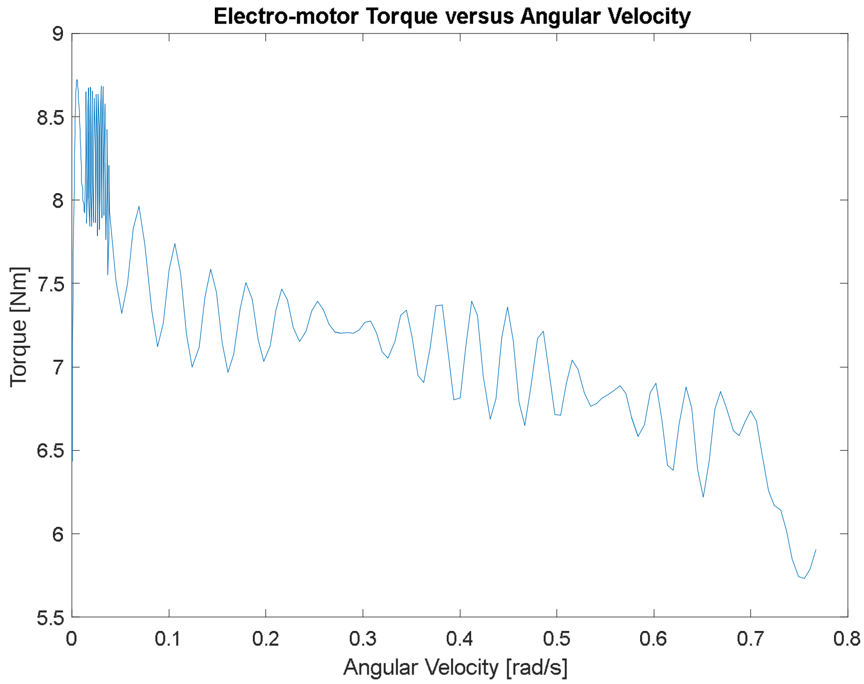

Figure 4.49 Electro-motor Torque versus Angular Velocity - Brake Situation - Theoretical Input Motion Parameters

- **Measured Input Motion Parameters**

Firstly, the various components that can be used to express the measured electro-motor torque are going to be investigated. As it can be observed in Figure 4.50, there are some differences between various components. The torques measured on the vertical shafts and reduced to the electro-motor and the torque measured on the electro-motor are very different. For the vertical shafts the torques were obtained for the addition of the northern and southern shaft measurements, only the northern shaft and only the southern shaft. These were then reduced to the electro-motor by means of transmission coefficients and drive efficiency. The measured electro-motor torque seems to follow a different pattern than the torques measured on the vertical shafts, and the magnitude is very large. For these reasons, the measured torques to be considered for comparisons will be the ones on the vertical shaft.

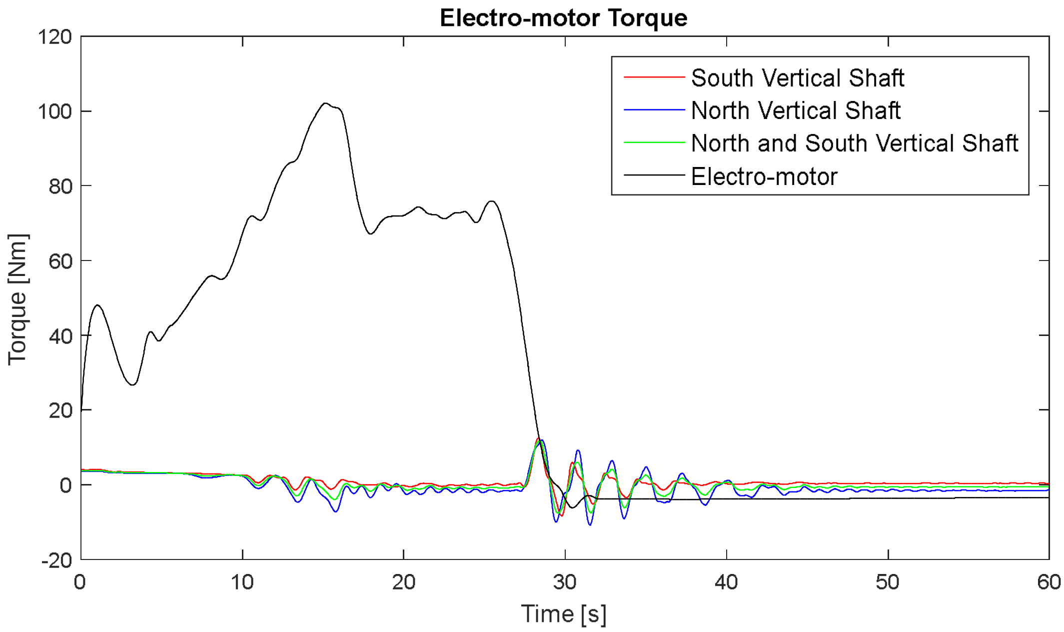

Figure 4.50 Electro-motor Torque - Brake Situation – Different Measured Components reduced to the Electro-motor

The model obtained from measured input motion parameters with the initial 10s delay plotted against the measured vertical shaft torques reduced on the electro-motor is shown in Figure 4.51. The model predictions show a higher starting torque, almost double the one measured, then a decrease is observed as in case of the measured one. When the brake is applied, the reaction of the bridge structure to the brake can be observed for all plots by a temporary increase of the torque. After some vibrations, the bridge stops and the magnitude of the electro-motor torque becomes constant around the value of the torque due to the self-weight of the bridge at the moment it stops. The model has a higher final magnitude of the torque when compared to the measured data. This is caused by the starting torque magnitude obtained from the model which is higher than the one in case of the measurements.

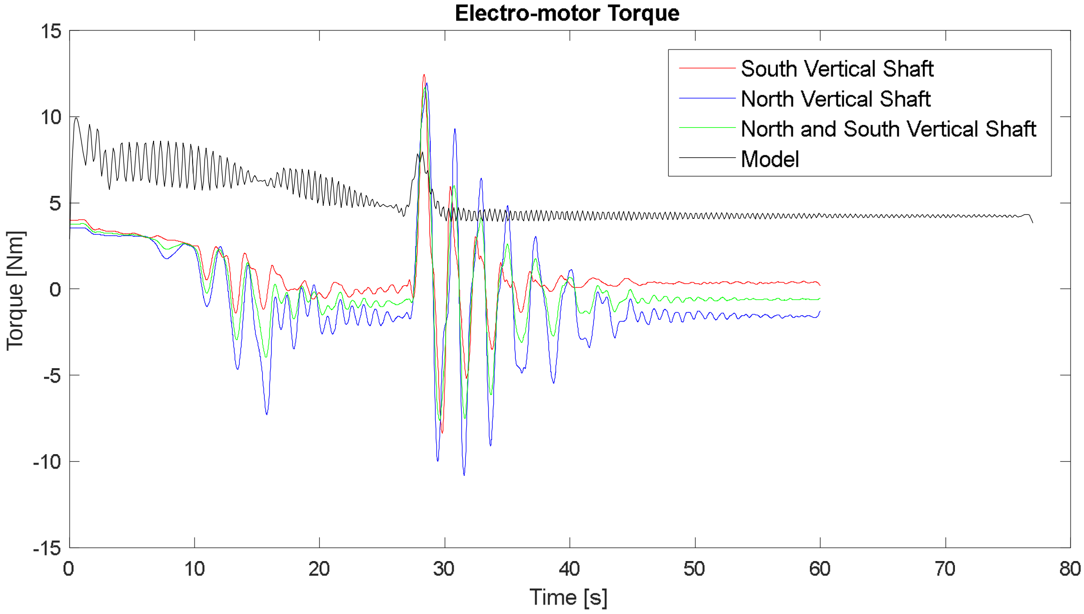

Figure 4.51 Electro-motor Torque - Brake Situation - Model versus Measurements

In Figure 4.52 the typical torques occurring in electric motors for this loading case can be observed when the torque obtained from the model is plotted against the angular velocity of the electro-motor. The same high initial starting torque is present also in this case, then a decrease towards the pull-up torque occurs, followed by a maximum torque obtained at a higher speed. This occurs just before the period of uniform movement, between 0.7 rad/s and 0.8 rad/s.

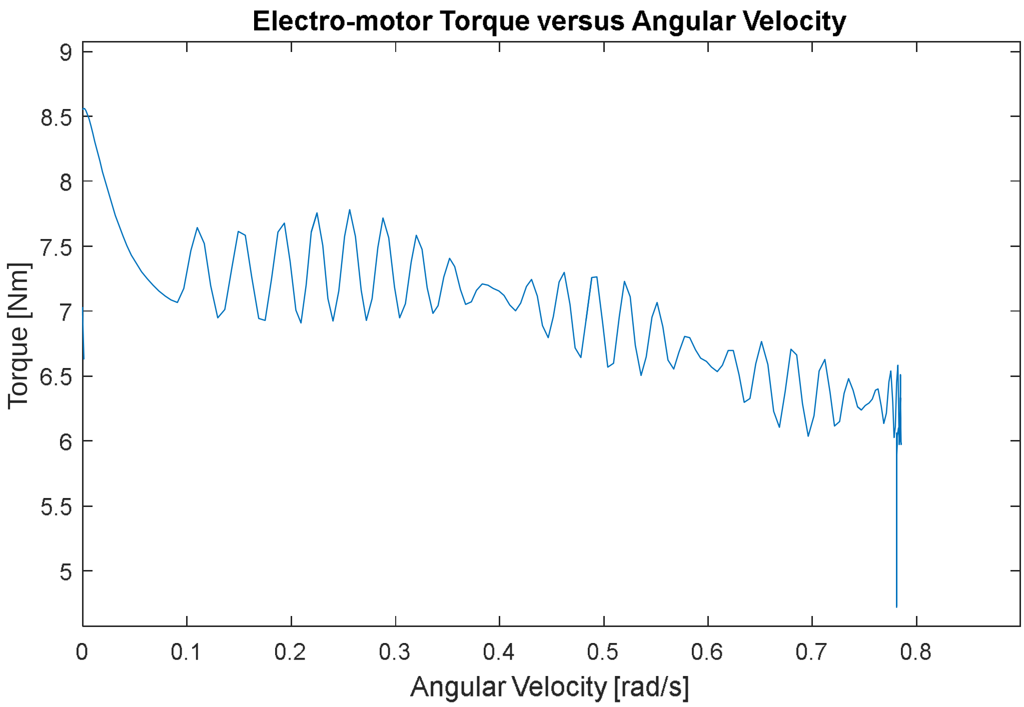

Figure 4.52 Electro-motor Torque versus Angular Velocity - Brake Situation - Measured Input Motion Parameters

5. CONCLUSIONS AND RECOMMENDATIONS

The comparisons drawn in chapter 4. Dynamic Model Verification helped gaining some insight into the factors having an influence on the dynamic loads acting on the operating systems of beam balanced bascule bridges. Based on these comparisons and with the main research question in mind, some final conclusions are drawn and recommendations are made with respect to how this research topic can be further investigated.

5.1. Conclusions

Firstly, the manner in which the beam balanced bascule bridge is modelled affects the behavior of the bridge during operation. The consideration of a straight rack type of operating mechanism in the model influences the outcome. When the theoretical motion parameters are input into the model and the results are compared with the theory, the model requires an increase of the input of 16.5% for normal operation and 8% for braking situation in order to have results at the same order of magnitude as the theory. In the theory, a curved rack type of operating mechanism was considered, thus the increase of the input motion parameters acts as an indirect transformation of the straight rack type of behavior into a curved rack type. For the model obtained from measured input motion parameters not only an increase is necessary to have a curved rack type of behavior, but also an initial delay of the beginning of the acceleration period. After considering an increase of 15% for normal operation and no increase for brake situation of the measured input motion parameters and an initial delay of 10s before the acceleration period, the behavior of the straight rack model is brought closer to the behavior of a bridge with a curved rack type of operating mechanism.

Furthermore, the operating system of the beam balanced bascule bridge depends on the motion of the bridge structure, more specifically the motion of the deck and/ or the balance part. The motion of the bridge structure can be described by three parameters: the angular displacement, the angular velocity and the angular acceleration. When these parameters were analyzed for both the deck and the balance part it was observed that they are the same for both components. This permitted the consideration of only one of the components to characterize the motion of the bridge structure.

In terms of angular displacements of the bridge structure, the results obtained from the model are in agreement with both theory and measurements. The shape of the angular displacement obtained from the model in normal situation shows an initial standing in the closed position of the bridge, at 0°, followed by an increase until the maximum opening angle and a period during which the bridge remains at that angle. For the brake situation, the angular displacement from the model has a similar shape, except the moment when the brake is applied, when the angular displacement stops increasing and remains at a value corresponding to the angle at which the bridge has stopped. Both theory and measurements follow the same path in terms of angular displacement, thus this parameter can be considered modelled accurately.

In terms of angular velocities of the bridge structure, the results are not so close to theory and measurements as the angular displacements, but similarities are present both in terms of shape and magnitudes. The angular velocity of the bridge structure obtained from the model during normal operation presents an initial creep speed, followed by an increase towards full speed, then a period of uniform movement when a slow decrease of the full speed occurs, a deceleration period characterized by a faster decrease of the angular velocity and it ends with another creep period until the bridge reaches a stop. For the brake situation, until the deceleration period, the same path is followed by the angular velocity of the bridge structure. However, the emergency brake is applied during the period of uniform movement, and after its application the angular velocity decreases abruptly to zero. The theory and the measurements present a similar path, with small differences in magnitudes with respect to the model predictions present before the deceleration period. In case of the theory, the differences are very small, about 1.3e-03, while for the measurements the differences are approximately 5e-03. This values are negligible, and since the shape is similar with theory and measurements, the angular velocity of the bridge structure can be considered an accurate parameter.

In terms of angular accelerations of the bridge structure, the model predictions resulted also very close to both theory and measurements. The angular acceleration obtained from the model for normal operation starts with a zero value, followed by a higher acceleration as the electro-motor tries to achieve full speed, then when the period of uniform movement begins a low constant acceleration occurs, then a higher deceleration occurs in order to stop the bridge and as the bridge stops the acceleration becomes again zero. For the brake situation, after the higher acceleration needed to achieve full speed, a high deceleration occurs as a result of the emergency brake, and afterwards the acceleration becomes zero. The theory and the measurements showed a similar shape, however, the deceleration needed for the emergency brake for the theory was smaller than the one for the model. On the other hand, this higher deceleration was present also in the measurements, thus it can be seen as a correct result. Taking into account that, overall, the angular acceleration of the bridge structure obtained from the model is similar to both theory and measurements, the parameter can be considered as an accurate one.

With regard to the electro-motor torque, all the above mentioned parameters and variables have an effect on its outcome. Moreover, variables as the stiffness and damping of the considered connecting elements (i.e. the straight rack, the hanger) also have an influence on the torque acting on the motor. In both loading situations this variable resulted always in-between the maximum theoretical design torque and the measured electro-motor torque. However, a definitive comparison cannot be established between the torque obtained from the model and the ones given by theory and measurements. The shape of the variable cannot be compared with the theory because only a constant value is considered in the design. On the other hand, the comparison with the measurements in terms of the shape is unreliable. The measured electro-motor torque and the measured vertical shaft torque reduced to the electro-motor are not coinciding, and this raises concerns about the accuracy of the measurements themselves and the modelling considerations regarding the motor. A simplistic model for the electro-motor seems not to be enough, and for this reason recommendations regarding both additional components to be considered in the model and considerations regarding the measurement campaign are given further on.

5.2. Recommendations

To improve research on this topic and ease the path of future researchers the following recommendations are given.

5.2.1. Modelling of the Bridge Structure

The advice regarding the modelling of the bridge structure is mainly meant to provide a simplification to this model. This recommendation should only be considered if the interest is not focused on the behaviour of the structural components of the bridge structure (e.g. counterweight, balance beam, hanger rod, deck, pivot points etc.).

When interested in the electro-motor torque, the bridge structure can be modelled in a future research study only by considering one rigid element. The hanger rod and balance part could be excluded, and their respective geometrical characteristics reduced on a rigid element located at the deck level. This recommendation is supported by the fact that the difference between the balance part and the deck various variables were found to be negligible, implying a similar behaviour of the two component parts of the bridge structure. By considering this type of model the mathematical expression will be largely reduced as well as the computation time.

When interested in structural dynamics, a flexible type of element can be considered to model the deck and the balance part. The equations of motion can be developed on the basis of the Euler-Bernoulli beam theory. This approach is more useful when the characteristics at different locations are of interest. An advantage of this approach is that the flexibility of the component elements can be accounted for, and their influence on the overall behaviour of the operating mechanism can be analysed.

5.2.2. Modelling of the Operating System

The current model can be improved by considering more components of the operating system. In the model created during this project all the components located between the rack and the electro-motor were considered by means of a single mass. However, the various components can be considered in a future research separately, and the connection between them can be realized through rotational type of spring-dashpot elements. This will permit the in-depth investigation of every components, and comparisons could be drawn at the level of each of them.

5.2.3. Revision of Standards

The current Design Codes for Movable Bridges should make some exemptions with regard to existing movable bridges. It is clear that the theory is rather conservative, but for existing movable bridges this is even more profound. Provisional exemptions should be given for the assessment of current functional movable bridges, so that the owner is not restricted by the codes. If performed measurements on movable bridges prove that the operating system is still functional, while the codes show failure, then further investigation should be allowed and the bridge should not be declared non-operational based only on the standards.

5.2.4. Measurements Data Collection

One of the most important improvements that can be done is the verification through measurements of more movable bridges. Moreover, if similar bridges are subjected to these types of verifications, then the model can be better improved by a generalization of the measured input motion parameters. Malfunctioning bridges should not be accounted for in this generalization, but their defects could be analysed from a different perspective. For example, for the reference project used in this research, it would be beneficial to analyse the influence of the defect spring buffer on the magnitude of the loads and behaviour of the bridge structure and of the operating mechanism. The repetition of the measurements for these bridges would be more interesting, especially if for instance a concentrated load would be placed conveniently in order to observe either a detrimental or beneficial effect on the bad functioning component.

On the other hand, data collection by means of measurements should be focused on the measurement of other variables than the ones available in the reference project. Instead of measuring the angular displacement of the deck, the angular acceleration would be a more adequate parameter. This is because the angular velocity and angular displacement could be obtained by numerical integration. This leads to more accurate results than numerical differentiation, which was used in this project. The same recommendation applies to the measurement of the electro-motor. The angular acceleration should be measured instead of the angular velocity. This will result in a more accurate angular acceleration for the electro-motor. A more ideal situation, but costly, would involve the measurements of all variables, angular displacement, angular velocity and angular acceleration, for both the electro-motor and the deck.

BIBLIOGRAPHY

[1] G. Parke and N. Hewson, ICE Manual of Bridge Engineering, Thomas Telford Publishing, 2008.

[2] D. Stroosma, Dynamica van Beweegbare Bruggen - Het Aandrijfmechanisme, Rijkswaterstaat - Directie Bruggen, 1980.

[3] NEN 6786 - Rules for the Design of Movable Bridges, Delft: Nederlands Normalisatie-Instituut, 2015.

[4] W.-F. Chen and L. Duan, Bridge Engineering Handbook, Boca Raton: CRC Press, 2000.

[5] T. L. Koglin, Movable Bridge Engineering, Wiley, 2003.

[6] S. D, “Dynamica van Beweegbare Bruggen - Deel I - Het Aandrijfmechanisme,” Rijkswaterstaat, 1980.

TABLE OF FIGURES

- **General Input Data**

Drawing Scheme

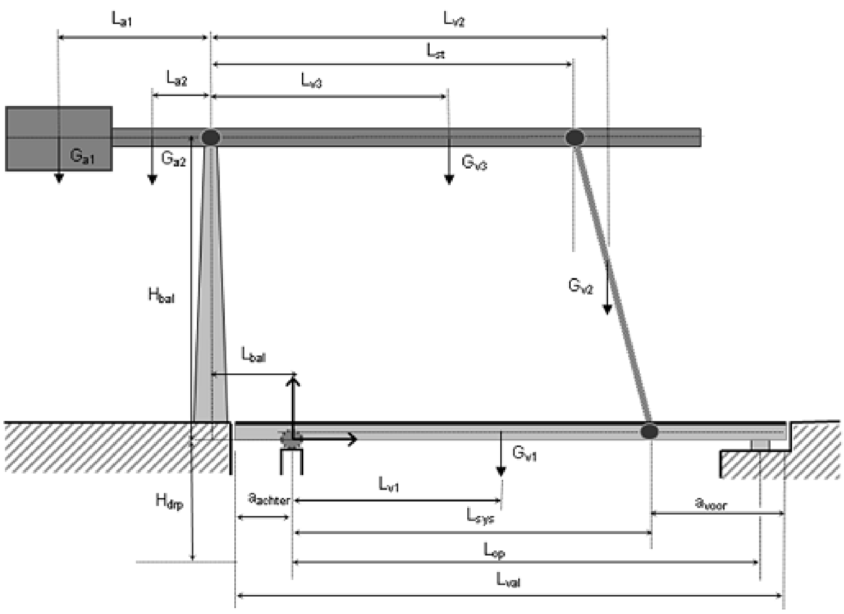

Geometrical Dimensions of the Bridge

Main pivot level above water level $H_{drp} := (5.09 - 0.80) \cdot m = 4.29\,m$

Deck length $L_{val} := 15.835m$

Vertical distance between balance pivot point and main pivot point of the deck $H_{bal} := (17.16 - 5.09) \cdot m = 12.07\,m$

Horizontal distance btween balance pivot point and main pivot point of the deck $L_{bal} := (1.200 + 1.650)m = 2.85\,m$

Distance between main pivot point and the back point of the deck $a_{achter} := 0.38m$

Distance between the pivot point of the tie rod and the front point of the deck $a_{voor.1} := 2.85m + 0.355m = 3.205\,m$

Distance between the support point the extreme point of the deck $a_{voor.2} := 0.355m$

Afstand tussen hoofddraaipunt en vooroplegging van het val $L_{op} := L_{val} - a_{achter} - a_{voor.2} = 15.1\,m$

Length from the main pivt point to the extreme point of the deck $a_{voorpunt} := L_{val} - a_{achter} = 15.455\,m$

Horizontal distance between main pivot point and the pivot point of the tie rod $L_{sys} := L_{val} - a_{achter} - a_{voor.1} = 12.25\,m$

Vertical distance between main pivot point and pivot point of the tie rod $H_{sys} := (5.170 - 5.090) \cdot m = 0.08\,m$

Angle between the tie rod and the vertical axis $\alpha_{hst} := \operatorname{atan2}(H_{bal}, L_{bal}) = 13.285 \cdot deg$

Angle between the connection line between deck pivot point and tie rod and the horizontal axis $\alpha_{dek} := \operatorname{atan2}(L_{sys}, H_{sys}) = 0.374 \cdot deg$

Deck width $b_{val} := 10.248m$

Deck area $A_{val} := L_{val} \cdot b_{val} = 162.277\,m^2$

Distance from pivot point to the centre of the deck $ah_{val} := \dfrac{L_{val}}{2} - a_{achter} = 7.538\,m$

Deck length to width ratio $lbv := \dfrac{L_{val}}{b_{val}} = 1.545$

Structural Elements Self-weights

Deck weight (according to VOBB annex B) $G_{v1} := (41025 + 6192 - 1200)\cdot kg\cdot g = 451.273\cdot kN$

Horizontal distance from main pivot point to the deck centre of gravity $L_{v1} := 8.004m$

Vertical distance from main pivot point to the deck centre of gravity $H_{v1} := 0.0755m$

Weight of the tie rod $G_{v2} := 2000\cdot kg\cdot g = 19.613\cdot kN$

Horizontal distance from deck main pivot point to the tie rod centre of gravity

$$L_{v2} := L_{sys} - \frac{\sqrt{H_{bal}^2 + L_{bal}^2}}{2}\cdot \sin(\alpha_{hst}) = 10.825\,m$$

Vertical distance from deck main pivot point to the tie rod centre of gravity

$$H_{v2} := H_{sys} + \frac{\sqrt{H_{bal}^2 + L_{bal}^2}}{2}\cdot \cos(\alpha_{hst}) = 6.115\,m$$

Weight of the balance part before the pivot point $G_{v3} := 0N$

Distance from balance centre of gravity to the above pivot point $L_{v3} := 0m$

Height from balance centre of gravity to above pivot point $H_{v3} := 0m$

Variable excess load (according to VOBB page 103) $F_{var} := 50\,\frac{N}{m^2}$

Counterweight $G_{a1} := (64275)\cdot kg\cdot g = 630.322\cdot kN$

Horizontal distance from balance pivot point to counterweight centre of gravity $L_{a1} := 4.604m$

Vertical distance from balance pivot point to counterweight centre of gravity $H_{a1} := 0.0115m$

Weight of the balance part after the pivot point $G_{a2} := (3814 + 5880 + 1000)\cdot kg\cdot g = 104.872\cdot kN$

Horizontal distance from balance pivot point to the centre of gravity $L_{a2} := 8.500m$

Vertical distance from balance pivot point to the centre of gravity $H_{a2} := 0.5m$

Total self-weight before the pivot point (excluding variable excess load)

Resulting weight before pivot point $G_{voor} := G_{v1} + G_{v2} + G_{v3} = 470.886\cdot kN$

Resulting x-direction eccentricity

$$e_{voor.x} := \frac{G_{v1}\cdot L_{v1} + G_{v2}\cdot L_{v2} + G_{v3}\cdot L_{v3}}{G_{voor}} = 8.122\,m$$

Resulting torque before pivot point $M_{x.voor} := -G_{voor}\cdot e_{voor.x} = -3.824\times 10^{3}\cdot kNm$

Resulting z-direction eccentricity

$$e_{voor.z} := \frac{G_{v1}\cdot H_{v1} + G_{v2}\cdot H_{v2} + G_{v3}\cdot H_{v3}}{G_{voor}} = 0.327\,m$$

Total self-weight after the pivot point

Resulting weight for the after part $G_{achter} := G_{a1} + G_{a2} = 735.195\cdot kN$

Resulting x-direction eccentricity

$$e_{achter.x} := -\frac{G_{a1}\cdot L_{a1} + G_{a2}\cdot L_{a2}}{G_{achter}} = -5.16\,m$$

Resulting torque after pivot point $M_{x.achter} := -G_{achter}\cdot e_{achter.x} = 3.793\times 10^{3}\cdot kNm$

Resulting z-direction eccentricity

$$e_{achter.z} := -\frac{G_{a1}\cdot H_{a1} + G_{a2}\cdot H_{a2}}{G_{achter}} = -0.081\,m$$

Mass Moments of Inertia

Gravitational acceleration $g = 9.807\,\frac{m}{s^2}$

Mass moment of inertia of the deck before the pivot point including the excess load:

$$I_{voor1} := \left(G_{v1} + F_{var}\cdot L_{val}\cdot b_{val}\right)\cdot\left(\frac{L_{val}^2}{12} + L_{v1}^2 + H_{v1}^2\right)\cdot\frac{1}{g} = 3.98\times 10^6\,m^2\cdot kg$$

Total mass moment of inertia before the pivot point:

$$I_{voor} := I_{voor1} + \left[G_{v3}\cdot\left(L_{v3}^2 + H_{v3}^2\right) + G_{v2}\cdot\left(L_{v2}^2 + H_{v2}^2\right)\right]\cdot\frac{1}{g} = 4.289\times 10^6\,m^2\cdot kg$$

Total mass moment of inertia after the pivot point:

$$I_{achter} := \left[G_{a1}\cdot\left(L_{a1}^2 + H_{a1}^2\right) + G_{a2}\cdot\left(L_{a2}^2 + H_{a2}^2\right)\right]\cdot\frac{1}{g} = 2.138\times 10^6\,m^2\cdot kg$$

Total mass moment of inertia (before and after the pivot point):

$$I_{tot} := I_{voor} + I_{achter} = 6.427\times 10^6\,m^2\cdot kg$$

Mass moment of inertia of the electro-motor

Mass moment of inertia of couplings on the motor shaft $I_{kop} := 0.01 kg\cdot m^2$

Mass moment of inertia of electromotor on the motor shaft $I_{motor} := 0.111 kg\cdot m^2$

Mass moment of inertia of brakes on the motor shaft $I_{rem} := 0.2 kg\cdot m^2$

Mass moment of inertia of flywheel on the motor shaft $I_{vw} := \frac{1}{8}\cdot\left[7850\cdot\frac{kg}{m^3}\cdot\frac{\pi}{4}\cdot(0.365\cdot m)^2\cdot 0.15\cdot m\right]\cdot(0.365\cdot m)^2 = 2.052\cdot kg\cdot m^2$

Total mass moment of inertia on the motor shaft $I_1 := I_{kop} + I_{motor} + I_{rem} + I_{vw} = 2.373\cdot kg\cdot m^2$

Drive Components Considerations

Efficiency Factors

The load acting on the components of the operating mechanism is affected by energy losses that occur in the mechanism. The efficiency factor of a worm wheel that is not protected against dust and dirt is estimated at 35%. This is in fact dependent on the pitch S and the radius Rs of the steel circle of the worm wheel. The load acting on the components of the operating mechanism is calculated with the following efficiency factor :

Drive components efficiency $\eta_{baew} := 13.5\% = 13.5\cdot\%$

Drive efficiency $\eta_{aandr} := 100\%$

Transmission Factors

Bevel gear transmission factor $i_{kglw} := \frac{75}{17} = 4.412$

Corner gearbox transmission factor $i_{htwk} := 6.53$

Main gearbox transmission factor $i_{rtwk} := 6.61$

Total gearbox transmission factor $i_{twk} := \frac{1}{i_{kglw}\cdot i_{htwk}\cdot i_{rtwk}} = 5.251\times 10^{-3}$

Operational Scheme of the Curved Rack

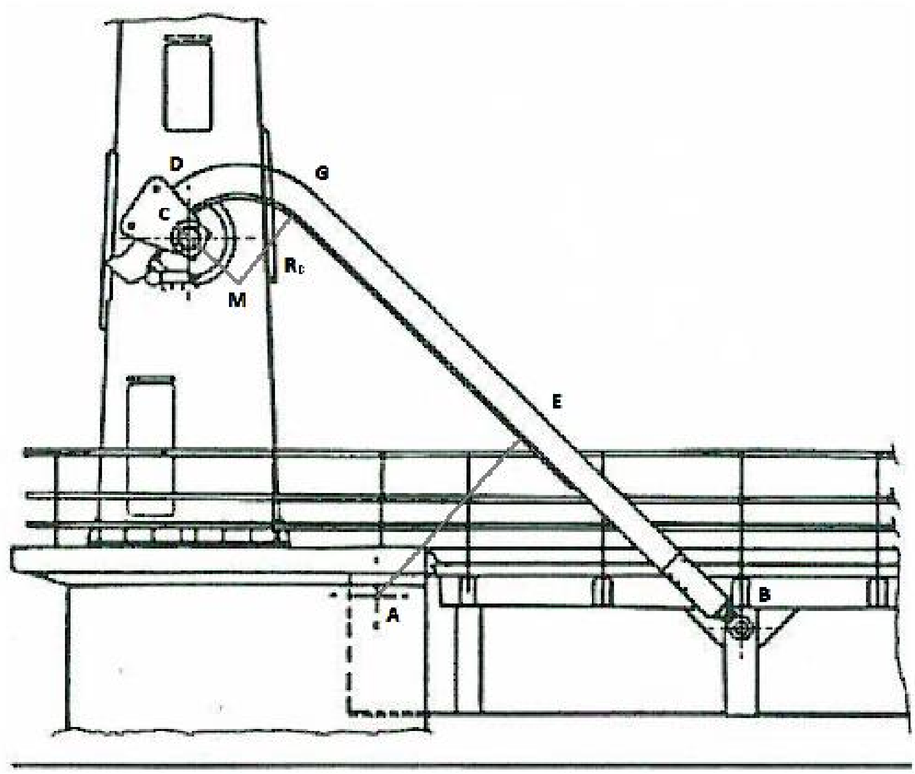

Rack Coordinates

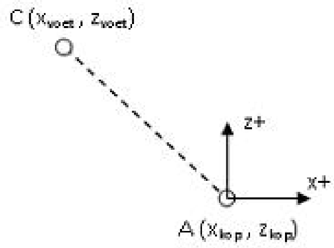

x-coordinate foot pivot point wrt. main pivot point $x_{voet} := -1.600m$

z-coordinate foot pivot point wrt. main pivot point $z_{voet} := (8.760 - 5.090) \cdot m = 3.67\,m$

x-coordinate head pivot point wrt. main pivot point $x_{kop} := 3.700m$

z-coordinate head pivot point wrt. main pivot point $z_{kop} := (5.090 - 5.090) \cdot m = 0 \cdot m$

$$A_1 := \begin{pmatrix} 0m \\ 0m \\ 0m \end{pmatrix} \qquad B_1 := \begin{pmatrix} x_{kop} \\ 0m \\ z_{kop} \end{pmatrix} = \begin{pmatrix} 3.7 \\ 0 \\ 0 \end{pmatrix} m \qquad C_1 := \begin{pmatrix} x_{voet} \\ 0 \cdot m \\ z_{voet} \end{pmatrix} = \begin{pmatrix} -1.6 \\ 0 \\ 3.67 \end{pmatrix} m$$

Pinion radius $R_{rond} := \dfrac{0.272 + 2 \cdot 0.008 \cdot 0}{2} m = 0.136\,m$

Curvature radius of the rack $Rh := 0.600m$

Length of the straight part of the rack $Lhm := 6.732$

Length from main pivot point to engagement point of the deck AB $L_{ab} := \left| B_1 - A_1 \right| = 3.7\,m$

Maximum opening angle of the structure $\alpha_{val.m} := 84deg$

Start delaying opening angle of the structure $\alpha_{val.r} := 11deg$

Start opening from closed position angle of the structure $\alpha_{val.bo} := 0.5deg$

Start opening from closed position length of the structure $L_{val} \cdot \sin(\alpha_{val.bo}) = 0.138\,m$

Start opening from closed position distance done by the rack $L_{ab} \cdot \sin(\alpha_{val.bo}) = 0.032\,m$

Rack Cross-Section

Rack bar cross-sectional area	: $A_{hst} := [264\cdot(2\cdot 28) + 170\cdot(2\cdot 35)]\text{mm}^2 = 0.027\,\text{m}^2$
Number of rack bars	: $n_{heugel} := 2$
Total rack bar cross-sectional area	: $A_{hst.tot} := n_{heugel}\cdot A_{hst} = 5.337\times 10^4\cdot\text{mm}^2$
Length of spring buffer	: $l_{buffer} := 500\text{mm}$
Bogie length	: $l_{sch} := 390\text{mm}$
Reserve	: $slr := 100\text{mm}$

Rack Stiffness

Spring buffer stiffnes : $C_{veerbuffer} := \dfrac{152.3}{2}\dfrac{\text{kN}}{\text{mm}}$

Steel elasticity modulus : $E_s := 210000\dfrac{\text{N}}{\text{mm}^2}$

Rack bar stiffness :
$$C_{heugel} := \left|\begin{array}{l} i \leftarrow 0 \\ j \leftarrow 0 \\ \text{for } j \in i \\ \quad C_j \leftarrow \dfrac{A_{hst}\cdot E_s}{\left|vbc_j\right|} \\ C \end{array}\right. = \left(8.692\times 10^8\right)\frac{\text{kg}}{\text{s}^2}$$

Total rack bar stiffness :
$$C_{h.tot} := \left|\begin{array}{l} i \leftarrow 0 \\ \text{for } j \in i \\ \quad C_j \leftarrow \dfrac{C_{heugel_j}\cdot C_{veerbuffer}}{C_{heugel_j} + C_{veerbuffer}} \\ C \end{array}\right. = \left(7.002\times 10^7\right)\frac{\text{kg}}{\text{s}^2}$$

Steel Poisson's coefficient : $\nu_s := 0.3$

Steel shear modulus : $G_s := \dfrac{E_s}{2\cdot(1+\nu_s)} = 8.077\times 10^4\cdot\dfrac{\text{N}}{\text{mm}^2}$

Vertical shaft length : $L_{v.as} := 5.200\cdot\text{m} = 5.2\,\text{m}$

Vertical shaft diameter : $D_{v.as} := 0.105\text{m}$

Vertical shaft polar moment of inertia : $I_{v.as} := \dfrac{\pi}{32}\cdot D_{v.as}{}^4 = 1.193\times 10^{-5}\,\text{m}^4$

Horizontal shaft length : $L_{h.as} := (2.700 + 2.900)\cdot\text{m} = 5.6\,\text{m}$

Horizontal shaft diameter : $D_{h.as} := 0.100\text{m}$

Horizontal shaft polar moment of inertia : $I_{h.as} := \dfrac{\pi}{32}\cdot D_{h.as}{}^4 = 9.817\times 10^{-6}\,\text{m}^4$

Rack bar stiffness on the motor shaft : $C_{hgl} := n_{heugel}\,C_{h.tot}\cdot R_{rond}{}^2\cdot i_{twk} = \left(1.36\times 10^4\right)\text{J}$

Total stiffness on the motor shaft : $C_{mot.t} := \left(\dfrac{1}{C_{hgl}}\right)^{-1} = \left(1.36\times 10^4\right)\text{J}$

- **Motion Parameters for the Electro-motor – VOBB Calculation Model**

$$
vd_{as}(v_{.geschat}) :=
\left|
\begin{array}{l}
\omega \leftarrow v_{.geschat} \\
\Delta t \leftarrow 0.1s \\
tt \leftarrow 0, \Delta t .. t_{.o} \\
i \leftarrow 0 \\
\text{for } t \in tt \\
\quad \left|
\begin{array}{l}
v_i \leftarrow 0 \\
ss_i \leftarrow 0 \\
a_i \leftarrow 0 \\
time_i \leftarrow t \\
i \leftarrow i + 1
\end{array}
\right. \\
0 \\
0 \\
i \leftarrow 0 \\
\text{for } t \in tt \\
\quad \left|
\begin{array}{l}
v_i \leftarrow \left(\dfrac{\xi \cdot \omega}{t_{.k}} \cdot t\right) \text{ if } 0 \le t < t_{.k} \\
v_i \leftarrow \xi \cdot \omega + \dfrac{\omega \cdot (1 - \xi)}{t_{.v}} (t - t_{.k}) \text{ if } t_{.k} \le t < (t_{.k} + t_{.v}) \\
v_i \leftarrow \omega \text{ if } (t_{.k} + t_{.v}) \le t < (t_{.k} + t_{.v} + t_{.e}) \\
v_i \leftarrow \omega - \dfrac{\omega \cdot (1 - \xi)}{t_{.s}} (t - t_{.k} - t_{.v} - t_{.e}) \text{ if } t_{.k} + t_{.v} + t_{.e} \le t < (t_{.o} - t_{.k}) \\
v_i \leftarrow \omega - \omega \cdot (1 - \xi) - \dfrac{\omega \cdot \xi}{t_{.k}} \cdot (t - t_{.k} - t_{.v} - t_{.e} - t_{.s}) \text{ if } t_{.k} + t_{.v} + t_{.e} + t_{.s} \le t < t_{.o} \\
i \leftarrow i + 1
\end{array}
\right. \\
i \leftarrow 0 \\
v_0 \leftarrow v_1 \\
0 \\
\text{for } t \in tt \\
\quad \left|
\begin{array}{l}
a_i \leftarrow \dfrac{\xi \cdot \omega}{t_{.k}} \text{ if } 0 \le t < t_{.k} \\
a_i \leftarrow \left[\dfrac{\omega \cdot (1 - \xi)}{t_{.v}}\right] \text{ if } t_{.k} \le t < (t_{.k} + t_{.v}) \\
a_i \leftarrow 0 \text{ if } (t_{.k} + t_{.v}) \le t < (t_{.k} + t_{.v} + t_{.e}) \\
a_i \leftarrow \left[\dfrac{-[\omega \cdot (1 - \xi)]}{t_{.s}}\right] \text{ if } t_{.k} + t_{.v} + t_{.e} \le t < (t_{.o} - t_{.k}) \\
a_i \leftarrow \left(\dfrac{-\omega \cdot \xi}{t_{.k}}\right) \text{ if } t_{.k} + t_{.v} + t_{.e} + t_{.s} \le t \le t_{.o} \\
i \leftarrow i + 1
\end{array}
\right. \\
i \leftarrow 0 \\
0 \\
0 \\
\text{for } t \in tt \\
\quad \left|
\begin{array}{l}
ss_i \leftarrow \displaystyle\sum_{aa = 0}^{i} (v_{aa} \cdot \Delta t) \\
i \leftarrow i + 1
\end{array}
\right. \\
\begin{pmatrix}
ss \\
v \cdot s \\
a \cdot s^2 \\
\dfrac{time}{s} \\
\dfrac{\Delta t}{s} \\
i - 1
\end{pmatrix}
\end{array}
\right.
$$

The function vd_{as} calculates the angular displacement, angular velocity and angular acceleration of the pinion:

Drive data range	$:vds := vd_{as}(\omega_{geschat})$
Pinion rotation data range	$:srs := vds_0 \cdot rad$
Pinion angular velocity data range	$:\omega rs := vds_1 \cdot \frac{1}{s}$
Pinion angular acceleration data range	$:\gamma rs := vds_2 \cdot \frac{1}{s^2}$
Time data range	$:ti := vds_3 \cdot s$
Time increment	$:\Delta T := vds_4 \cdot s$
Number of elements	$:ii := vds_5$
Range of steps	$:ir := 0, 1 .. ii$

Electro-motor Motion

The graph below shows the relative displacement in radians, from the closed position to the open position of the pinion as a function of time with respect to the fixed position.

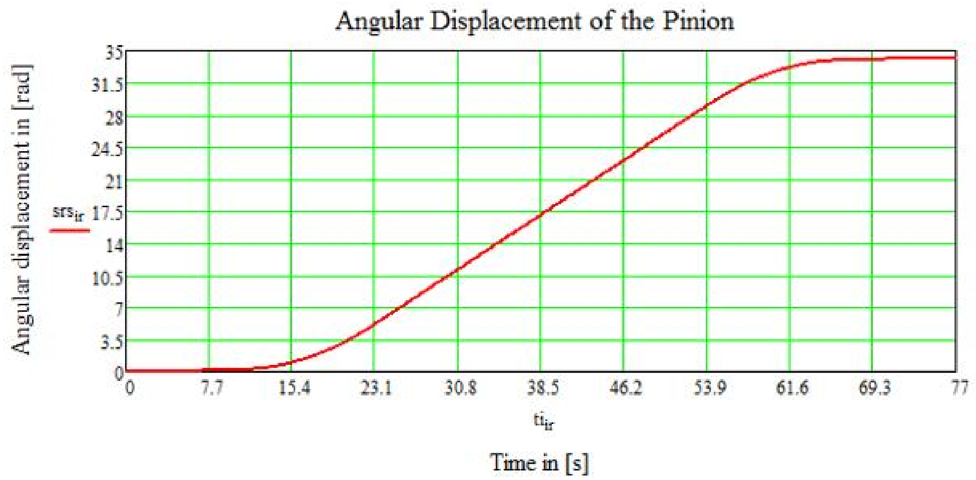

The graph below shows the angular velocity of the pinion from the closed position to the open position or from the open position to the closed position as a function of the time.

The graph below shows the angular velocity of the pinion from the closed position to the open position or from the open position to the closed position as a function of the time.

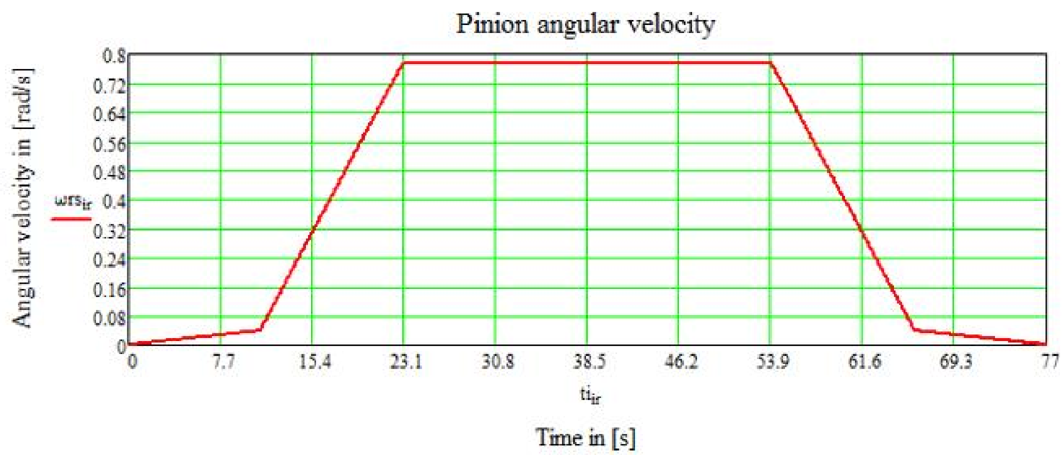

The following graph shows the relative angular acceleration of the pinion from the closed position to the open position or from the open position to the closed position as a function of the time.

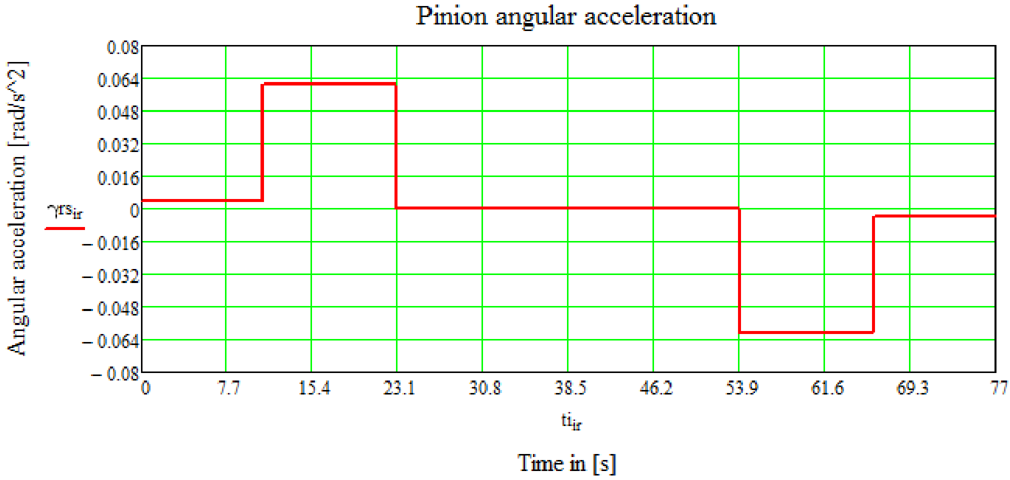

- **Motion Parameters for the Bridge Structure – VOBB Calculation Model**

Bridge Structure Motion

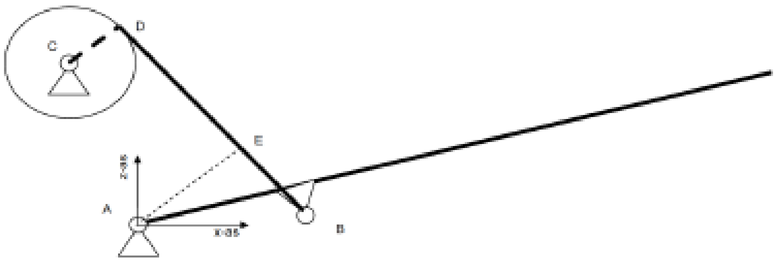

Data generation of motion parameters of the structure and the rack

$$
vd_{val} := \left|
\begin{array}{l}
i \leftarrow 0,1..ii \\
k \leftarrow 0,1..ii-1 \\
vac \leftarrow Si_2 - Si_0 \\
\quad val \leftarrow d\ \ valc \\
vbc \leftarrow dbccA \\
x \leftarrow 0m \\
\quad v \leftarrow 0deg \\
j \leftarrow i \\
j \leftarrow 0 \\
jr \leftarrow 0 \\
0 \\
\text{for } j \in i \\
\quad \left| \begin{array}{l}
vab_j \leftarrow B_2(\ val_j, Si) \\
vae_j \leftarrow uv(vbc_j) \cdot \dfrac{\left| vac \times vab_j \right|}{\left| vbc_j \right|} \\
\quad bc_j \leftarrow \ \ vc(vbc_j)
\end{array} \right. \\
0 \\
\text{for } j \in k \\
\quad \left| \begin{array}{l}
\quad val_j \leftarrow \dfrac{val_{j+1} - \ val_j}{T} \\
vval_{b_j} \leftarrow \ \ val_j \cdot L_{ab} \\
\quad bc_j \leftarrow \dfrac{bc_{j+1} - \ bc_j}{T} \\
0
\end{array} \right. \\
\quad val_{ii} \leftarrow \ \ val_{ii-1} \\
vval_{b_{ii}} \leftarrow vval_{b_{ii-1}} \\
\quad bc_{ii} \leftarrow \ \ bc_{ii-1} \\
0
\end{array}
\right.
$$

$$
\left|
\begin{array}{l}
\text{for } j \in k \\
\quad \left|
\begin{array}{l}
ival_j \leftarrow \dfrac{val_j}{rs_j} \\
val_j \leftarrow \dfrac{val_{j+1} - val_j}{T} \\
aval_{b_j} \leftarrow val_j \cdot \left| vab_0 \right| \cdot nv\left(vab_j\right) \\
bc_j \leftarrow \dfrac{bc_{j+1} - bc_j}{T}
\end{array}
\right. \\
val_{ii} \leftarrow val_{ii-1} \\
aval_{b_{ii}} \leftarrow aval_{b_{ii-1}} \\
ival_{ii} \leftarrow ival_{ii-1} \\
ival_0 \leftarrow ival_1 \\
0 \\
\begin{pmatrix}
val \\
vbc \cdot \dfrac{1}{m} \\
vab \cdot \dfrac{1}{m} \\
vae \cdot \dfrac{1}{m} \\
vval_b \cdot \dfrac{s}{m} \\
val \cdot s \\
aval_b \cdot \dfrac{s^2}{m} \\
val \cdot s^2 \\
bc \\
bc \cdot s \\
bc \cdot s^2 \\
0 \\
ival \\
0
\end{pmatrix}
\end{array}
\right.
$$

Data generation of motion parameters for structure and rack : $vdval := vd_{val}$

Data for angle of the structure around the main pivot point : $val := vdval_0 \cdot rad$

Data for vector from B to C : $vbc := vdval_1 \cdot m$

Data for vector from A to B : $vab := vdval_2 \cdot m$

Data for vector from A to BC normal on BC : $vae := vdval_3 \cdot m$

Data for speed vector in point B : $vval_b := vdval_4 \cdot \dfrac{m}{s}$

Data for angular velocity vector of the structure : $val := vdval_5 \cdot \dfrac{rad}{s}$

Data for accelerai on vector in point B : $aval_b := vdval_6 \cdot \dfrac{m}{s^2}$

Data for angular acceleration vector around the main pivot point $\quad val := vdval_7 \cdot \frac{rad}{s^2}$

Data for vector of the angle of the rack wrt the horizontal $\quad bc := vdval_8 \cdot rad$

Data for vector of the angular velocity of the rack $\quad bc := vdval_9 \cdot \frac{rad}{s}$

Data for vector of the angular acceleration of the rack $\quad bc := vdval_{10} \cdot \frac{rad}{s^2}$

Rack overlength $\quad ol_{cil} := L_{heugel2}$

Transmission ratio of the structure to the drive $\quad ival := vdval_{12}$

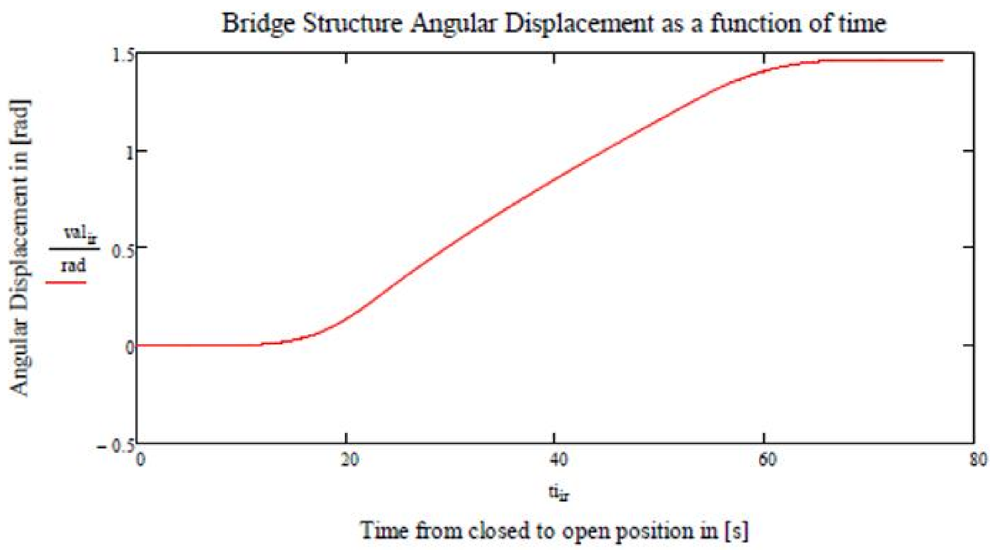

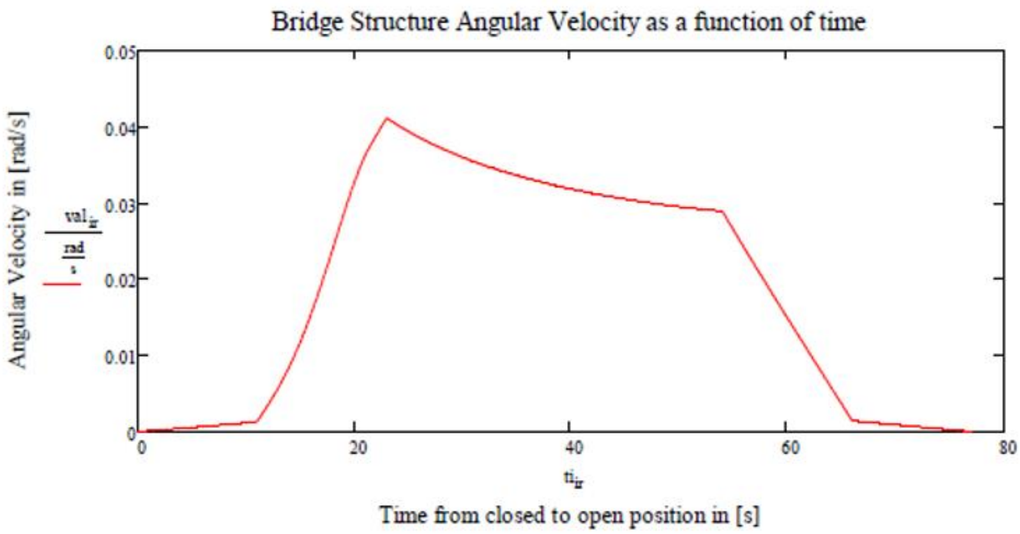

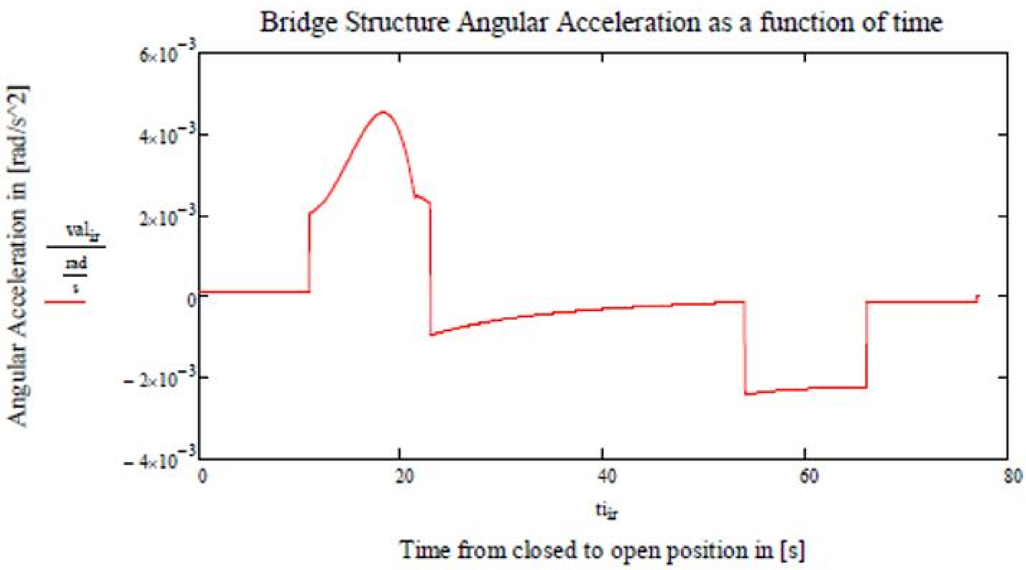

- **Electro-motor Torque Calculation Model according to VOBB**

Table 11a - Ultimate Limit State: Transmission Moment

Index from table 11 $\quad$ $:id := 1$

Characteristic value of the motor torque due to wind

$$:M_{w.rep} := \left| \begin{array}{l} i \leftarrow 0, 1 .. ii \\ k \leftarrow 0, 1 .. ii - 1 \\ \text{for } \alpha \in \alpha val \\ \quad \left| \begin{array}{l} Mw1_j \leftarrow P_{w.rep}(\alpha, 1, P_{w.1}) \cdot A_{val} \cdot L_{v1} \cdot ival_j \cdot i_{twk} \cdot 0 \\ Mw2_j \leftarrow P_{w.rep}(\alpha, 0, P_{w.1}) \cdot A_{val} \cdot L_{v1} \cdot (ival_j \cdot i_{twk}) \cdot 0 \\ j \leftarrow j + 1 \end{array} \right. \\ \begin{pmatrix} Mw1 \\ Mw2 \end{pmatrix} \end{array} \right.$$

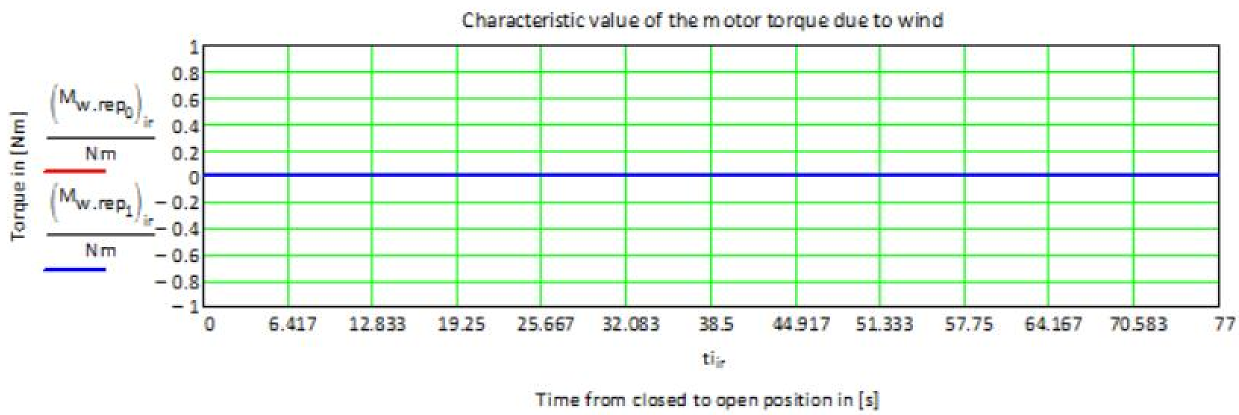

Characteristic value of the motor torque due to selfweight

$$:M_{o.LS.rep} := \left| \begin{array}{l} i \leftarrow 0,1..ii \\ \text{for } j \in i \\ \quad \left| \begin{array}{l} M_{zv_j} \leftarrow (vev \times vzv_j)\cdot ival_j \cdot i_{twk} \\ M_{zh_j} \leftarrow \left[veh \times (vaho_j + vzh)\right]\cdot(ival_j \cdot i_{twk}) \\ M_{zbv_j} \leftarrow (vebv \times vzbv_j)\cdot(ival_j \cdot i_{twk}) \\ M_{zba_j} \leftarrow (veba \times vzba_j + veb \times vzb_j)\cdot(ival_j \cdot i_{twk}) \\ M_j \leftarrow -\left[\left(M_{zv_j}\right)_1 + \left(M_{zh_j}\right)_1 + \left(M_{zbv_j}\right)_1 + \left(M_{zba_j}\right)_1\right] \end{array} \right. \\ M \end{array} \right.$$

Characteristic value of the motor torque due to selfweight

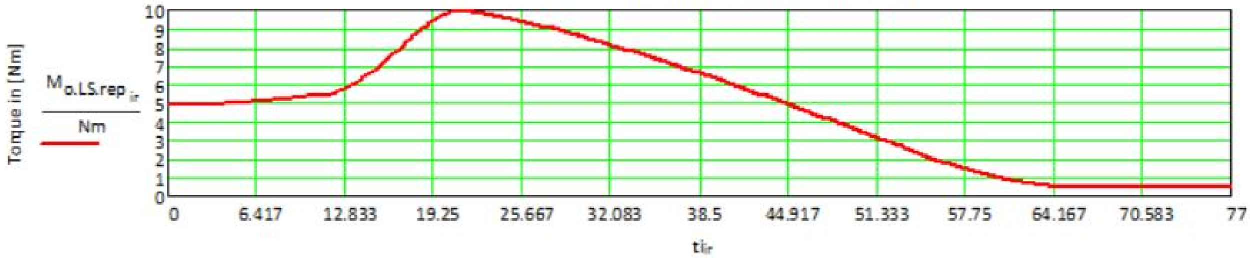

Time from closed to open position in [s]

Design value of the static moment on the motor shaft :

$$M_{s.d} := \left| \begin{array}{l} i \leftarrow 0,1..ii \\ k \leftarrow 0,1..1 \\ \text{for } n \in k \\ \quad \text{for } j \in ii \\ \qquad FF_{s.d_{n,j}} \leftarrow 0 \\ \text{for } j \in i \\ \quad \left| \begin{array}{l} MM_{s.d_{0,j}} \leftarrow \left[\left(M_{w.rep_0}\right)_j + \left[M_{o.LS.rep_j} + (vvo \times vzv_j)_1 \cdot ival_j \cdot i_{twk}\right]\right] \\ MM_{s.d_{1,j}} \leftarrow \left[\left(M_{w.rep_1}\right)_j + \left[M_{o.LS.rep_j} - (vvo \times vzv_j)_1 \cdot ival_j \cdot i_{twk}\right]\right] \\ MM_j \leftarrow \dfrac{\max\left(\max\left(MM_{s.d_{0,j}}, MM_{s.d_{1,j}}\right), \left|\min\left(MM_{s.d_{0,j}}, MM_{s.d_{1,j}}\right)\right|\right)}{\eta_{bew}} \end{array} \right. \\ \begin{pmatrix} \dfrac{MM_{s.d}}{\eta_{bew}} \\ MM \end{pmatrix} \end{array} \right.$$

Design value of the motor torque due to wind acting from above $:Msd_{boven} := \left({M_{s.d_0}}^{T}\right)^{\langle 0 \rangle}$

Design value of the motor torque due to wind acting from below $:Msd_{onder} := \left({M_{s.d_0}}^{T}\right)^{\langle 1 \rangle}$

Design value of the static moment on the motor - maximum absolute value $:Msd := M_{s.d_1}$

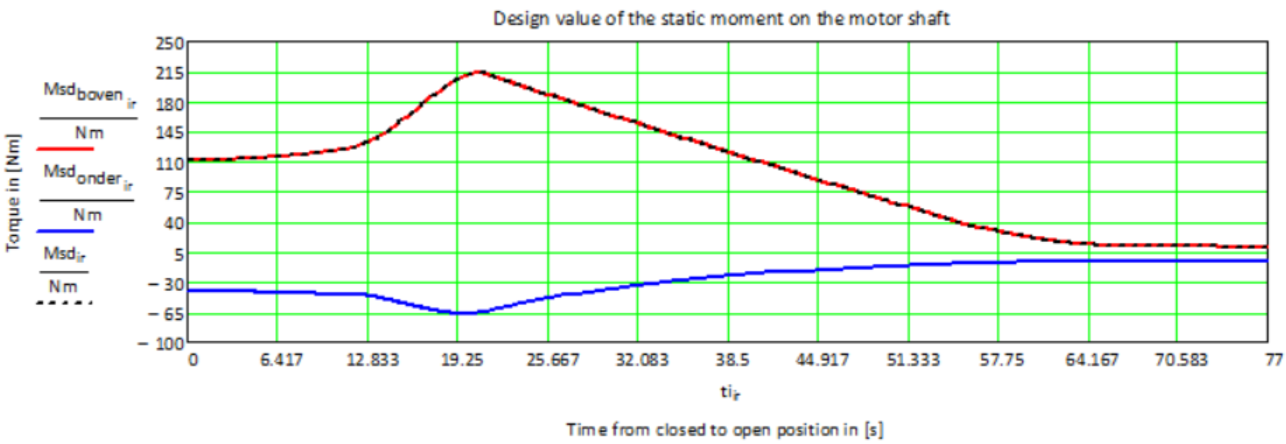
Design value of the static moment on the motor shaft
Torque in [Nm]
Msd_boven_ir / Nm
Msd_onder_ir / Nm
Msd_ir / Nm
250
215
180
145
110
75
40
5
− 30
− 65
− 100
0
6.417
12.833
19.25
25.667
32.083
38.5
44.917
51.333
57.75
64.167
70.583
77
ti_ir
Time from closed to open position in [s]

APPENDIX 2 MATLAB SCRIPTS FOR TWO DEGREES OF FREEDOM MODEL

- **Normal Operation - Model for comparison with theory**

```
% Mechanical Devices Transmission Factor (from the bridge to the electro-motor
itwk = 0.005251;

% Mechanical Devices Efficiency
eta = 1;

% Loading Electro-motor Motion Parameters
load('T.mat');
load('motor.mat');
load('bridgetorque.mat');

% Time
T = T(:,1);
% Angular Acceleration
A = motor(:,3);
% Angular Velocity
V = motor(:,2);
% Angular Displacement
D = motor(:,1);
% Angular Displacement
M = bridgetorque(:,1);

figure;
subplot(2,2,1), plot(T,D); xlabel('Time (s)'); ylabel('Angular Displacement (rad)');
subplot(2,2,2), plot(T,V); xlabel('Time (s)'); ylabel('Angular Velocity (rad/s)');
subplot(2,2,3), plot(T,A); xlabel('Time (s)'); ylabel('Angular Acceleration (rad/s^2)');
subplot(2,2,4), plot(T,M); xlabel('Time (s)'); ylabel('Bridge Torque (Nm)');
```

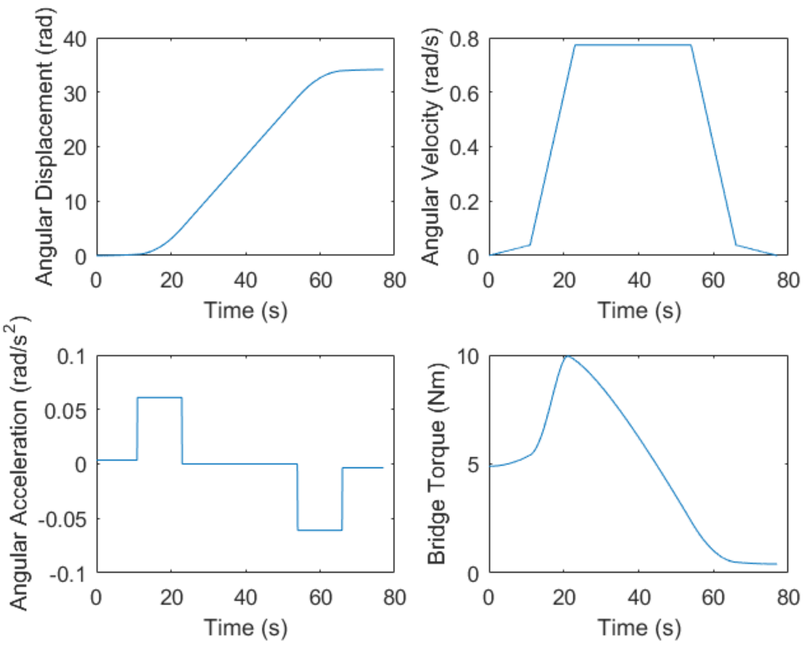

```
% Equations of Motion of the Beam Balanced Bascule Bridge for Normal Operation

function ydot = eom6(t,y,C,K,J1,J2,A,V,D,M,T)

% y =   [ fi2    ]
%       [ fi2dot ]

fi2 = y(1);     % angular displacement of the bridge structure
fi2dot = y(2);  % angular velocity of the bridge structure

% Linear Interpolation of the angular displacement, angular velocity and
% angular acceleration of the electro-motor and the bridge torque


kIndex = find(T>t);

if isempty(kIndex)
    Dm = D(end);
    Vm = V(end);
    Am = A(end);
    Mm = M(end);
else
    kIndex1 = kIndex(1);
    kIndex0 = kIndex1-1;
    dd = (D(kIndex1)-D(kIndex0))/(T(kIndex1)-T(kIndex0));
    Dm = D(kIndex0)+dd*(t-T(kIndex0));
    dv = (V(kIndex1)-V(kIndex0))/(T(kIndex1)-T(kIndex0));
    Vm = V(kIndex0)+dv*(t-T(kIndex0));
    da = (A(kIndex1)-A(kIndex0))/(T(kIndex1)-T(kIndex0));
    Am = A(kIndex0)+da*(t-T(kIndex0));
    dm = (M(kIndex1)-M(kIndex0))/(T(kIndex1)-T(kIndex0));
    Mm = M(kIndex0)+dm*(t-T(kIndex0));

end

fi1 = Dm;       % angular displacement of the electro-motor
fi1dot = Vm;    % angular velocity of the electro-motor

y1 = fi2dot;

y2 = 1/J2*(Mm-C*(fi2dot-fi1dot)-K*(fi2-fi1));
                % angular acceleration of the bridge structure

y3 = fi2;


ydot = [y1;y2;y3];


end

 %function eom
```

```
% Input Data

J1 = 2.373;                      % mass moment of inertia of the electro-motor
J2 = 6427000;                    % mass moment of inertia of the bridge structure
K = 350000;                      % stiffness of the mechanical devices
psi = 0.05;                      % considered damping ratio
Jmd = 1.708052063;                % mass of the mechanical devices
C = 2*psi*sqrt(K*Jmd);       % damping coefficient of the mechanical devices


ti = 0;                          % initial time
dt = 0.1;                        % time increment
tf = 77;                         % final time
Time = ti:dt:tf;
y0=[0;0;0];                      % initial conditions


% Solving the EOMs with ode45 function

[t,y] = ode45(@(t,y) eom6(t,y,C,K,J1,J2,A,V,D,M,T),T,y0);

disp2 = y(:,3);
vel2 = y(:,1);
acc2 = y(:,2);

disp1 = zeros(size(t));
vel1 = zeros(size(t));
acc1 = zeros(size(t));
torquem = zeros(size(t));

for it = 1: 1: length(t)
    kIndex = find(T>t(it));
    if isempty(kIndex)
        Dm = D(end);
        Vm = V(end);
        Am = A(end);
    else
        kIndex1 = kIndex(1);
        kIndex0 = kIndex1-1;
        dd = (D(kIndex1)-D(kIndex0))/(T(kIndex1)-T(kIndex0));
        Dm = D(kIndex0)+dd*(t(it)-T(kIndex0));
        dv = (V(kIndex1)-V(kIndex0))/(T(kIndex1)-T(kIndex0));
        Vm = V(kIndex0)+dv*(t(it)-T(kIndex0));
        da = (A(kIndex1)-A(kIndex0))/(T(kIndex1)-T(kIndex0));
        Am = A(kIndex0)+da*(t(it)-T(kIndex0));
    end

    disp1(it) = Dm;
    vel1(it) = Vm;
    acc1(it) = Am;
    torquem(it)= J1*acc1(it)+C*(vel1(it)-vel2(it))+K*(disp1(it)-disp2(it));
end
```

```
% Plotting the results

figure;
subplot(3,3,1), plot(t,disp1); xlabel('Time (s)'); ylabel('Disp1');
subplot(3,3,2), plot(t,vel1); xlabel('Time (s)'); ylabel('Vel1');
subplot(3,3,3), plot(t,acc1); xlabel('Time (s)'); ylabel('Acc1');
subplot(3,3,4), plot(t,disp2); xlabel('Time (s)'); ylabel('Disp2');
subplot(3,3,5), plot(t,vel2); xlabel('Time (s)'); ylabel('Vel2');
subplot(3,3,6), plot(t,acc2); xlabel('Time (s)'); ylabel('Acc2');
subplot(3,3,7), plot(t,torquem); xlabel('Time (s)'); ylabel('Torquem');

figure;
plot (t, torquem); xlabel('Time (s)'); ylabel('Torquem');
```

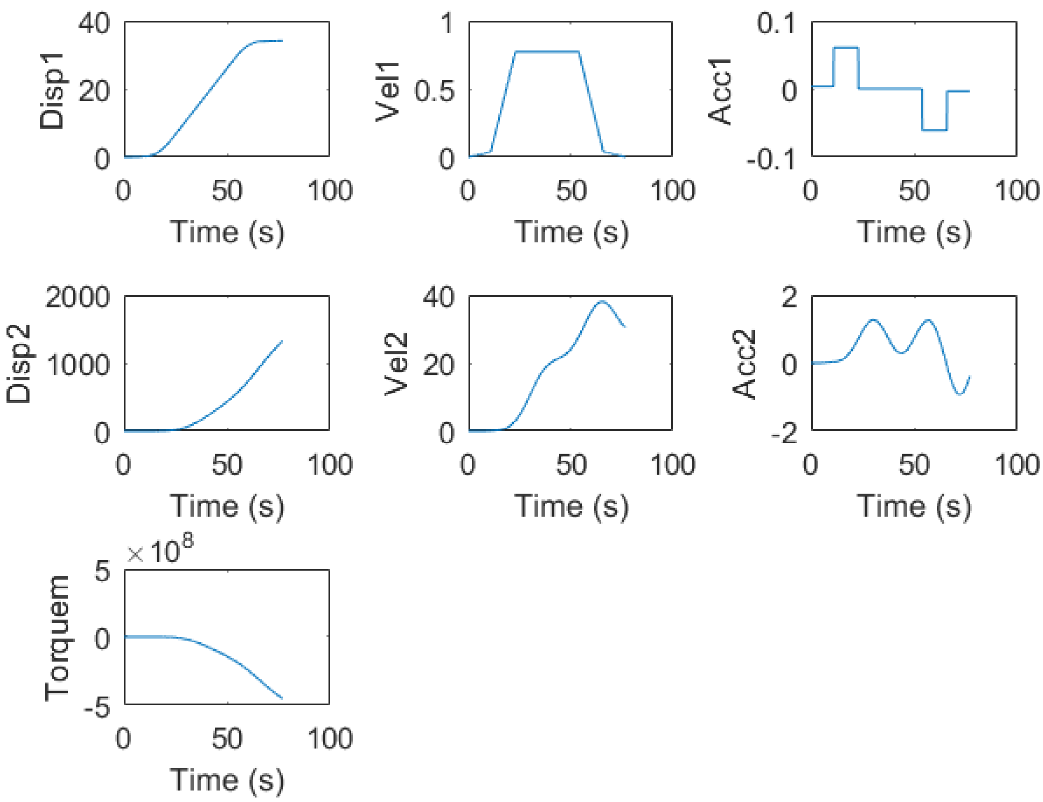

- **Normal Operation – Model for comparison with measurements**

```
% Mechanical Devices Transmission Factor (from the bridge to the electro-motor
itwk = 0.005251;

% Mechanical Devices Efficiency
eta = 1;

% Loading Electro-motor Motion Parameters
load('TBS1.mat');
load('VBS1.mat');
load('MBS1.mat');
load('MBS1filt.mat');
load('MBS1vas.mat');

% Time
T = TBS1(:,1);
% Angular Velocity
V = 2*3.14/60*VBS1(:,1)*itwk;
% Electromotor Torque
Me = MBS1(:,1)*itwk;
% Electromotor Torque - Filtered Data for every 10 elements
Mef = MBS1filt(:,1)*itwk;
% Bridge Torque
M = MBS1vas(:,1);

Index = find(T);
for i = 2:1:length(T)
    A(1) = 0;
    A(i) = (V(i)-V(i-1))/(T(i)-T(i-1));     % Angular Acceleration
end

D = cumtrapz(T,V);                          % Angular Displacement

A = A';

figure;
subplot(2,2,1), plot(T,D); xlabel('Time (s)'); ylabel('Angular Displacement (rad)');
subplot(2,2,2), plot(T,V); xlabel('Time (s)'); ylabel('Angular Velocity (rad/s)');
subplot(2,2,3), plot(T,A); xlabel('Time (s)'); ylabel('Angular Acceleration (rad/s^2)');
subplot(2,2,4), plot(T,M); xlabel('Time (s)'); ylabel('Bridge Torque (Nm)');

figure;
plot(T,Mef);xlabel('Time (s)'); ylabel('Electromotor Torque (Nm)');
```

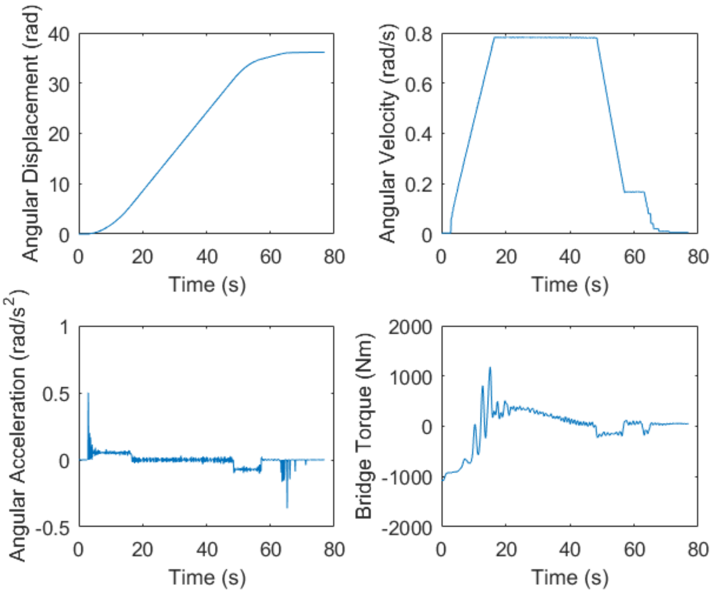


```
% Equations of Motion of the Beam Balanced Bascule Bridge for Normal Operation

function ydot = eom6(t,y,C,K,J1,J2,A,V,D,M,T)

% y =   [ fi2    ]
%       [ fi2dot ]

fi2 = y(1);     % angular displacement of the bridge structure
fi2dot = y(2);  % angular velocity of the bridge structure

% Linear Interpolation of the angular displacement, angular velocity and
% angular acceleration of the electro-motor and the bridge torque

kIndex = find(T>t);

if isempty(kIndex)
    Dm = D(end);
    Vm = V(end);
    Am = A(end);
    Mm = M(end);
else
    kIndex1 = kIndex(1);
    kIndex0 = kIndex1-1;
    dd = (D(kIndex1)-D(kIndex0))/(T(kIndex1)-T(kIndex0));
    Dm = D(kIndex0)+dd*(t-T(kIndex0));
    dv = (V(kIndex1)-V(kIndex0))/(T(kIndex1)-T(kIndex0));
    Vm = V(kIndex0)+dv*(t-T(kIndex0));
    da = (A(kIndex1)-A(kIndex0))/(T(kIndex1)-T(kIndex0));
    Am = A(kIndex0)+da*(t-T(kIndex0));
    dm = (M(kIndex1)-M(kIndex0))/(T(kIndex1)-T(kIndex0));
    Mm = M(kIndex0)+dm*(t-T(kIndex0));

end
```

```
fi1 = Dm;       % angular displacement of the electro-motor
fi1dot = Vm;    % angular velocity of the electro-motor

y1 = fi2dot;

y2 = 1/J2*(Mm-C*(fi2dot-fi1dot)-K*(fi2-fi1));
                % angular acceleration of the bridge structure

y3 = fi2;

ydot = [y1;y2;y3];

end

%function eom
% Input Data

J1 = 2.373;                     % mass moment of inertia of the electro-motor
J2 = 6427000;                   % mass moment of inertia of the bridge structure
K = 333155;                     % stiffness of the mechanical devices
psi = 0.05;                     % considered damping ratio
Jmd = 1.708052063;               % mass of the mechanical devices
C = 2*psi*sqrt(K*Jmd);      % damping coefficient of the mechanical devices


ti = 0;                         % initial time
dt = 0.1;                       % time increment
tf = 77;                        % final time
Time = ti:dt:tf;
y0=[0;0;0];                     % initial conditions

% Solving the EOMs with ode45 function

[t,y] = ode45(@(t,y) eom6(t,y,C,K,J1,J2,A,V,D,M,T),T,y0);

vel2 = y(:,1);
acc2 = y(:,2);
disp2 = y(:,3);


disp1 = zeros(size(t));
vel1 = zeros(size(t));
acc1 = zeros(size(t));
torquem = zeros(size(t));

for it = 1: 1: length(t)
    kIndex = find(T>t(it));
    if isempty(kIndex)
        Dm = D(end);
        Vm = V(end);
        Am = A(end);
```

```
    else
        kIndex1 = kIndex(1);
        kIndex0 = kIndex1-1;
        dd = (D(kIndex1)-D(kIndex0))/(T(kIndex1)-T(kIndex0));
        Dm = D(kIndex0)+dd*(t(it)-T(kIndex0));
        dv = (V(kIndex1)-V(kIndex0))/(T(kIndex1)-T(kIndex0));
        Vm = V(kIndex0)+dv*(t(it)-T(kIndex0));
        da = (A(kIndex1)-A(kIndex0))/(T(kIndex1)-T(kIndex0));
        Am = A(kIndex0)+da*(t(it)-T(kIndex0));
    end

    disp1(it) = Dm;
    vel1(it) = Vm;
    acc1(it) = Am;
    torquem(it)= J1*acc1(it)+C*(vel1(it)-vel2(it))+K*(disp1(it)-disp2(it));
end

% Plotting the results

figure;
subplot(3,3,1), plot(t,disp1); xlabel('Time (s)'); ylabel('Disp1');
subplot(3,3,2), plot(t,vel1); xlabel('Time (s)'); ylabel('Vel1');
subplot(3,3,3), plot(t,acc1); xlabel('Time (s)'); ylabel('Acc1');
subplot(3,3,4), plot(t,disp2); xlabel('Time (s)'); ylabel('Disp2');
subplot(3,3,5), plot(t,vel2); xlabel('Time (s)'); ylabel('Vel2');
subplot(3,3,6), plot(t,acc2); xlabel('Time (s)'); ylabel('Acc2');
subplot(3,3,7), plot(t,torquem); xlabel('Time (s)'); ylabel('Torquem');
```

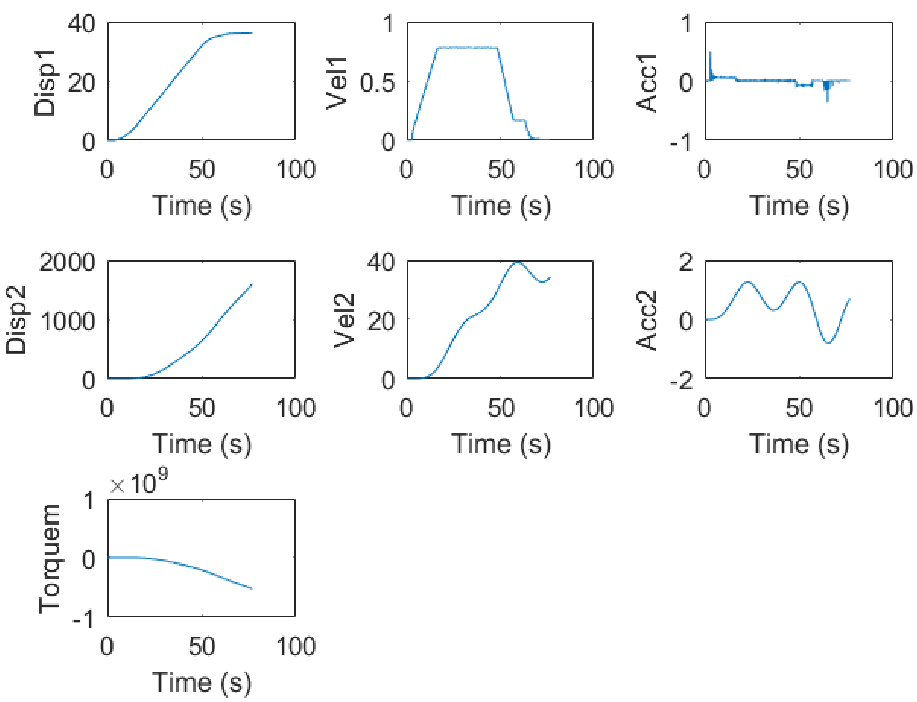

- **Brake Situation – Model for comparison with theory**

```
% Mechanical Devices Transmission Factor (from the bridge to the electro-motor
itwk = 0.005251;

% Mechanical Devices Efficiency
eta = 1;

% Loading Electro-motor Motion Parameters
load('T.mat');
load('motor.mat');
load('bridgetorque.mat');

% Time
T = T(:,1);
% Angular Acceleration
A = motor(:,3);
% Angular Velocity
V = motor(:,2);
% Angular Displacement
D = motor(:,1);
% Angular Displacement
M = bridgetorque(:,1);

figure;
subplot(2,2,1), plot(T,D); xlabel('Time (s)'); ylabel('Angular Displacement (rad)');
subplot(2,2,2), plot(T,V); xlabel('Time (s)'); ylabel('Angular Velocity (rad/s)');
subplot(2,2,3), plot(T,A); xlabel('Time (s)'); ylabel('Angular Acceleration (rad/s^2)');
subplot(2,2,4), plot(T,M); xlabel('Time (s)'); ylabel('Bridge Torque (Nm)');
```

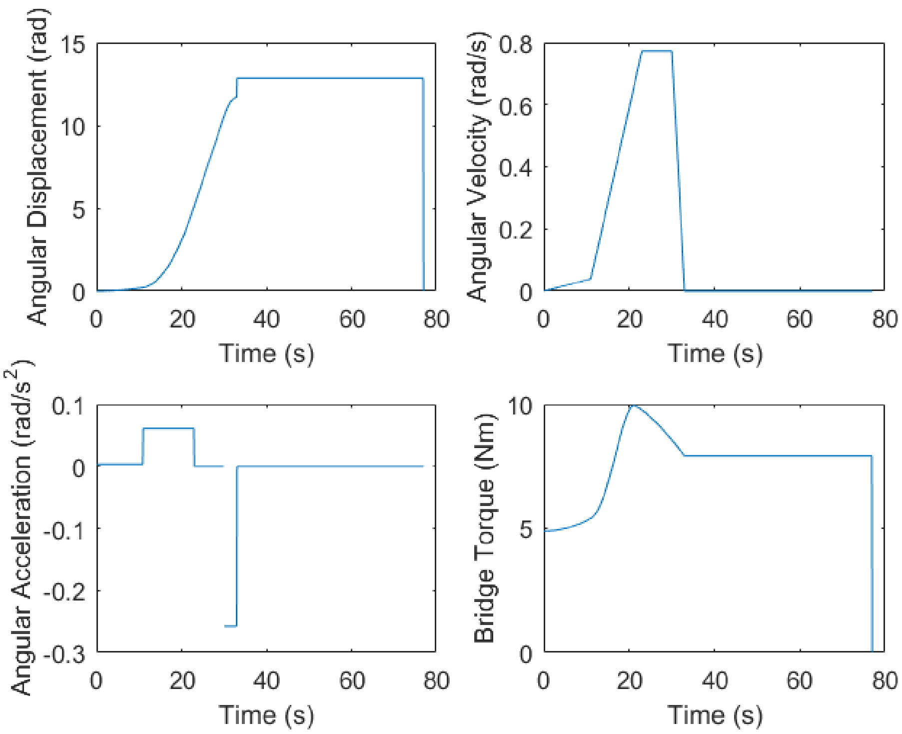

```
% Equations of Motion of the Beam Balanced Bascule Bridge for Brake Situation

function ydot = eom6brake(t,y,C,K,J1,J2,A,V,D,M,T,tbrake)

% y =   [ fi2    ]
%       [ fi2dot ]


fi2 = y(1);     % angular displacement of the bridge structure
fi2dot = y(2);  % angular velocity of the bridge structure

% Linear Interpolation of the angular displacement, angular velocity and angular acceleration of
the electro-motor

kIndex = find(T>t);
tbindex = find(T==tbrake);

if isempty(kIndex)
    Dm = D(end);
    Vm = V(end);
    Am = A(end);
    Mm = M(end);
else
    kIndex1 = kIndex(1);
    kIndex0 = kIndex1-1;

    if t<tbrake

        dd = (D(kIndex1)-D(kIndex0))/(T(kIndex1)-T(kIndex0));
        Dm = D(kIndex0)+dd*(t-T(kIndex0));
        dv = (V(kIndex1)-V(kIndex0))/(T(kIndex1)-T(kIndex0));
        Vm = V(kIndex0)+dv*(t-T(kIndex0));
        da = (A(kIndex1)-A(kIndex0))/(T(kIndex1)-T(kIndex0));
        Am = A(kIndex0)+da*(t-T(kIndex0));
        dm = (M(kIndex1)-M(kIndex0))/(T(kIndex1)-T(kIndex0));
        Mm = M(kIndex0)+dm*(t-T(kIndex0));

    else
        if t>(tbrake+3)
            indexstop = find(T==tbrake+3);
            Vm = 0;
            Dm = D(indexstop);
            Am = 0;
            Mm = M(indexstop);

        else
                dv = V(tbindex)/(-3);
                Vm = V(tbindex)+dv*(t-tbrake);
                Dm = D(tbindex)+(t-tbrake)*(Vm+V(tbindex))/2;
                Am = A(tbindex)+(Vm-V(tbindex))/(t-tbrake);
                dm = (M(kIndex1)-M(kIndex0))/(T(kIndex1)-T(kIndex0));
                Mm = M(kIndex0)+dm*(t-T(kIndex0));
```

```
        end
end
end

fi1 = Dm;       % angular displacement of the electro-motor
fi1dot = Vm;    % angular velocity of the electro-motor
bridgetorque = Mm;

y1 = fi2dot;

y2 = 1/J2*(bridgetorque-C*(fi2dot-fi1dot)-K*(fi2-fi1));
                % angular acceleration of the bridge structure

y3 = fi2;

if fi2<0
    fi2 = 0;
end

ydot = [y1;y2;y3];

end

 %function eom

% Input Data

J1 = 2.373;                     % mass moment of inertia of the electro-motor
J2 = 6427000;                   % mass moment of inertia of the bridge structure
K = 350000;                     % stiffness of the mechanical devices
psi = 0.05;                     % considered damping ratio
Jmd = 1.708052063;               % mass of the mechanical devices
C = 2*psi*sqrt(K*Jmd);      % damping coefficient of the mechanical devices

tbrake = 30;                    % time at which the brake is applied

ti = 0;                         % initial time
dt = 0.1;                       % time increment
tf = 77;                        % final time
Time = ti:dt:tf;
y0=[0;0;0];               % initial conditions


% Solving the EOMs with ode45 function

[t,y] = ode45(@(t,y) eom6brake(t,y,C,K,J1,J2,A,V,D,M,T,tbrake),T,y0);


vel2 = y(:,1);
acc2 = y(:,2);
disp2 = y(:,3);
```

```
disp1 = zeros(size(t));
vel1 = zeros(size(t));
acc1 = zeros(size(t));
torquem = zeros(size(t));
bridgetorque = zeros(size(t));

for it = 1: 1: length(t)
    kIndex = find(T>t(it));
    tbindex = find(T==tbrake);

    if isempty(kIndex)
        Dm = D(end);
        Vm = V(end);
        Am = A(end);
        Mm = M(end);
    else
        kIndex1 = kIndex(1);
        kIndex0 = kIndex1-1;

        if t(it)<tbrake

            dd = (D(kIndex1)-D(kIndex0))/(T(kIndex1)-T(kIndex0));
            Dm = D(kIndex0)+dd*(t(it)-T(kIndex0));
            dv = (V(kIndex1)-V(kIndex0))/(T(kIndex1)-T(kIndex0));
            Vm = V(kIndex0)+dv*(t(it)-T(kIndex0));
            da = (A(kIndex1)-A(kIndex0))/(T(kIndex1)-T(kIndex0));
            Am = A(kIndex0)+da*(t(it)-T(kIndex0));
            dM = (M(kIndex1)-M(kIndex0))/(T(kIndex1)-T(kIndex0));
            Mm = M(kIndex0)+dM*(t(it)-T(kIndex0));

        else
            indexstop = find(T==tbrake+3);
            if t(it)<=(tbrake+3)
                dv = V(tbindex)/(-3);
                Vm = V(tbindex)+dv*(t(it)-tbrake);
                Dm = D(tbindex)+(t(it)-tbrake)*(Vm+V(tbindex))/2;
                Am = A(tbindex)+(Vm-V(tbindex))/(t(it)-tbrake);
                dM = (M(kIndex1)-M(kIndex0))/(T(kIndex1)-T(kIndex0));
                Mm = M(kIndex0)+dM*(t(it)-T(kIndex0));
            else
                Vm = 0;
                Dm = D(indexstop);
                Am = 0;
                Mm = M(indexstop);
            end
        end

    disp1(it) = Dm;
    vel1(it) = Vm;
    acc1(it) = Am;
    bridgetorque(it) = Mm;
```

```
    torquem(it)= J1*acc1(it)+C*(vel1(it)-vel2(it))+K*(disp1(it)-disp2(it));
    end
end

% Plotting the results

figure;

subplot(3,3,1), plot(t,disp1); xlabel('Time (s)'); ylabel('Disp1');
subplot(3,3,2), plot(t,vel1); xlabel('Time (s)'); ylabel('Vel1');
subplot(3,3,3), plot(t,acc1); xlabel('Time (s)'); ylabel('Acc1');
subplot(3,3,4), plot(t,disp2); xlabel('Time (s)'); ylabel('Disp2');
subplot(3,3,5), plot(t,vel2); xlabel('Time (s)'); ylabel('Vel2');
subplot(3,3,6), plot(t,acc2); xlabel('Time (s)'); ylabel('Acc2');
subplot(3,3,7), plot(t,torquem); xlabel('Time (s)'); ylabel('Torquem');

figure;
subplot(2,2,1), plot(T,disp1); xlabel('Time (s)'); ylabel('Angular Displacement (rad)');
subplot(2,2,2), plot(T,vel1); xlabel('Time (s)'); ylabel('Angular Velocity (rad/s)');
subplot(2,2,3), plot(T,acc1); xlabel('Time (s)'); ylabel('Angular Acceleration (rad/s^2)');
subplot(2,2,4), plot(T,bridgetorque); xlabel('Time (s)'); ylabel('Bridge Torque (Nm)');
```

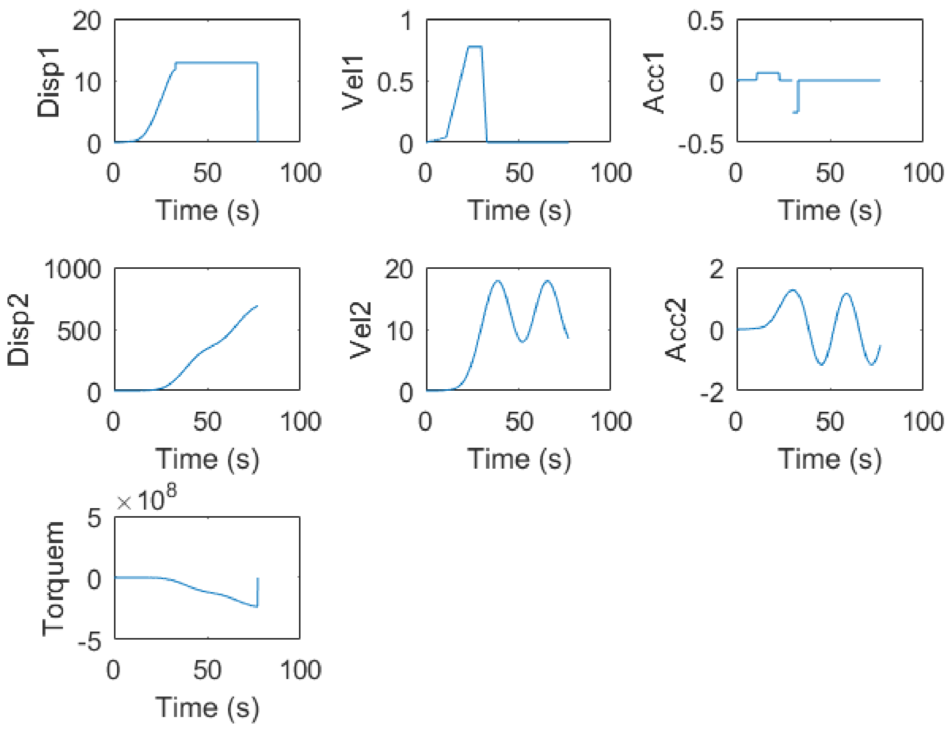

- **Brake Situation – Model for comparison with measurements**

```
% Mechanical Devices Transmission Factor (from the bridge to the electro-motor
itwk = 0.005251;

% Mechanical Devices Efficiency
eta = 1;

% Loading Electro-motor Motion Parameters
load('TBS4.mat');
load('VBS4.mat');
load('MBS4.mat');
load('MBS4filt.mat');
load('MBS4vas.mat');

% Time
T = TBS4(:,1);
% Angular Velocity
V = 2*3.14/60*VBS4(:,1)*itwk;
% Electromotor torque
Me = MBS4(:,1)*itwk;
% Electromotor torque - Filtered data for every 10 elements
Mef = MBS4filt(:,1)*itwk;
% Electromotor torque
M = MBS4vas(:,1);

Index = find(T);
for i = 2:1:length(T)
    A(1) = 0;
    A(i) = (V(i)-V(i-1))/(T(i)-T(i-1));     % Angular Acceleration

end

D = cumtrapz(T,V);                          % Angular Displacement


A = A';

figure;
subplot(2,2,1), plot(T,D); xlabel('Time (s)'); ylabel('Angular Displacement (rad)');
subplot(2,2,2), plot(T,V); xlabel('Time (s)'); ylabel('Angular Velocity (rad/s)');
subplot(2,2,3), plot(T,A); xlabel('Time (s)'); ylabel('Angular Acceleration (rad/s^2)');
subplot(2,2,4), plot(T,M); xlabel('Time (s)'); ylabel('Bridge Torque (Nm)');

figure;
plot(T,Mef);xlabel('Time (s)'); ylabel('Electromotor Torque (Nm)');
```

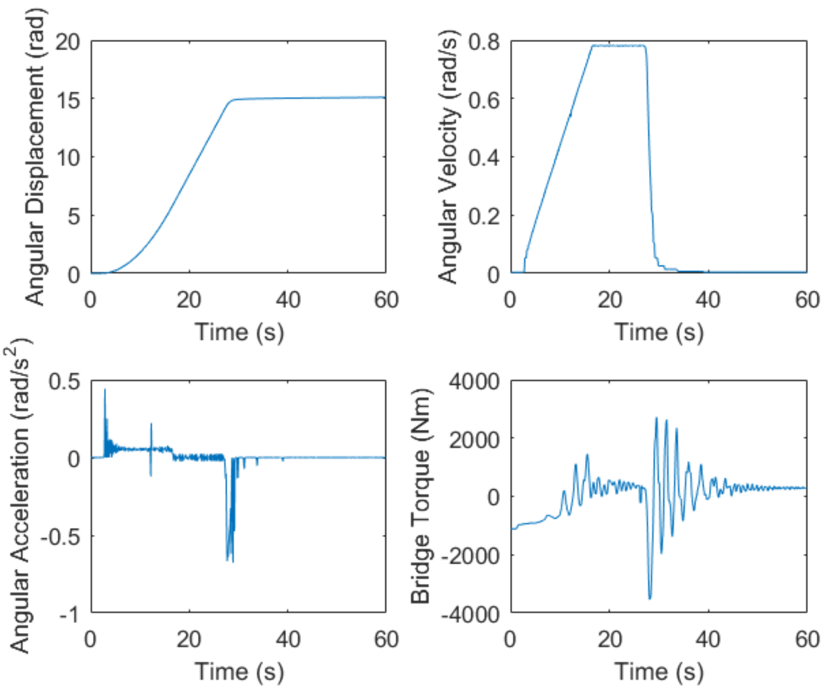


```
% Equations of Motion of the Beam Balanced Bascule Bridge for Brake Situation

function ydot = eom6(t,y,C,K,J1,J2,A,V,D,M,T)

% y =   [ fi2    ]
%       [ fi2dot ]

fi2 = y(1);      % angular displacement of the bridge structure
fi2dot = y(2);   % angular velocity of the bridge structure

% Linear Interpolation of the angular displacement, angular velocity and
% angular acceleration of the electro-motor and the bridge torque

kIndex = find(T>t);

if isempty(kIndex)
    Dm = D(end);
    Vm = V(end);
    Am = A(end);
    Mm = M(end);
else
    kIndex1 = kIndex(1);
    kIndex0 = kIndex1-1;
    dd = (D(kIndex1)-D(kIndex0))/(T(kIndex1)-T(kIndex0));
    Dm = D(kIndex0)+dd*(t-T(kIndex0));
    dv = (V(kIndex1)-V(kIndex0))/(T(kIndex1)-T(kIndex0));
    Vm = V(kIndex0)+dv*(t-T(kIndex0));
    da = (A(kIndex1)-A(kIndex0))/(T(kIndex1)-T(kIndex0));
    Am = A(kIndex0)+da*(t-T(kIndex0));
    dm = (M(kIndex1)-M(kIndex0))/(T(kIndex1)-T(kIndex0));
    Mm = M(kIndex0)+dm*(t-T(kIndex0));
```

```
end

fi1 = Dm;       % angular displacement of the electro-motor
fi1dot = Vm;    % angular velocity of the electro-motor

y1 = fi2dot;

y2 = 1/J2*(Mm-C*(fi2dot-fi1dot)-K*(fi2-fi1));
                % angular acceleration of the bridge structure

y3 = fi2;

ydot = [y1;y2;y3];

end

 %function eom
% Input Data

J1 = 2.373;                     % mass moment of inertia of the electro-motor
J2 = 6427000;                   % mass moment of inertia of the bridge structure
K = 333155;                     % stiffness of the mechanical devices
psi = 0.05;                     % considered damping ratio
Jmd = 1.708052063;               % mass of the mechanical devices
C = 2*psi*sqrt(K*Jmd);      % damping coefficient of the mechanical devices

ti = 0;                         % initial time
dt = 0.1;                       % time increment
tf = 77;                        % final time
Time = ti:dt:tf;
y0=[0;0;0];                     % initial conditions

% Solving the EOMs with ode45 function

[t,y] = ode45(@(t,y) eom6(t,y,C,K,J1,J2,A,V,D,M,T),T,y0);

vel2 = y(:,1);
acc2 = y(:,2);
disp2 = y(:,3);

disp1 = zeros(size(t));
vel1 = zeros(size(t));
acc1 = zeros(size(t));
torquem = zeros(size(t));

for it = 1: 1: length(t)
    kIndex = find(T>t(it));
    if isempty(kIndex)
        Dm = D(end);
        Vm = V(end);
        Am = A(end);
```

```
    else
        kIndex1 = kIndex(1);
        kIndex0 = kIndex1-1;
        dd = (D(kIndex1)-D(kIndex0))/(T(kIndex1)-T(kIndex0));
        Dm = D(kIndex0)+dd*(t(it)-T(kIndex0));
        dv = (V(kIndex1)-V(kIndex0))/(T(kIndex1)-T(kIndex0));
        Vm = V(kIndex0)+dv*(t(it)-T(kIndex0));
        da = (A(kIndex1)-A(kIndex0))/(T(kIndex1)-T(kIndex0));
        Am = A(kIndex0)+da*(t(it)-T(kIndex0));
    end

    disp1(it) = Dm;
    vel1(it) = Vm;
    acc1(it) = Am;
    torquem(it)= J1*acc1(it)+C*(vel1(it)-vel2(it))+K*(disp1(it)-disp2(it));
end

% Plotting the results

figure;
subplot(3,3,1), plot(t,disp1); xlabel('Time (s)'); ylabel('Disp1');
subplot(3,3,2), plot(t,vel1); xlabel('Time (s)'); ylabel('Vel1');
subplot(3,3,3), plot(t,acc1); xlabel('Time (s)'); ylabel('Acc1');
subplot(3,3,4), plot(t,disp2); xlabel('Time (s)'); ylabel('Disp2');
subplot(3,3,5), plot(t,vel2); xlabel('Time (s)'); ylabel('Vel2');
subplot(3,3,6), plot(t,acc2); xlabel('Time (s)'); ylabel('Acc2');
subplot(3,3,7), plot(t,torquem); xlabel('Time (s)'); ylabel('Torquem');
```

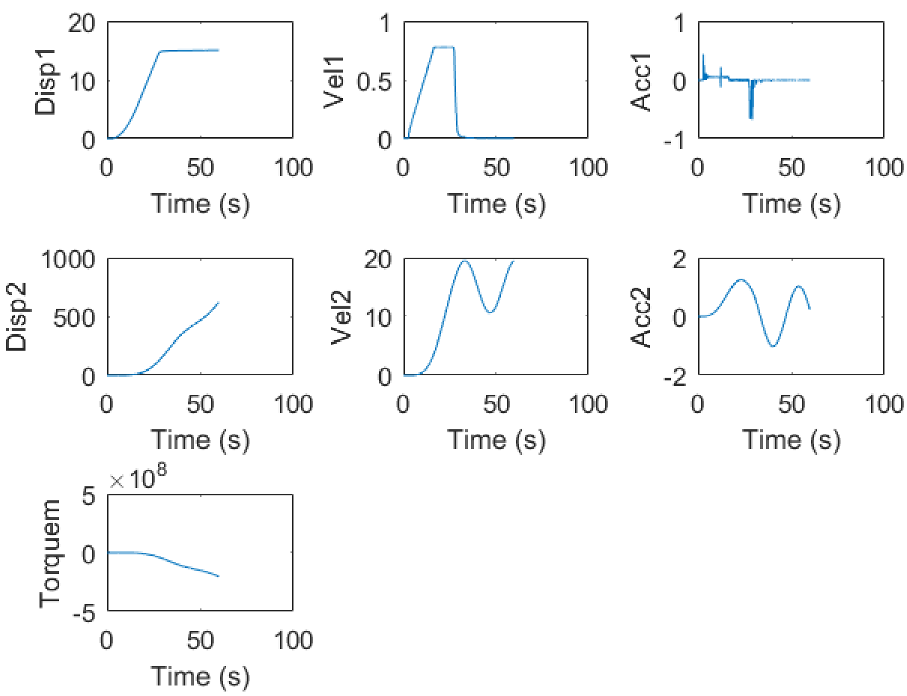

APPENDIX 3 MATLAB SCRIPTS FOR THREE DEGREES OF FREEDOM MODEL

- **Equations of motion derived by Newton's Second Law**

```
function ydot = eom(t,y,Jb,Jd,lh,beta,ch,kh,mb,md,g,lb,ld,H,Lr,gamai,lc,rm,Disp,Vel,T,kmd,cmd)

% y = [ fib
%       fibdot
%       fid
%       fiddot ]

fib = y(1);
fibdot = y(2);
fid = y(3);
fiddot = y(4);

% Interpolation of the input motion parameters for the time t of the solver
kIndex = find(T>t);

if isempty(kIndex)
    Dm = Disp(end);
    Vm = Vel(end);
else
    kIndex1 = kIndex(1);
    kIndex0 = kIndex1-1;
    dd = (Disp(kIndex1)-Disp(kIndex0))/(T(kIndex1)-T(kIndex0));
    Dm = Disp(kIndex0)+dd*(t-T(kIndex0));
    dv = (Vel(kIndex1)-Vel(kIndex0))/(T(kIndex1)-T(kIndex0));
    Vm = Vel(kIndex0)+dv*(t-T(kIndex0));
end

% Angular Displacement of the Motor
fim = Dm;
% Angular Velocity of the Motor
fimdot = Vm;
% Length of the hanger at any position
D = ((H+sin(fib)*lh-sin(fid)*lh)^2+(H*tan(beta)+lh*(1-cos(fib))-lh*(1-cos(fid)))^2)^(1/2);
% The first derivative of the elongation of the hanger
Dprim = 1/2*D^(-1)*(2*lh*(H+sin(fib)*lh-sin(fid)*lh)*(cos(fib)*fibdot-
cos(fid)*fiddot)+2*lh*(H*tan(beta)+lh*(1-cos(fib))-lh*(1-cos(fid)))*(sin(fib)*fibdot-
sin(fid)*fiddot));
% Angle between the hanger and the vertical axis at any position
ang = atan((H*tan(beta)+lh*(1-cos(fib))-lh*(1-cos(fid)))/(H+sin(fib)*lh-sin(fid)*lh));
% Vertical length of the rack at any position
H1 = Lr*sin(gamai)-lc*sin(fid)+2*fim*rm/3.14;
% Horizontal length of the rack at any position
L1 = Lr*cos(gamai)-lc*(1-cos(fid))+2*fim*rm/3.14;
% Length of the rack at any position
D1 = (H1^2+L1^2)^(1/2);
% First Derivative of the elongation of the rack
```

```
D1prim = 1/2*(D1)^(-1)*((-2*H1*lc*cos(fid)-
2*L1*lc*sin(fid))*fiddot+(4*H1*rm/3.14+4*L1*rm/3.14)*fimdot);
% Angle between the rack and the horizontal axis at any position
ang1 = atan(H1/L1);
% Equation of Motion of the Balance Part
fib2dot = (+mb*g*lb*cos(fib)-(kh*(D-
H/cos(beta))+ch*Dprim)*(cos(ang)*lh*cos(fib)+sin(ang)*lh*sin(fib)))/Jb;
% Equation of Motion of the Deck
fid2dot = (-md*g*ld*cos(fid)+(kh*(D-
H/cos(beta))+ch*Dprim)*(cos(ang)*lh*cos(fid)+sin(ang)*lh*sin(fid))+(kmd*(D1-
Lr)+cmd*D1prim)*(cos(ang1)*lc*sin(fid)+sin(ang1)*lc*cos(fid)))/Jd;

ydot = [fibdot;fib2dot;fiddot;fid2dot];

fprintf(1, 'time = %d s\n', t);
end
```

- **Equations of motion derived by Lagrangian Approach**

The translational degrees of freedom necessary to express the potential energy stored in the springs are expressed function of the angular displacement of the component parts of the bridge. The elongation of the hanger is denoted by uh and the elongation of the mechanical devices (rack bar) is denoted by ur.

The vertical length of the hanger:

$> H := H_h + l_h \cdot \sin(\varphi_b(t)) - l_h \cdot \sin(\varphi_d(t)) :$

The horizontal length of the hanger:

$> L := H_h \cdot \tan(\text{beta}) + l_h \cdot (1 - \cos(\varphi_b(t))) - l_h \cdot (1 - \cos(\varphi_d(t))) :$

The length of the hanger:

$> D_h := \text{sqrt}(L^2 + H^2) :$

The angle between the hanger and the vertical axis:

$> beta_h := \arctan\left(\frac{L}{H}\right);$

$$\beta_h := \arctan\left(\frac{H_h \tan(\beta) + l_h (1 - \cos(\varphi_b(t))) - l_h (1 - \cos(\varphi_d(t)))}{H_h + l_h \sin(\varphi_b(t)) - l_h \sin(\varphi_d(t))}\right) \tag{1}$$

The elongation of the hanger:

$> u_h := \left(D_h - \frac{H_h}{\cos(\text{beta})}\right);$

$$u_h := \sqrt{(H_h + l_h \sin(\varphi_b(t)) - l_h \sin(\varphi_d(t)))^2 + (H_h \tan(\beta) + l_h (1 - \cos(\varphi_b(t))) - l_h (1 - \cos(\varphi_d(t))))^2} - \frac{H_h}{\cos(\beta)} \tag{2}$$

The vertical length of the rack:

$$> H_1 := L_y \cdot \sin(gama_i) - l_c \cdot \sin(\varphi_d(t)) + \frac{2 \cdot r_m \cdot \varphi_m(t)}{3.14};$$

$$H_1 := L_y \sin(gama_i) - l_c \sin(\varphi_d(t)) + 0.6369426752\, r_m\, \varphi_m(t) \tag{3}$$

The horizontal length of the rack:

$$> L_1 := L_y \cdot \cos(gama_i) - l_c \cdot (1 - \cos(\varphi_d(t))) + \frac{2 \cdot r_m \cdot \varphi_m(t)}{3.14};$$

$$L_1 := L_y \cos(gama_i) - l_c \left(1 - \cos(\varphi_d(t))\right) + 0.6369426752\, r_m\, \varphi_m(t) \tag{4}$$

The length of the rack:

$$> D_1 := \mathrm{sqrt}(L_1^2 + H_1^2);$$

$$D_1 := \left(\left(L_y \sin(gama_i) - l_c \sin(\varphi_d(t)) + 0.6369426752\, r_m\, \varphi_m(t)\right)^2 + \left(L_y \cos(gama_i) - l_c \left(1 - \cos(\varphi_d(t))\right) + 0.6369426752\, r_m\, \varphi_m(t)\right)^2\right)^{1/2} \tag{5}$$

The angle between the rack and the horizontal axis:

$$> gama_1 := \arctan\left(\frac{H_1}{L_1}\right);$$

$$gama_1 := \arctan\left(\frac{L_y \sin(gama_i) - l_c \sin(\varphi_d(t)) + 0.6369426752\, r_m\, \varphi_m(t)}{L_y \cos(gama_i) - l_c \left(1 - \cos(\varphi_d(t))\right) + 0.6369426752\, r_m\, \varphi_m(t)}\right) \tag{6}$$

The elongation of the rack:

$$> u_y := (D_1 - L_y);$$

$$u_y := \left(\left(L_y \sin(gama_i) - l_c \sin(\varphi_d(t)) + 0.6369426752\, r_m\, \varphi_m(t)\right)^2 + \left(L_y \cos(gama_i) - l_c \left(1 - \cos(\varphi_d(t))\right) + 0.6369426752\, r_m\, \varphi_m(t)\right)^2\right)^{1/2} - L_y \tag{7}$$

The Lagrangian approach for deriving the equations of motion is a analytical dynamics method based upon conservation of energy. The considered energies are kinetic K and potential P. The potential energy considers both the energy stored in springs and the energy due to gravity. An additional energy is also considered, the dissipation energy Diss, which accounts for the dampers present in the system.

$$> K := \frac{1}{2} \cdot J_b \cdot \left(\mathit{diff}\left(\varphi_b(t), t\right)\right)^2 + \frac{1}{2} \cdot J_d \cdot \left(\mathit{diff}\left(\varphi_d(t), t\right)\right)^2 + \frac{1}{2} \cdot J_m \cdot \left(\mathit{diff}\left(\varphi_m(t), t\right)\right)^2;$$

$$K := \frac{1}{2} J_b \left(\frac{d}{dt} \varphi_b(t)\right)^2 + \frac{1}{2} J_d \left(\frac{d}{dt} \varphi_d(t)\right)^2 + \frac{1}{2} J_m \left(\frac{d}{dt} \varphi_m(t)\right)^2 \tag{8}$$

$$> P := \frac{1}{2} \cdot k_h \cdot (u_h)^2 + \frac{1}{2} \cdot k_{md} (u_y)^2 - m_b \cdot g \cdot l_b \cdot \sin(\varphi_b(t)) + m_d \cdot g \cdot l_d \cdot \sin(\varphi_d(t));$$

$$P := \frac{1}{2} k_k \left(\sqrt{\left(H_k + l_k \sin(\varphi_b(t)) - l_k \sin(\varphi_d(t))\right)^2 + \left(H_k \tan(\beta) + l_k \left(1 - \cos(\varphi_b(t))\right) - l_k \left(1 - \cos(\varphi_d(t))\right)\right)^2} - \frac{H_k}{\cos(\beta)} \right)^2 + \frac{1}{2} k_{md} \left(\left(\left(L_y \sin(gama_i) - l_c \sin(\varphi_d(t)) + 0.6369426752\, r_m \varphi_m(t)\right)^2 + \left(L_y \cos(gama_i) - l_c \left(1 - \cos(\varphi_d(t))\right) + 0.6369426752\, r_m \varphi_m(t)\right)^2 \right)^{1/2} - L_y \right)^2 - m_b g\, l_b \sin(\varphi_b(t)) + m_d g\, l_d \sin(\varphi_d(t)) \tag{9}$$

> $Diss := \frac{1}{2} \cdot c_k \cdot (diff(u_k, t))^2 + \frac{1}{2} \cdot c_{md} (diff(u_y, t))^2;$

$$Diss := \frac{1}{8} \left(c_k \left(2 \left(H_k + l_k \sin(\varphi_b(t)) - l_k \sin(\varphi_d(t))\right) \left(l_k \cos(\varphi_b(t)) \left(\frac{d}{dt} \varphi_b(t)\right) - l_k \cos(\varphi_d(t)) \left(\frac{d}{dt} \varphi_d(t)\right) \right) + 2 \left(H_k \tan(\beta) + l_k \left(1 - \cos(\varphi_b(t))\right) - l_k \left(1 - \cos(\varphi_d(t))\right)\right) \left(l_k \sin(\varphi_b(t)) \left(\frac{d}{dt} \varphi_b(t)\right) - l_k \sin(\varphi_d(t)) \left(\frac{d}{dt} \varphi_d(t)\right) \right) \right)^2 \right) \Big/ \left(\left(H_k + l_k \sin(\varphi_b(t)) - l_k \sin(\varphi_d(t))\right)^2 + \left(H_k \tan(\beta) + l_k \left(1 - \cos(\varphi_b(t))\right) - l_k \left(1 - \cos(\varphi_d(t))\right)\right)^2 \right) + \frac{1}{8} \left(c_{md} \left(2 \left(L_y \sin(gama_i) - l_c \sin(\varphi_d(t)) + 0.6369426752\, r_m \varphi_m(t)\right) \left(-l_c \cos(\varphi_d(t)) \left(\frac{d}{dt} \varphi_d(t)\right) + 0.6369426752\, r_m \left(\frac{d}{dt} \varphi_m(t)\right) \right) + 2 \left(L_y \cos(gama_i) - l_c \left(1 - \cos(\varphi_d(t))\right) + 0.6369426752\, r_m \varphi_m(t)\right) \left(-l_c \sin(\varphi_d(t)) \left(\frac{d}{dt} \varphi_d(t)\right) + 0.6369426752\, r_m \left(\frac{d}{dt} \varphi_m(t)\right) \right) \right)^2 \right) \Big/ \left(\left(L_y \sin(gama_i) - l_c \sin(\varphi_d(t)) + 0.6369426752\, r_m \varphi_m(t)\right)^2 + \left(L_y \cos(gama_i) - l_c \left(1 - \cos(\varphi_d(t))\right) + 0.6369426752\, r_m \varphi_m(t)\right)^2 \right) \tag{10}$$

> $L := K - P;$

$$L := \frac{1}{2} J_b \left(\frac{d}{dt} \varphi_b(t)\right)^2 + \frac{1}{2} J_d \left(\frac{d}{dt} \varphi_d(t)\right)^2 + \frac{1}{2} J_m \left(\frac{d}{dt} \varphi_m(t)\right)^2 - \frac{1}{2} k_k \left(\sqrt{\left(H_k + l_k \sin(\varphi_b(t)) - l_k \sin(\varphi_d(t))\right)^2 + \left(H_k \tan(\beta) + l_k \left(1 - \cos(\varphi_b(t))\right) - l_k \left(1 - \cos(\varphi_d(t))\right)\right)^2} - \frac{H_k}{\cos(\beta)} \right)^2 - \frac{1}{2} k_{md} \left(\left(\left(L_y \sin(gama_i) - l_c \sin(\varphi_d(t)) + 0.6369426752\, r_m \varphi_m(t)\right)^2 + \left(L_y \cos(gama_i) - l_c \left(1 - \cos(\varphi_d(t))\right) + 0.6369426752\, r_m \varphi_m(t)\right)^2 \right)^{1/2} - L_y \right)^2 + m_b g\, l_b \sin(\varphi_b(t)) - m_d g\, l_d \sin(\varphi_d(t)) \tag{11}$$

The Lagrange's equations are used to find the equations of motion of the system. This is accomplished by generating generalized forces Qi(t) for each degree of freedom qi.

> $Lb := subs\left(\left\{\varphi_b(t) = var1, diff\left(\varphi_b(t), t\right) = var2, \varphi_d(t) = var3, diff\left(\varphi_d(t), t\right) = var4, \varphi_m(t) = var5, diff\left(\varphi_m(t), t\right) = var6\right\}, L\right):$

Equation of motion of the balance part (degree of freedom φ_b)

> $Eq11 := diff(Lb, var2):$

> $Eq12 := diff(Lb, var1):$

> $Eq13 := subs\left(\left\{var1 = \varphi_b(t), var2 = diff\left(\varphi_b(t), t\right), var3 = \varphi_d(t), var4 = diff\left(\varphi_d(t), t\right)\right\}, Eq11\right):$

> $Eq14 := subs\left(\left\{var1 = \varphi_b(t), var2 = diff\left(\varphi_b(t), t\right), var3 = \varphi_d(t), var4 = diff\left(\varphi_d(t), t\right)\right\}, Eq12\right):$

> $Eq15 := diff(Eq13, t):$

> $Eq18 := subs\left(\left\{\varphi_b(t) = var1, diff\left(\varphi_b(t), t\right) = var2, \varphi_d(t) = var3, diff\left(\varphi_d(t), t\right) = var4\right\}, Diss\right):$

> $Eq19 := diff(Eq18, var2):$

> $Eq20 := subs\left(\left\{var1 = \varphi_b(t), var2 = diff\left(\varphi_b(t), t\right), var3 = \varphi_d(t), var4 = diff\left(\varphi_d(t), t\right)\right\}, Eq19\right):$

> $Eq16 := Eq15 - Eq14 + Eq20:$

> $Eq17 := collect(Eq16, diff);$

$$\begin{aligned}
Eq17 := {} & J_b\left(\frac{d^2}{dt^2}\varphi_b(t)\right) + \frac{1}{4}\Bigg(c_k\Big(2\left(H_k + l_k\sin(\varphi_b(t)) - l_k\sin(\varphi_d(t))\right)l_k\cos(\varphi_b(t)) + 2\left(H_k\tan(\beta) + l_k(1\right.\\
& \left.-\cos(\varphi_b(t))) - l_k(1-\cos(\varphi_d(t)))\right)l_k\sin(\varphi_b(t))\Big)^2\left(\frac{d}{dt}\varphi_b(t)\right)\Bigg)\Bigg/\Big(\left(H_k + l_k\sin(\varphi_b(t))\right.\\
& \left.- l_k\sin(\varphi_d(t))\right)^2 + \left(H_k\tan(\beta) + l_k(1-\cos(\varphi_b(t))) - l_k(1-\cos(\varphi_d(t)))\right)^2\Big) + \frac{1}{4}\Bigg(c_k\Big(-2\left(H_k\right.\\
& \left.+ l_k\sin(\varphi_b(t)) - l_k\sin(\varphi_d(t))\right)l_k\cos(\varphi_d(t)) - 2\left(H_k\tan(\beta) + l_k(1-\cos(\varphi_b(t))) - l_k(1\right.\\
& \left.-\cos(\varphi_d(t)))\right)l_k\sin(\varphi_d(t))\Big)\Big(2\left(H_k + l_k\sin(\varphi_b(t)) - l_k\sin(\varphi_d(t))\right)l_k\cos(\varphi_b(t)) + 2\left(H_k\tan(\beta) + l_k(1\right.\\
& \left.-\cos(\varphi_b(t))) - l_k(1-\cos(\varphi_d(t)))\right)l_k\sin(\varphi_b(t))\Big)\left(\frac{d}{dt}\varphi_d(t)\right)\Bigg)\Bigg/\Big(\left(H_k + l_k\sin(\varphi_b(t))\right.\\
& \left.- l_k\sin(\varphi_d(t))\right)^2 + \left(H_k\tan(\beta) + l_k(1-\cos(\varphi_b(t))) - l_k(1-\cos(\varphi_d(t)))\right)^2\Big)\\
& + \frac{1}{2}\Bigg(k_k\Bigg(\\
& \sqrt{\left(H_k + l_k\sin(\varphi_b(t)) - l_k\sin(\varphi_d(t))\right)^2 + \left(H_k\tan(\beta) + l_k(1-\cos(\varphi_b(t))) - l_k(1-\cos(\varphi_d(t)))\right)^2}\\
& - \frac{H_k}{\cos(\beta)}\Bigg)\Big(2\left(H_k + l_k\sin(\varphi_b(t)) - l_k\sin(\varphi_d(t))\right)l_k\cos(\varphi_b(t)) + 2\left(H_k\tan(\beta) + l_k(1-\cos(\varphi_b(t))\right)
\end{aligned} \quad (12)$$

$$-l_k\left(1-\cos(\varphi_d(t))\right)l_k\sin(\varphi_b(t))\Big)\Big/\sqrt{\left(H_k+l_k\sin(\varphi_b(t))-l_k\sin(\varphi_d(t))\right)^2+\left(H_k\tan(\beta)+l_k\left(1-\cos(\varphi_b(t))\right)-l_k\left(1-\cos(\varphi_d(t))\right)\right)^2}$$
$$-m_b\,g\,l_b\cos(\varphi_b(t))$$

Equation of motion of the deck (degree of freedom φ_d)

```
> Eq21 := diff(Lb, var4) :
> Eq22 := diff(Lb, var3) :
> Eq23 := subs({var1=φb(t), var2=diff(φb(t), t), var3=φd(t), var4=diff(φd(t), t), var5=φm(t), var6
  =diff(φm(t), t)}, Eq21) :
> Eq24 := subs({var1=φb(t), var2=diff(φb(t), t), var3=φd(t), var4=diff(φd(t), t), var5=φm(t), var6
  =diff(φm(t), t)}, Eq22) :
> Eq25 := diff(Eq23, t) :
> Eq28 := subs({φb(t) = var1, diff(φb(t), t) = var2, φd(t) = var3, diff(φd(t), t) = var4, φm(t) = var5, diff(φm(t), t)
  = var6}, Diss) :
> Eq29 := diff(Eq28, var4) :
> Eq30 := subs({var1=φb(t), var2=diff(φb(t), t), var3=φd(t), var4=diff(φd(t), t), var5=φm(t), var6
  =diff(φm(t), t)}, Eq29) :
> Eq26 := Eq25 − Eq24 + Eq30 :
> Eq27 := collect(Eq26, diff);
```

$$Eq27 := J_d\left(\frac{d^2}{dt^2}\varphi_d(t)\right)+\Big(0.2500000000\,c_k\Big(2.\left(l_k\sin(\varphi_b(t))-1.\,l_k\sin(\varphi_d(t))+H_k\right)l_k\cos(\varphi_b(t))$$
$$+2.\left(H_k\tan(\beta)+l_k\left(1.-1.\cos(\varphi_b(t))\right)-1.\,l_k\left(1.-1.\cos(\varphi_d(t))\right)\right)l_k\sin(\varphi_b(t))\Big)\Big(-2.\left(l_k\sin(\varphi_b(t))\right.$$
$$\left.-1.\,l_k\sin(\varphi_d(t))+H_k\right)l_k\cos(\varphi_d(t))-2.\left(H_k\tan(\beta)+l_k\left(1.-1.\cos(\varphi_b(t))\right)-1.\,l_k\left(1.\right.\right.$$
$$\left.\left.-1.\cos(\varphi_d(t))\right)\right)l_k\sin(\varphi_d(t))\Big)\left(\frac{d}{dt}\varphi_b(t)\right)\Big)\Big/\Big(\left(l_k\sin(\varphi_b(t))-1.\,l_k\sin(\varphi_d(t))+H_k\right)^2 \tag{13}$$
$$+\left(H_k\tan(\beta)+l_k\left(1.-1.\cos(\varphi_b(t))\right)-1.\,l_k\left(1.-1.\cos(\varphi_d(t))\right)\right)^2\Big)+\Big(\Big(0.2500000000\,c_{md}\Big($$
$$-2.\left(L_y\sin(gama_i)-1.\,l_c\sin(\varphi_d(t))+0.6369426752\,r_m\varphi_m(t)\right)l_c\cos(\varphi_d(t))-2.\left(L_y\cos(gama_i)-1.\,l_c\left(1.\right.\right.$$

$$-1.\cos(\varphi_d(t))) + 0.6369426752\, r_m \varphi_m(t))\, l_c \sin(\varphi_d(t)))^2) \Big/ ((L_y \sin(gama_i) - 1.\, l_c \sin(\varphi_d(t))$$

$$+ 0.6369426752\, r_m \varphi_m(t))^2 + (L_y \cos(gama_i) - 1.\, l_c (1. - 1.\cos(\varphi_d(t))) + 0.6369426752\, r_m \varphi_m(t))^2)$$

$$+ \Big(0.2500000000\, c_k \big(-2.\, (l_k \sin(\varphi_b(t)) - 1.\, l_k \sin(\varphi_d(t)) + H_k)\, l_k \cos(\varphi_d(t)) - 2.\, (H_k \tan(\beta) + l_k (1. - 1.\cos$$

$$-1.\cos(\varphi_d(t))))^2)\big) \left(\frac{d}{dt} \varphi_d(t)\right) + \Big(0.2500000000\, c_{md} (1.273885350\, (L_y \sin(gama_i)$$

$$-1.\, l_c \sin(\varphi_d(t)) + 0.6369426752\, r_m \varphi_m(t))\, r_m + 1.273885350\, (L_y \cos(gama_i) - 1.\, l_c (1. - 1.\cos(\varphi_d(t)))$$

$$+ 0.6369426752\, r_m \varphi_m(t))\, r_m)\, (-2.\, (L_y \sin(gama_i) - 1.\, l_c \sin(\varphi_d(t))$$

$$+ 0.6369426752\, r_m \varphi_m(t))\, l_c \cos(\varphi_d(t)) - 2.\, (L_y \cos(gama_i) - 1.\, l_c (1. - 1.\cos(\varphi_d(t)))$$

$$+ 0.6369426752\, r_m \varphi_m(t))\, l_c \sin(\varphi_d(t)))\, \left(\frac{d}{dt} \varphi_m(t)\right)\Big) \Big/ ((L_y \sin(gama_i) - 1.\, l_c \sin(\varphi_d(t))$$

$$+ 0.6369426752\, r_m \varphi_m(t))^2 + (L_y \cos(gama_i) - 1.\, l_c (1. - 1.\cos(\varphi_d(t))) + 0.6369426752\, r_m \varphi_m(t))^2)$$

$$+ \Big(0.5000000000\, k_{md} \Big(\sqrt{(L_y \sin(gama_i) - l_c \sin(\varphi_d(t)) + 0.6369426752\, r_m \varphi_m(t))^2 + (L_y \cos(gama_i) - l_c (1 -}$$

$$r_m \varphi_m(t))\, l_c \sin(\varphi_d(t)))\Big) \Big/$$

$$((L_y \sin(gama_i) - l_c \sin(\varphi_d(t)) + 0.6369426752\, r_m \varphi_m(t))^2 + (L_y \cos(gama_i) - l_c (1$$

$$- \cos(\varphi_d(t))) + 0.6369426752\, r_m \varphi_m(t))^2)^{1/2}$$

$$+ \Big(0.5000000000\, k_k \Big(\sqrt{(H_k + l_k \sin(\varphi_b(t)) - l_k \sin(\varphi_d(t)))^2 + (H_k \tan(\beta) + l_k (1 - \cos(\varphi_b(t))) - l_k (1 - \mathrm{cc}}$$

$$-1.\, l_k (1. - 1.\cos(\varphi_d(t))))\, l_k \sin(\varphi_d(t)))\Big) \Big/$$

$$\sqrt{(H_k + l_k \sin(\varphi_b(t)) - l_k \sin(\varphi_d(t)))^2 + (H_k \tan(\beta) + l_k (1 - \cos(\varphi_b(t))) - l_k (1 - \cos(\varphi_d(t))))^2}$$

$$+ m_d\, g\, l_d \cos(\varphi_d(t))$$

Equation of motion of the motor (degree of freedom φ_m)

> $Eq31 := diff(Lb, var6):$

> $Eq32 := diff(Lb, var5):$

> $Eq33 := subs(\{var1 = \varphi_b(t), var2 = diff(\varphi_b(t), t), var3 = \varphi_d(t), var4 = diff(\varphi_d(t), t), var5 = \varphi_m(t), var6 = diff(\varphi_m(t), t)\}, Eq31):$

> $Eq34 := subs(\{var1 = \varphi_b(t), var2 = diff(\varphi_b(t), t), var3 = \varphi_d(t), var4 = diff(\varphi_d(t), t), var5 = \varphi_m(t), var6 = diff(\varphi_m(t), t)\}, Eq32):$

> $Eq35 := diff(Eq33, t):$

> $Eq38 := subs(\{\varphi_b(t) = var1, diff(\varphi_b(t), t) = var2, \varphi_d(t) = var3, diff(\varphi_d(t), t) = var4, \varphi_m(t) = var5, diff(\varphi_m(t), t) = var6\}, Diss):$

> $Eq39 := diff(Eq38, var6):$

> $Eq40 := subs\left(\left\{var1 = \varphi_b(t), var2 = diff\left(\varphi_b(t), t\right), var3 = \varphi_d(t), var4 = diff\left(\varphi_d(t), t\right), var5 = \varphi_m(t), var6 = diff\left(\varphi_m(t), t\right)\right\}, Eq39\right):$

> $Eq36 := Eq35 - Eq34 + Eq40:$

> $Eq37 := collect(Eq36, diff);$

$$
\begin{aligned}
Eq37 := {} & J_m \left(\frac{d^2}{dt^2} \varphi_m(t)\right) + \Big(0.2500000000\, c_{md} \big(1.273885350\, \left(L_y \sin(gama_i) - 1.\, l_c \sin(\varphi_d(t))\right. \\
& \left.+ 0.6369426752\, r_m \varphi_m(t)\right) r_m + 1.273885350\, \left(L_y \cos(gama_i) - 1.\, l_c \left(1. - 1.\cos(\varphi_d(t))\right)\right. \\
& \left.+ 0.6369426752\, r_m \varphi_m(t)\right) r_m\big) \big(-2.\, \left(L_y \sin(gama_i) - 1.\, l_c \sin(\varphi_d(t))\right. \\
& \left.+ 0.6369426752\, r_m \varphi_m(t)\right) l_c \cos(\varphi_d(t)) - 2.\, \left(L_y \cos(gama_i) - 1.\, l_c \left(1. - 1.\cos(\varphi_d(t))\right)\right. \\
& \left.+ 0.6369426752\, r_m \varphi_m(t)\right) l_c \sin(\varphi_d(t))\big) \left(\frac{d}{dt} \varphi_d(t)\right)\Big) \Big/ \Big(\left(L_y \sin(gama_i) - 1.\, l_c \sin(\varphi_d(t))\right. \\
& \left.+ 0.6369426752\, r_m \varphi_m(t)\right)^2 + \left(L_y \cos(gama_i) - 1.\, l_c \left(1. - 1.\cos(\varphi_d(t))\right) + 0.6369426752\, r_m \varphi_m(t)\right)^2\Big) \\
& + \Big(0.2500000000\, c_{md} \big(1.273885350\, \left(L_y \sin(gama_i) - 1.\, l_c \sin(\varphi_d(t)) + 0.6369426752\, r_m \varphi_m(t)\right) r_m + 1.2738853 \\
& - 1.\cos(\varphi_d(t))\big) + 0.6369426752\, r_m \varphi_m(t)\big)^2\Big) \\
& + \Big(0.5000000000\, k_{md} \Big(\sqrt{\left(L_y \sin(gama_i) - l_c \sin(\varphi_d(t)) + 0.6369426752\, r_m \varphi_m(t)\right)^2 + \left(L_y \cos(gama_i) - l_c (1 -\right.} \\
& \Big(\left(L_y \sin(gama_i) - l_c \sin(\varphi_d(t)) + 0.6369426752\, r_m \varphi_m(t)\right)^2 + \left(L_y \cos(gama_i) - l_c \left(1\right.\right. \\
& \left.\left. - \cos(\varphi_d(t))\right) + 0.6369426752\, r_m \varphi_m(t)\right)^2\Big)^{1/2}
\end{aligned}
\tag{14}
$$

- **Normal Operation – Model for comparison with theory**

```
clear all
close all
clc

% Loading Motor Motion Parameters

itwk = 5.251*10^(-3);          % Mechanical Devices Transmission Factor
eta = 0.135;                   % Mechanical Devices Efficiency


load('T.mat');                 % Loading Time
load('motor.mat');             % Loading Motor Motion Parameters
% Time
T = T(:,1);
% Angular Acceleration
Acc = motor(:,3);
% Angular Velocity
Vel = motor(:,2);
% Angular Displacement
Disp = motor(:,1);

figure;
```

```
subplot(1,3,1), plot(T,Disp); xlabel('Time (s)'); ylabel('Angular Displacement');
subplot(1,3,2), plot(T,Vel); xlabel('Time (s)'); ylabel('Angular Velocity');
subplot(1,3,3), plot(T,Acc); xlabel('Time (s)'); ylabel('Angular Acceleration');

% Input Data

g = 9.81;                          % gravitational acceleration
Jb = 2.138*10^6;                   % mass moment of inertia of the balance part
mb = 74969;                        % mass of the balance part
Jd = 3.98*10^6;                    % mass moment of inertia of the deck
md = 46017;                        % mass of the deck
Jm = 2.373;                        % mass moment of inertia of the electro-motor
kh = 347858326.1;                  % stiffness of the hanger 347858326.1
kmd = 140000000;                   % stiffness of the mechanical devices 140000000
mh = 2000;                         % mass of the hanger
psi = 0.05;                        % considered damping ratio
ch = 2*psi*sqrt(kh/mh)*mh;         % damping coefficient of the hanger
mmd = 1366.44165;                  % mass of the mechanical devices
cmd = 2*psi*sqrt(kmd/mmd)*mmd;     % damping coefficient of the mechanical devices
lb = 5.16;                         % distance from the center of gravity of the balance part to the
upper pivot point
beta = 0.23;                       % the angle between the hanger and the vertical axis (in closed
position)
ld = 8.004;                        % distance from the center of gravity of the deck to the lower
pivot point
lh = 12.63;                        % distance from the connection point of the hanger to the pivot
points
lc = 3.7;                          % distance from the connection point of the rack and the deck to
the lower pivot point
rm = 0.136;                        % the angle between the rack and the horizontal axis (in closed
position)
H = 12.07;                         % vertical length of the hanger
gamai = 0.604;                     % initial angle between the rack and the deck
Lr = 6.445;                        % initial length of the rack

ti = 0;                            % initial time
dt = 0.1;                          % time increment
tf = 77;                           % final time
Time = ti:dt:tf;                   % time range
y0 = [0;0;0;0];                    % initial conditions

% Ordinary Differential Equations Solver

[t,y] = ode45(@(t,y)
eom(t,y,Jb,Jd,lh,beta,ch,kh,mb,md,g,lb,ld,H,Lr,gamai,lc,rm,Disp,Vel,T,kmd,cmd),Time,y0);

% Angular Displacement of the Balance Part
dispb = y(:,1);
% Angular Velocity of the Balance Part
velb = y(:,2);
% Angular Displacement of the Deck
dispd = y(:,3);
```

```
% Angular Velocity of the Deck
veld = y(:,4);

accb = zeros(size(t));
accd = zeros(size(t));

% Algorithm for computing the angular accelerations and the motor torque

for it = 1:1:length(t)

    kIndex = find(T>t(it));
    if isempty(kIndex)
        Dm = Disp(end);
        Vm = Vel(end);
        Am = Acc(end);
    else
        kIndex1 = kIndex(1);
        kIndex0 = kIndex1-1;
        dd = (Disp(kIndex1)-Disp(kIndex0))/(T(kIndex1)-T(kIndex0));
        Dm = Disp(kIndex0)+dd*(t(it)-T(kIndex0));
        dv = (Vel(kIndex1)-Vel(kIndex0))/(T(kIndex1)-T(kIndex0));
        Vm = Vel(kIndex0)+dv*(t(it)-T(kIndex0));
        da = (Acc(kIndex1)-Acc(kIndex0))/(T(kIndex1)-T(kIndex0));
        Am = Acc(kIndex0)+da*(t(it)-T(kIndex0));
    end

    % Angular Displacement of the Motor
    dispm(it) = Dm;
    % Angular Velocity of the Motor
    velm(it) = Vm;
    % Angular Acceleration of the Motor
    accm(it) = Am;
    % Length of the hanger at any position
    D = ((H+sin(dispb(it))*lh-sin(dispd(it))*lh)^2+(H*tan(beta)+lh*(1-cos(dispb(it)))-lh*(1-
cos(dispd(it))))^2)^(1/2);
    % The first derivative of the elongation of the hanger
    Dprim = 1/2*D^(-1)*(2*lh*(H+sin(dispb(it))*lh-sin(dispd(it))*lh)*(cos(dispb(it))*velb(it)-
cos(dispd(it))*veld(it))+2*lh*(H*tan(beta)+lh*(1-cos(dispb(it)))-lh*(1-
cos(dispd(it))))*(sin(dispb(it))*velb(it)-sin(dispd(it))*veld(it)));
    % Angle between the hanger and the vertical axis at any position
    ang = atan((H*tan(beta)+lh*(1-cos(dispb(it)))-lh*(1-cos(dispd(it))))/(H+sin(dispb(it))*lh-
sin(dispd(it))*lh));
    % Vertical length of the rack at any position
    H1 = Lr*sin(gamai)-lc*sin(dispd(it))+2*dispm(it)*rm/3.14;
    % Horizontal length of the rack at any position
    L1 = Lr*cos(gamai)-lc*(1-cos(dispd(it)))+2*dispm(it)*rm/3.14;
    % Length of the rack at any position
    D1 = (H1^2+L1^2)^(1/2);
    % First Derivative of the elongation of the rack
    D1prim = 1/2*(D1)^(-1)*((-2*H1*lc*cos(dispd(it))-
2*L1*lc*sin(dispd(it)))*veld(it)+(4*H1*rm/3.14+4*L1*rm/3.14)*velm(it));
    % Angle between the rack and the horizontal axis at any position
```

```
    ang1 = atan(H1/L1);

    % Angular Acceleration of the Balance Part
    accb(it) = (+mb*g*lb*cos(dispb(it))-(kh*(D-
H/cos(beta))+ch*Dprim)*(cos(ang)*lh*cos(dispb(it))+sin(ang)*lh*sin(dispb(it))))/Jb;
    % Angular Acceleration of the Deck
    accd(it) = (-md*g*ld*cos(dispd(it))+(kh*(D-
H/cos(beta))+ch*Dprim)*(cos(ang)*lh*cos(dispd(it))+sin(ang)*lh*sin(dispd(it)))+(kmd*(D1-
Lr)+cmd*D1prim)*(cos(ang1)*lc*sin(dispd(it))+sin(ang1)*lc*cos(dispd(it))))/Jd;
    % Torque acting on the Motor
    Mmotor(it) = -rm*(kmd*(D1-Lr)+cmd*D1prim)+Jm*accm(it);

end

% Plotting Results (Unfiltered)

figure;
subplot(3,3,1), plot(t,dispb); xlabel('Time (s)'); ylabel('Angular Displacement - Balance Part
[rad]');
subplot(3,3,2), plot(t,velb); xlabel('Time (s)'); ylabel('Angular Velocity - Balance Part
[rad/s]');
subplot(3,3,3), plot(t,accb); xlabel('Time (s)'); ylabel('Angular Acceleration - Balance Part
[rad/s^2]');
subplot(3,3,4), plot(t,dispd); xlabel('Time (s)'); ylabel('Angular Displacement - Deck [rad]');
subplot(3,3,5), plot(t,veld); xlabel('Time (s)'); ylabel('Angular Velocity - Deck [rad/s]');
subplot(3,3,6), plot(t,accd); xlabel('Time (s)'); ylabel('Angular Acceleration - Deck
[rad/s^2]');
subplot(3,3,7), plot(t,Mmotor); xlabel('Time (s)'); ylabel('Motor Torque [Nm]');
```

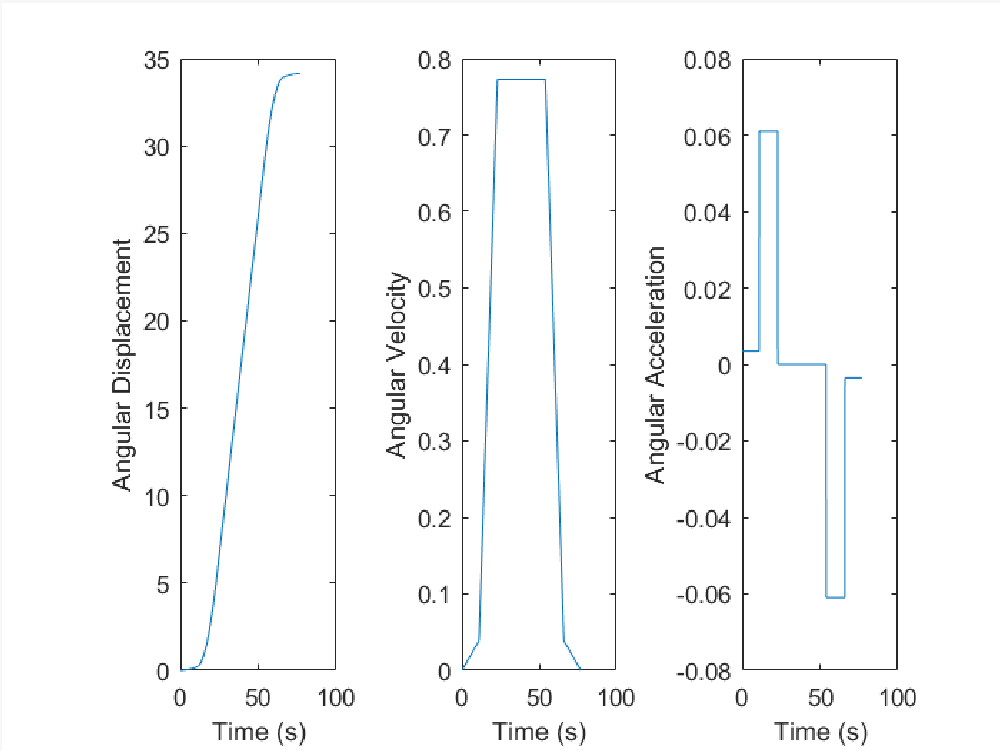

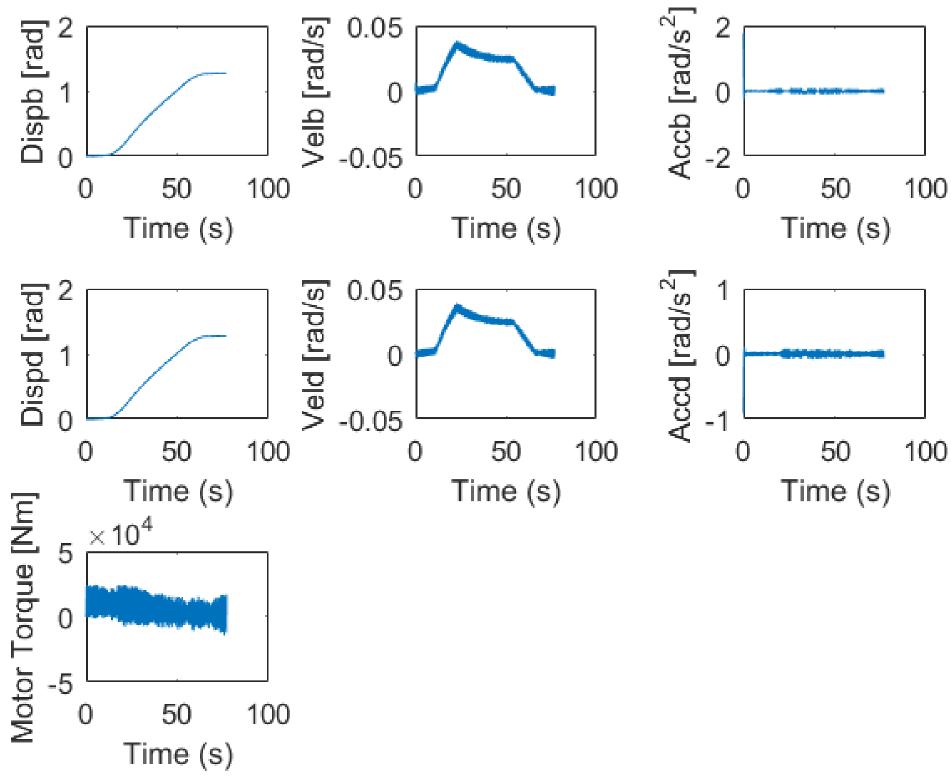

- **Normal Operation – Model for comparison with measurements**

```
clear all
close all
clc

% Loading Motor Motion Parameters

itwk = 0.005251;         % Mechanical Devices Transmission Factor
eta = 0.135;             % Mechanical Devices Efficiency

load('Tmeas.mat');       % Loading Measurements Time
load('Vmeas.mat');       % Loading Measurements Angular Velocity
% Time
T = Tmeas(:,1);
% Angular Velocity (filtered)
Vmeasf = smooth(Vmeas(:)*itwk,0.1,'sgolay');
Vel = Vmeasf(:,1);
% Angular Acceleration Calculation
Index = find(T);
for i = 2:1:length(T)
    A(1) = 0;
    A(i) = (Vel(i)-Vel(i-1))/(T(i)-T(i-1));
end
```

```
% Angular Displacement Calculation
Disp = cumtrapz(T,Vel);
% Angular Acceleration
Acc = A';

figure;
subplot(1,3,1), plot(T,Disp); xlabel('Time (s)'); ylabel('Angular Displacement');
subplot(1,3,2), plot(T,Vel); xlabel('Time (s)'); ylabel('Angular Velocity');
subplot(1,3,3), plot(T,Acc); xlabel('Time (s)'); ylabel('Angular Acceleration');

% Input Data

g = 9.81;                        % gravitational acceleration
Jb = 2.138*10^6;                 % mass moment of inertia of the balance part
mb = 74969;                      % mass of the balance part
Jd = 3.98*10^6;                  % mass moment of inertia of the deck
md = 46017;                      % mass of the deck
Jm = 2.373;                      % mass moment of inertia of the electro-motor
kh = 347858326.1;                % stiffness of the hanger 347858326.1
kmd = 133262000;                 % stiffness of the mechanical devices 140000000
mh = 2000;                       % mass of the hanger
psi = 0.05;                      % considered damping ratio
ch = 2*psi*sqrt(kh/mh)*mh;       % damping coefficient of the hanger
mmd = 1366.44165;                % mass of the mechanical devices
cmd = 2*psi*sqrt(kmd/mmd)*mmd;   % damping coefficient of the mechanical devices
lb = 5.16;                       % distance from the center of gravity of the balance part to the
upper pivot point
beta = 0.23;                     % the angle between the hanger and the vertical axis (in closed
position)
ld = 8.004;                      % distance from the center of gravity of the deck to the lower
pivot point
lh = 12.63;                      % distance from the connection point of the hanger to the pivot
points
lc = 3.7;                        % distance from the connection point of the rack and the deck to
the lower pivot point
rm = 0.136;                      % the angle between the rack and the horizontal axis (in closed
position)
H = 12.07;                       % vertical length of the hanger
gamai = 0.604;                   % initial angle between the rack and the deck
Lr = 6.445;                      % initial length of the rack

ti = 0;                          % initial time
dt = 0.1;                        % time increment
tf = 77;                         % final time
Time = ti:dt:tf;                 % time range
y0 = [0;0;0;0];                  % initial conditions

% Ordinary Differential Equations Solver

[t,y] = ode45(@(t,y)
eom(t,y,Jb,Jd,lh,beta,ch,kh,mb,md,g,lb,ld,H,Lr,gamai,lc,rm,Disp,Vel,T,kmd,cmd),Time,y0);
```

```
% Angular Displacement of the Balance Part
dispb = y(:,1);
% Angular Velocity of the Balance Part
velb = y(:,2);
% Angular Displacement of the Deck
dispd = y(:,3);
% Angular Velocity of the Deck
veld = y(:,4);

accb = zeros(size(t));
accd = zeros(size(t));

% Algorithm for computing the angular accelerations and the motor torque

for it = 1:1:length(t)

    kIndex = find(T>t(it));
    if isempty(kIndex)
        Dm = Disp(end);
        Vm = Vel(end);
        Am = Acc(end);
    else
        kIndex1 = kIndex(1);
        kIndex0 = kIndex1-1;
        dd = (Disp(kIndex1)-Disp(kIndex0))/(T(kIndex1)-T(kIndex0));
        Dm = Disp(kIndex0)+dd*(t(it)-T(kIndex0));
        dv = (Vel(kIndex1)-Vel(kIndex0))/(T(kIndex1)-T(kIndex0));
        Vm = Vel(kIndex0)+dv*(t(it)-T(kIndex0));
        da = (Acc(kIndex1)-Acc(kIndex0))/(T(kIndex1)-T(kIndex0));
        Am = Acc(kIndex0)+da*(t(it)-T(kIndex0));
    end

    % Angular Displacement of the Motor
    dispm(it) = Dm;
    % Angular Velocity of the Motor
    velm(it) = Vm;
    % Angular Acceleration of the Motor
    accm(it) = Am;
    % Length of the hanger at any position
    D = ((H+sin(dispb(it))*lh-sin(dispd(it))*lh)^2+(H*tan(beta)+lh*(1-cos(dispb(it)))-lh*(1-
cos(dispd(it))))^2)^(1/2);
    % The first derivative of the elongation of the hanger
    Dprim = 1/2*D^(-1)*(2*lh*(H+sin(dispb(it))*lh-sin(dispd(it))*lh)*(cos(dispb(it))*velb(it)-
cos(dispd(it))*veld(it))+2*lh*(H*tan(beta)+lh*(1-cos(dispb(it)))-lh*(1-
cos(dispd(it))))*(sin(dispb(it))*velb(it)-sin(dispd(it))*veld(it)));
    % Angle between the hanger and the vertical axis at any position
    ang = atan((H*tan(beta)+lh*(1-cos(dispb(it)))-lh*(1-cos(dispd(it))))/(H+sin(dispb(it))*lh-
sin(dispd(it))*lh));
    % Vertical length of the rack at any position
    H1 = Lr*sin(gamai)-lc*sin(dispd(it))+2*dispm(it)*rm/3.14;
    % Horizontal length of the rack at any position
    L1 = Lr*cos(gamai)-lc*(1-cos(dispd(it)))+2*dispm(it)*rm/3.14;
```

```
    % Length of the rack at any position
    D1 = (H1^2+L1^2)^(1/2);
    % First Derivative of the elongation of the rack
    D1prim = 1/2*(D1)^(-1)*((-2*H1*lc*cos(dispd(it))-
2*L1*lc*sin(dispd(it)))*veld(it)+(4*H1*rm/3.14+4*L1*rm/3.14)*velm(it));
    % Angle between the rack and the horizontal axis at any position
    ang1 = atan(H1/L1);

    % Angular Acceleration of the Balance Part
    accb(it) = (+mb*g*lb*cos(dispb(it))-(kh*(D-
H/cos(beta))+ch*Dprim)*(cos(ang)*lh*cos(dispb(it))+sin(ang)*lh*sin(dispb(it))))/Jb;
    % Angular Acceleration of the Deck
    accd(it) = (-md*g*ld*cos(dispd(it))+(kh*(D-
H/cos(beta))+ch*Dprim)*(cos(ang)*lh*cos(dispd(it))+sin(ang)*lh*sin(dispd(it)))+(kmd*(D1-
Lr)+cmd*D1prim)*(cos(ang1)*lc*sin(dispd(it))+sin(ang1)*lc*cos(dispd(it))))/Jd;
    % Torque acting on the Motor
    Mmotor(it) = -rm*(kmd*(D1-Lr)+cmd*D1prim)+Jm*accm(it);

end

% Plotting Results (Unfiltered)

figure;
subplot(3,3,1), plot(t,dispb); xlabel('Time (s)'); ylabel('Dispb [rad]');
subplot(3,3,2), plot(t,velb); xlabel('Time (s)'); ylabel('Velb [rad/s]');
subplot(3,3,3), plot(t,accb); xlabel('Time (s)'); ylabel('Accb [rad/s^2]');
subplot(3,3,4), plot(t,dispd); xlabel('Time (s)'); ylabel('Dispd [rad]');
subplot(3,3,5), plot(t,veld); xlabel('Time (s)'); ylabel('Veld [rad/s]');
subplot(3,3,6), plot(t,accd); xlabel('Time (s)'); ylabel('Accd [rad/s^2]');
subplot(3,3,7), plot(t,Mmotor); xlabel('Time (s)'); ylabel('Motor Torque [Nm]');
```

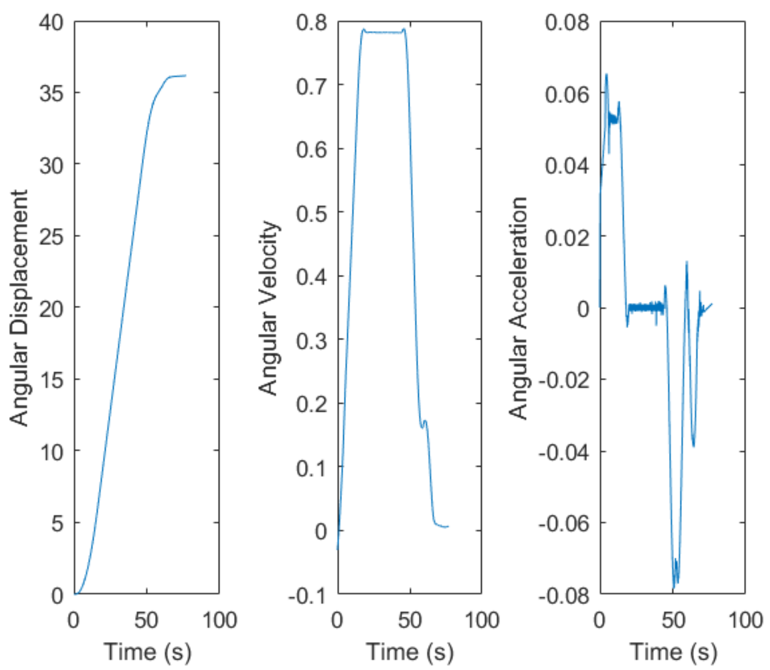

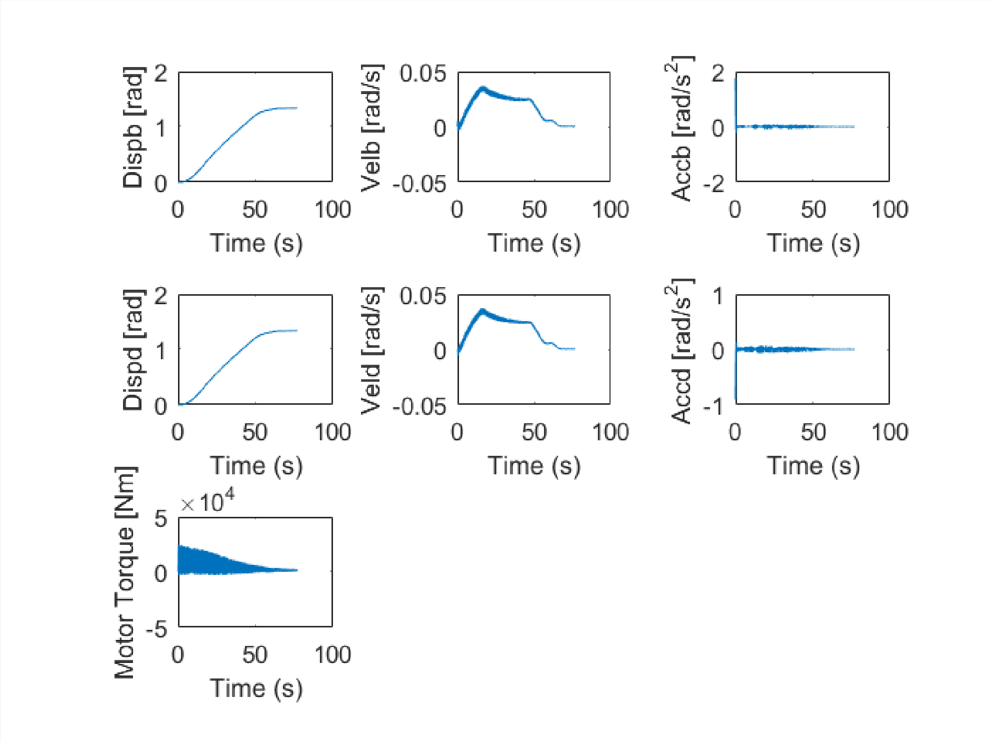

- **Braking Situation – Model for comparison with theory**

```
clear all
close all
clc
```

```
% Loading Motor Motion Parameters
```

```
itwk = 5.251*10^(-3);           % Mechanical Devices Transmission Factor
eta = 0.135;                    % Mechanical Devices Efficiency
tbrake = 25;                  % Time at which the brake is applied

load('T.mat');                  % Loading Time
load('motor.mat');              % Loading Motor Motion Parameters
% Time
T = T(:,1);
% Angular Velocity
Vel = motor(:,2);

% Algorithm for computing the motor motion parameters in case of a brake
Index = find(T);
tbindex = find(T==tbrake);
for it =1:1:length(T)
    if isempty(Index)
        Vm(it) = Vel(end);
    else
        Index1 = Index(1);
```

```
        Index0 = Index1-1;

        if T(it)<=tbrake
            Vm(it) = Vel(it);
        else
            indexstop = find(T(it)==tbrake+3);
            if T(it)<=(tbrake+3)
                Vm(it) = Vel(tbindex)-Vel(tbindex)/3*(T(it)-tbrake);
            else
                Vm(it) = 0;
            end
        end
    end
end

Vel = Vm;
% Angular Displacement Calculation
Disp = cumtrapz(T,Vel);
% Angular Acceleration
for ib = 2:1:length(T)
    Acc(1) = 0;
    Acc(ib) = (Vel(ib)-Vel(ib-1))/(T(ib)-T(ib-1));
end
Acc = Acc';

figure;
subplot(1,3,1), plot(T,Disp); xlabel('Time (s)'); ylabel('Angular Displacement');
subplot(1,3,2), plot(T,Vel); xlabel('Time (s)'); ylabel('Angular Velocity');
subplot(1,3,3), plot(T,Acc); xlabel('Time (s)'); ylabel('Angular Acceleration');

% Input Data
```

```
g = 9.81;                        % gravitational acceleration
Jb = 2.138*10^6;                 % mass moment of inertia of the balance part
mb = 74969;                      % mass of the balance part
Jd = 3.98*10^6;                  % mass moment of inertia of the deck
md = 46017;                      % mass of the deck
Jm = 2.373;                      % mass moment of inertia of the electro-motor
kh = 347858326.1;                % stiffness of the hanger 347858326.1
kmd = 140000000;                 % stiffness of the mechanical devices 140000000
mh = 2000;                       % mass of the hanger
psi = 0.05;                      % considered damping ratio
ch = 2*psi*sqrt(kh/mh)*mh;       % damping coefficient of the hanger
mmd = 1366.44165;                % mass of the mechanical devices
cmd = 2*psi*sqrt(kmd/mmd)*mmd;   % damping coefficient of the mechanical devices
lb = 5.16;                       % distance from the center of gravity of the balance part to the
upper pivot point
beta = 0.23;                     % the angle between the hanger and the vertical axis (in closed
position)
ld = 8.004;                      % distance from the center of gravity of the deck to the lower
pivot point
```

```
lh = 12.63;                     % distance from the connection point of the hanger to the pivot
points
lc = 3.7;                       % distance from the connection point of the rack and the deck to
the lower pivot point
rm = 0.136;                     % the angle between the rack and the horizontal axis (in closed
position)
H = 12.07;                      % vertical length of the hanger
gamai = 0.604;                  % initial angle between the rack and the deck
Lr = 6.445;                     % initial length of the rack

ti = 0;                         % initial time
dt = 0.1;                       % time increment
tf = 77;                        % final time
Time = ti:dt:tf;                % time range
y0 = [0;0;0;0];                 % initial conditions

% Ordinary Differential Equations Solver

[t,y] = ode45(@(t,y)
eom(t,y,Jb,Jd,lh,beta,ch,kh,mb,md,g,lb,ld,H,Lr,gamai,lc,rm,Disp,Vel,T,kmd,cmd),Time,y0);

% Angular Displacement of the Balance Part
dispb = y(:,1);
% Angular Velocity of the Balance Part
velb = y(:,2);
% Angular Displacement of the Deck
dispd = y(:,3);
% Angular Velocity of the Deck
veld = y(:,4);

accb = zeros(size(t));
accd = zeros(size(t));
```

```
% Algorithm for computing the angular accelerations and the motor torque

for it = 1:1:length(t)

    kIndex = find(T>t(it));
    if isempty(kIndex)
        Dm = Disp(end);
        Vm = Vel(end);
        Am = Acc(end);
    else
        kIndex1 = kIndex(1);
        kIndex0 = kIndex1-1;
        dd = (Disp(kIndex1)-Disp(kIndex0))/(T(kIndex1)-T(kIndex0));
        Dm = Disp(kIndex0)+dd*(t(it)-T(kIndex0));
        dv = (Vel(kIndex1)-Vel(kIndex0))/(T(kIndex1)-T(kIndex0));
        Vm = Vel(kIndex0)+dv*(t(it)-T(kIndex0));
        da = (Acc(kIndex1)-Acc(kIndex0))/(T(kIndex1)-T(kIndex0));
        Am = Acc(kIndex0)+da*(t(it)-T(kIndex0));
    end
```

```
    % Angular Displacement of the Motor
    dispm(it) = Dm;
    % Angular Velocity of the Motor
    velm(it) = Vm;
    % Angular Acceleration of the Motor
    accm(it) = Am;
    % Length of the hanger at any position
    D = ((H+sin(dispb(it))*lh-sin(dispd(it))*lh)^2+(H*tan(beta)+lh*(1-cos(dispb(it)))-lh*(1-
cos(dispd(it))))^2)^(1/2);
    % The first derivative of the elongation of the hanger
    Dprim = 1/2*D^(-1)*(2*lh*(H+sin(dispb(it))*lh-sin(dispd(it))*lh)*(cos(dispb(it))*velb(it)-
cos(dispd(it))*veld(it))+2*lh*(H*tan(beta)+lh*(1-cos(dispb(it)))-lh*(1-
cos(dispd(it))))*(sin(dispb(it))*velb(it)-sin(dispd(it))*veld(it)));
    % Angle between the hanger and the vertical axis at any position
    ang = atan((H*tan(beta)+lh*(1-cos(dispb(it)))-lh*(1-cos(dispd(it))))/(H+sin(dispb(it))*lh-
sin(dispd(it))*lh));
    % Vertical length of the rack at any position
    H1 = Lr*sin(gamai)-lc*sin(dispd(it))+2*dispm(it)*rm/3.14;
    % Horizontal length of the rack at any position
    L1 = Lr*cos(gamai)-lc*(1-cos(dispd(it)))+2*dispm(it)*rm/3.14;
    % Length of the rack at any position
    D1 = (H1^2+L1^2)^(1/2);
    % First Derivative of the elongation of the rack
    D1prim = 1/2*(D1)^(-1)*((-2*H1*lc*cos(dispd(it))-
2*L1*lc*sin(dispd(it)))*veld(it)+(4*H1*rm/3.14+4*L1*rm/3.14)*velm(it));
    % Angle between the rack and the horizontal axis at any position
    ang1 = atan(H1/L1);

    % Angular Acceleration of the Balance Part
    accb(it) = (+mb*g*lb*cos(dispb(it))-(kh*(D-
H/cos(beta))+ch*Dprim)*(cos(ang)*lh*cos(dispb(it))+sin(ang)*lh*sin(dispb(it))))/Jb;

    % Angular Acceleration of the Deck

    accd(it) = (-md*g*ld*cos(dispd(it))+(kh*(D-
H/cos(beta))+ch*Dprim)*(cos(ang)*lh*cos(dispd(it))+sin(ang)*lh*sin(dispd(it)))+(kmd*(D1-
Lr)+cmd*D1prim)*(cos(ang1)*lc*sin(dispd(it))+sin(ang1)*lc*cos(dispd(it))))/Jd;
    % Torque acting on the Motor
    Mmotor(it) = -rm*(kmd*(D1-Lr)+cmd*D1prim)+Jm*accm(it);

end

% Plotting Results (Unfiltered)

figure;
subplot(3,3,1), plot(t,dispb); xlabel('Time (s)'); ylabel('Dispb [rad]');
subplot(3,3,2), plot(t,velb); xlabel('Time (s)'); ylabel('Velb [rad/s]');
subplot(3,3,3), plot(t,accb); xlabel('Time (s)'); ylabel('Accb [rad/s^2]');
subplot(3,3,4), plot(t,dispd); xlabel('Time (s)'); ylabel('Dispd [rad]');
subplot(3,3,5), plot(t,veld); xlabel('Time (s)'); ylabel('Veld [rad/s]');
subplot(3,3,6), plot(t,accd); xlabel('Time (s)'); ylabel('Accd [rad/s^2]');
subplot(3,3,7), plot(t,Mmotor); xlabel('Time (s)'); ylabel('Motor Torque [Nm]');
```

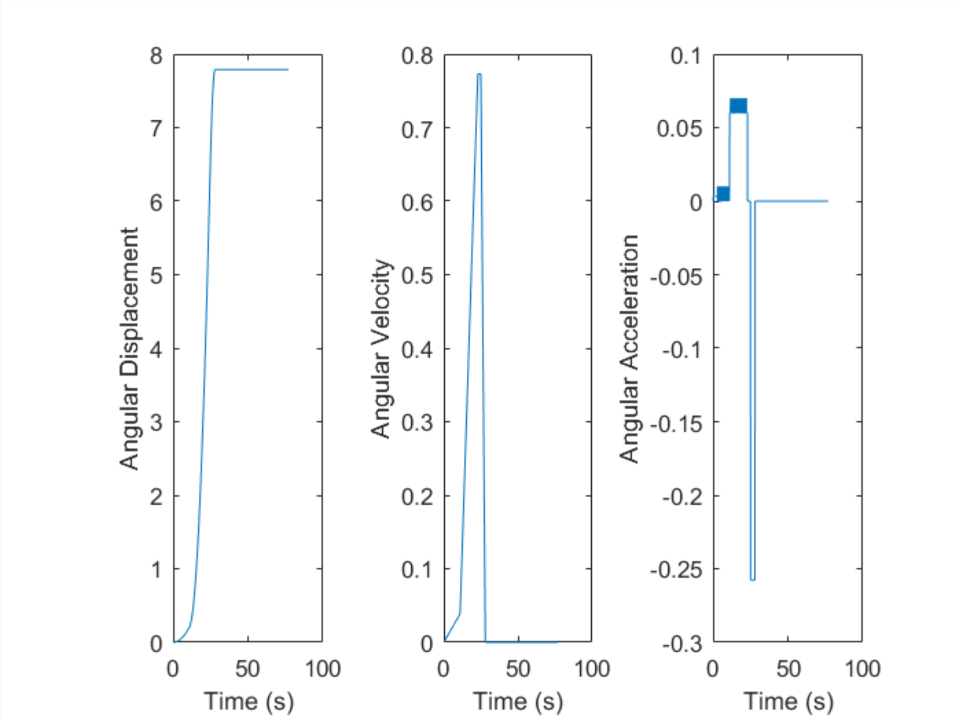
Angular Displacement
Time (s)
Angular Velocity
Time (s)
Angular Acceleration
Time (s)

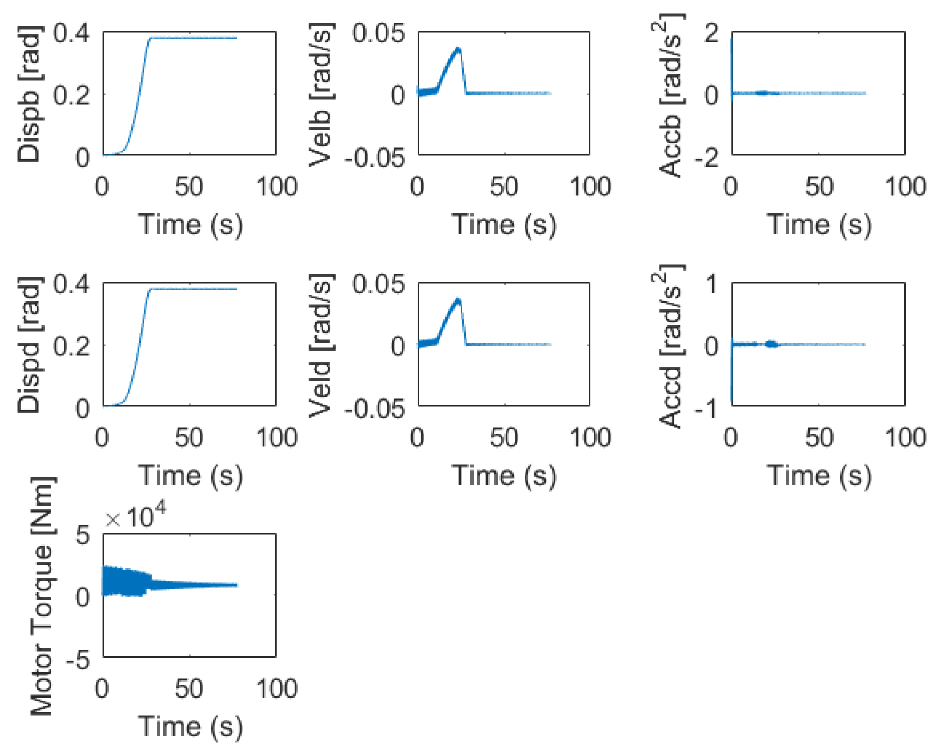
Dispb [rad]
Time (s)
Velb [rad/s]
Time (s)
Accb [rad/s2]
Time (s)
Dispd [rad]
Time (s)
Veld [rad/s]
Time (s)
Accd [rad/s2]
Time (s)
Motor Torque [Nm]
×10^4
Time (s)

- **Brake Situation – Model for comparison with measurements**

```
clear all
close all
clc

% Loading Motor Motion Parameters

itwk = 0.005251;        % Mechanical Devices Transmission Factor
eta = 0.135;            % Mechanical Devices Efficiency

load('Tmeasbrake.mat');      % Loading Measurements Time
load('Vmeasbrake.mat');      % Loading Measurements Angular Velocity
% Time
T = Tmeasbrake(:,1);
% Angular Velocity (filtered)
Vmeasf = smooth(Vmeasbrake(:)*itwk*2*3.14/60,0.1,'sgolay');
Vel = Vmeasf(:,1);
% Angular Acceleration Calculation
Index = find(T);
for i = 2:1:length(T)
    A(1) = 0;
    A(i) = (Vel(i)-Vel(i-1))/(T(i)-T(i-1));
end
% Angular Displacement Calculation
Disp = cumtrapz(T,Vel);
% Angular Acceleration
Acc = A';

figure;
subplot(1,3,1), plot(T,Disp); xlabel('Time (s)'); ylabel('Angular Displacement');
subplot(1,3,2), plot(T,Vel); xlabel('Time (s)'); ylabel('Angular Velocity');
subplot(1,3,3), plot(T,Acc); xlabel('Time (s)'); ylabel('Angular Acceleration');

% Input Data

g = 9.81;                       % gravitational acceleration
Jb = 2.138*10^6;                % mass moment of inertia of the balance part
mb = 74969;                     % mass of the balance part
Jd = 3.98*10^6;                 % mass moment of inertia of the deck
md = 46017;                     % mass of the deck
Jm = 2.373;                     % mass moment of inertia of the electro-motor
kh = 347858326.1;               % stiffness of the hanger 347858326.1
kmd = 133262000;                % stiffness of the mechanical devices 140000000
mh = 2000;                      % mass of the hanger
psi = 0.05;                     % considered damping ratio
ch = 2*psi*sqrt(kh/mh)*mh;      % damping coefficient of the hanger
mmd = 1366.44165;               % mass of the mechanical devices
cmd = 2*psi*sqrt(kmd/mmd)*mmd;  % damping coefficient of the mechanical devices
lb = 5.16;                      % distance from the center of gravity of the balance part to the
upper pivot point
```

```
beta = 0.23;                    % the angle between the hanger and the vertical axis (in closed
position)
ld = 8.004;                     % distance from the center of gravity of the deck to the lower
pivot point
lh = 12.63;                     % distance from the connection point of the hanger to the pivot
points
lc = 3.7;                       % distance from the connection point of the rack and the deck to
the lower pivot point
rm = 0.136;                     % the angle between the rack and the horizontal axis (in closed
position)
H = 12.07;                      % vertical length of the hanger
gamai = 0.604;                  % initial angle between the rack and the deck
Lr = 6.445;                     % initial length of the rack

ti = 0;                         % initial time
dt = 0.1;                       % time increment
tf = 77;                        % final time
Time = ti:dt:tf;                % time range
y0 = [0;0;0;0];                 % initial conditions

% Ordinary Differential Equations Solver

[t,y] = ode45(@(t,y)
eom(t,y,Jb,Jd,lh,beta,ch,kh,mb,md,g,lb,ld,H,Lr,gamai,lc,rm,Disp,Vel,T,kmd,cmd),Time,y0);

% Angular Displacement of the Balance Part
dispb = y(:,1);
% Angular Velocity of the Balance Part
velb = y(:,2);
% Angular Displacement of the Deck
dispd = y(:,3);
% Angular Velocity of the Deck
veld = y(:,4);

accb = zeros(size(t));
accd = zeros(size(t));

% Algorithm for computing the angular accelerations and the motor torque

for it = 1:1:length(t)

    kIndex = find(T>t(it));
    if isempty(kIndex)
        Dm = Disp(end);
        Vm = Vel(end);
        Am = Acc(end);
    else
        kIndex1 = kIndex(1);
        kIndex0 = kIndex1-1;
        dd = (Disp(kIndex1)-Disp(kIndex0))/(T(kIndex1)-T(kIndex0));
        Dm = Disp(kIndex0)+dd*(t(it)-T(kIndex0));
        dv = (Vel(kIndex1)-Vel(kIndex0))/(T(kIndex1)-T(kIndex0));
```

```
        Vm = Vel(kIndex0)+dv*(t(it)-T(kIndex0));
        da = (Acc(kIndex1)-Acc(kIndex0))/(T(kIndex1)-T(kIndex0));
        Am = Acc(kIndex0)+da*(t(it)-T(kIndex0));
    end

    % Angular Displacement of the Motor
    dispm(it) = Dm;
    % Angular Velocity of the Motor
    velm(it) = Vm;
    % Angular Acceleration of the Motor
    accm(it) = Am;
    % Length of the hanger at any position
    D = ((H+sin(dispb(it))*lh-sin(dispd(it))*lh)^2+(H*tan(beta)+lh*(1-cos(dispb(it)))-lh*(1-
cos(dispd(it))))^2)^(1/2);
    % The first derivative of the elongation of the hanger
    Dprim = 1/2*D^(-1)*(2*lh*(H+sin(dispb(it))*lh-sin(dispd(it))*lh)*(cos(dispb(it))*velb(it)-
cos(dispd(it))*veld(it))+2*lh*(H*tan(beta)+lh*(1-cos(dispb(it)))-lh*(1-
cos(dispd(it))))*(sin(dispb(it))*velb(it)-sin(dispd(it))*veld(it)));
    % Angle between the hanger and the vertical axis at any position
    ang = atan((H*tan(beta)+lh*(1-cos(dispb(it)))-lh*(1-cos(dispd(it))))/(H+sin(dispb(it))*lh-
sin(dispd(it))*lh));
    % Vertical length of the rack at any position
    H1 = Lr*sin(gamai)-lc*sin(dispd(it))+2*dispm(it)*rm/3.14;
    % Horizontal length of the rack at any position
    L1 = Lr*cos(gamai)-lc*(1-cos(dispd(it)))+2*dispm(it)*rm/3.14;
    % Length of the rack at any position
    D1 = (H1^2+L1^2)^(1/2);
    % First Derivative of the elongation of the rack
    D1prim = 1/2*(D1)^(-1)*((-2*H1*lc*cos(dispd(it))-
2*L1*lc*sin(dispd(it)))*veld(it)+(4*H1*rm/3.14+4*L1*rm/3.14)*velm(it));
    % Angle between the rack and the horizontal axis at any position
    ang1 = atan(H1/L1);

    % Angular Acceleration of the Balance Part
    accb(it) = (+mb*g*lb*cos(dispb(it))-(kh*(D-
H/cos(beta))+ch*Dprim)*(cos(ang)*lh*cos(dispb(it))+sin(ang)*lh*sin(dispb(it))))/Jb;
    % Angular Acceleration of the Deck
    accd(it) = (-md*g*ld*cos(dispd(it))+(kh*(D-
H/cos(beta))+ch*Dprim)*(cos(ang)*lh*cos(dispd(it))+sin(ang)*lh*sin(dispd(it)))+(kmd*(D1-
Lr)+cmd*D1prim)*(cos(ang1)*lc*sin(dispd(it))+sin(ang1)*lc*cos(dispd(it))))/Jd;
    % Torque acting on the Motor
    Mmotor(it) = -rm*(kmd*(D1-Lr)+cmd*D1prim)+Jm*accm(it);

end

% Plotting Results (Unfiltered)

figure;
subplot(3,3,1), plot(t,dispb); xlabel('Time (s)'); ylabel('Dispb [rad]');
subplot(3,3,2), plot(t,velb); xlabel('Time (s)'); ylabel('Velb [rad/s]');
subplot(3,3,3), plot(t,accb); xlabel('Time (s)'); ylabel('Accb [rad/s^2]');
subplot(3,3,4), plot(t,dispd); xlabel('Time (s)'); ylabel('Dispd [rad]');
```

```
subplot(3,3,5), plot(t,veld); xlabel('Time (s)'); ylabel('Veld [rad/s]');
subplot(3,3,6), plot(t,accd); xlabel('Time (s)'); ylabel('Accd [rad/s^2]');
subplot(3,3,7), plot(t,Mmotor); xlabel('Time (s)'); ylabel('Motor Torque [Nm]');
```

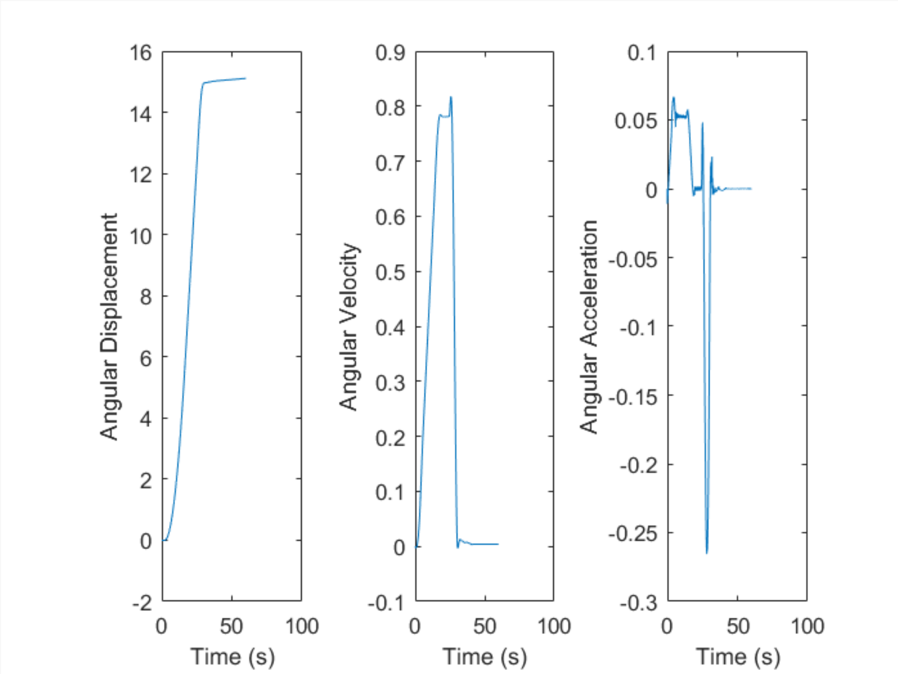

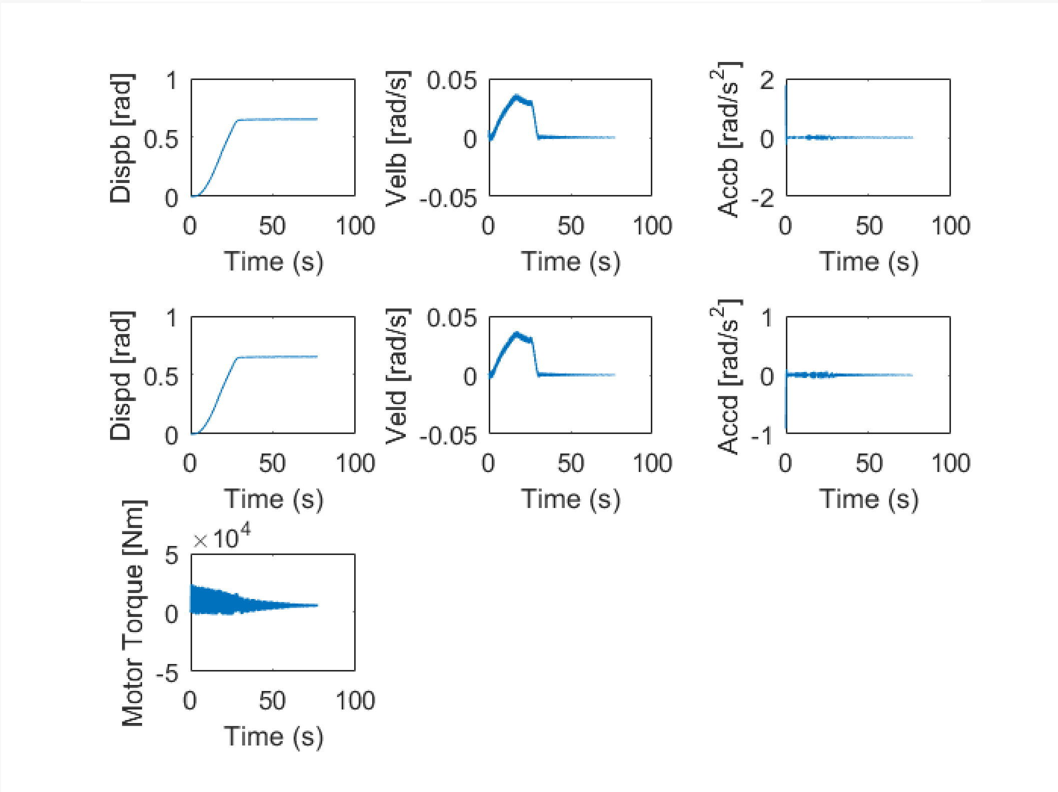

- **Linearization of the three degrees of freedom model**

Linearizing the first equation of motion (degree of freedom φ_b)

> $EOMb := Eq14 - Eq20;$

$$
\begin{aligned}
EOMb :=& \\
&-\frac{1}{2}\Bigg(k_k\Bigg(\sqrt{\left(H_k+l_k\sin(\varphi_b(t))-l_k\sin(\varphi_d(t))\right)^2+\left(H_k\tan(\beta)+l_k\left(1-\cos(\varphi_b(t))\right)-l_k\left(1-\cos(\varphi_d(t))\right)\right)^2} \\
&-\frac{H_k}{\cos(\beta)}\Bigg)\Big(2\left(H_k+l_k\sin(\varphi_b(t))-l_k\sin(\varphi_d(t))\right)l_k\cos(\varphi_b(t))+2\left(H_k\tan(\beta)+l_k\left(1-\cos(\varphi_b(t))\right)\right. \\
&\left.-l_k\left(1-\cos(\varphi_d(t))\right)\right)l_k\sin(\varphi_b(t))\Big)\Bigg)\Bigg/ \\
&\sqrt{\left(H_k+l_k\sin(\varphi_b(t))-l_k\sin(\varphi_d(t))\right)^2+\left(H_k\tan(\beta)+l_k\left(1-\cos(\varphi_b(t))\right)-l_k\left(1-\cos(\varphi_d(t))\right)\right)^2} \\
&+m_b\,g\,l_b\cos(\varphi_b(t))-\frac{1}{4}\Bigg(c_k\Bigg(2\left(H_k+l_k\sin(\varphi_b(t))-l_k\sin(\varphi_d(t))\right)\left(l_k\cos(\varphi_b(t))\left(\frac{d}{dt}\varphi_b(t)\right)\right. \\
&\left.-l_k\cos(\varphi_d(t))\left(\frac{d}{dt}\varphi_d(t)\right)\right)+2\left(H_k\tan(\beta)+l_k\left(1-\cos(\varphi_b(t))\right)-l_k\left(1\right.\right. \\
&\left.\left.-\cos(\varphi_d(t))\right)\right)\left(l_k\sin(\varphi_b(t))\left(\frac{d}{dt}\varphi_b(t)\right)-l_k\sin(\varphi_d(t))\left(\frac{d}{dt}\varphi_d(t)\right)\right)\Bigg)\Big(2\left(H_k+l_k\sin(\varphi_b(t))\right. \\
&\left.-l_k\sin(\varphi_d(t))\right)l_k\cos(\varphi_b(t))+2\left(H_k\tan(\beta)+l_k\left(1-\cos(\varphi_b(t))\right)-l_k\left(1-\cos(\varphi_d(t))\right)\right)l_k\sin(\varphi_b(t))\Big) \\
&\Bigg)\Bigg/\left(\left(H_k+l_k\sin(\varphi_b(t))-l_k\sin(\varphi_d(t))\right)^2+\left(H_k\tan(\beta)+l_k\left(1-\cos(\varphi_b(t))\right)-l_k\left(1-\cos(\varphi_d(t))\right)\right)^2\right)
\end{aligned}
\qquad (15)
$$

> $Eqb1 := subs(\{\varphi_b(t)=var1, diff(\varphi_b(t),t)=var2, \varphi_d(t)=var3, diff(\varphi_d(t),t)=var4\}, EOMb):$

> $Eqb2 := -diff(Eqb1, var2):$

> $Eqb3 := -diff(Eqb1, var1):$

> $Eqb4 := -diff(Eqb1, var4):$

> $Eqb5 := -diff(Eqb1, var3):$

> $a1b := subs(\{var1=0, var2=0, var3=0, var4=0\}, Eqb2):$

> $a0b := subs(\{var1=0, var2=0, var3=0, var4=0\}, Eqb3):$

> $a1d := subs(\{var1=0, var2=0, var3=0, var4=0\}, Eqb4):$

> $a0d := subs(\{var1=0, var2=0, var3=0, var4=0\}, Eqb5):$

> $Eqblin := Eq15 + a1b\cdot diff(\varphi_b(t),t) + a0b\cdot\varphi_b(t) + a1d\cdot diff(\varphi_d(t),t) + a0d\cdot\varphi_d(t);$

$$
\begin{aligned}
Eqblin := {} & J_b\left(\frac{d^2}{dt^2}\varphi_b(t)\right) + \frac{c_k H_k^2 l_k^2 \left(\frac{d}{dt}\varphi_b(t)\right)}{H_k^2 + H_k^2\tan(\beta)^2} + \Bigg(\frac{k_k H_k^2 l_k^2}{H_k^2 + H_k^2\tan(\beta)^2} \\
& - \frac{k_k\left(\sqrt{H_k^2 + H_k^2\tan(\beta)^2} - \frac{H_k}{\cos(\beta)}\right) H_k^2 l_k^2}{\left(H_k^2 + H_k^2\tan(\beta)^2\right)^{3/2}} \\
& + \frac{1}{2}\,\frac{k_k\left(\sqrt{H_k^2 + H_k^2\tan(\beta)^2} - \frac{H_k}{\cos(\beta)}\right)\left(2\,l_k^2 + 2\,H_k\tan(\beta)\,l_k\right)}{\sqrt{H_k^2 + H_k^2\tan(\beta)^2}}\Bigg)\varphi_b(t) - \frac{c_k H_k^2 l_k^2\left(\frac{d}{dt}\varphi_d(t)\right)}{H_k^2 + H_k^2\tan(\beta)^2} + \Bigg(\\
& - \frac{k_k H_k^2 l_k^2}{H_k^2 + H_k^2\tan(\beta)^2} + \frac{k_k\left(\sqrt{H_k^2 + H_k^2\tan(\beta)^2} - \frac{H_k}{\cos(\beta)}\right) H_k^2 l_k^2}{\left(H_k^2 + H_k^2\tan(\beta)^2\right)^{3/2}} \\
& - \frac{k_k\left(\sqrt{H_k^2 + H_k^2\tan(\beta)^2} - \frac{H_k}{\cos(\beta)}\right) l_k^2}{\sqrt{H_k^2 + H_k^2\tan(\beta)^2}}\Bigg)\varphi_d(t)
\end{aligned}
\tag{16}
$$

Linearizing the second equation of motion (degree of freedom φ_d)

> $EOMd := Eq24 - Eq30;$

$$
\begin{aligned}
& EOMd := \\
& -\frac{1}{2}\Big(k_k\Big(\\
& \sqrt{(H_k + l_k\sin(\varphi_b(t)) - l_k\sin(\varphi_d(t)))^2 + (H_k\tan(\beta) + l_k(1 - \cos(\varphi_b(t))) - l_k(1 - \cos(\varphi_d(t))))^2} \\
& - \frac{H_k}{\cos(\beta)}\Big)(-2(H_k + l_k\sin(\varphi_b(t)) - l_k\sin(\varphi_d(t)))\,l_k\cos(\varphi_d(t)) - 2(H_k\tan(\beta) + l_k(1 - \cos(\varphi_b(t))) \\
& - l_k(1 - \cos(\varphi_d(t))))\,l_k\sin(\varphi_d(t)))\Big)\Big/ \\
& \sqrt{(H_k + l_k\sin(\varphi_b(t)) - l_k\sin(\varphi_d(t)))^2 + (H_k\tan(\beta) + l_k(1 - \cos(\varphi_b(t))) - l_k(1 - \cos(\varphi_d(t))))^2} \\
& - \frac{1}{2}\Big(k_{md}\Big(((L_\gamma\sin(gama_j) - l_c\sin(\varphi_d(t)) + 0.6369426752\,r_m\varphi_m(t))^2 + (L_\gamma\cos(gama_j) \\
& - l_c(1 - \cos(\varphi_d(t))) + 0.6369426752\,r_m\varphi_m(t))^2)^{1/2} - L_\gamma\Big)(-2(L_\gamma\sin(gama_j) - l_c\sin(\varphi_d(t)) \\
& + 0.6369426752\,r_m\varphi_m(t))\,l_c\cos(\varphi_d(t)) - 2(L_\gamma\cos(gama_j) - l_c(1 - \cos(\varphi_d(t))) \\
& + 0.6369426752\,r_m\varphi_m(t))\,l_c\sin(\varphi_d(t)))\Big)\Big/ \\
& ((L_\gamma\sin(gama_j) - l_c\sin(\varphi_d(t)) + 0.6369426752\,r_m\varphi_m(t))^2 + (L_\gamma\cos(gama_j) - l_c(1 \\
& - \cos(\varphi_d(t))) + 0.6369426752\,r_m\varphi_m(t))^2)^{1/2} - m_d\,g\,l_d\cos(\varphi_d(t)) - \frac{1}{4}\Big(c_k\Big(2(H_k + l_k\sin(\varphi_b(t)) \\
& - l_k\sin(\varphi_d(t)))\Big(l_k\cos(\varphi_b(t))\left(\frac{d}{dt}\varphi_b(t)\right) - l_k\cos(\varphi_d(t))\left(\frac{d}{dt}\varphi_d(t)\right)\Big) + 2(H_k\tan(\beta) + l_k(1 \\
& - \cos(\varphi_b(t))) - l_k(1 - \cos(\varphi_d(t))))\Big(l_k\sin(\varphi_b(t))\left(\frac{d}{dt}\varphi_b(t)\right) - l_k\sin(\varphi_d(t))\left(\frac{d}{dt}\varphi_d(t)\right)\Big)\Big)(-2(H_k \\
& + l_k\sin(\varphi_b(t)) - l_k\sin(\varphi_d(t)))\,l_k\cos(\varphi_d(t)) - 2(H_k\tan(\beta) + l_k(1 - \cos(\varphi_b(t))) - l_k(1 \\
& - \cos(\varphi_d(t))))\,l_k\sin(\varphi_d(t)))\Big)\Big/((H_k + l_k\sin(\varphi_b(t)) - l_k\sin(\varphi_d(t)))^2 + (H_k\tan(\beta) + l_k(1 \\
& - \cos(\varphi_b(t))) - l_k(1 - \cos(\varphi_d(t))))^2) - \frac{1}{4}\Big(c_{md}\Big(2(L_\gamma\sin(gama_j) - l_c\sin(\varphi_d(t))
\end{aligned}
\tag{17}
$$

$$+0.6369426752\, r_m \varphi_m(t)\Big)\left(-l_c \cos(\varphi_d(t))\left(\frac{d}{dt}\varphi_d(t)\right)+0.6369426752\, r_m\left(\frac{d}{dt}\varphi_m(t)\right)\right)$$
$$+2\left(L_\gamma \cos(gama_i)-l_c\left(1-\cos(\varphi_d(t))\right)+0.6369426752\, r_m \varphi_m(t)\right)\left(-l_c \sin(\varphi_d(t))\left(\frac{d}{dt}\varphi_d(t)\right)\right.$$
$$\left.+0.6369426752\, r_m\left(\frac{d}{dt}\varphi_m(t)\right)\right)\Big)\Big)\Big(-2\left(L_\gamma \sin(gama_i)-l_c \sin(\varphi_d(t))\right.$$
$$\left.+0.6369426752\, r_m \varphi_m(t)\right) l_c \cos(\varphi_d(t))-2\left(L_\gamma \cos(gama_i)-l_c\left(1-\cos(\varphi_d(t))\right)\right.$$
$$\left.+0.6369426752\, r_m \varphi_m(t)\right) l_c \sin(\varphi_d(t))\Big)\Big)\Big/\Big(\left(L_\gamma \sin(gama_i)-l_c \sin(\varphi_d(t))+0.6369426752\, r_m \varphi_m(t)\right)^2$$
$$+\left(L_\gamma \cos(gama_i)-l_c\left(1-\cos(\varphi_d(t))\right)+0.6369426752\, r_m \varphi_m(t)\right)^2\Big)$$

> $Eqd1 := subs(\{\varphi_b(t) = var1, diff(\varphi_b(t), t) = var2, \varphi_d(t) = var3, diff(\varphi_d(t), t) = var4, \varphi_m(t) = var5, diff(\varphi_m(t), t) = var6\}, EOMd)$:

> $Eqd2 := -diff(Eqd1, var2)$:

> $Eqd3 := -diff(Eqd1, var1)$:

> $Eqd4 := -diff(Eqd1, var4)$:

> $Eqd5 := -diff(Eqd1, var3)$:

> $Eqd6 := -diff(Eqd1, var6)$:

> $Eqd7 := -diff(Eqd1, var5)$:

> $a1m := subs(\{var1=0, var2=0, var3=0, var4=0, var5=0, var6=0\}, Eqd6)$:

> $a0m := subs(\{var1=0, var2=0, var3=0, var4=0, var5=0, var6=0\}, Eqd7)$:

> $a1b := subs(\{var1=0, var2=0, var3=0, var4=0, var5=0, var6=0\}, Eqd2)$:

> $a0b := subs(\{var1=0, var2=0, var3=0, var4=0, var5=0, var6=0\}, Eqd3)$:

> $a1d := subs(\{var1=0, var2=0, var3=0, var4=0, var5=0, var6=0\}, Eqd4)$:

> $a0d := subs(\{var1=0, var2=0, var3=0, var4=0, var5=0, var6=0\}, Eqd5)$:

> $Eqdlin := Eq25 + a1b\cdot diff(\varphi_b(t), t) + a0b\cdot\varphi_b(t) + a1d\cdot diff(\varphi_d(t), t) + a0d\cdot\varphi_d(t) + a1m\cdot diff(\varphi_m(t), t) + a0m\cdot\varphi_m(t)$;

$$Eqdlin := J_d\left(\frac{d^2}{dt^2}\varphi_d(t)\right) - \frac{c_h H_h^2 l_h^2\left(\frac{d}{dt}\varphi_b(t)\right)}{H_h^2 + H_h^2\tan(\beta)^2} + \left(-\frac{k_h H_h^2 l_h^2}{H_h^2 + H_h^2\tan(\beta)^2} + \frac{k_h\left(\sqrt{H_h^2 + H_h^2\tan(\beta)^2} - \frac{H_h}{\cos(\beta)}\right)H_h^2 l_h^2}{\left(H_h^2 + H_h^2\tan(\beta)^2\right)^{3/2}} - \frac{k_h\left(\sqrt{H_h^2 + H_h^2\tan(\beta)^2} - \frac{H_h}{\cos(\beta)}\right)l_h^2}{\sqrt{H_h^2 + H_h^2\tan(\beta)^2}}\right)\varphi_b(t)$$
$$+\left(\frac{c_h H_h^2 l_h^2}{H_h^2 + H_h^2\tan(\beta)^2} + \frac{c_{md}L_y^2\sin(gama_i)^2 l_c^2}{L_y^2\sin(gama_i)^2 + L_y^2\cos(gama_i)^2}\right)\left(\frac{d}{dt}\varphi_d(t)\right) + \left(\frac{k_h H_h^2 l_h^2}{H_h^2 + H_h^2\tan(\beta)^2} - \frac{k_h\left(\sqrt{H_h^2 + H_h^2\tan(\beta)^2} - \frac{H_h}{\cos(\beta)}\right)H_h^2 l_h^2}{\left(H_h^2 + H_h^2\tan(\beta)^2\right)^{3/2}}\right.$$
$$+\frac{1}{2}\frac{k_h\left(\sqrt{H_h^2 + H_h^2\tan(\beta)^2} - \frac{H_h}{\cos(\beta)}\right)\left(2 l_h^2 - 2 H_h\tan(\beta)\, l_h\right)}{\sqrt{H_h^2 + H_h^2\tan(\beta)^2}} + \frac{k_{md}L_y^2\sin(gama_i)^2 l_c^2}{L_y^2\sin(gama_i)^2 + L_y^2\cos(gama_i)^2}$$
$$-\frac{k_{md}\left(\sqrt{L_y^2\sin(gama_i)^2 + L_y^2\cos(gama_i)^2} - L_y\right)L_y^2\sin(gama_i)^2 l_c^2}{\left(L_y^2\sin(gama_i)^2 + L_y^2\cos(gama_i)^2\right)^{3/2}} \tag{18}$$
$$\left.+\frac{1}{2}\frac{k_{md}\left(\sqrt{L_y^2\sin(gama_i)^2 + L_y^2\cos(gama_i)^2} - L_y\right)\left(2 l_c^2 - 2 L_y\cos(gama_i)\, l_c\right)}{\sqrt{L_y^2\sin(gama_i)^2 + L_y^2\cos(gama_i)^2}}\right)\varphi_d(t)$$
$$-\frac{1}{2}\frac{c_{md}(1.273885350\, L_y\sin(gama_i)\, r_m + 1.273885350\, L_y\cos(gama_i)\, r_m)\, L_y\sin(gama_i)\, l_c\left(\frac{d}{dt}\varphi_m(t)\right)}{L_y^2\sin(gama_i)^2 + L_y^2\cos(gama_i)^2}$$
$$+\left(-\frac{1}{2}\frac{k_{md}(1.273885350\, L_y\sin(gama_i)\, r_m + 1.273885350\, L_y\cos(gama_i)\, r_m)\, L_y\sin(gama_i)\, l_c}{L_y^2\sin(gama_i)^2 + L_y^2\cos(gama_i)^2}\right.$$
$$+\frac{1}{2}\frac{1}{\left(L_y^2\sin(gama_i)^2 + L_y^2\cos(gama_i)^2\right)^{3/2}}\left(k_{md}\left(\sqrt{L_y^2\sin(gama_i)^2 + L_y^2\cos(gama_i)^2}\right.\right.$$
$$\left.\left.-L_y\right)L_y\sin(gama_i)\, l_c\,(1.273885350\, L_y\sin(gama_i)\, r_m + 1.273885350\, L_y\cos(gama_i)\, r_m)\right)$$
$$\left.-\frac{0.6369426750\, k_{md}\left(\sqrt{L_y^2\sin(gama_i)^2 + L_y^2\cos(gama_i)^2} - L_y\right)r_m l_c}{\sqrt{L_y^2\sin(gama_i)^2 + L_y^2\cos(gama_i)^2}}\right)\varphi_m(t)$$

Linearizing the third equation of motion (degree of freedom φ_m)

> $EOMm := Eq34 - Eq40;$

$$EOMm :=$$
$$-\frac{1}{2}\left(k_{md}\left(\left(\left(L_y\sin(gama_i) - l_c\sin(\varphi_d(t)) + 0.6369426752\, r_m\varphi_m(t)\right)^2 + \left(L_y\cos(gama_i) - l_c\left(1 - \cos(\varphi_d(t))\right) + 0.6369426752\, r_m\varphi_m(t)\right)^2\right)^{1/2} - L_y\right)\left(1.273885350\left(L_y\sin(gama_i) - l_c\sin(\varphi_d(t)) + 0.6369426752\, r_m\varphi_m(t)\right)r_m + 1.273885350\left(L_y\cos(gama_i) - l_c\left(1 - \cos(\varphi_d(t))\right)\right)\right.\right. \tag{19}$$

$$+0.6369426752\, r_m \varphi_m(t)\big)\, r_m\big)\big) \Big/ \Big(\big(\big(L_\gamma \sin(gama_i) - l_c \sin(\varphi_d(t)) + 0.6369426752\, r_m \varphi_m(t)\big)^2 + \big(L_\gamma \cos(gama_i) - l_c\,(1 - \cos(\varphi_d(t))) + 0.6369426752\, r_m \varphi_m(t)\big)^2\big)^{1/2} - \frac{1}{4}\Big(c_{md}\Big(2\,\big(L_\gamma \sin(gama_i) - l_c \sin(\varphi_d(t)) + 0.6369426752\, r_m \varphi_m(t)\big)\Big(-l_c \cos(\varphi_d(t))\Big(\frac{d}{dt}\varphi_d(t)\Big) + 0.6369426752\, r_m\Big(\frac{d}{dt}\varphi_m(t)\Big)\Big) + 2\,\big(L_\gamma \cos(gama_i) - l_c\,(1 - \cos(\varphi_d(t))) + 0.6369426752\, r_m \varphi_m(t)\big)\Big(-l_c \sin(\varphi_d(t))\Big(\frac{d}{dt}\varphi_d(t)\Big) + 0.6369426752\, r_m\Big(\frac{d}{dt}\varphi_m(t)\Big)\Big)\Big)\Big(1.273885350\,\big(L_\gamma \sin(gama_i) - l_c \sin(\varphi_d(t)) + 0.6369426752\, r_m \varphi_m(t)\big)\, r_m + 1.273885350\,\big(L_\gamma \cos(gama_i) - l_c\,(1 - \cos(\varphi_d(t))) + 0.6369426752\, r_m \varphi_m(t)\big)\, r_m\Big)\Big/\Big(\big(L_\gamma \sin(gama_i) - l_c \sin(\varphi_d(t)) + 0.6369426752\, r_m \varphi_m(t)\big)^2 + \big(L_\gamma \cos(gama_i) - l_c\,(1 - \cos(\varphi_d(t))) + 0.6369426752\, r_m \varphi_m(t)\big)^2\Big)$$

> $Eqm1 := subs(\{\varphi_b(t) = var1, diff(\varphi_b(t), t) = var2,\ \varphi_d(t) = var3, diff(\varphi_d(t), t) = var4, \varphi_m(t) = var5, diff(\varphi_m(t), t) = var6\}, EOMm):$

> $Eqm4 := -diff(Eqm1, var4):$

> $Eqm5 := -diff(Eqm1, var3):$

> $Eqm6 := -diff(Eqm1, var6):$

> $Eqm7 := -diff(Eqm1, var5):$

> $a1m := subs(\{var1=0, var2=0,\ var3=0, var4=0, var5=0, var6=0\}, Eqm6):$

> $a0m := subs(\{var1=0, var2=0,\ var3=0, var4=0, var5=0, var6=0\}, Eqd7):$

> $a1d := subs(\{var1=0, var2=0,\ var3=0, var4=0, var5=0, var6=0\}, Eqm4):$

> $a0d := subs(\{var1=0, var2=0,\ var3=0, var4=0, var5=0, var6=0\}, Eqm5):$

> $Eqmlin := Eq35 + a1d \cdot diff(\varphi_d(t), t) + a0d \cdot \varphi_d(t) + a1m \cdot diff(\varphi_m(t), t) + a0m \cdot \varphi_m(t);$

$$Eqmlin := J_m\Big(\frac{d^2}{dt^2}\varphi_m(t)\Big) - \frac{1}{2}\,\frac{c_{md}\,(1.273885350\, L_\gamma \sin(gama_i)\, r_m + 1.273885350\, L_\gamma \cos(gama_i)\, r_m)\, L_\gamma \sin(gama_i)\, l_c \Big(\frac{d}{dt}\varphi_d(t)\Big)}{L_\gamma^2 \sin(gama_i)^2 + L_\gamma^2 \cos(gama_i)^2} + \Big(-\frac{1}{2}\,\frac{k_{md}\,(1.273885350\, L_\gamma \sin(gama_i)\, r_m + 1.273885350\, L_\gamma \cos(gama_i)\, r_m)\, L_\gamma \sin(gama_i)\, l_c}{L_\gamma^2 \sin(gama_i)^2 + L_\gamma^2 \cos(gama_i)^2} + \frac{1}{2}\,\frac{1}{(L_\gamma^2 \sin(gama_i)^2 + L_\gamma^2 \cos(gama_i)^2)^{3/2}}\Big(k_{md}\Big(\sqrt{L_\gamma^2 \sin(gama_i)^2 + L_\gamma^2 \cos(gama_i)^2} \tag{20}$$

$$-L_r\Big)\, L_r \sin(gama_i)\, l_c\, (1.273885350\, L_r \sin(gama_i)\, r_m + 1.273885350\, L_r \cos(gama_i)\, r_m)\Big)$$

$$-\frac{0.6369426750\, k_{md} \left(\sqrt{L_r^2 \sin(gama_i)^2 + L_r^2 \cos(gama_i)^2} - L_r\right) r_m\, l_c}{\sqrt{L_r^2 \sin(gama_i)^2 + L_r^2 \cos(gama_i)^2}}\Bigg)\, \varphi_d(t)$$

$$+\frac{1}{4}\, \frac{c_{md}\, (1.273885350\, L_r \sin(gama_i)\, r_m + 1.273885350\, L_r \cos(gama_i)\, r_m)^2 \left(\frac{d}{dt}\, \varphi_m(t)\right)}{L_r^2 \sin(gama_i)^2 + L_r^2 \cos(gama_i)^2} + \Bigg($$

$$-\frac{1}{2}\, \frac{k_{md}\, (1.273885350\, L_r \sin(gama_i)\, r_m + 1.273885350\, L_r \cos(gama_i)\, r_m)\, L_r \sin(gama_i)\, l_c}{L_r^2 \sin(gama_i)^2 + L_r^2 \cos(gama_i)^2}$$

$$+\frac{1}{2}\, \frac{1}{\left(L_r^2 \sin(gama_i)^2 + L_r^2 \cos(gama_i)^2\right)^{3/2}} \Big(k_{md} \Big(\sqrt{L_r^2 \sin(gama_i)^2 + L_r^2 \cos(gama_i)^2}$$

$$-L_r\Big)\, L_r \sin(gama_i)\, l_c\, (1.273885350\, L_r \sin(gama_i)\, r_m + 1.273885350\, L_r \cos(gama_i)\, r_m)\Big)$$

$$-\frac{0.6369426750\, k_{md} \left(\sqrt{L_r^2 \sin(gama_i)^2 + L_r^2 \cos(gama_i)^2} - L_r\right) r_m\, l_c}{\sqrt{L_r^2 \sin(gama_i)^2 + L_r^2 \cos(gama_i)^2}}\Bigg)\, \varphi_m(t)$$

- **Linear three degrees of freedom model**

```
function ydot =
eomlin(t,y,Jb,Jd,Jm,lh,beta,ch,kh,mb,md,g,lb,ld,H,Lr,gamai,lc,rm,Disp,Vel,T,kmd,cmd)

% y = [ fib
%       fibdot
%       fid
%       fiddot ]

fib = y(1);
fibdot = y(2);
fid = y(3);
fiddot = y(4);

% Mass Matrix

m11 = Jb;
m12 = 0;
m13 = 0;
m21 = 0;
m22 = Jd;
m23 = 0;
m31 = 0;
m32 = 0;
m33 = Jm;

% Stiffness Matrix
```

```
k11 = kh*H^2*lh^2/(H^2+H^2*(tan(beta))^2)-
kh*H^2*lh^2/(H^2+H^2*(tan(beta))^2)^(3/2)*((H^2+H^2*(tan(beta))^2)^(1/2)-
H/cos(beta))+kh*((H^2+H^2*(tan(beta))^2)^(1/2)-
H/cos(beta))*(lh^2+H*tan(beta)*lh)/(H^2+H^2*(tan(beta))^2)^(1/2);
k12 = -
kh*H^2*lh^2/(H^2+H^2*(tan(beta))^2)+kh*H^2*lh^2/(H^2+H^2*(tan(beta))^2)^(3/2)*((H^2+H^2*(tan(beta
))^2)^(1/2)-H/cos(beta))-kh*((H^2+H^2*(tan(beta))^2)^(1/2)-
H/cos(beta))*(lh^2)/(H^2+H^2*(tan(beta))^2)^(1/2);
k13 = 0;
k21 = k12;
k22 = kh*H^2*lh^2/(H^2+H^2*(tan(beta))^2)-
kh*H^2*lh^2/(H^2+H^2*(tan(beta))^2)^(3/2)*((H^2+H^2*(tan(beta))^2)^(1/2)-
H/cos(beta))+kh*((H^2+H^2*(tan(beta))^2)^(1/2)-H/cos(beta))*(lh^2-
H*tan(beta)*lh)/(H^2+H^2*(tan(beta))^2)^(1/2)+kmd*Lr^2*(sin(gamai))^2*lc^2/(Lr^2*(sin(gamai))^2+L
r^2*(cos(gamai))^2)-kmd*((Lr^2*(sin(gamai))^2+Lr^2*(cos(gamai))^2)^(1/2)-
Lr)*Lr^2*(sin(gamai))^2*lc^2/(Lr^2*(sin(gamai))^2+Lr^2*(cos(gamai))^2)^(3/2)+kmd*((Lr^2*(sin(gama
i))^2+Lr^2*(cos(gamai))^2)^(1/2)-Lr)*(lc^2-
Lr*cos(gamai)*lc)/(Lr^2*(sin(gamai))^2+Lr^2*(cos(gamai))^2)^(1/2);
k23 = -
kmd*(2/3.14*Lr*sin(gamai)*rm+2/3.14*Lr*cos(gamai)*rm)*Lr*sin(gamai)*lc/(Lr^2*(sin(gamai))^2+Lr^2*
(cos(gamai))^2)+kmd*((Lr^2*(sin(gamai))^2+Lr^2*(cos(gamai))^2)^(1/2)-
Lr)*Lr*sin(gamai)*lc*(2/3.14*Lr*sin(gamai)*rm+2/3.14*Lr*cos(gamai)*rm)/(Lr^2*(sin(gamai))^2+Lr^2*
(cos(gamai))^2)^(3/2)-2/3.14*kmd*((Lr^2*(sin(gamai))^2+Lr^2*(cos(gamai))^2)^(1/2)-
Lr)*rm*lc/(Lr^2*(sin(gamai))^2+Lr^2*(cos(gamai))^2)^(1/2);
k31 = 0;
k32 = k23;
k33 = k23;

% Damping Matrix

c11 = ch*H^2*lh^2/(H^2+H^2*(tan(beta))^2);
c12 = -c11;
c13 = 0;
c21 = c12;
c22 =
ch*H^2*lh^2/(H^2+H^2*(tan(beta))^2)+cmd*Lr^2*(sin(gamai))^2*lc^2/(Lr^2*(sin(gamai))^2+Lr^2*(cos(g
amai))^2);
c23 = -
cmd*(2/3.14*Lr*sin(gamai)*rm+2/3.14*Lr*cos(gamai)*rm)*Lr*sin(gamai)*lc/(Lr^2*(sin(gamai))^2+Lr^2*
(cos(gamai))^2);
c31 = 0;
c32 = c23;
c33 =
cmd*(1/3.14*Lr*sin(gamai)*rm+1/3.14*Lr*cos(gamai)*rm)^2/(Lr^2*(sin(gamai))^2+Lr^2*(cos(gamai))^2)
;

% Interpolation of the input motion parameters for the time t of the solver
kIndex = find(T>t);

if isempty(kIndex)
    Dm = Disp(end);
    Vm = Vel(end);
```

```
else
    kIndex1 = kIndex(1);
    kIndex0 = kIndex1-1;
    dd = (Disp(kIndex1)-Disp(kIndex0))/(T(kIndex1)-T(kIndex0));
    Dm = Disp(kIndex0)+dd*(t-T(kIndex0));
    dv = (Vel(kIndex1)-Vel(kIndex0))/(T(kIndex1)-T(kIndex0));
    Vm = Vel(kIndex0)+dv*(t-T(kIndex0));
end

% Angular Displacement of the Motor
fim = Dm;
% Angular Velocity of the Motor
fimdot = Vm;
% Equation of Motion of the Balance Part
fib2dot = 1/m11*(-c11*fibdot-k11*fib-c12*fiddot-k12*fid);
% Equation of Motion of the Deck
fid2dot = 1/m22*(-c21*fibdot-k21*fib-c22*fiddot-k22*fid-c23*fimdot-k23*fim);

ydot = [fibdot;fib2dot;fiddot;fid2dot];

fprintf(1, 'time = %d s\n', t);
end
clear all
close all
clc

% Loading Motor Motion Parameters

itwk = 5.251*10^(-3);           % Mechanical Devices Transmission Factor
eta = 0.135;                    % Mechanical Devices Efficiency


load('T.mat');                  % Loading Time
load('motor.mat');              % Loading Motor Motion Parameters
% Time
T = T(:,1);
% Angular Acceleration
Acc = motor(:,3);
% Angular Velocity
Vel = motor(:,2);
% Angular Displacement
Disp = motor(:,1);

figure;
subplot(1,3,1), plot(T,Disp); xlabel('Time (s)'); ylabel('Angular Displacement');
subplot(1,3,2), plot(T,Vel); xlabel('Time (s)'); ylabel('Angular Velocity');
subplot(1,3,3), plot(T,Acc); xlabel('Time (s)'); ylabel('Angular Acceleration');

% Input Data

g = 9.81;                       % gravitational acceleration
Jb = 2.138*10^6;                % mass moment of inertia of the balance part
```

```
mb = 74969;                     % mass of the balance part
Jd = 3.98*10^6;                 % mass moment of inertia of the deck
md = 46017;                     % mass of the deck
Jm = 2.373;                     % mass moment of inertia of the electro-motor
kh = 347858326.1;               % stiffness of the hanger 347858326.1
kmd = 140000000;                % stiffness of the mechanical devices 140000000
mh = 2000;                      % mass of the hanger
psi = 0.05;                     % considered damping ratio
ch = 2*psi*sqrt(kh/mh)*mh;      % damping coefficient of the hanger
mmd = 1366.44165;               % mass of the mechanical devices
cmd = 2*psi*sqrt(kmd/mmd)*mmd;  % damping coefficient of the mechanical devices
lb = 5.16;                      % distance from the center of gravity of the balance part to the
upper pivot point
beta = 0.23;                    % the angle between the hanger and the vertical axis (in closed
position)
ld = 8.004;                     % distance from the center of gravity of the deck to the lower
pivot point
lh = 12.63;                     % distance from the connection point of the hanger to the pivot
points
lc = 3.7;                       % distance from the connection point of the rack and the deck to
the lower pivot point
rm = 0.136;                     % the angle between the rack and the horizontal axis (in closed
position)
H = 12.07;                      % vertical length of the hanger
gamai = 0.604;                  % initial angle between the rack and the deck
Lr = 6.445;                     % initial length of the rack

ti = 0;                         % initial time
dt = 0.1;                       % time increment
tf = 77;                        % final time
Time = ti:dt:tf;                % time range
y0 = [0;0;0;0];                 % initial conditions

% Mass Matrix

m11 = Jb;
m12 = 0;
m13 = 0;
m21 = 0;
m22 = Jd;
m23 = 0;
m31 = 0;
m32 = 0;
m33 = Jm;

% Stiffness Matrix

k11 = kh*H^2*lh^2/(H^2+H^2*(tan(beta))^2)-
kh*H^2*lh^2/(H^2+H^2*(tan(beta))^2)^(3/2)*((H^2+H^2*(tan(beta))^2)^(1/2)-
H/cos(beta))+kh*((H^2+H^2*(tan(beta))^2)^(1/2)-
H/cos(beta))*(lh^2+H*tan(beta)*lh)/(H^2+H^2*(tan(beta))^2)^(1/2);
```

```
k12 = -
kh*H^2*lh^2/(H^2+H^2*(tan(beta))^2)+kh*H^2*lh^2/(H^2+H^2*(tan(beta))^2)^(3/2)*((H^2+H^2*(tan(beta
))^2)^(1/2)-H/cos(beta))-kh*((H^2+H^2*(tan(beta))^2)^(1/2)-
H/cos(beta))*(lh^2)/(H^2+H^2*(tan(beta))^2)^(1/2);
k13 = 0;
k21 = k12;
k22 = kh*H^2*lh^2/(H^2+H^2*(tan(beta))^2)-
kh*H^2*lh^2/(H^2+H^2*(tan(beta))^2)^(3/2)*((H^2+H^2*(tan(beta))^2)^(1/2)-
H/cos(beta))+kh*((H^2+H^2*(tan(beta))^2)^(1/2)-H/cos(beta))*(lh^2-
H*tan(beta)*lh)/(H^2+H^2*(tan(beta))^2)^(1/2)+kmd*Lr^2*(sin(gamai))^2*lc^2/(Lr^2*(sin(gamai))^2+L
r^2*(cos(gamai))^2)-kmd*((Lr^2*(sin(gamai))^2+Lr^2*(cos(gamai))^2)^(1/2)-
Lr)*Lr^2*(sin(gamai))^2*lc^2/(Lr^2*(sin(gamai))^2+Lr^2*(cos(gamai))^2)^(3/2)+kmd*((Lr^2*(sin(gama
i))^2+Lr^2*(cos(gamai))^2)^(1/2)-Lr)*(lc^2-
Lr*cos(gamai)*lc)/(Lr^2*(sin(gamai))^2+Lr^2*(cos(gamai))^2)^(1/2);
k23 = -
kmd*(2/3.14*Lr*sin(gamai)*rm+2/3.14*Lr*cos(gamai)*rm)*Lr*sin(gamai)*lc/(Lr^2*(sin(gamai))^2+Lr^2*
(cos(gamai))^2)+kmd*((Lr^2*(sin(gamai))^2+Lr^2*(cos(gamai))^2)^(1/2)-
Lr)*Lr*sin(gamai)*lc*(2/3.14*Lr*sin(gamai)*rm+2/3.14*Lr*cos(gamai)*rm)/(Lr^2*(sin(gamai))^2+Lr^2*
(cos(gamai))^2)^(3/2)-2/3.14*kmd*((Lr^2*(sin(gamai))^2+Lr^2*(cos(gamai))^2)^(1/2)-
Lr)*rm*lc/(Lr^2*(sin(gamai))^2+Lr^2*(cos(gamai))^2)^(1/2);
k31 = 0;
k32 = k23;
k33 = k23;

% Damping Matrix

c11 = ch*H^2*lh^2/(H^2+H^2*(tan(beta))^2);
c12 = -c11;
c13 = 0;
c21 = c12;
c22 =
ch*H^2*lh^2/(H^2+H^2*(tan(beta))^2)+cmd*Lr^2*(sin(gamai))^2*lc^2/(Lr^2*(sin(gamai))^2+Lr^2*(cos(g
amai))^2);
c23 = -
cmd*(2/3.14*Lr*sin(gamai)*rm+2/3.14*Lr*cos(gamai)*rm)*Lr*sin(gamai)*lc/(Lr^2*(sin(gamai))^2+Lr^2*
(cos(gamai))^2);
c31 = 0;
c32 = c23;
c33 =
cmd*(1/3.14*Lr*sin(gamai)*rm+1/3.14*Lr*cos(gamai)*rm)^2/(Lr^2*(sin(gamai))^2+Lr^2*(cos(gamai))^2)
;

% Ordinary Differential Equations Solver

[t,y] = ode45(@(t,y)
eomlin(t,y,Jb,Jd,Jm,lh,beta,ch,kh,mb,md,g,lb,ld,H,Lr,gamai,lc,rm,Disp,Vel,T,kmd,cmd),Time,y0);

% Angular Displacement of the Balance Part
dispb = y(:,1);
% Angular Velocity of the Balance Part
velb = y(:,2);
% Angular Displacement of the Deck
```

```
dispd = y(:,3);
% Angular Velocity of the Deck
veld = y(:,4);

accb = zeros(size(t));
accd = zeros(size(t));

% Algorithm for computing the angular accelerations and the motor torque

for it = 1:1:length(t)

    kIndex = find(T>t(it));
    if isempty(kIndex)
        Dm = Disp(end);
        Vm = Vel(end);
        Am = Acc(end);
    else
        kIndex1 = kIndex(1);
        kIndex0 = kIndex1-1;
        dd = (Disp(kIndex1)-Disp(kIndex0))/(T(kIndex1)-T(kIndex0));
        Dm = Disp(kIndex0)+dd*(t(it)-T(kIndex0));
        dv = (Vel(kIndex1)-Vel(kIndex0))/(T(kIndex1)-T(kIndex0));
        Vm = Vel(kIndex0)+dv*(t(it)-T(kIndex0));
        da = (Acc(kIndex1)-Acc(kIndex0))/(T(kIndex1)-T(kIndex0));
        Am = Acc(kIndex0)+da*(t(it)-T(kIndex0));
    end

    % Angular Displacement of the Motor
    dispm(it) = Dm;
    % Angular Velocity of the Motor
    velm(it) = Vm;
    % Angular Acceleration of the Motor
    accm(it) = Am;
     % Angular Acceleration of the Balance Part
    accb(it) = 1/m11*(-c11*velb(it)-k11*dispb(it)-c12*veld(it)-k12*dispd(it));
    % Angular Acceleration of the Deck
    accd(it) = 1/m22*(-c21*velb(it)-k21*dispb(it)-c22*veld(it)-k22*dispd(it)-c23*velm(it)-
k23*dispm(it));
    % Torque acting on the Motor
    Mmotor(it) = m33*accm(it)+c32*veld(it)+k32*dispd(it)+c33*velm(it)+k33*dispm(it);

end

% Plotting Results (Unfiltered)

figure;
subplot(3,3,1), plot(t,dispb); xlabel('Time (s)'); ylabel('Dispb [rad]');
subplot(3,3,2), plot(t,velb); xlabel('Time (s)'); ylabel('Velb [rad/s]');
subplot(3,3,3), plot(t,accb); xlabel('Time (s)'); ylabel('Accb [rad/s^2]');
subplot(3,3,4), plot(t,dispd); xlabel('Time (s)'); ylabel('Dispd [rad]');
subplot(3,3,5), plot(t,veld); xlabel('Time (s)'); ylabel('Veld [rad/s]');
subplot(3,3,6), plot(t,accd); xlabel('Time (s)'); ylabel('Accd [rad/s^2]');
```

```
subplot(3,3,7), plot(t,Mmotor); xlabel('Time (s)'); ylabel('Motor Torque [Nm]');
```

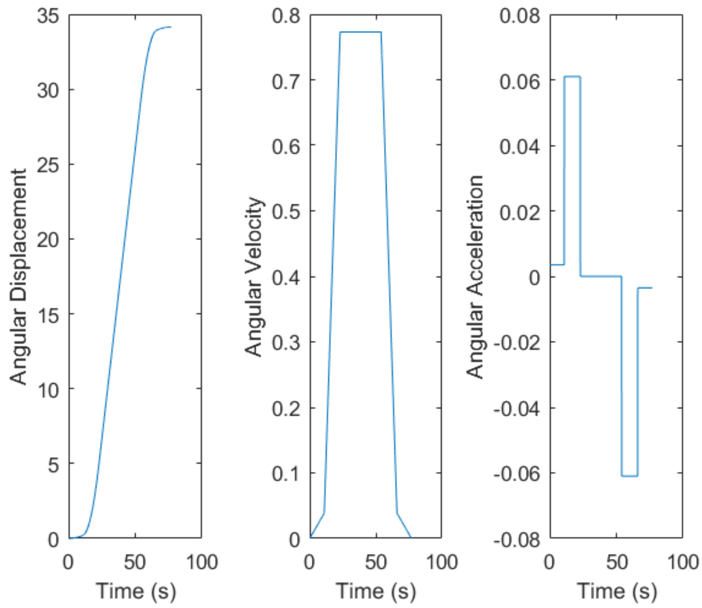

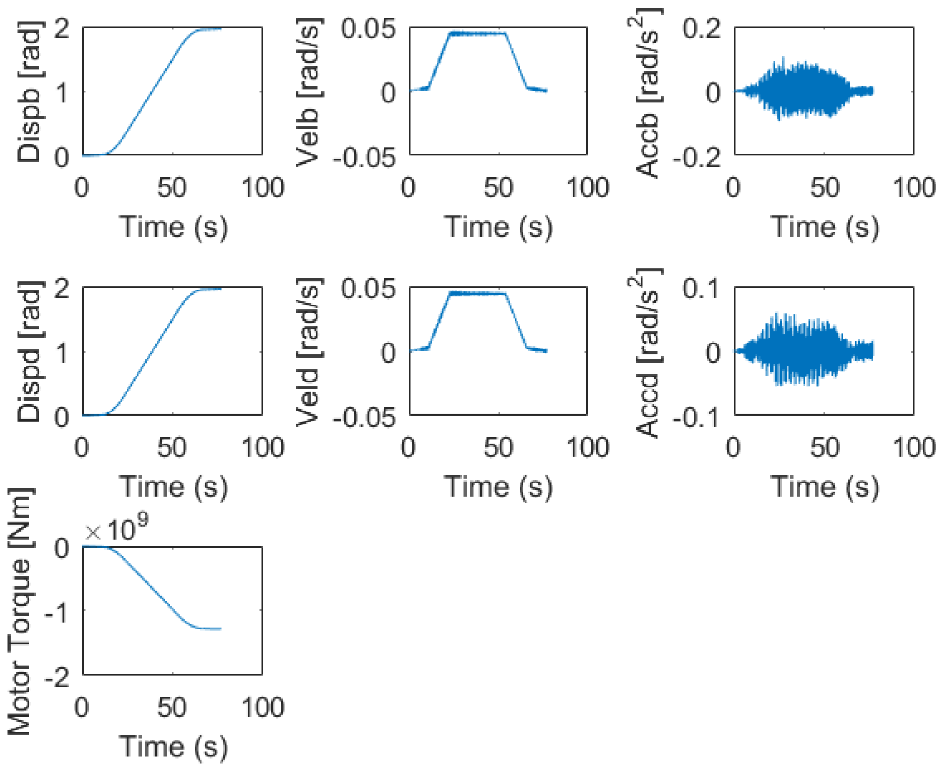

- **Eigenvalue Problem**

```
clear all
close all
clc

% Eigenvalue Problem for Normal Operation

% Input Data

g = 9.81;                         % gravitational acceleration
Jb = 2.138*10^6;                  % mass moment of inertia of the balance part
mb = 74969;                       % mass of the balance part
Jd = 3.98*10^6;                   % mass moment of inertia of the deck
md = 46017;                       % mass of the deck
Jm = 2.373;                       % mass moment of inertia of the electro-motor
kh = 347858326.1;                 % stiffness of the hanger 347858326.1
kmd = 140000000;                  % stiffness of the mechanical devices 140000000
mh = 2000;                        % mass of the hanger
psi = 0.05;                       % considered damping ratio
ch = 2*psi*sqrt(kh/mh)*mh;        % damping coefficient of the hanger
mmd = 1366.44165;                 % mass of the mechanical devices
cmd = 2*psi*sqrt(kmd/mmd)*mmd;    % damping coefficient of the mechanical devices
lb = 5.16;                        % distance from the center of gravity of the balance part to the
upper pivot point
beta = 0.23;                      % the angle between the hanger and the vertical axis (in closed
position)
ld = 8.004;                       % distance from the center of gravity of the deck to the lower
pivot point
lh = 12.63;                       % distance from the connection point of the hanger to the pivot
points
lc = 3.7;                         % distance from the connection point of the rack and the deck to
the lower pivot point
rm = 0.136;                       % the angle between the rack and the horizontal axis (in closed
position)
H = 12.07;                        % vertical length of the hanger
gamai = 0.604;                    % initial angle between the rack and the deck
Lr = 6.445;                       % initial length of the rack

% Mass Matrix

Mm = [[Jb 0]; [0 Jd]];

% Stiffness Matrix

k11 = kh*H^2*lh^2/(H^2+H^2*(tan(beta))^2)-
kh*H^2*lh^2/(H^2+H^2*(tan(beta))^2)^(3/2)*((H^2+H^2*(tan(beta))^2)^(1/2)-
H/cos(beta))+kh*((H^2+H^2*(tan(beta))^2)^(1/2)-
H/cos(beta))*(lh^2+H*tan(beta)*lh)/(H^2+H^2*(tan(beta))^2)^(1/2);
k12 = -
kh*H^2*lh^2/(H^2+H^2*(tan(beta))^2)+kh*H^2*lh^2/(H^2+H^2*(tan(beta))^2)^(3/2)*((H^2+H^2*(tan(beta
))^2)^(1/2)-H/cos(beta))-kh*((H^2+H^2*(tan(beta))^2)^(1/2)-
H/cos(beta))*(lh^2)/(H^2+H^2*(tan(beta))^2)^(1/2);
```

```
k21 = k12;
k22 = kh*H^2*lh^2/(H^2+H^2*(tan(beta))^2)-
kh*H^2*lh^2/(H^2+H^2*(tan(beta))^2)^(3/2)*((H^2+H^2*(tan(beta))^2)^(1/2)-
H/cos(beta))+kh*((H^2+H^2*(tan(beta))^2)^(1/2)-H/cos(beta))*(lh^2-
H*tan(beta)*lh)/(H^2+H^2*(tan(beta))^2)^(1/2)+kmd*Lr^2*(sin(gamai))^2*lc^2/(Lr^2*(sin(gamai))^2+L
r^2*(cos(gamai))^2)-kmd*((Lr^2*(sin(gamai))^2+Lr^2*(cos(gamai))^2)^(1/2)-
Lr)*Lr^2*(sin(gamai))^2*lc^2/(Lr^2*(sin(gamai))^2+Lr^2*(cos(gamai))^2)^(3/2)+kmd*((Lr^2*(sin(gama
i))^2+Lr^2*(cos(gamai))^2)^(1/2)-Lr)*(lc^2-
Lr*cos(gamai)*lc)/(Lr^2*(sin(gamai))^2+Lr^2*(cos(gamai))^2)^(1/2);

Km = [[k11 k12]; [k21 k22]];

% Eigenvalues and Eigenvectors Computation

[Vm,Dm] = eig(Km,Mm);

% Squared Eigenvalues
display(Dm);
% Eigenvectors
display(Vm);

% Check

Check = Km*Vm-Mm*Vm*Dm;
display(Check);

% Natural angular frequencies [rad/s]
nat_freq_1=sqrt(Dm(1,1));
nat_freq_2=sqrt(Dm(2,2));

display(nat_freq_1);
display(nat_freq_2);


% Natural angular frequencies [Hz]
f_1 = nat_freq_1/(2*3.14);
f_2 = nat_freq_2/(2*3.14);

display(f_1);
display(f_2);

% Natural Mode Shapes
mode_shape_1=Vm(:,1);
mode_shape_2=Vm(:,2);

display(mode_shape_1);
display(mode_shape_2);

time = 0:0.1:77;
```

```
% Set Frequency
```

```
omega = nat_freq_1;
```

```
fi_11 = exp(1i*omega*time)*mode_shape_1(1);
fi_12 = exp(1i*omega*time)*mode_shape_1(2);
fi_21 = exp(1i*omega*time)*mode_shape_2(1);
fi_22 = exp(1i*omega*time)*mode_shape_2(2);


figure;
subplot(1,2,1), plot(time,fi_11,'r',time,fi_21,'b');xlabel('Time (s)'); ylabel('Displacement');
subplot(1,2,2), plot(time,fi_12,'r',time,fi_22,'b');xlabel('Time (s)'); ylabel('Displacement');
legend('balance part', 'deck')

% Set Frequency
omega = nat_freq_2;

fi_11 = exp(1i*omega*time)*mode_shape_1(1);
fi_12 = exp(1i*omega*time)*mode_shape_1(2);
fi_21 = exp(1i*omega*time)*mode_shape_2(1);
fi_22 = exp(1i*omega*time)*mode_shape_2(2);


figure;
subplot(1,2,1), plot(time,fi_11,'r',time,fi_21,'b');xlabel('Time (s)'); ylabel('Displacement');
subplot(1,2,2), plot(time,fi_12,'r',time,fi_22,'b');xlabel('Time (s)'); ylabel('Displacement');
legend('balance part', 'deck')
```

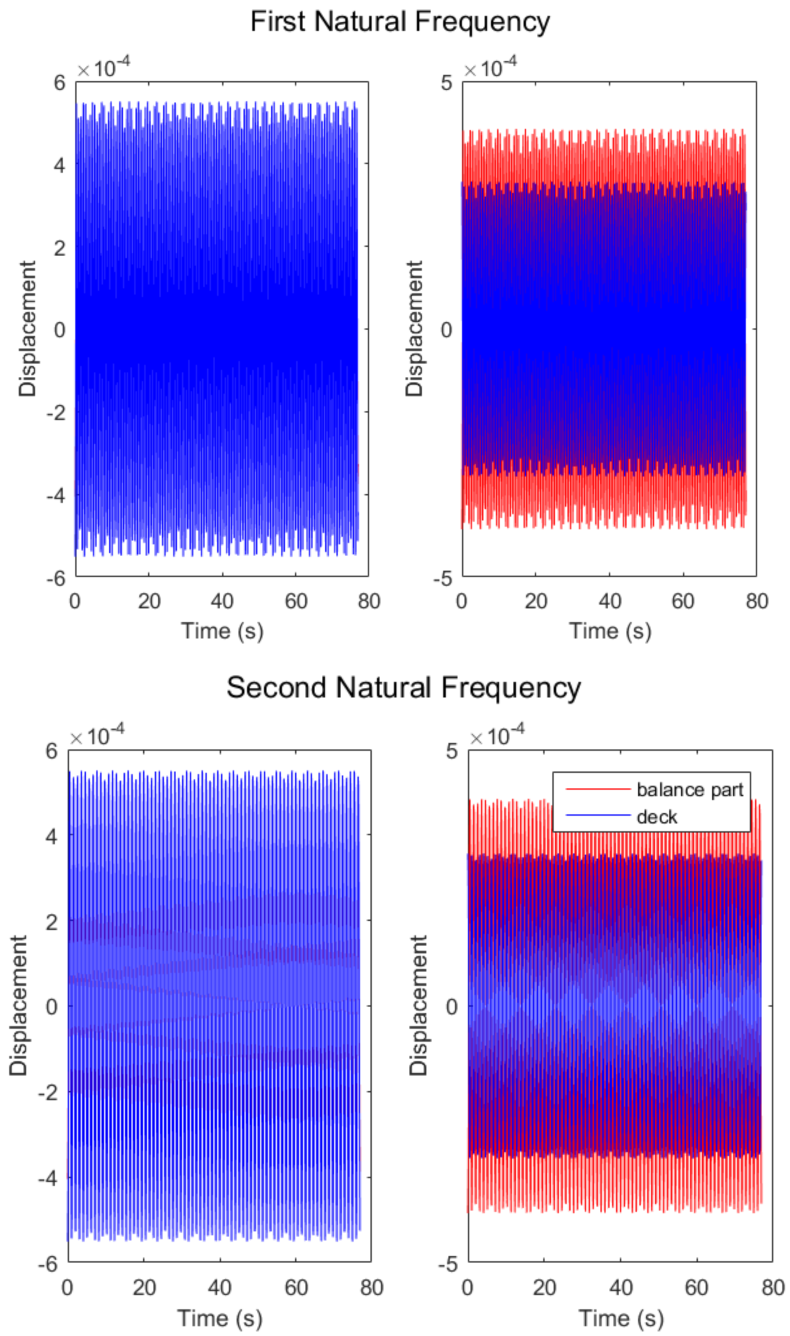
First Natural Frequency
Second Natural Frequency
Displacement
Time (s)
×10^-4
balance part
deck